Atmospheric Polycyclic Aromatic Hydrocarbons: Identification, Abundances and Spatio-Temporal Variation

A Thesis

submitted for the Award of Ph.D. degree of

MOHANLAL SUKHADIA UNIVERSITY

in the

Faculty of Science

By

Prashant Rajput

Under the supervision of

Dr. M. M. Sarin

SENIOR PROFESSOR
GEOSCIENCES DIVISION
PHYSICAL RESEARCH LABORATORY
AHMEDABAD – 380 009, INDIA

DEPARTMENT OF CHEMISTRY
FACULTY OF SCIENCE
MOHANLAL SUKHADIA UNIVERSITY
UDAIPUR (RAJ)

Year of submission – 2012

*Learn from **yesterday**, live for **today**, hope for **tomorrow**.*

*The important thing is not to stop **questioning**.*

-Albert Einstein

DECLARATION

I, **Mr. Prashant Rajput**, S/o Mr. Satya Deo Singh, resident of C-19, PRL Residences, Navrangpura, Ahmedabad – 380 009, hereby declare that the research work incorporated in the present thesis entitled **"Atmospheric Polycyclic Aromatic Hydrocarbons: Identification, Abundances and Spatio-Temporal Variation"** is my own work and is original. This work f has not been submitted to any University for the award of a Degree or a Diploma. I have properly acknowledged the material collected from secondary sources wherever required.

I solely owe the responsibility for the originality of the entire content.

Date: Prashant Rajput

GEOSCIENCES DIVISION
PHYSICAL RESEARCH LABORATORY
AHMEDABAD – 380 009, INDIA

C E R T I F I C A T E

I feel great pleasure in certifying that the thesis entitled **"Atmospheric Polycyclic Aromatic Hydrocarbons: Identification, Abundances and Spatio-Temporal Variation"** embodies a record of the results of investigations carried out by **Prashant Rajput** under my guidance.

He has completed the following requirements as per Ph.D. regulations of the University

a) Course work as per the University rules.

b) Residential requirements of the University

c) Regularly submitted six monthly/ annual progress report

d) Presented his work in the Departmental Committee

e) Published/accepted minimum of one research paper in a referred research journal.

I am satisfied with the analysis of data, interpretation of results and conclusions drawn.

I recommend the submission of thesis.

Date:

Name and Designation of Supervisor

Dr. M. M. Sarin

Senior Professor

Countersigned by

Head of the Department

Dedicated to

Mummy

&

Papa

ACKNOWLEDGEMENTS

After spending the most valuable five years of my life and remembering those sweet and eventful years at the Physical Research Laboratory (PRL), Ahmedabad, India; I realize that there are many without whom this thesis would not have been a reality. To me, this thesis is by far the most challenging and significant scientific accomplishment in my career. With deep sense of gratitude and respect, I wish to express my sincere thanks and appreciation for fatherly behavior to my thesis supervisor, Prof. M. M. Sarin - a person who believes in the perfection, and introducing me to the field of Atmospheric Chemistry. His enthusiasm, integral view of handling a research project, timely planning and his submission of providing "high quality research with great perfection", has taught me very important lesson of life. His constant and enormous support, inspiration and encouragement throughout my Ph. D. period have helped to bring out the best from me in the form of this thesis. He has always been an immense source of inspiration and I am extremely grateful to him for providing me the opportunity to work with him. I am greatly indebt to him in making me what I am today.

I thank Prof. J. N. Goswami, the Director, and Prof. Utpal Sarkar, the Dean, Physical Research Laboratory, for providing me all the necessary facilities to carry out my thesis work.

I would like to thank Prof. S. Krishnaswami who inspired me to do better work and keeping me awake all the time. It was a great opportunity and privilege for me to work in the foundation made by him. The scientific discussions with him were simply outstanding and amazing which helped me to bring out the best from me.

The course-work taughts by Drs. Raghavan Rangarajan, Angom D. K. Singh, Jyotiranjan S. Ray, D. Banerjee, K. K. Marhas, Vinay Kumar Rai, S. Ramachandran, D. Pallamraju, Bhas Bapat, K. P. Subramanian, N. M. Ashok, Prasanta K. Panigrahi, M. M. Sarin and R. Ramesh was extraordinary and knowledgeable.

With great respect and gratitude, I thank Dr. S. K. Singh and Ravi Bhushan (Ravi Daa) - the persons with great sense of humanity whom you can always trust. I wish to thank Dr. R. Rengarajan and Mr. A. K. Sudheer for helping me in learning the instrumentation skills. The scientific discussion and advices from them were very helpful. To run a good laboratory, one would always wish to have a person like Mr. J. P. Bhavsar (Bhavsar Bhai). Thank to Ms. Sneha Acharya and Vaishali Patel for the help in computer related work. I thank Mrs. Pauline Joseph for all the help, care and support provided to me. I thank all the family members of the Chemistry group for a nice and comfortable company throughout the tenure of my research at PRL.

I thank all the faculties, scientists and staff members of the Geosciences Division. My special thanks to Drs. A. K. Singhvi, R. Ramesh, J. S. Ray, S. K. Singh, R. D. Deshpande, Ravi Bhushan, M. G. Yadava, A. D. Shukla, Navin Juyal, Neeraj Rastogi and Sanjeev Kumar for their help and kind support during my stay at PRL. I must thank Pranav Bhai, Manan and Lakhan bhai for helping in instrumental related problems. I am always benefited by the discussion made with Venkat Ji, T. A. Rajesh, Neeraj Srivastava and Panda Ji. I thank Prof. Shyam Lal and Drs. Neeraj Rastogi, Lokesh Kumar Sahu, Varun Sheel, Som Kumar Sharma and P. R. Sinha for their constructive suggestions during this study.

The time spent at PRL hostel with my close friends will be unforgettable moment of my life. I must thank all my seniors (Drs. Kirpa Ram, Ashwini Kumar, Timmy Francis, Rohit Srivastava, Gyan Ranjan Tripathy, Waliur Rahman, Vineet Goswami, Amzad H. Laskar, Sumita Kedia, Naveen Gandhi, Naveen Chauhan, Arvind Singh, Shailendra Kumar Singh, Mala S. Bagiya, Ashok Kumar, Sandeep Gautam, Harinder Pal, Bhaswar, Joydeep, Naveen Kumar Singh, Soumya Rao, Vivek Vyas, Shreyas Managave, Ritesh Mishra, P. Morthekai, Uma Kota, Sanat Das, Rajesh Kushwaha, Suchita Srivastava, Sumanta Sarkhel, Vimal Kishore, Suman Acharyya, Rabiul H. Biswas, Salman Silotri, H. Zeen Devi, Alok Kumar Saini, Nawaz, Anjishnu Sarkar and A. S. Maurya), my batch-mates (Srinivas, Satinder, Jayati, Moumita, Neeraj, Arvind, Tapas, Ketan, Pravin, Patra, Iman, Suruchi and Ashish) and junior-mates (Arun, Chinmay, Rajlakshmi, Medha,

Damodar, Reddy, Aadhi, Shashi, Fazlul, Siddharta, Lakshmi, Bhavya, Midhun, Manojith, Gaurav, Gulab, Tomar, Yashpal, Negi, Anirban Chatterjee, Abhaya Kumar Swain, Chithrabhanu P., Guruprasad Kadam, Ikshu Gautam, Kuldeep Suthar, Manu George, Shraddha Band, Sanjay Kumar Saini, Saweeta Kumari and Venkatesh). I also thank Sharad Chandra Tripathi, Arvind S. Rajpurohit and Jaspreet S. Randhawa for being like younger brothers to me.

I also thank kids, Mahin, Golu, Markandeya, Monu, Nandana, Devkrishnan and Yatharth, for receiving positive energy while watching their play and actions.

I am also thankful to the tea-stall, Barber and laundry-service people, outside the PRL hostel, for providing me the service in-time with affection.

I take this opportunity to thank all the members of PRL workshop. I specially thank Mr. G. P. Ubale, Vishnu Patel, Bankim, Jayanti Bhai for the help and fulfilling the requirements to carry out my research work at various stages. I must thank Jokhakar Ji, Sivadasan bhai, Jitu bhai, Rakesh bhai and all the members of electronic section for their help and support. I thank all the members of the administration department for their help and support for admin related works. My special thanks to Deekshitulu Ji, Ghanshyam bhai, Yadav Ji, Ranganathan Ji, Bhupendra Ji, Senthil bhai, Pradeep Sharma, Hemal bhai, Nandini Rao, Usha Ji, Gandhi Ji, Virendra K. Padhya, S. P. Pillai, K. K. Sasi Kumar, Suresh K. Patel, Hitesh C. Panchal, Parul Ji, Panchasara Ji, D. J. Panchal and Yugal Jain for their help and support at various levels.

I must thank all the members of the Computer Center: Subedar and Dholakia Ji, Jigar bhai, Tejas, Alok bhai, Mishra Ji, Kailash, Rushit, Renyca, Disha, Heena and Pramila behen.

I am glad to acknowledge Dr. Darshan Singh and his group members (Deepti Sharma, Atinder Pal Singh and Manjeet Singh) for the help provided in the aerosol sampling at Patiala.

With great respect and gratitude, I wish to thank all the faculties, scientists, staff members and the students of PRL, whose names are missing, for their love, care and support provided during my stay at PRL.

I wish to thank to our PRL medical doctors, Dr. (Mrs.) Sheetal Patel and Dr. Sameer Dani, and staff members who kept me aware to the ways to maintain a good health.

I would like to share this moment of achievement and happiness with my entire family, friends: Shakti Singh, Mrigendra Dubey, Rakesh Mishra, Vishnu Dubey, Prakash Chandra, Vinay Pathak, Shyam Singh, Prabhakar Rai and Santosh Yadav. Once again I thank Srinivas and Satinder, without their support, care and understanding it would have been not possible to complete my research work. I hope they will continue their encouragement and support in the same way in future too.

I am very grateful to have juniors like Upasana, Balaji, Sneha, Aslam and Saweeta, who helped me a lot in making the presentation of the thesis effectively. Further, I wish to thank Ms. Upasana Banerji to make me learn the Corel-Draw.

I am highly indebted to my parents (Smt. Bimla Singh and Shree Satya Deo Singh), brother (Prabhat) and sisters (Leena and Padma), who always have been a source of inspiration and motivation to me. They never let me down throughout my study period and taught me the real meaning of hard work and honesty by setting their own examples. I thank my brother-in-laws, Engineers B. K. Singh and Brijesh Singh. I thank my fiancée Ms. Neha Singh for her moral support and patience provided to me during the last stage of this work.

Finally, I thank all the persons who have, directly or indirectly, helped me during my Ph. D. Thesis.

ABSTRACT

This thesis presents a systematic study on the atmospheric concentrations of particulate bound polycyclic aromatic hydrocarbons (PAHs), together with a suit of chemical constituents [elemental and organic carbon (EC, OC) and water-soluble organic carbon (WSOC) and inorganic species (WSIS)], from two distinct biomass burning emissions (post-harvest paddy- and wheat-residue burning) in the Indo-Gangetic Plain (IGP). The seasonal variability in atmospheric constituents, as studied from a strategically located sampling site (Patiala: 30.2 ˚N, 76.3 ˚E; 250 m amsl), reveals that mass concentrations of PM2.5 (Av: 195 μg m^{-3}), OC (70 μg m^{-3}), WSOC (40 μg m^{-3}) and ΣWSIS (44 μg m^{-3}) from paddy-residue burning (during October–November) are about 4─5 times higher than those from wheat-residue burning emissions (in April–May); whereas, EC (6 μg m^{-3}) and ΣPAHs (27 ng m^{-3}) are higher by a factor of 2 and 6, respectively, from paddy-residue burning. However, the WSOC/OC ratios (~0.60) are somewhat similar from the two emissions. The ΣPAHs/EC ratios are also significantly different, 4.2 and 1.2 mg g^{-1}, for paddy- and wheat-residue burning emissions. The cross plots of PAHs show distinct differences in isomer ratios from agricultural-waste burning emissions vis-à-vis fossil-fuel combustion. Furthermore, diagnostic ratios of nss-K^+/OC, nss-K^+/EC and nss-SO_4^{2-}/OC have been used for the characterization of paddy- and wheat-residue burning emissions. The long-range transport of particulate OC and PAHs, from the source regions in the IGP to NE-Himalaya (Barapani: 25.7 ˚N, 91.9 ˚E; 1064 m amsl), has been studied in order to assess the atmospheric aging of organic aerosols. Using OC/EC (range: 2─26) and PAH isomer ratios, it is inferred that biomass burning emission dominates (~80%) the abundance of carbonaceous aerosols over NE-H. These results have implications to the impact of biomass burning emissions on the atmospheric chemistry and radiative forcing.

Keywords: *Agricultural-waste burning, Indo-Gangetic Plain (IGP), Northeastern-Himalaya, Long-range transport, Elemental and organic carbon (EC, OC), Water-soluble organic carbon (WSOC), Polycyclic aromatic hydrocarbons (PAHs), Water-soluble inorganic species (WSIS).*

TABLE OF CONTENTS

CHAPTER 1 ..... **1**

Introduction ***1***

1.1. Introduction *3*

1.2. Atmospheric impact of carbonaceous aerosols *5*

1.3. Laboratory experiments on SOA formation *8*

1.4. Chemical reactivity of PAHs *8*

1.5. Rationale and objectives *13*

1.6. Thesis outline *15*

CHAPTER 2 ..... **17**

Aerosol collection and chemical analysis ***17***

2.1. Introduction *19*

2.2. Field-campaign *20*

2.2.1 Patiala: Semi-urban location, upwind in the Indo-Gangetic Plain 21

2.2.2 Shillong: High-altitude location in NE-Himalaya (NE-H) 22

2.2.3 Ahmedabad: Urban site in semi-arid region of western India 22

2.2.4 Mt Abu: High-altitude location in semi-arid western India 23

2.2.5 Hisar: Semi-urban location in the Indo-Gangetic Plain 24

2.2.6 Kanpur: Typical urban location in the Indo-Gangetic Plain 24

2.3. Ambient aerosol sampling *25*

2.4. Chemical Analysis *25*

2.4.1 Analytical scheme 25

2.4.2 Determination of aerosol loading (PM2.5) 26

2.4.3 Analysis of elemental carbon and organic carbon (EC, OC) 26

2.4.4 Analysis of water-soluble organic carbon (WSOC) 31

2.4.5 Analysis of polycyclic aromatic hydrocarbons (PAHs) 33

2.4.5.1 Materials 33

2.4.5.2 Optimization of GC-MS parameters 33

2.4.5.3 Optimization of purification step on silica cartridge 36

2.4.5.4 Optimization of extraction parameters on ASE 37

2.4.5.5 Investigation of loss of 2- to 3-ring PAHs.....38
2.4.5.6 Time-dependent record of analytical conditions on GC-MS.....40
2.4.6 Analysis of water-soluble inorganic species (WSIS).....42
2.5. Summary.....*46*

CHAPTER 3.....**47**

Biomass burning emissions in northern India: Chemical characterization and atmospheric impact.....***47***
3.1. Introduction.....*49*
3.2. Field-campaign and meteorology.....*50*
3.2.1 Sampling site description.....50
3.2.2 Aerosol sampling.....52
3.2.3 Meteorology.....53
3.3. Results and Discussion.....*57*
3.3.1 Inter-annual variability.....58
3.3.1.1 Emissions from paddy-residue burning: October–November.....58
3.3.1.2 Emissions from bio- and fossil-fuel combustion: December–March 61
3.3.1.3 Emissions from wheat-residue burning: April–May.....61
3.3.1.4 Summary of the field-based concentrations of EC, OC, WSOC and ΣPAHs in PM2.5 during three different emission scenarios:.....62
3.3.2 Estimation of primary- and secondary-organic carbon.....64
3.3.3 Water-soluble OC and the SOA.....67
3.3.4 Correlation analysis of particulate ΣPAHs with EC and OC.....69
3.3.5 Variability of particulate PAHs.....71
3.3.6 PAHs isomer ratios and source-characterization.....73
3.3.7 Ambient measurements versus chamber simulation:.....74
3.3.7.1 Paddy-residue burning:.....74
3.3.7.2 Wheat-residue burning:.....76
3.3.8 Inter-annual variability in WSIS for paddy-residue burning emissions.82
3.3.9 Inter-annual variability in WSIS for bio- and fossil-fuel combustion emission.....84
3.3.10 Inter-annual variability in WSIS for wheat-residue burning emissions.85
3.3.11 Summary on water-soluble inorganic species in aerosols.....85

3.3.12 Secondary inorganic species from paddy- and wheat-residue burning emissions 87
3.3.13 nss-K^+, nss-SO_4^{2-}, OC and EC 87
3.3.14 Field burning versus chamber combustion of paddy-residue 91
3.3.14.1 Field-based 91
3.3.14.2 Chamber experiment 91
3.3.15 Field burning versus chamber combustion of wheat-residue 91
3.3.15.1 Field-based 91
3.3.15.2 Chamber experiment 92
3.3.15.3 Equivalent ratios of cations and anions for paddy- and wheat-residues burning emissions 93
3.4. Inferences 95
3.4.1 Emission factors and emissions of aerosol from agricultural-waste burning 95
3.4.2 Emission factors (EF) 97
3.4.3 Fuel load (FL) 97
3.4.4 Area burned (AB) 98
3.5. Global scenario on biomass burning emissions 98
3.5.1 Agricultural-waste burning emissions in southern China and Korea (East Asia) 99
3.5.2 Agricultural-waste burning emissions in Thailand (Southeast Asia) 99
3.5.3 Emissions from savanna-fires in Africa 99
3.5.4 Emissions from cerrado/tropical forest fires in the Amazon basin in South America 100
3.5.5 Boreal forest fires in US/Canada (North America) 101
3.6. Summary and Implications 102

CHAPTER 4 105

Atmospheric long-range transport of carbonaceous aerosols to NE-Himalaya… ……..... 105

4.1. Introduction 107
4.2. Methodology 108
4.2.1 Field-campaign 108
4.2.2 Air-mass back trajectories: 110
4.3. Results and Discussion 110

4.3.1 Mass concentrations of PM2.5, EC, OC, WSOC and ΣPAHs 110
4.3.1.1 TYPE-I Air-masses (Passing over the IGP) 110
4.3.1.2 TYPE-II Air-masses (Passing over the south-China) 114
4.3.2 Atmospheric aging/mixing of aerosols during long-range transport 116
4.3.3 Atmospheric concentration of ΣPAHs and ΣPAHs/EC ratio 119
4.3.4 PAHs isomer ratios 122
4.3.5 Finger-printing of source regions for carbonaceous aerosols 122
4.3.6 Atmospheric aging of carbonaceous aerosols: Use of PAH isomers ... 125
4.3.7 Chemical reactivity of PAHs 126
4.4. Summary and Implications 128

CHAPTER 5 131

Spatio-temporal variation of PAHs from different geographical locations in India: Urban, semi-urban and high-altitude sites 131

5.1. Introduction 133
5.2. Results and Discussion 133
5.2.1 Meteorological wind-fields over the sampling locations: 133
5.2.2 PM2.5, EC, OC and ΣPAHs over Ahmedabad: A Wintertime study ... 134
5.2.3 PM2.5, EC, OC and ΣPAHs over Ahmedabad: A Summertime study 135
5.2.4 PAHs isomer ratios from Ahmedabad: Wintertime versus summer 137
5.2.5 Aerosol composition over Mt Abu: A wintertime study 137
5.2.6 PAHs composition from Hisar and Kanpur during winter in the IGP.. 138
5.2.7 Characteristic ratios of OC/EC and ΣPAHs/EC from different geographical locations in India 141
5.2.8 PAHs isomer ratios 142
5.2.9 Chemical reactivity of PAHs 142
5.3. Summary and Implications 150

CHAPTER 6 151

Synthesis and scope of future research 151

6.1. Synthesis 153
6.2. Scope of the future research 157

References **159**

List of Publications **175**

LIST OF TABLES

Table 2.1: Experimental parameters for the measurement of PAHs 36

Table 2.2: Analysis of 16-PAHs in SRM 1649b, Urban Dust (n = 32)..... 42

Table 3.1: Integration period of aerosol sampling for different emission scenario 53

Table 3.2: Aerosols concentration (Av ± sd; with range in parenthesis) and characteristic ratios for different emission scenarios..... 63

Table 3.3: Number of data points grouped by lowest OC/EC ratio for different emissions to determine the primary OC in aerosols. 65

Table 3.4: Relative rate constants (Av ± 1σ) of PAH isomers for their heterogeneous reactivity in ambient aerosols 81

Table 3.5: Chemical composition of water-soluble inorganic species (WSIS) for different emission sources..... 86

Table 3.6: Characteristic ratios of nss-K^+/OC, nss-K^+/EC and SO_4^{2-}/OC for distinct sources..... 91

Table 3.7: Equivalent ratios among water-soluble inorganic ions in aerosol from paddy- and wheat-residue burning emissions 94

Table 3.8: Estimation of emission factor and emission of aerosols for the agricultural-waste burning of paddy- and wheat-residues 96

Table 4.1: Average mass fractions of PM2.5-bound PAHs (mg g^{-1} OC) 115

Table 4.2: Relative rate constants (Av ± 1σ) of PAH isomers for heterogeneous-phase reactions in ambient aerosols..... 128

Table 5.1: Average mass fractions of PM2.5-bound PAHs (mg g^{-1} OC) from semi-arid locations (Ahmedabad and Mt Abu) in western India 138

Table 5.2: Relative rate constants (Av ± 1σ) of PAH isomers for heterogeneous-phase reactions in ambient aerosols from this study..... 150

LIST OF FIGURES

Figure 1.1: Reaction of acenaphthene with OH radical. 10

Figure 1.2: Reaction of acenaphthylene with OH radical. 10

Figure 1.3: Reaction of acenaphthylene with NO_X radical. 10

Figure 2.1: Map showing aerosol sampling locations: Patiala, Hisar, Kanpur, Shillong, Ahmedabad and Mt Abu.. 23

Figure 2.2: Analytical scheme for chemical analysis of aerosol samples. 25

Figure 2.3: The schematic diagram of the thermo-optical EC-OC analyzer (Sunset Laboratory, US). 27

Figure 2.4: A real-time thermograph of sample (PTA-76) analyzed on the thermo-optical EC-OC analyzer..... 28

Figure 2.5: Analytical accuracy for total carbon (TC) on EC-OC analyzer. 29

Figure 2.6: Replicate measurements of OC and EC (in μg C cm^{-2}) in aerosol samples with different punch area (1.5, 0.7 and 0.5 cm^2).. 30

Figure 2.7: A typical calibration of water-soluble total and inorganic carbon (WSTC and WSIC) on TOC Analyzer, using KHP and $(Na_2CO_3)/(NaHCO_3)$, respectively. 31

Figure 2.8: Uncertainty on analytical accuracy of the measurements (± 8%) is obtained from analysis of (a) several organic standards (n = 8) and; (b) aerosol samples (n = 21). 32

Figure 2.9: Molecular structure of 16-PAHs analyzed in this study. 34

Figure 2.10: Investigation for (a) Optimum ion-source temperature and (b) Variation in retention time for the 16-PAHs on GC-MS. 35

Figure 2.11: The consistent recovery (~100%) of 16-PAHs after purification on silica cartridge 37

Figure 2.12: Replicate analysis (n = 12) of three isomer pairs in SRM-1649b..... 38

Figure 2.13: The extraction efficiency of PAHs, as determined in aerosol samples collected from different geographical regions. 39

Figure 2.14: Typical chromatographs of 16-PAHs on GC-MS in the standard (QTM PAH Mix; 47930-U) and aerosol sample..... 40

Figure 2.15: Time dependent analyses (n = 95; over 2 years) of 16-PAHs (QTM PAH Mix; 47930-U).....41

Figure 2.16: : A typical calibration used for the quantification of water-soluble cations and anions in aerosol samples.....43

Figure 2.17: Scatter plot of replicate measurements (in ppm; μg mL^{-1}) of cations and anions in aerosols on Ion-Chromatograph.....44

Figure 2.18: Typical chromatographs of cations and anions on Ion-Chromatograph in aerosol sample (PTA-75).....45

Figure 3.1: MODIS image of fire-counts during paddy- and wheat-residue burning in the IGP. 52

Figure 3.2: The monthly average meteorological record on temperature and relative humidity during the aerosol sampling over Patiala. ...54

Figure 3.3: Seasonal wind-rose plots for the sampling period from October '08–May '09 and October '10–May '11. N: North; E: East; S: South and W: West. 55

Figure 3.4: Rainfall records over Patiala for the years from 2008–2011 suggest efficient cleaning of the ambient atmosphere during south-west monsoon. 56

Figure 3.5: Inter-annual variability in: (a) PM2.5; (b) mass fraction of OC and (c) mass fraction of EC. 58

Figure 3.6: Inter-annual variability in the characteristic ratios of: (a) OC/EC (b) WSOC/OC and (c) ΣPAHs/EC. 59

Figure 3.7: The OC and EC concentrations in aerosols with lowest 40% of OC/EC ratio are plotted to obtain primary organic carbon (POC).....66

Figure 3.8: Percentage contribution of EC (elemental carbon), POC (primary organic carbon) and SOC (secondary organic carbon) to TC (carbonaceous aerosol) during different emission scenarios. 67

Figure 3.9: Scatter plot of secondary OC (SOC) and WSOC in aerosols during: (a) paddy-residue burning; (b) bio- and fossil-fuel combustion and (c) wheat-residue burning. 68

Figure 3.10: Mass closures of organic carbon (OC = WSOC+WIOC), where WSOC and WIOC are referred for water soluble- and water insoluble-organic carbon. 69

Figure 3.11: Scatter plot of: (a, b, c) EC versus ΣPAHs and (d, e, f) OC versus ΣPAHs for different emissions. 70

Figure 3.12: Percentage contribution of 16-PAHs for paddy- and wheat-residue burning and bio- and fossil-fuel combustion emissions. 71

Figure 3.13: Variation of PM2.5-bound PAHs with varying number of aromatic rings for different emission sources. 72

Figure 3.14: Cross plots of diagnostic ratios of PAH isomers: (a) FLA/(FLA+PYR) vs. ANTH/(ANTH+PHEN) and, (b) FLA/(FLA+PYR) vs. IcdP/(IcdP+BghiP). 73

Figure 3.15: Comparison in relative abundances of carbonaceous species in ambient aerosol (this study) and that from chamber-experiment. 75

Figure 3.16: PAHs ratios in ambient aerosol (this study) and chamber-experiment..... 77

Figure 3.17: Scatter plot showing the relative reactivity of: (a) 3-; (b, c) 4-; (d) 5- and (e) 6-ring PAH isomers under ambient atmospheric conditions, for paddy-residue burning. 78

Figure 3.18: Scatter plot showing the relative reactivity of: (a) 3-; (b, c) 4-; (d) 5- and (e) 6-ring PAH isomers under ambient atmospheric conditions, for bio- and fossil-fuel combustion emission. 79

Figure 3.19: Scatter plot showing the relative reactivity of: (a) 3-; (b, c) 4-; (d) 5- and (e) 6-ring PAH isomers under ambient atmospheric conditions, for wheat-residue burning emissions..... 80

Figure 3.20: Variability in atmospheric abundances of: (a) water-soluble inorganic species (WSIS); and mass fraction of (b) Na^+; (c) NH_4^+; (d) K^+; (e) Mg^{2+}; (f) Ca^{2+}; (g) Cl^-; (h) NO_3^- and (i) SO_4^{2-} for different emission scenario..... 83

Figure 3.21: Temporal variability in: (a) nss-K^+/OC; (b) nssK^+/EC and (c) nss-SO_4^{2-}/OC concentration ratios.. 88

Figure 3.22: Scatter plot among (a, b, c) nss-K^+ and OC; (d, e, f) nss-K^+ and EC; and (g, h, i) nss-SO_4^{2-} and OC for three distinct emission scenarios. 89

Figure 3.23: Abundances of WSIS measured in ambient aerosols (this study) and that reported from the chamber experiment [Hays et al., 2005] for: (a) paddy-residue and (b) wheat-residue burning emissions. 92

Figure 3.24: Cross plot exhibits distinctly different ratio for paddy- and wheat-residues burning emission (in ambient aerosols; this study) with that from mineral dust: [a][Formenti et al., 2003]; and seawater composition: [b][Keene et al., 1986]. 95

Figure 4.1: Air-mass back trajectories (at 500 m AGL) arriving at Barapani (NE-Himalaya), indicate dominant impact from the IGP (TYPE-I). 111

Figure 4.2: Temporal variability of (a) PM2.5 and the associated carbonaceous species: (b) OC; (c) EC; (d) WSOC; (e) carbonate carbon (CC) and (f) ΣPAHs, over NE-H. 112

Figure 4.3: Spatial variability in: (a) OC/TC ratio; (b) EC/TC ratio and (b) TC (total carbon: OC+EC) concentration. 113

Figure 4.4: Scatter plot showing a significant correlation (TYPE-I air-masses) between water soluble- and water insoluble-organic carbon (WSOC and WIOC) in aerosols. 116

Figure 4.5: Spatial variability in: (a) OC/EC and (b) WSOC/OC ratios to assess the atmospheric aging of aerosols. 118

Figure 4.6: Scatter plot shows a significant decrease in ΣPAHs/EC ratio (mg g^{-1}): from 3.54 mg g^{-1} at Upwind IGP (Patiala) to 1.72 mg g^{-1} at NE-H. 120

Figure 4.7: Comparison of PAH isomer ratios from NE-H and Upwind IGP. The data for Upwind IGP (Patiala) is adopted from [Rajput et al., 2011b]. 121

Figure 4.8: Cross plot of FLA/(FLA+PYR) versus: (a) ANTH/(ANTH+PHEN); (b) BaA/(BaA+CHRY+TRIPH); (c) BaP/(BaP+B[b,j,k]FLA) and; (d) IcdP/(IcdP+BghiP). 123

Figure 4.9: Dominant impact of biomass burning emissions accounting for ~80% to the total budget of carbonaceous aerosol over NE-H, from the IGP is depicted. 125

Figure 4.10: Scatter plot of PAH isomers for its potential sources and that from the NE-H to assess atmospheric aging of carbonaceous aerosols.. 127

Figure 5.1: Typical wind-fields during wintertime over Ahmedabad and Mt Abu, modified after [Rastogi and Sarin, 2005]. 134

Figure 5.2: Typical wind-fields during summer over Ahmedabad and Mt Abu, modified after [Rastogi and Sarin, 2005]. 135

Figure 5.3: (a) Ambient concentration of PM2.5, (b) Contribution of OC and EC to PM2.5 and, (c) Characteristic ratio of OC/EC and ΣPAHs/EC over Ahmedabad during winter and summer..... 136

Figure 5.4: PAH isomer ratios (3- to 6-ring) in aerosols for winter and summertime over Ahmedabad. 137

Figure 5.5: Percentage contribution of 16-PAHs from two locations in the IGP (Hisar and Kanpur) during wintertime. 139

Figure 5.6: Spatial variability in (a) OC/EC and, (b) ΣPAHs/EC ratios for wintertime over India.. 140

Figure 5.7: Spatial variability in PAHs isomer ratios in aerosols for wintertime in India. 141

Figure 5.8: Scatter plot of PAH isomers (normalized to EC) in aerosols from Ahmedabad during winter and summertime. 145

Figure 5.9: Scatter plot of PAH isomers (normalized to EC) in aerosols from Mt Abu during wintertime. 146

Figure 5.10: Scatter plot of PAH isomers (normalized to EC) in aerosols from Hisar during winter. 147

Figure 5.11: Scatter plot of PAH isomers (normalized to EC) in aerosols from Kanpur during winter. 148

Figure 5.12: Cross-plot of PAH isomer ratios FLA/(FLA+PYR) and IcdP/(IcdP+BghiP) from different geographical location within and outside the India.. 149

LIST OF ABBREVIATIONS

NE-Himalaya	North eastern-Himalaya
PM2.5	Particulate matter of aerodynamic diameter ≤ 2.5 micron
OC	Organic Carbon
EC	Elemental Carbon
TC	Total carbon (= OC+EC)
WSOC	Water-Soluble Organic Carbon
WSIS	Water-Soluble Inorganic Species
ΣWSIS	Summation of all the cations and anions assessed
POA	Primary Organic Aerosol
SOA	Secondary Organic Aerosol
VOC	Volatile Organic Compound
WIOC	Water-Insoluble Organic Carbon
PAH	Polycyclic Aromatic Hydrocarbon
NAPH	Naphthalene
ACY	Acenaphthylene
2-BrNAPH	2-Bromonaphthalene
ACE	Acenaphthene
FLU	Fluorene
PHEN	Phenanthrene
ANTH	Anthracene
FLA	Fluoranthene
PYR	Pyrene
BaA	Benzo[*a*]anthracene
CHRY+TRIPH	Chrysene/Triphenylene
B[b,j,k]FLA	Benjo[*b*+*j*+*k*]fluoranthene
BaP	Benzo[*a*]pyrene
IcdP	Indeno[1,2,3-*cd*]pyrene
D[ah,ac]ANTH	Dibenzo[*a,h*+*a,c*]anthracene
BghiP	Benzo[*g,h,i*]perylene
ΣPAHs	Summation of all the 16-PAHs

CHAPTER 1

INTRODUCTION

1.1. Introduction

Troposphere is a highly dynamic component of the atmosphere, and responds very quickly to the processes occurring on the earth's surface. For example, the effect of dust storms, volcanic eruption and emission of aerosols and trace gases from biomass burning vis-à-vis fossil-fuel combustion is recorded in the atmospheric composition soon after the occurrence of these events. In contrary to their emissions, the atmospheric budget of aerosols is controlled by their removal due to wet precipitations and/or dry deposition (gravitational settling). The intermediate process between the emission of the chemical constituents and their atmospheric removal occurs during their transport. During the course of their transport, the chemical composition and atmospheric abundances of atmospheric aerosols change due to their mixing with other atmospheric constituents and/or the chemical reactive nature of some of them.

To characterize the emission sources and their source strength a significant work has been carried out over the globe and represented in the literature. Furthermore, the deposition fluxes of several constituents have been also studied over the atmospheric- and marine-boundary layer. However, the process associated with the transport of chemical constituents has been less understood due to varying chemical composition depending on their residence time in the ambient atmosphere.

Atmospheric particulate matter (PM) is broadly comprised of inorganic salts, siliceous crustal minerals, carbonaceous matter, and water [*Seinfeld and Pandis*, 2006]. Reliable analytical techniques exist to characterize the inorganic salt, mineral fractions to determine particulate-phase water content. However, the information on the chemical composition of carbonaceous aerosols is limited, with the analytical techniques available till date. However, a wide range of chemical and thermodynamic properties of organic compounds, present in particulate organic carbon (OC), makes characterization of particulate OC difficult using any single direct analytical technique. Moreover, the analytical distinction between the organic and elemental carbon (OC and EC) fractions is currently not well defined. In most of the methods, EC is operationally defined as

that portion of the aerosol carbon that is resistant to decomposition under high temperature and inert gas conditions.

Particulate carbon contributes significantly to the total aerosol burden in ambient atmosphere. Aerosol carbon (carbonaceous aerosol) consists of three fractions: organic carbon (OC), elemental carbon (EC), and carbonate carbon (CC). The latter is originated almost exclusively from soil dust. Organic aerosols can have primary origin (referred to as primary organic aerosols; POA), from direct emission source, or formed in the atmosphere (referred to as secondary organic aerosols; SOA) on oxidation of certain volatile organic compound (VOC). As a matter of fact, the oxidized products have higher molecular weight as compared to its parent compound, and therefore, it facilitates for mass transfer into the particulate-phase.

The conversion efficiency of an organic (gas-phase) into PM is represented in terms of mass yield: the mass of PM formed on oxidation of a given mass of gaseous organic compound. EC has been found in the particulate-phase, attributable to its non-volatility. EC is considered as a useful tracer for the primary component in aerosols, in view of its emission from the primary sources. Furthermore, EC absorbs visible and near-IR light, and so also referred to as "black carbon". Both the primary- and secondary-aerosols can have natural vis-à-vis anthropogenic origin. However, an individual aerosol in the atmosphere may comprise of both the secondary and primary particles.

Atmospheric aerosol composition is important in governing their interaction with solar radiations and affecting the cloud properties [*Menon et al.*, 2002; *Ramanathan et al.*, 2007]. However, the aerosol composition is highly variable on a temporal (day/night and seasonal) and spatial scale due to change in its emission from natural vis-à-vis anthropogenic sources [*Decesari et al.*, 2010; *Ram et al.*, 2010a; *Ram et al.*, 2010b; *Srinivas et al.*, 2011]. Besides the varying sources, aerosol composition can also change during its chemical processing and/or mixing (with particles from different origin) within the atmosphere. Assessing the aerosol characteristics is essential to infer about their sources, formation mechanism, and understand their role in atmospheric chemistry and radiation impacts (through direct interaction and indirectly via entrainment into

clouds) on a regional-to-global scale [*Ervens et al.*, 2011; *Huang et al.*, 2011; *Pathak et al.*, 2009; *Rastogi and Sarin*, 2006]. Atmospheric aerosols, either of natural origin or from anthropogenic emission/chemical transformation (gas-particle conversion), exist in three distinct size range.

The particle of the size, peaking in the range 0.005–0.1 μm is referred as the nuclei mode, 0.1–2.5 μm as the accumulation mode and >2.5 μm as the coarse mode aerosol. The interaction of carbonaceous aerosols directly with the solar radiation (absorption and scattering) and, via entrainment into clouds is estimated usually as a first approximation to assess its impact on regional to global climate. However, recent studies have addressed the issue on complexity in estimating the radiative impacts of aerosols arising due to their mixing as a function of transport/time. For example, the absorption efficiency of black carbon (BC) can increase by a factor of two when mixed with scattering species such as sulfate and nitrate as compared to that when freshly emitted. Assessing the interaction between atmospheric constituents though critical but essentially required to understand certain key processes e.g. the impact of heterogeneous reactivity of organic compounds for new particle formation mechanism.

1.2. Atmospheric impact of carbonaceous aerosols

Carbonaceous aerosols consist of both the light-scattering organic carbon (OC) and light-absorbing elemental/black carbon (EC) fraction [*Bond et al.*, 2004; *Kondo et al.*, 2011; *Novakov et al.*, 2000; *Ram et al.*, 2010a]. The EC is emitted only due to incomplete combustion of fossil-fuel and biomass burning. However, the particulate OC can form within the atmosphere (referred to as secondary organic carbon) due to physico-chemical transformations, in addition to its emission from combustion sources. Recent estimates show that carbonaceous aerosols, emitted from open biomass burning has a net cooling effect, in contrast to that emitted from the bio- and fossil-fuel combustion [*Jacobson*, 2004]. Furthermore, mixing of EC with sulphate (scattering aerosol), enhances the absorption efficiency of the EC [*Ramana et al.*, 2010].

Biomass burning emissions produce a huge amount of smoke along with several gases and the particles. Depending on the source-intensity and the

convective mixing of the atmosphere, aerosols can be uplifted to as high as upper troposphere. This is expected to increase the aerosol optical depth (AOD), probability of aerosols interaction with solar photons and the high-level clouds. In this context, large-scale (~100s of million tons) agricultural-waste burning emission in the Northern India has a profound impact on the atmospheric chemistry and physics [*Rajput et al.*, 2011b]. However, the first-hand information on the chemical characterization of carbonaceous species for post-harvest agricultural-waste burning emissions through field-based measurements is lacking in the literature.

Organic aerosols constitute a major fraction of particulate matter and are important in the atmosphere due to their interaction with other chemical constituents present in the atmosphere. One of the important classes of organic aerosols is the Polycyclic Aromatic Hydrocarbons (PAHs), emitted in the atmosphere primarily due to the incomplete combustion of fossil-fuels and biomass burning. The widespread generation and subsequent release of PAHs into the environment is the consequence of their presence in air, water, and soil samples. Due to their semi-volatile nature PAHs get partitioned between the gas- and particulate-phase in the atmosphere [*Allen*, 1997].

PAHs are characterized by their fused-ring structures consisting of aromatic rings. The conjugated electron systems of these aromatic compounds determine their physical and chemical properties. Naphthalene, for instance, a two ringed compound, is the smallest member of the class and is found predominantly in the vapor phase in the atmosphere, while PAHs consisting of three to four rings are present in the air in both the vapor and particulate phases. The PAHs with five or more rings are commonly found as solids adsorbed onto particulate matter in the atmosphere. The incorporation of PAH into the particles has been explained by a general condensation and adsorption mechanism: PAHs are initially generated in the gas phase, and then adsorbed onto pre-existing particles while undergoing condensation upon cooling of the emission [*Baek et al.*, 1991]. As a result a considerable amount of airborne PAHs can be expected to be present in the accumulation mode of the particles, which have a large specific surface-area.

In contrast to the least volatile PAH, for which the gas-to-particle conversion step may be determined shortly after emission, a considerable fraction of the more volatile PAHs will escape particle incorporation and persist in the gas phase in the atmosphere.

The distribution of PAH in the atmosphere between the gas and particulate phases is determined by several factors such as the oxidation of PAHs, vapor pressure of the PAHs as a function of temperature, the amount of fine particles which could provide surface for adsorption/scavenging of PAHs. The PAHs found in the particulate phase in the atmosphere have the residence time governed by the residence time of aerosols (carrier particles). Scavenging (physical removal) and transport of airborne particles is again a function of the particle size and the prevailing meteorological conditions.

It has been well established that although the atmospheric residence time for either coarse-mode particles or nuclei range particles are similar, their removal mechanisms are different. The former tends to be efficiently removed from the atmosphere by sedimentation such as dry or wet deposition, while the latter are removed by coagulation with each other and/or larger particles. However particles in the size range between 0.1 and 2 or 3 μm, with which airborne PAHs are predominantly associated, are known to diffuse slowly and have little inertia, and may be expected to remain airborne for a few days or longer. Furthermore they are also known not to be efficiently removed by rain. Therefore fine-mode aerosols may be transported over large distances depending on the meteorological conditions.

The association of PAHs with the fine-mode aerosols is important in terms of their persistence in the atmosphere, where they can undergo chemical transformations and be transported over long distances. While studying the oxidation reaction of PAHs adsorbed onto graphite particles, the inhibiting potential of graphite particles has been observed as compared to its reactivity in the gas-phase [*Atkinson and Arey*, 1994; *Esteve et al.*, 2004].

Measurements of the size-distribution of PAHs indicate that while they are found in the 0.01–0.5 μm diameter mode of fresh combustion emissions they

exhibit a bimodal distribution in ambient urban aerosol, with an additional mode in the 0.5–1.0 μm diameter range [*Venkataraman and Friedlander*, 1994]. The PAH isomer ratios can be used as a diagnostic finger-print tracer of the sources of PAHs in atmospheric aerosols [*Liu et al.*, 2007; *Yunker et al.*, 2002].

1.3. Laboratory experiments on SOA formation

A main goal of current aerosol chamber experiments is to determine the aerosol formation potential of either a single parent hydrocarbon or a mixture of parent hydrocarbons, and to determine the mechanism of particle formation through measurement of specific gas and aerosol-phase oxidation products [*Rudich*, 2003; *Seinfeld and Pankow*, 2003].

The amount of aerosol formed from the atmospheric oxidation of VOCs depends on the structure of the parent molecule. For unsaturated molecules, the location of double bonds is important in determining the nature of the oxidation products. For example, cyclic compounds generally have higher yields of secondary organic PM than acyclic compounds because most of the carbon backbone of cyclic compounds remains intact when the double bond(s) is (are) cleaved on oxidation.

Chamber experiments provide a tool to enhance the mechanism of chemical transformation and microphysical processes (such as water uptake), known to occur in the atmosphere. Both the gas-phase chemistry and aerosol formation and growth process has been studied through chamber based experiments. However, simulating the ambient conditions within the chambers is problematic in terms of sunlight, clouds cover and weather aspects.

1.4. Chemical reactivity of PAHs

O_3 concentration in unpolluted troposphere is typically about 7×10^{11} molecules cm^{-3} (30 ppb mixing ratio at ground level). On a global scale concentration of OH radical is 8×10^5 molecules cm^{-3} in the troposphere. The potential reactivity of one of the most reactive compounds among carbonaceous species, the PAHs, has been the subject of several studies.

Homogeneous reactivity of PAHs has been considered as one of the potential sources of SOA formation and heterogeneous reactivity for altering the surface characteristics of aerosol. In terms of chemical kinetics, the heterogeneous reaction is a first order reaction whereas the homogeneous reaction is of the second order.

The formation of O_3, OH radicals and NO_X can be viewed by the following reactions occurring in the atmosphere. The photolysis of O_3 in the troposphere to yield the O (^{1}D) atom leads to the formation of the OH radical [*Seinfeld and Pandis*, 2006].

$$NO_2 + h\nu(\lambda < 424\,nm) \rightarrow NO + O$$

$$O + O_2 + M(O_2, N_2) \rightarrow O_3$$

$$O_3 + h\nu(\lambda < 320nm) \xrightarrow{Photolysis} O_2 + O(^1D)$$

$$O(^1D) + H_2O \rightarrow 2OH$$

The NO_3 radical formation and destruction is shown below:

$$NO + O_3 \rightarrow NO_2 + O_2$$

$$NO_2 + O_3 \rightarrow NO_3 + O_2$$

$$NO_3 + NO \rightarrow 2NO_2$$

$$NO + h\nu \rightarrow NO_2 + O(^3P)$$

$$NO + h\nu \rightarrow NO + O_2$$

$$NO_3 + NO_2 \leftrightarrow N_2O_5$$

(NO_3 radical concentrations are relatively low during day time).

Some of the typical reactions of individual PAHs with OH and NO_3 radicals are shown below:

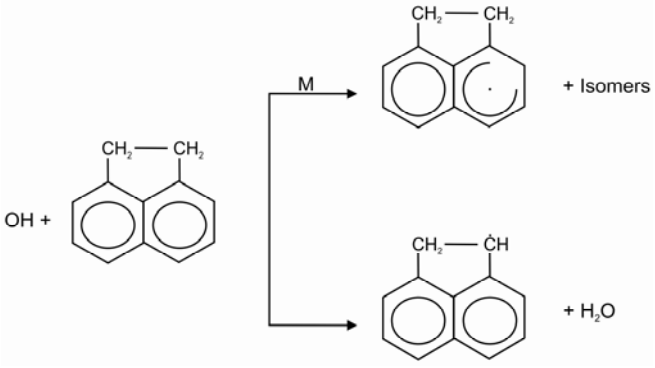

Figure 1.1: Reaction of acenaphthene with OH radical.

where M = N_2, O_2

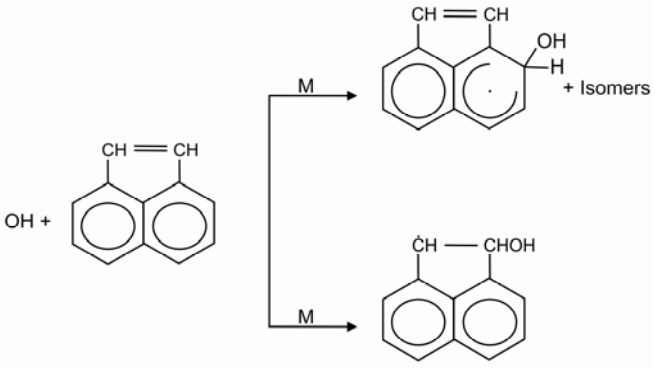

Figure 1.2: Reaction of acenaphthylene with OH radical.

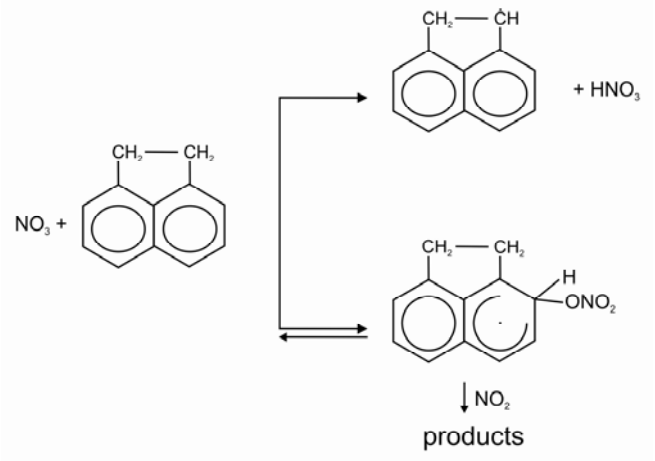

Figure 1.3: Reaction of acenaphthylene with NO_X radical.

$$PAH(soot) + Nitrating\ agent(g) \xrightarrow{heterogeneous} Nitro - PAH$$

$$PAH(g) + Nitrating\ agent(g) \xrightarrow{homogeneous} Nitro - PAH$$

Water-soluble organic compounds have potential to, alter the surface characteristic of aerosols through coating, affect the activation efficiency of CCN (cloud-condensation nuclei), alter single scattering albedo (SSA) and, enhance the cloud cover over the earth [*Ervens et al.*, 2011; *Novakov and Penner*, 1993; *Turpin et al.*, 2000; *Weber et al.*, 2007]. It has been recognized long-back in 1990s that the characterization of water-soluble organics is essential to comprehend their role in atmospheric processes [*Saxena and Hildemann*, 1996].

With the advent of analytical skills, the chemical characterization of water-extractable organic compounds has revealed that mono- and di-carboxylic acids constitute a major fraction of the water-soluble organic carbon (WSOC) mass [*Decesari et al.*, 2000; *Pavuluri et al.*, 2011]. As of current findings, the water-soluble organic compounds are predominantly comprised of a group of compounds collectively referred as humic-like substances (HULIS). The HULIS can exist as water-soluble (fulvic acid), base-soluble (humic acid) and insoluble (humin) categories [*Graber and Rudich*, 2006]. The two accepted mechanisms of HULIS formation include: primary emissions from biomass burning and secondary formation from the oxidation of soot [*Decesari et al.*, 2002]. Furthermore, the H-NMR (Proton-Nuclear Magnetic Resonance) characterization coupled with ^{14}C measurements of water-extractable organic compounds, produced from biomass burning, exhibits the most abundant proton signal, corresponding to the aliphatic compounds [*Song et al.*, 2012]. In contrast, the water-extractable organics produced from the oxidation of soot particles have been observed to be relatively enriched in aromatic fraction [*Decesari et al.*, 2002]. Furthermore, secondary organic aerosol (SOA) formation in the ambient atmosphere, an important process, can be studied only through the ground-based measurements [*Kondo et al.*, 2007; *Rudich et al.*, 2007; *Seinfeld and Pankow*, 2003].

Recently, chamber- and field-based measurements have shown that the gas-phase polycyclic aromatic hydrocarbons (PAHs) can yield to as high as 50% of the total SOA mass [*Chan et al.*, 2009; *Lee et al.*, 2012; *Zhang and Ying*, 2012]. Moreover, the heterogeneous reactions of PAHs with atmospheric oxidants O_3, NO_X and OH radical show efficient conversion of hydrophobic surface into more hygroscopic particles, and thus, can have significant role in aerosol-cloud interaction and altering the aerosol albedo (SSA) [*Esteve et al.*, 2006; *Evagelpoulos et al.*, 2010; *Kaiser et al.*, 2011; *Perraudin et al.*, 2007]. The potential of PAHs in determining the atmospheric budget of SOA and trace gases (NO_X and O_3), in addition to affect the cloud nucleation activity through surface alteration characteristics (of aerosols), has been well recognized.

The Indo-Gangetic Plain (IGP) extending from NW- to eastern part of India occupies 4, 37,000 sq. km. area (~13% of total geographical area of the country) and produces ~50% of total food grains in the nation. Due to emissions from different types of biomass (agricultural-waste and bio-fuels) burning and fossil-fuel combustion in the IGP, the chemical characterization of atmospheric aerosols is essential to assess the atmospheric impact of these transient practices on annual and seasonal basis [*Rajput et al.*, 2011b; *Ram and Sarin*, 2009; *Ram et al.*, 2010b; *Ramanathan et al.*, 2001; *Ramanathan et al.*, 2007; *Rengarajan et al.*, 2007]. The large-scale biomass burning practice in the states of Punjab, Haryana and western part of Uttar Pradesh in the Indo-Gangetic Plain (IGP), is one of the dominant sources of carbonaceous aerosols [Badarinath et al., 2006; Venkataraman et al., 2006].

There are major gaps in the literature on the factors controlling the emissions of carbonaceous aerosols from different types of biomass burning, interaction of these particles with the water vapor and trace gases [*Andreae and Merlet*, 2001; *Crutzen and Andreae*, 1990]. However, the field evidence of these processes in the ambient atmosphere is lacking. For example, the understanding of the processes driving the occurrence of EC, OC, WSOC and PAHs is essential to comprehend not only for its fate (transformation and concentration), but also their interaction with trace gases and fog droplets, in addition to the formation of haze in the lower atmosphere.

Assessing the transport of aerosols is certainly important in order to understand the occurrence of pollutants in downwind locations, affecting the mixing state of aerosols (chemical aging) and thereby changing the earth's radiation budget and the cloud-albedo on a regional scale. However, this knowledge is scarce in general and lacking for the IGP.

1.5. Rationale and objectives

Carbonaceous aerosols, consisting of primary species (elemental carbon: EC and organic carbon: OC) and secondary organic compounds, contribute significantly to the particulate matter in the lower atmosphere [*Chan et al.*, 2009; *Hallquist et al.*, 2009; *Jimenez*, 2009; *Rudich et al.*, 2007; *Seinfeld and Pankow*, 2003]. Several studies have assessed the chemical composition of carbonaceous aerosols from the source region. However, the complexity in assessing aerosol characteristics after their long-range transport arises mainly due to atmospheric mixing and chemical processing.

The lack of adequate information on aerosol mixing and chemical aging of chemical constituents during their transport is a major cause of uncertainty in assessing the aerosol chemical composition and radiative forcing in the lower atmosphere [*Haywood and Boucher*, 2000; *Novakov and Penner*, 1993; *Sokolik et al.*, 2001]. Furthermore, interaction of several carbonaceous species with trace constituents in the troposphere, not only change the aerosol composition but in turn also influence the abundance of trace gases [*Andreae and Crutzen*, 1997; *Hallquist et al.*, 2009].

Importantly, the water-soluble organic carbon (WSOC) has secondary formation pathway in the atmosphere via photochemical reactions of volatile organic compound (VOC) and/or aging (oxidation) of organic aerosols, besides their primary production from biomass burning emission [*Decesari et al.*, 2002; *Mayol-Bracero et al.*, 2002b; *Saxena and Hildemann*, 1996; *Turpin et al.*, 2000; *Weber et al.*, 2007]. And therefore, this characteristic feature (of secondary formation) of WSOC can be used to provide information on the chemical oxidation of organic compounds during their long-range atmospheric transport by assessing the mass fraction of WSOC to OC in conjunction with OC/EC ratio.

The significance of these water-soluble organic compounds in influencing the number density of cloud condensation nuclei (CCN) by changing the surface characteristics of aerosols from hydrophobic to hydrophilic and also alter the radiation balance of the atmosphere is well known [*Kaiser et al.*, 2011; *Shapiro et al.*, 2009].

Moreover, the applicability of polycyclic aromatic hydrocarbons (PAHs) as tracers to the emission from fossil-fuel combustion and biomass burning [*Yunker et al.*, 2002], can also be extended to ascertain the prominent affect of atmospheric mixing and chemical aging of carbonaceous aerosols, as they are potentially reactive with O_3, NO_X and OH radical [*Chan et al.*, 2009; *Decesari et al.*, 2002; *Esteve et al.*, 2004; *Kaiser et al.*, 2011; *Perraudin et al.*, 2007]. With this rationale, the present thesis focus on:

(1) Chemical characterization and atmospheric impact of two distinct large-scale post-harvest agricultural-waste burning emission of paddy- and wheat-residues occurring on a seasonal and annual basis in the northern India during October-November and April-May, respectively, (2) Aerosol characterization in the IGP during wintertime (December–March), when fog-events are intense. (3) Chemical aging of carbonaceous aerosols in the Northeastern-Himalaya and, (4) Heterogeneous chemical reactivity of PAHs under different environmental conditions.

The objectives of this thesis are as follows

1. *To investigate the temporal and spatial variations of PAHs from different environmental regions.*
2. *To assess the relative abundances of PAHs and the source-apportionment in conjunction with carbonaceous aerosols (EC, OC & WSOC).*
3. *To assess the chemical aging of carbonaceous aerosols during their long-range transport.*

The 16-PAHs, measured in this study, include Naphthalene {NAPH}, Acenaphthylene {ACY}, 2-Bromonaphthalene {2-BrNAPH}, Acenaphthene

{ACE}, Fluorene {FLU}, Phenanthrene {PHEN}, Anthracene {ANTH}, Fluoranthene {FLA}, Pyrene {PYR}, Benzo[*a*]anthracene {BaA}, Chrysene/Triphenylene {CHRY+TRIPH}, Benzo[*b*+*j*+*k*]fluoranthene {B[b,j,k]FLA}, Benzo[*a*]pyrene [BaP], Indeno[*1,2,3-cd*]pyrene {IcdP}, Dibenzo[*a*,*h*+*a*,*c*]anthracene {D[ah,ac]ANTH}, and Benzo[*g,h,i*]perylene {BghiP}.

1.6. Thesis outline

Chapter 1 will provide an introduction of the subject and review of previous research work in brief. In addition, the rationale and objectives of this study will be defined here.

Chapter 2 will describe relevant analytical details on aerosol sampling and analysis of various chemical constituents in aerosol. The significance of sampling locations in context to this study will also be discussed.

Chapter 3 describes the results and discussion on the analytical data set on carbonaceous (EC, OC, WSOC and PAHs) and water-soluble inorganic species (WSIS) in aerosol from a semi-urban sampling location (Patiala), located upwind of major industrial pollution sources in the Indo-Gangetic Plain (IGP) will be given in this chapter.

Chapter 4 will describe the chemical processing of carbonaceous species during their long-range transport over the Northeastern-Himalaya (NE-H).

Chapter 5 will provide the scenario on spatial variability of PAHs from different geographical locations in India (urban, semi-urban, high-altitude, low-dust and high-dust region).

Chapter 6 will summarize important findings of this study and their implications in assessing aerosols impact on regional climate. This chapter will also present future research scope in the area.

CHAPTER 2

AEROSOL COLLECTION AND CHEMICAL ANALYSIS

2.1. Introduction

Atmospheric aerosols are composed of mineral dust, inorganic constituents, carbonaceous matter (organic carbon and elemental carbon) and sea-salts [*Baek et al.*, 1991; *Mayol-Bracero et al.*, 2002b; *Ram and Sarin*, 2010; *Rengarajan et al.*, 2007; *Seinfeld and Pankow*, 2003; *Seinfeld and Pandis*, 2006]. Among the various components, physical adsorption characteristics of mineral dust, sea-salt (polar), and graphitic carbon (non-polar) are well understood [*Baek et al.*, 1991; *Jacobson et al.*, 2000; *Rudich et al.*, 2007]. These characteristics affect the high precision measurements of organic compounds and compromise their application as proxies to trace the aerosol sources and to understand their chemical reactivity with the atmospheric oxidants (O_3, OH and NO_x) [*Miet et al.*, 2009a; b; *Perraudin et al.*, 2005b; *Richter et al.*, 1996]. It is, thus, essential to establish an analytical protocol for the measurements of organic compounds in atmospheric aerosols with varying mass concentration and matrix.

Analytical schemes for the quantitative determination of PAHs in environmental samples and standard reference materials are available in the literature e.g. [*Alexandrou et al.*, 2001; *Kiss et al.*, 1996; *Kiss et al.*, 1997; *Richter et al.*, 1996; *Schantz et al.*, 1997; *Wise et al.*, 1986; *Wise et al.*, 2000]. However, suitability of many of these is limited to low aerosol loading. More importantly, these analytical methods have not adequately investigated the matrix effect (of tarry matter emitted from agricultural-waste burning) on mass recovery of PAHs.

Therefore, development of an analytical protocol is required for the quantitative mass recovery of PAHs, by eliminating the matrix from high atmospheric loading of aerosols. Present study reports a quantitative method established for the determination of PAHs by suitable combination of accelerated solvent extraction (ASE), followed by purification on a silica cartridge and subsequent determination on a gas chromatograph coupled to a mass spectrometer (GC-MS). The suitability of the analytical method has been ascertained from the field-based samples collected from different geographical locations in India.

The analyses of organic compounds by the conventional extraction techniques such as Soxhlet extraction and ultrasonication [*Duan et al.*, 2005;

Mandalakis et al., 2005; *Wise et al.*, 2000], though provide their quantitative recovery, require large volume of solvents (> 100 mL) and are often labour intensive. In spite of this, the Soxhlet extraction technique has been successfully used for the extraction of PAHs from standard reference materials (SRM-National Institute of Standards and Technology) [*Wise et al.*, 1986; *Wise et al.*, 2000]. However, the current demand for eco-friendly environment requires minimum consumption of solvents and rapid sample preparation, without compromising the accuracy and precision.

Among the two conventional techniques (ultrasonication and Soxhlet extraction), the former provides rapid sample preparation with comparatively lower consumption of solvent. An alternative extraction technique involving supercritical fluid extraction (SFE) requires longer extraction time and also suffers from the incomplete recovery of PAHs in environmental samples due to analyte-matrix interactions [*Hawthorne et al.*, 1993].

In contrast, the microwave-assisted solvent extraction (MASE) and the accelerated solvent extraction (ASE) approach are beneficial in terms of lower consumption of solvent and perform extraction in shorter time [*Alvarez-Avilés et al.*, 2007; *Chee et al.*, 1997; *Richter et al.*, 1996; *Schantz et al.*, 1997; *Turrio-Baldassarri et al.*, 2003].

However, the MASE technique requires centrifugation and filtration; thus, amounting to the loss of analyte. For the quantitative determination of PAHs, gas chromatography (GC), for its high-resolution and sensitivity, is often preferred rather than liquid chromatography (LC). Recently, the wide range of applications of GC-MS technique has been reviewed [*Poster et al.*, 2006].

This chapter describes the collection and analysis of aerosol samples. The results are presented in subsequent chapters 3, 4 and 5. The analytical protocol established for the quantitative determination of PAHs has been published [*Rajput et al.*, 2011a].

2.2. Field-campaign

To assess the aerosol composition and chemistry from different environmental regions, the aerosols sampling was conducted from upwind

location in the Indo-Gangetic Plain (IGP) at Patiala, foot-hills of North-eastern Himalaya (NE-H), urban and high-altitude locations in the western India at Ahmedabad and Mt. Abu respectively. Some of the archive aerosols from Hisar and Kanpur locations have also been studied to assess the spatial variability in aerosol composition, particularly for the Polycyclic Aromatic Hydrocarbons (PAHs), in the IGP. The details and significance of different sampling sites are described as below:

2.2.1 Patiala: Semi-urban location, upwind in the Indo-Gangetic Plain

The sampling site at Patiala (30.2 ˚N, 76.3 ˚E; 250 m above mean sea level) is located upwind of the major industrial polluting sources in the Indo-Gangetic Plain (IGP; Figure 2.1). The site is influenced by the downwind transport of carbonaceous aerosols and pollutants from two distinct seasonal post-harvest biomass burning emissions in October–November and April–May. In order to assess the aerosol chemical composition from the biomass burning emissions, PM2.5 samples (n = 141) were collected during the dry season (from October ’08–May ’09 and October ’10–May ’11).

The sampling during the wet period (south-west monsoon; July–September) is not relevant due to wash out of the atmosphere by frequent rain events. During summer months (May–June), transport of mineral dust from western India and northwest Desert regions is a conspicuous feature [*Jethva et al.*, 2005].

The entire study period from October–May is sub-divided into three seasons: October–November is referred to as post-monsoon, influenced by emissions from post-harvest burning of paddy-residue; December–March (wintertime) is dominated by bio-fuel (Babool, Cowdung cake, Eucalyptus, Jujube and Shisham) and fossil-fuel combustion, with occasional fog events. Due to shallow boundary layer height during wintertime, aerosols get confined within the lower atmosphere, making the aerosol loading higher in this plain relative to the other parts of India. The time period of April–May is influenced by emissions from post-harvest burning of wheat-residue.

2.2.2 Shillong: High-altitude location in NE-Himalaya (NE-H)

The sampling site at Barapani (25.7 °N; 91.9 °E; 1064 m asl) is located at the foot-hills of the NE-Himalaya (Figure 2.1), ~20 km upwind of the Shillong town. The annual-average rainfall in this region is ~1100 cm, spread over June–September (SW-monsoon) and October–December (NE-monsoon). In addition, pre-monsoon rain activity begins by early April. This facilitates the removal of ambient aerosols by wet-scavenging important during April–December over NE-Himalaya. During the winter months (January–March), long-range transport of pollutants from the Indo-Gangetic Plain (IGP) and south-east Asia is a conspicuous feature of the region.

With this background information and the importance of study site, PM2.5 samples (n = 51) were collected (whole week, mostly between the first and fourth week of the months) in two campaigns. First campaign was conducted in March 2009 (n = 12) and second campaign during January and March 2010 (n = 19 and 20, respectively). A high-volume air-sampler (flow rate: 1.2 m^3 min^{-1}; Thermo Scientific) was deployed at ~10 m above the ground level inside the premises of Space Applications Centre. On average, about 1200 m^3 of ambient air was filtered for each sample (sampling duration: ~18 h) through pre-combusted (at 450 °C for ~6 h) tissuquartz filters (PALLFLEX™, 2500QAT-UP, 20 cm x 25 cm).

2.2.3 Ahmedabad: Urban site in semi-arid region of western India

Ahmedabad (23.0 °N; 72.6 °E; 49 m amsl) is one of the major cities of India, located in western part, ~500 km southeast of the Thar Desert. The nearest distance to the Arabian Sea, in the southwest direction, is ~100 km. The local climate is of semi-arid type with the annual average rainfall for the city is ~700 mm. Furthermore, the precipitation events seldom occur outside the southwest-monsoon period (June–September; summer months). The period from May–August is dominated by southwesterly winds and that from November–February (wintertime) by the northeasterly winds. Small-scale industries are located about 20 km southeast of the site. The emissions from two coal-based thermal power plants, situated in the northeast at a distance of about 10 km (Sabarmati: ~350 MW per day) and 25 km (Gandhi Nagar: 700 MW per day), is an important

source of aerosols. The coastal zone represents a specific case of aerosol mixing of marine origin (sea salts) with that produced from natural and/or anthropogenic sources. As a result, aerosols are formed, which can be an unusual mixture of several aerosol types. Aerosol composition and characteristics assessed in PM2.5 samples collected during November–December '09 (n = 16) and May–June '10 (n = 11) over Ahmedabad are representative of their occurrence during NE- and SW-monsoon periods, respectively.

Figure 2.1: Map showing aerosol sampling locations: Patiala, Hisar, Kanpur, Shillong, Ahmedabad and Mt Abu. The Indo-Gangetic Plain (IGP) is shown by shaded area (light yellow).

2.2.4 Mt Abu: High-altitude location in semi-arid western India

Another sampling site for aerosol study was selected at Guru Shikhar, Mt. Abu (24.6 °N; 72.7 °E; 1680 m amsl). Guru Shikhar is a highest mountain peak in the southern end of Aravali range of mountains in western India. The annual

rainfall at Mt. Abu averages around 600–700 mm and occurs only during SW-monsoon (June–September). During wintertime, the sampling site at Guru Shikhar represents the free-troposphere whereas lies within the boundary layer during the summer.

Furthermore, the proximity of the site to the Thar Desert (~300 km in northeast direction), provides an opportunity to assess the role of mineral dust aerosols over the region. The main town of Mt Abu (altitude: 1220 m amsl) is situated about 10 km from sampling site. Therefore, the Guru Shikhar site provides an ideal site for sampling in a relatively clean environment in a semi-arid region. PM2.5 samples (n = 15) have been collected during February–March ’10 over Mt Abu to assess the atmospheric impact of long-range transport during NE-monsoon period (wintertime).

2.2.5 Hisar: Semi-urban location in the Indo-Gangetic Plain

The sampling site at Hisar (Figure 2.1, 29.2 °N; 75.7 °E; 219 m amsl) represents a semi-urban atmosphere in the IGP. The site is surrounded by agricultural-fields and is located downwind with respect to north-easterlies during wintertime [Rengarajan et al., 2007]. The sampling site is upwind to a metropolitan city (Delhi; ~150 km) during the sampling period in December, 2004 [Rengarajan et al., 2007]. For assessing the spatial variability and chemical reactivity of PAHs, some of the archive samples (PM10; n = 20) collected during December 2004 have been measured for PAHs.

2.2.6 Kanpur: Typical urban location in the Indo-Gangetic Plain

The aerosol sampling at Kanpur (26.5 °N, 80.3 °E, 142 m amsl) represents the urban environment in the northern part of IGP. The sampling site is situated ~15 km downwind of main city and is influenced by emissions from biomass burning as well as fossil-fuel combustion sources [Ram et al., 2010a]. Some of the archive samples (PM10; n = 20), collected during wintertime (January–March ’07 and December ’07–March ’08) have been measured for PAHs to assess their atmospheric concentrations, chemical reactivity and their isomer ratios.

2.3. Ambient aerosol sampling

Aerosol samples were collected using high-volume samplers (flow rate: 1.2 m^3 min^{-1}) by filtering ambient air through pre-combusted (at 450 ˚C for ~6 h) tissuquartz filters (PALLFLEX™, 2500QAT-UP, 20 cm x 25 cm). After sample collection, filters were wrapped in Al-foils, sealed in zip-lock plastic bags, and retrieved to the laboratory as per the protocol described in earlier studies [*Rajput et al.*, 2011a; *Ram and Sarin*, 2009; *Ram et al.*, 2010a; *Ram et al.*, 2010b; *Rastogi and Sarin*, 2008; *Rengarajan et al.*, 2007].

2.4. Chemical Analysis

2.4.1 Analytical scheme

The analytical scheme for chemical analysis of aerosols is presented in Figure 2.2.

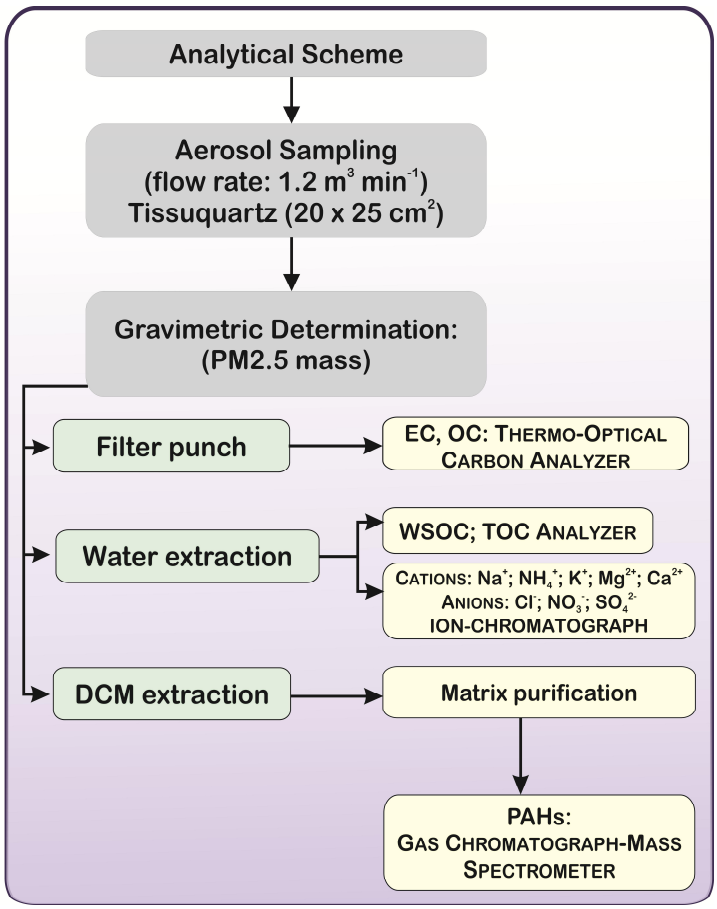

Figure 2.2: Analytical scheme for chemical analysis of aerosol samples.

The analysis of chemical constituents analyzed in aerosols can be summarized as

1. EC-OC: Using transmittance protocol (NIOSH-5040) on a thermo-optical carbon analyzer.
2. PAHs: Extraction in dichloromethane (DCM) using accelerated solvent extraction (ASE) followed by purification on silica-solid phase extraction (SPE) cartridge and subsequent determination on gas chromatograph/mass spectrometer (GC/MS). Quantification of PAHs is done by comparing MS response to that of perdeuterated internal standard (Pyrene-D10).
3. WSOC and Ionic-composition: In water extract of aerosols, WSOC is determined using total organic carbon (TOC) analyzer, whereas the ionic-composition (cations and anions) is determined on Ion-Chromatograph.

2.4.2 Determination of aerosol loading (PM2.5)

Particulate matter (PM2.5) mass was determined gravimetrically on a high precision analytical balance (0.1 mg; Sartorius, model LA130S-F) after equilibrating the filters at 24 ± 2 ˚C and relative humidity of 37 ± 2% for nearly 10 h. PM2.5 (μg m^{-3}) was obtained by dividing the sample weight ($w_{sample\ filter}$-$w_{blank\ filter}$, in unit of μg) with the volume of air filtered (m^3). The volume of air was determined by multiplying the flow rate of high-volume sampler (m^3 min^{-1}) with integrated sampling time (min).

2.4.3 Analysis of elemental carbon and organic carbon (EC, OC)

The concentrations of elemental carbon (EC) and organic carbon (OC) were measured on a EC-OC analyzer (Model 2000, Sunset Laboratory, Forest Grove, USA) using a temperature gradient (NIOSH-5040) thermo-optical transmittance (TOT) protocol [*Ram and Sarin*, 2009; *Rengarajan et al.*, 2007; *Schauer et al.*, 2003]. The typical schematic of EC-OC analyzer showing its three

main components: sample oven, oxidizer (manganese dioxide; MnO_2) and a methanator is presented in Figure 2.3 [*Birch and Cary*, 1996].

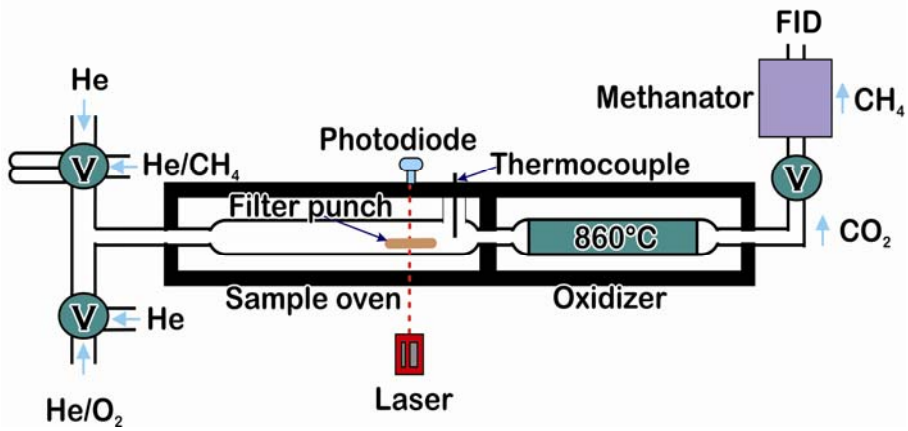

Figure 2.3: The schematic diagram of the thermo-optical EC-OC analyzer (Sunset Laboratory, US).

In brief a 1.5 sq. cm filter-punch was placed on a quartz boat, which is then inserted gently into the front oven of EC-OC analyzer. EC-OC analysis was carried out in two stages; during the first stage (in helium atmosphere) OC is evolved, whereas during the second stage of analysis in an oxidizing atmosphere (98% He + 2% O_2), EC is evolved. The total time taken per analysis was about 13 minutes. The evolved carbon during each temperature step was oxidized to CO_2 (in back oven, held @ 880 ˚C) followed by reduction to CH_4 for its quantification using flame-ionization detector (FID). Reported abundances of OC and EC are corrected for the pyrolyzed carbon (PC) and carbonate carbon (CC). To set the OC-EC split point and correct for PC, transmittance of light from a He-Ne laser source (@ 678 nm), passing through the filter-punch was monitored continuously. The transmittance first decreases and then increases, so at a point of time when the optical transmittance becomes equal to the initial transmittance (at time t = 0, transmittance was due to EC in the sample), that point is referred as the split-point between OC and EC.

For the correction of inorganic carbonate carbon (CC) the thermograms were integrated manually between 220–280 s of the run time, where the carbonate peak was ascertained independently with a separate filter-punch from several

aerosol samples (n = 15), after de-carbonation in the fumes of 6 M HCl for 6–8 h [*Cachier et al.*, 1989; *Ram and Sarin*, 2009; *Rengarajan et al.*, 2007]. A real-time thermograph of an aerosol sample analyzed on EC-OC analyzer using thermo-optical transmittance protocol is represented in Figure 2.4. The corrections (explained above) applied to the reported concentrations of OC and EC can be mathematically expressed as

$$OC_{actual} = (OC_{measured} + PC - CC) - (OC_{blank})$$

$$EC_{actual} = EC_{measured} - PC$$

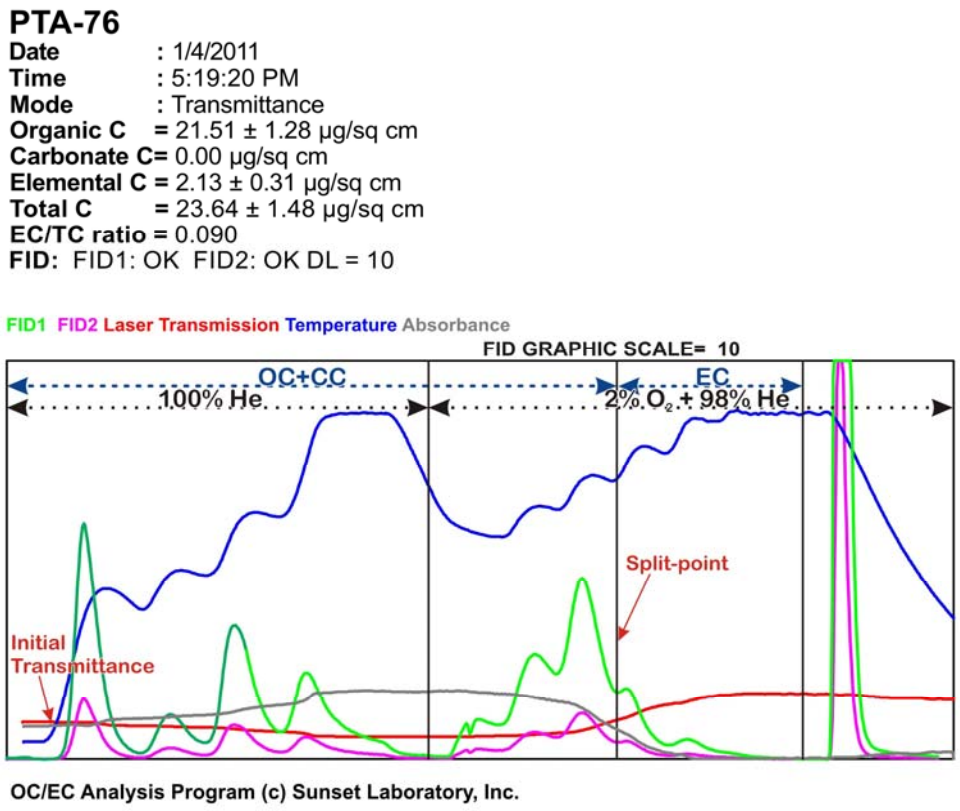

Figure 2.4: A real-time thermograph of sample (PTA-76) analyzed on the thermo-optical EC-OC analyzer.

At the end of every analysis known amount of methane (5% CH_4 + 95% He; v/v) was injected to check the response of detector (FID). In order to assess the instrumental detection limit, blank filters were also analyzed. The average

blank concentration of OC found to be 3.7 ± 0.6 μg cm^{-2} (n = 25; ± 1σ) has been subtracted from the measured abundances of OC in the aerosol samples. The detection limit (calculated using 3σ values of the procedural blanks) was 0.27 μg m^{-3} for the average volume of air sampled (~1300 m^3). The detection limit for EC was 0.06 μg m^{-3} (using EC signal of 0.2 μg cm^{-2} as the instrumental detection limit). Analytical accuracy in determining total carbon, was assessed by analyzing known amount of Potassium Hydrogen Phthalate (KHP) solution (n = 22; Figure 2.5a); the average ratio of measured carbon to expected carbon is 1.03 ± 0.05 (~3%).

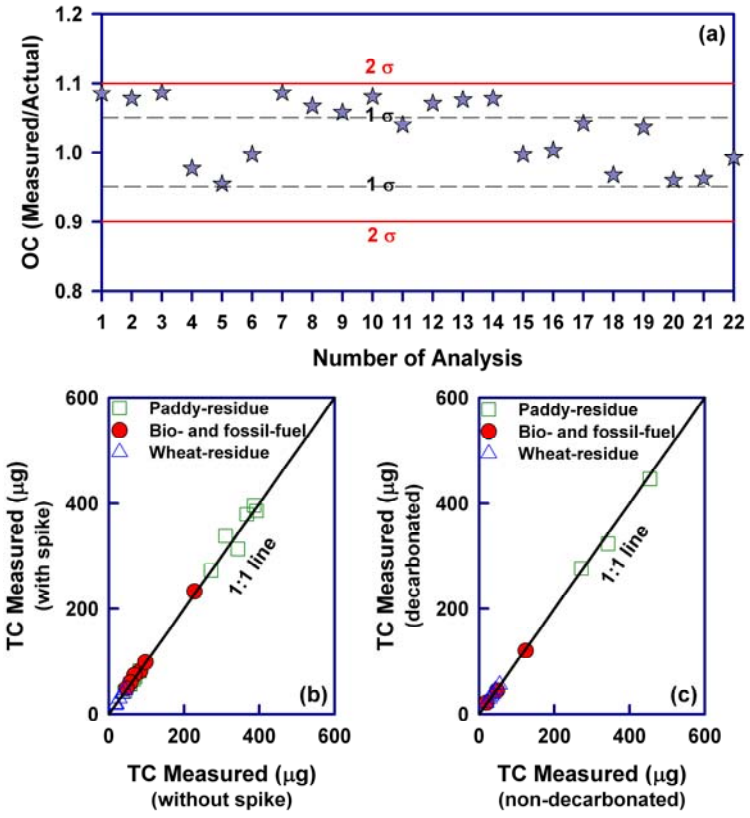

Figure 2.5: Analytical accuracy for total carbon (TC) on EC-OC analyzer: (a) potassium hydrogen phthalate (KHP) and (b) sucrose. (c) low content of inorganic carbon in aerosols is ascertained.

Analysis of several field-based samples (n = 20), spiked with sucrose (2000 ppm), further ascertained the OC-EC split point and provide accuracy of the

measurements to be ± 10% at most (Figure 2.5b). Several aerosol samples (n = 15) were de-carbonated in HCl fumes for assessing the peak positioning and content of carbonate carbon (CC) in aerosols. Data suggest that CC always contributes less than 5% of particulate carbon (= OC+EC+CC) in PM2.5 (Figure 2.5c). On analyzing the aerosol samples, area under the CC peak in thermograms was integrated manually and corrected for OC concentrations as reported in earlier publications. The CC corrected carbon in aerosols is referred to as TC (total carbon: OC+EC). Replicate analysis of the samples provided uncertainty on analytical precision (n = 45; ± σ), ± 3% for OC; ± 7% for EC and ± 3% for TC (= OC+EC). To ascertain the accuracy of OC-EC split point and the area corrected for PC (due to high content of OC), replicate analysis of samples (n = 45) was done and a few samples were also analyzed using 0.7 sq. cm and 0.5 sq. cm filter punch area (Figure 2.6).

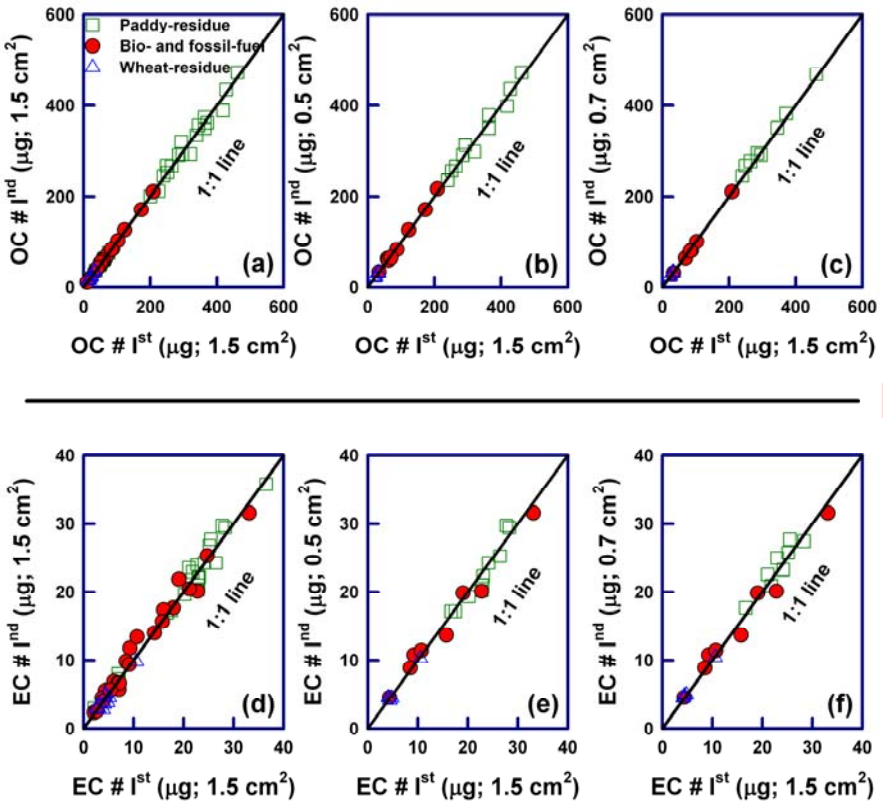

Figure 2.6: Replicate measurements of OC and EC (in µg C cm^{-2}) in aerosol samples with different punch area (1.5, 0.7 and 0.5 cm^2). The solid line represents the 1:1 line.

When compared, the OC and EC concentrations obtained using 0.7 sq. cm and 0.5 sq. cm filter punch area with that from 1.5 sq. cm, a good agreement was observed (Figure 2.6).

2.4.4 Analysis of water-soluble organic carbon (WSOC)

For water-soluble organic carbon analysis, 1/2 punches (3.14 cm^2 each) of sample filters were sonicated for ~30 minutes with 30/40 mL Milli-Q water. The resulting water extract was filtered using glass-syringe through glass-fiber filter (PALLFLEX^{TM}: 47 mm) into pre-cleaned amber colored glass vials, and analyzed for WSOC on a TOC analyzer (Shimadzu, model TOC-5000A).

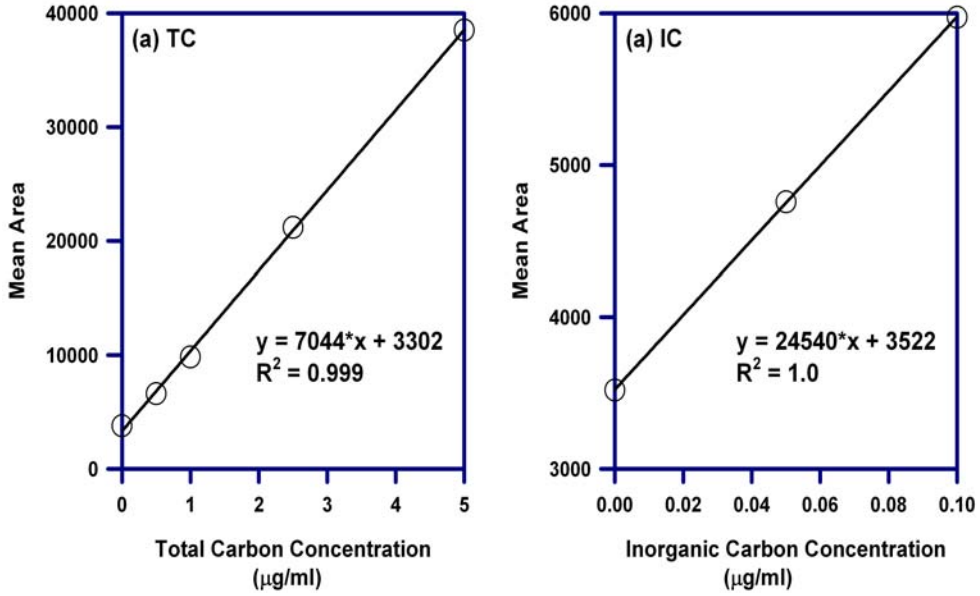

Figure 2.7: A typical calibration of water-soluble total and inorganic carbon (WSTC and WSIC) on TOC Analyzer, using KHP and (Na_2CO_3)/($NaHCO_3$), respectively.

The measurement protocol includes two steps: (i) the measurement of water-soluble total carbon (WSTC) by injecting 100 μl of water extract into the furnace (680 ˚C) and (ii) determination of water-soluble inorganic carbon (WSIC) by treating 250 μl of water extract with 25% H_3PO_4 v/v in-situ. The concentration of WSOC is calculated from the difference between these two sets of measurements (WSOC = WSTC-WSIC).

The instrument was calibrated using standard solutions of potassium hydrogen phthalate (KHP) and sodium carbonate-bicarbonate mixture (Na_2CO_3+$NaHCO_3$; 1:1 v/v) for WSTC and WSIC respectively (Figure 2.7a, b). Replicate injections (3–5 times) of water extracts showed the uncertainty on internal precision for WSTC and WSIC analysis to be within ± 2%.

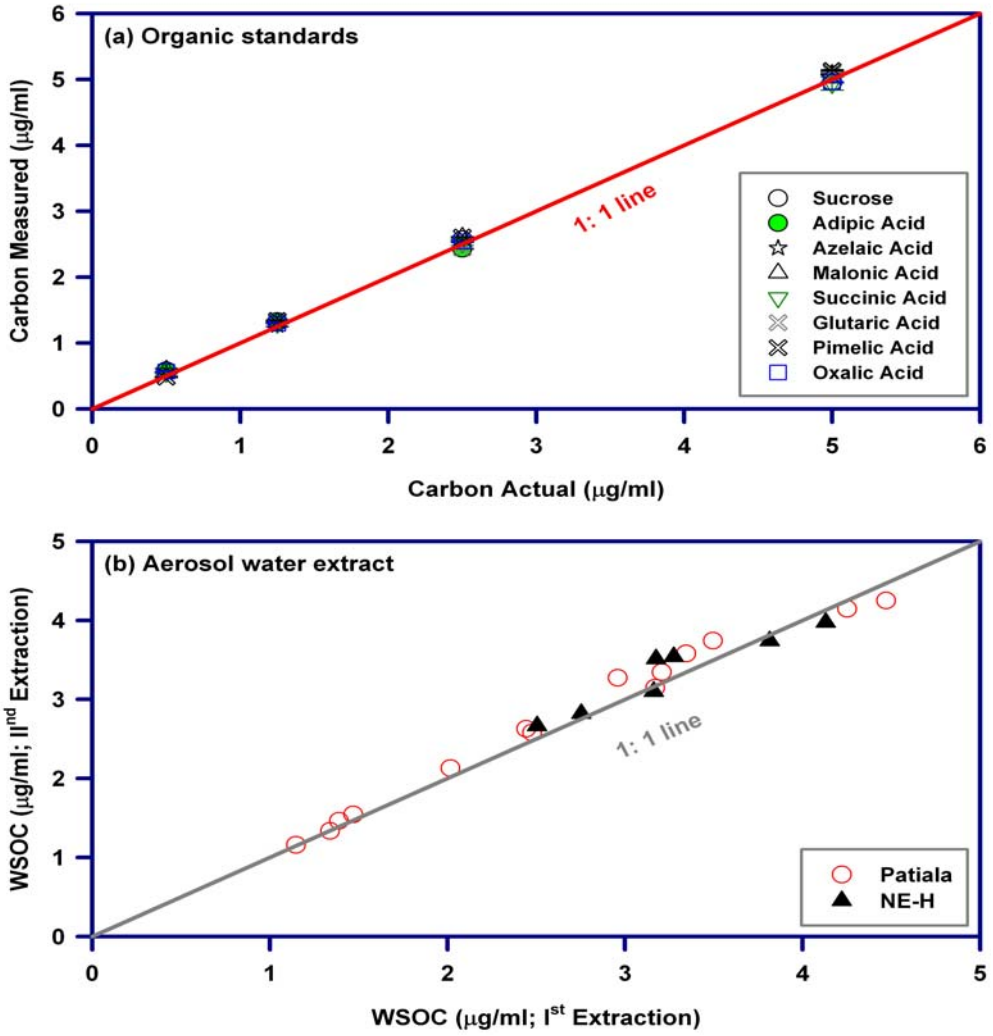

Figure 2.8: Uncertainty on analytical accuracy of the measurements (± 8%) is obtained from analysis of (a) several organic standards (n = 8) and; (b) aerosol samples (n = 21).

Uncertainty on analytical accuracy for WSOC measurements is within ± 8% on TOC analyzer, determined by analyzing several organic acids (n = 8) in triplicates (Figure 2.8a). Repeat extraction and analysis of samples (n = 21)

provided uncertainty of the WSOC measurements to be ~ ± 8% (Figure 2.8b). The WSOC in blank filters (n = 20) was simultaneously measured and the average value (401 ± 106 μg) is used to derive the WSOC concentrations in aerosol samples.

2.4.5 Analysis of polycyclic aromatic hydrocarbons (PAHs)

2.4.5.1 Materials

The HPLC grade solvents (≥ 95%), dichloromethane (DCM), acetone and hexane (Chromasolv® Plus, Sigma-Aldrich) are used for the extraction and sample preparation. The 16-PAHs mixture (QTM PAH Mix; 47930-U, in Methylene Chloride, Supelco) and Pyrene-D10 (in methanol, 71390 Absolute Standards INC.) are used as the external and internal standards respectively. The analytical accuracy of PAHs is determined using a standard reference material (SRM-1649b), procured from the National Institute of Standards & Technology (NIST, Gaithersburg, USA). In SRM, PAHs are extracted using the accelerated solvent extraction system (ASE 200, Dionex Corporation, Sunnyvale, USA), followed by evaporation in an evaporator (Turbo Vap LV® II, Caliper Life Sciences, Hopkinton, USA). Subsequently, extract was purified on silica-solid phase extraction cartridge (SPE; WAT020810, Waters Sep-Pak®, 3cc/500mg) placed over the vacuum manifold (20 positions, WAT200606). After removal of matrix, extracts were analyzed for PAHs on a GC-MS (Agilent: 7890A/5975C). The detailed approach involving optimization of experimental conditions for the determination of 16-PAHs is described in the following sections.

2.4.5.2 Optimization of GC-MS parameters

After several initial tests, a 30 min GC program (Table 2.1) was adopted for the separation of 16-PAHs (Figure 2.9). Subsequently the MS conditions, especially the ion-source (filament) temperature were standardized for optimum intensity to the PAHs. The PAHs were analyzed on a GC-MS in electron impact mode (70 eV). A 1-μL solution of 400 ppb (16-PAHs; QTM mixture) spiked with 200 ng of Pyrene-D10 (internal standard) is separated on a GC capillary column

(30 m x 0.25 mm x 0.25 μm; Agilent HP-5MS) at a constant flow rate of 1.3 mL/min of helium gas and analyzed at different filament temperatures (Figure 2.10 a); 280 ˚C (n = 4), 300 ˚C (n = 4) and 320 ˚C (n = 4). The PAHs are identified by comparing their retention times (RT) with that for 16-PAHs standard and their quantification is achieved by comparing the peak areas with that of the internal standard (Pyrene-D10).

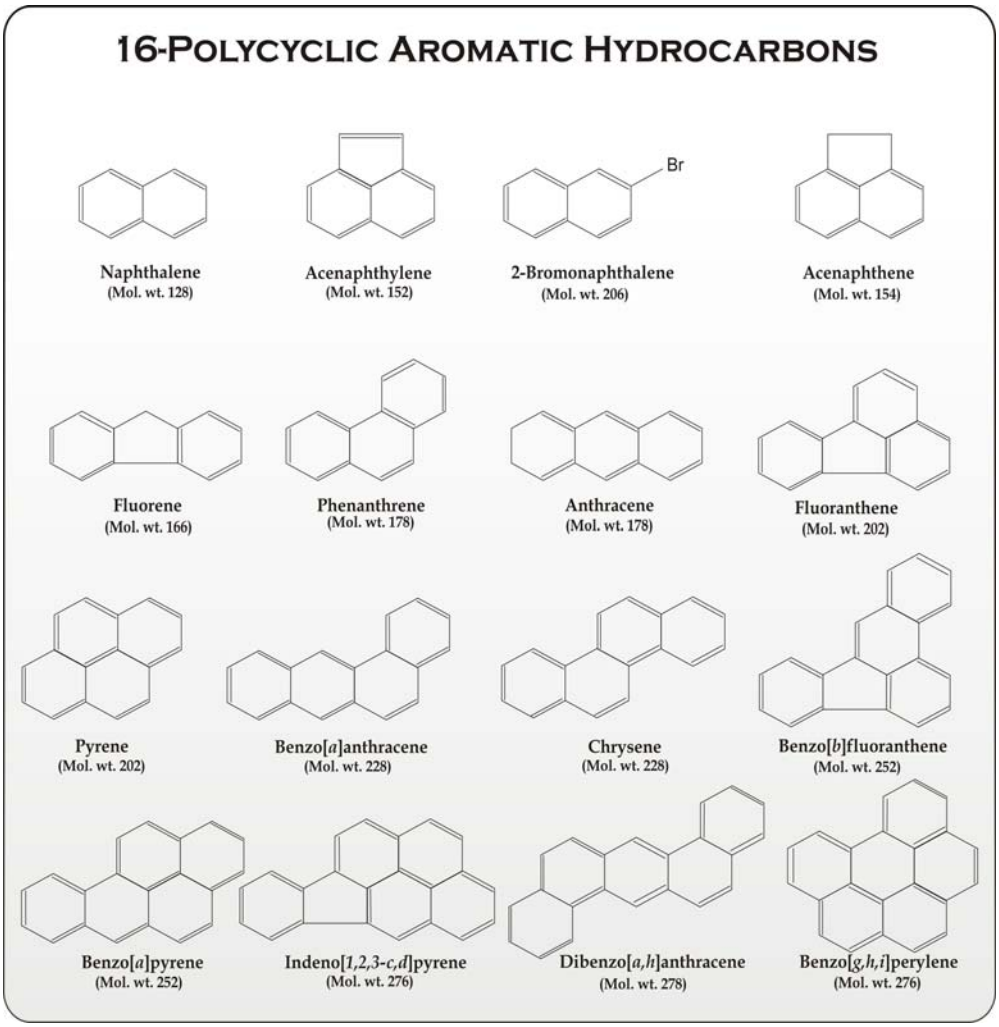

Figure 2.9: Molecular structure of 16-PAHs analyzed in this study.

The filament temperature at 300 ˚C appeared to be the threshold (Figure 2.10 a) for optimum relative response factors (RRF) for all the 16-PAHs, calculated as

$$RRF = \frac{\{Area_{Analyte} * Conc_{ISTD}\}}{\{Area_{ISTD} * Conc_{Analyte}\}} \quad (2.1)$$

The ISTD stands for Internal Standard. Likewise, retention time of PAHs at varying filament temperatures (as above), are investigated (Figure 2.10b), and are found to be invariable (RT < 0.001% shift).

The optimized GC-MS conditions for the determination of PAHs are listed in Table 2.1, and are used for the measurement of 16-PAHs in ambient aerosols.

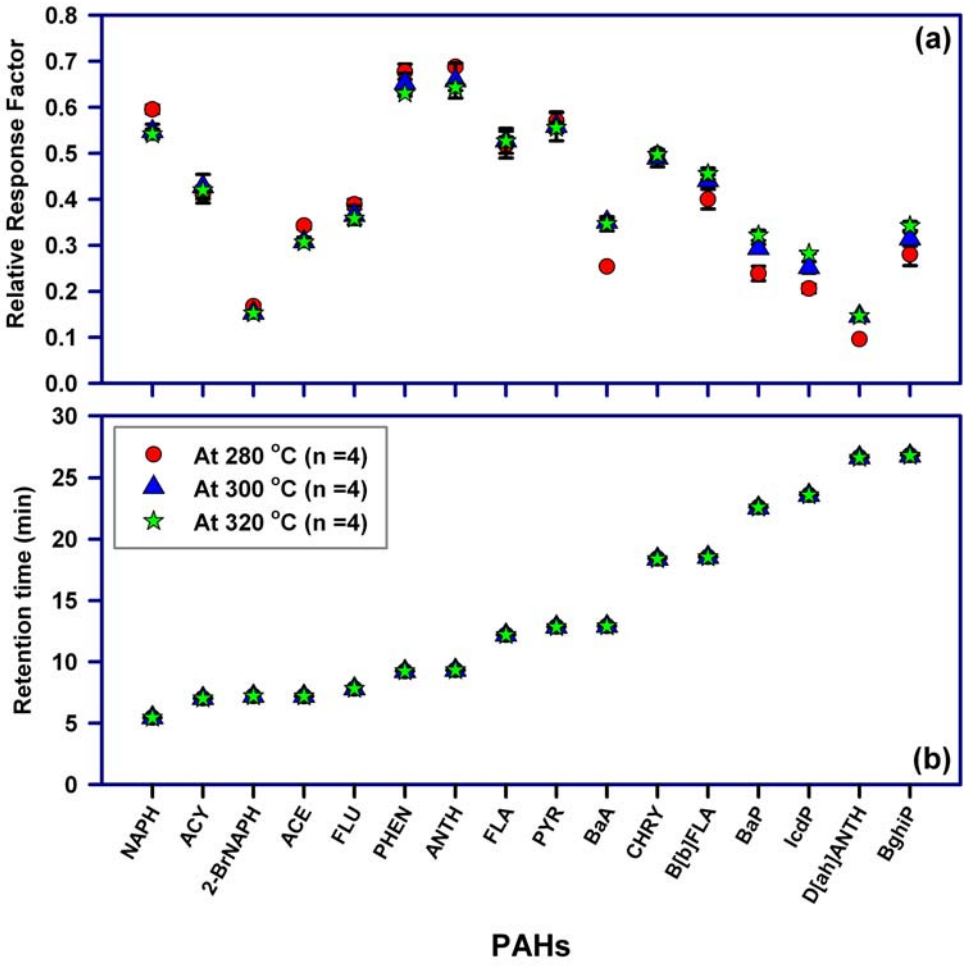

Figure 2.10: Investigation for (a) Optimum ion-source temperature and (b) Variation in retention time for the 16-PAHs on GC-MS.

Data acquisition and processing for the GC-MS analysis is performed on a HP-Enhanced Chemstation Data System.

Table 2.1: Experimental parameters for the measurement of PAHs

ASE		**GC-MS**		
Parameters	**Optimized conditions**	**GC** Inlet temp: 300 ˚C		
Solvent	DCM (30 mL)	**Heating Rate ˚C / min**	**Temp ˚C**	**Hold Time Min**
System pressure	1500 psi		50	1
Oven temperature	100 ˚C	25	150	-
		25	200	-
Oven heating time	5 min	3	230	-
		8	310	3
Static Cycles	3 (of 5 min each)	**MS**		
Nitrogen purge	60 s	Interface temp.	280	
Extraction Time	30 min	Ion-source temp.	300	
		Quadrupole temp.	180	

2.4.5.3 Optimization of purification step on silica cartridge

Aerosol samples contain a wide range of matrices involving mineral dust, organic carbon and elemental carbon. These matrices cause mass interferences with the analytes and affect the resolution of measurements, particularly for the measurements of PAHs on GC-MS. In this study, the silica-SPE (solid-phase extraction) cartridge has been used for the purification of PAHs [*Xie et al.*, 2003]. Prior to the application of silica-SPE cartridges for purification of PAHs in aerosol samples, the elution recovery from 16-PAHs standard on the cartridge is investigated (Figure 2.11).

Accordingly, the silica cartridges, installed over the vacuum manifold are conditioned through 10 mL DCM followed by 10 mL hexane under the vacuum (< 340 millibar). The cartridges are dried under normal conditions for 5 min. Subsequently, the 16-PAHs liquid mixture of varying amount 100 ng (n = 3), 400 ng (n = 3) and, 800 ng (n = 3), in 3 mL hexane are loaded on silica cartridges. The matrix is allowed to fall under gravity, and is discarded. The cartridges are dried again for 5 min. The affect of cartridge drying on the PAHs mass recovery has been discussed elsewhere [*Xie et al.*, 2003]. Subsequently, the elution of PAHs from each cartridge is performed under gravity with 3 mL, 20% DCM in hexane

(v/v). The eluate is evaporated to ~500 µL under gentle nitrogen gas stream, to which 200 ng of Pyrene-D10 is added. The final solution is made to 1 mL in hexane and stored in amber colored glass vials at -19 ˚C until analysis on GC-MS. The analytical recovery close to 100% (Figure 2.11), for all the 16-PAHs ensured no significant loss of these compounds while purification on silica-SPE cartridge.

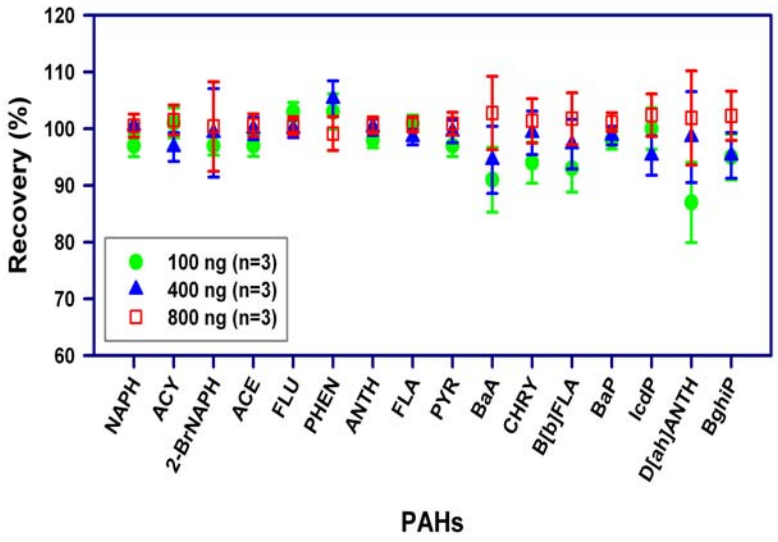

Figure 2.11: The consistent recovery (~100%) of 16-PAHs after purification on silica cartridge, as ascertained from a standard (QTM PAH Mix; 47930-U) is noteworthy.

2.4.5.4 Optimization of extraction parameters on ASE

The extraction parameters on accelerated solvent extraction (ASE) such as solvent selection, temperature and extraction time on the recovery efficiency of PAHs were investigated at a constant pressure of 1500 psi (103 bars). The extraction at 1500 psi pressure is considered to be optimal for the aerosol samples [*Richter et al.*, 1996]. The extraction protocol was developed based on the analysis of standard reference material (NIST, SRM-1649b, Urban Dust). The toxic solvents e.g. benzene and its derivatives were not used to assess the extraction efficiency of PAHs. Furthermore, the loss of analyte during extraction at different temperature and pressure [*Alexandrou et al.*, 2001], if any, was checked with the low boiling point solvents e.g. DCM (40 ˚C), which not only extract PAHs quantitatively from aerosols but also can undergo rapid evaporation (Figure 2.12). The extraction protocol for the PAHs, employing 100 ˚C for 15

minutes is considered to be optimal on ASE (Figure 2.12). Furthermore, the PAHs were also extracted from SRM in two different solvents viz. DCM (n = 6) and DCM/Acetone (n = 6; 1:1 v/v) at 100 ˚C, 1500 psi and 3 static cycles of 5 min each. These extracts were evaporated to 1 mL in evaporator (< 30 ˚C) and further to near dryness by gentle nitrogen gas purge. The residue was dissolved in 3 mL hexane. Subsequently, the optimized protocol, described in the previous sections is used for the purification and sample preparation for PAHs analysis. The results suggest that, within the uncertainty of measurements on GC-MS, the yields for individual PAHs were equal with DCM or DCM:Acetone (1:1 v/v).

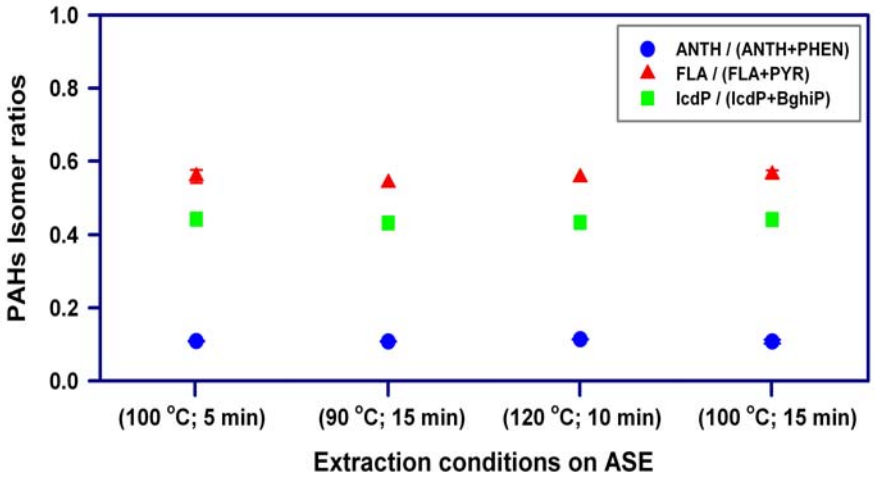

Figure 2.12: Replicate analysis (n = 12) of three isomer pairs in SRM-1649b ascertain that accelerated solvent extraction (ASE) does not lead to their fractionation.

However, DCM was used for the PAHs extraction, due to its rapid evaporation (b.p. 40 ˚C) in comparison to its mixture with acetone (56.3 ˚C). The analytical accuracy (Table 2.2) of the protocol was determined by the SRM analysis (n = 32) following the protocol listed in Table 2.1. The molecular weight (quantification ion), retention times and the detection limits (inferred from analyses of n = 22 blanks) for 16-PAHs are also given in Table 2.2.

2.4.5.5 Investigation of loss of 2- to 3-ring PAHs

The 100 ng of 16-PAHs mixture (QTM PAH Mix; 47930-U, in Methylene Chloride, Supelco) was spiked on pre-cleaned quartz fiber filters (1.5 sq cm; n =

6). The extraction of PAHs in DCM, followed by matrix purification and sample preparation is done in the similar way to aerosol samples. The analyses on GC-MS ensure recovery close to 100% for the individual PAHs. A total of (n = 17) ambient aerosol samples, collected from different geographical locations in India; from Patiala (n = 8), Hisar (n = 2) and Shillong (n = 7), were analyzed for the mass recovery of PAHs. Repeat extractions and analyses of these samples (n = 17; Figure 4) reveal that the extraction efficiency for 2- to 3-ring PAHs is 85% whereas the recovery is ~100% for 4- to 6-ring compounds. The overall extraction efficiency of PAHs is 97 ± 2%. The extraction efficiency (EF) of PAHs in aerosol samples (Figure 4) is calculated as

$$EF = 100 \times \frac{PAHs\ recovery\ in\ first\ extraction}{PAHs\ recovery\ in \{first + second\} extraction} \qquad (2.2)$$

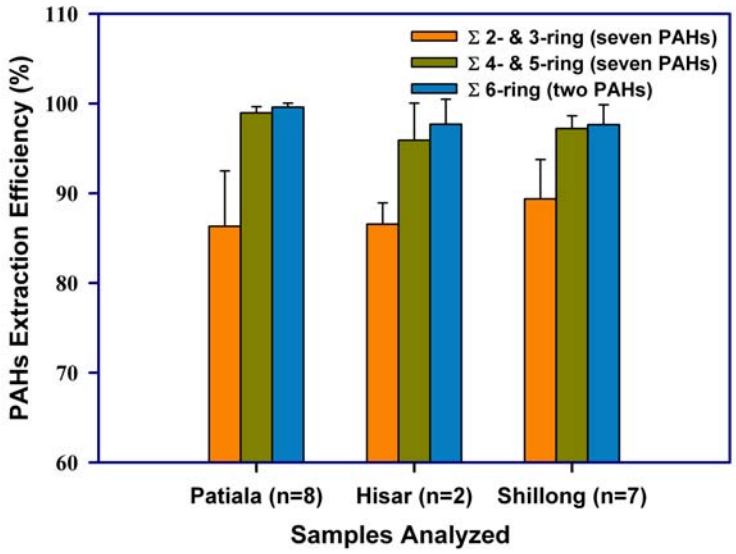

Figure 2.13: The extraction efficiency of PAHs, as determined in aerosol samples collected from different geographical regions.

Analysis of several sample repeats (n = 17) showed that on an average the uncertainty on external precision of the measurements is ± 4%. It is relevant to reemphasis that these samples are representative of tarry matter and soot (along with the mineral dust), and therefore, the analytical protocol investigate the extraction efficiency of PAHs in the presence of varying matrices. However, in

aerosol samples the low recovery for 2- to 3-ring PAH, in contrast to the high recovery for 4- to 6-ring PAHs is attributable to their low concentrations in aerosol samples (Figure 2.13).

2.4.5.6 Time-dependent record of analytical conditions on GC-MS

The DCM based commercial standard of 16-PAHs mixture is diluted in hexane to prepare a 2 ppm stock solution.

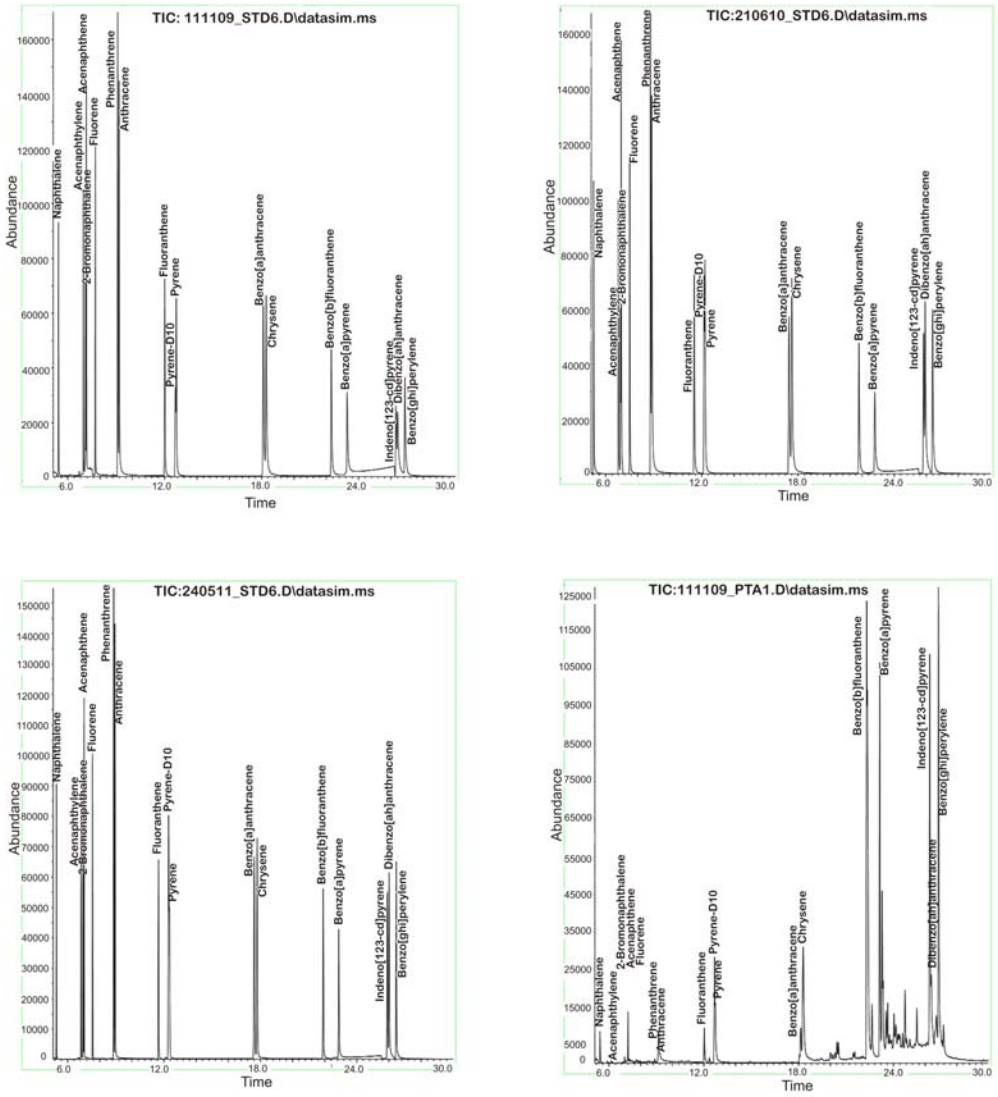

Figure 2.14: Typical chromatographs of 16-PAHs on GC-MS in the standard (QTM PAH Mix; 47930-U) and aerosol sample.

From this stock solution, seven working standards between the concentration ranges from 0–1500 ppb are prepared in hexane and analyzed routinely on GC-MS. The operating conditions for PAHs analysis on GC-MS are given in Table 2.1. Typical chromatographs on analyzing the 16-PAHs standard mixture and aerosol sample on GC-MS is shown in Figure 2.14.

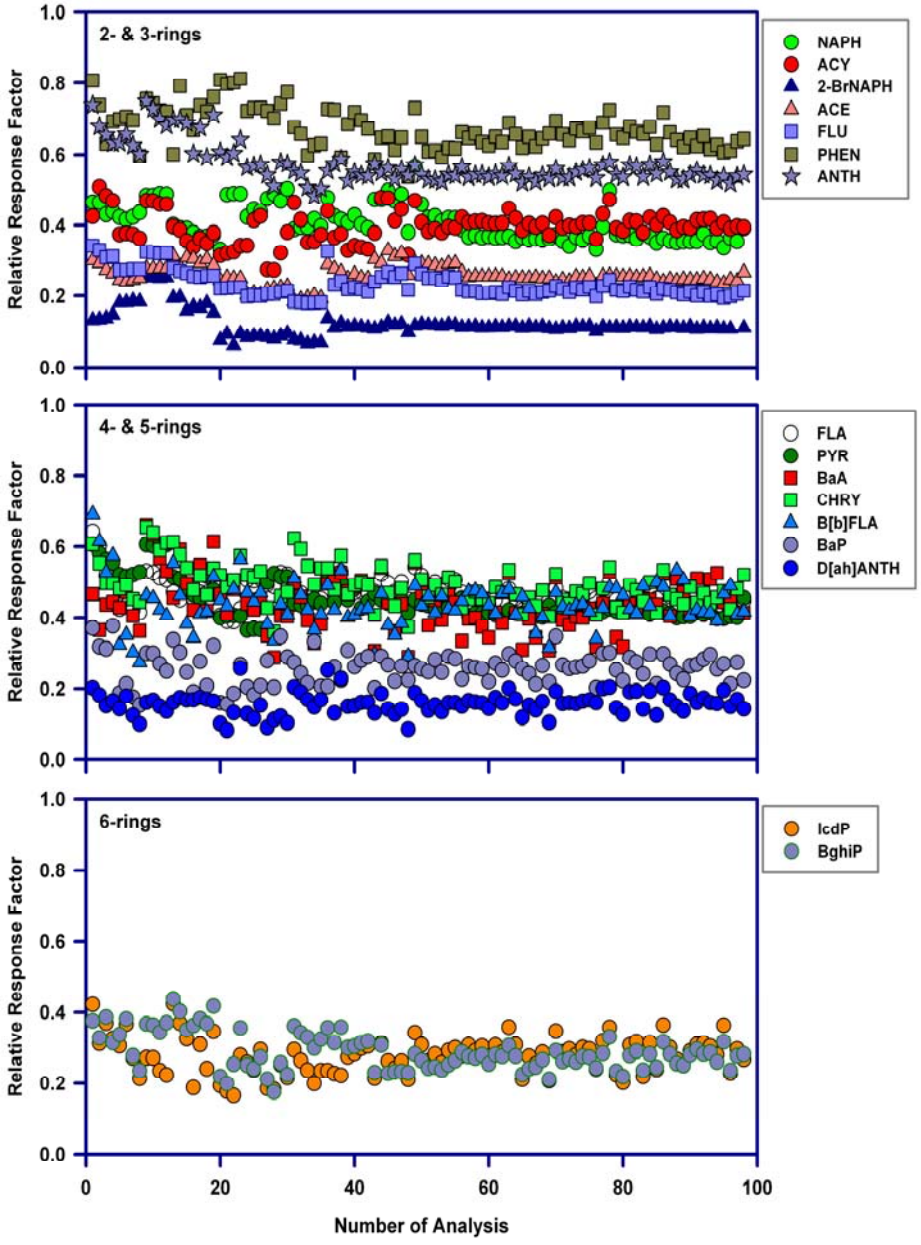

Figure 2.15: Time dependent analyses (n = 95; over 2 years) of 16-PAHs (QTM PAH Mix; 47930-U) ascertain the variability (20% at most) in response factors on GC-MS.

The two years record in temporal variations (insignificant for n = 95 injections of 16-PAHs standard) of the RRF of 16-PAHs (equation 2.1) show the stability of GC-MS (Figure 2.15). Furthermore, several analyses of SRM aliquots (~100 mg; n = 32) over a period of one year, determine the analytical accuracy (Table 2.2).

Table 2.2: Analysis of 16-PAHs in SRM 1649b, Urban Dust (n = 32)

16-PAHs	Molecular weight	Retention time (min)	DL (n=22)	Measured Conc.[§] (ng / 100 mg SRM)	Reported Conc. (ng / 100 mg SRM)
Naphthalene {NAPH}*	128	5.448 ± 0.002	2.8	83 ± 17	112 ± 42
Acenaphthylene {ACY}*	152	7.000 ± 0.004	3.6	14 ± 3	18 ± 3
2-Bromonaphthalene {2-BrNAPH}	206	7.154 ± 0.019	3.4	NR	NR
Acenaphthene {ACE}*	154	7.180 ± 0.003	2.2	10 ± 1	19 ± 4
Fluorene {FLU}*	166	7.760 ± 0.016	2.1	16 ± 2	22 ± 2
Phenanthrene {PHEN}	178	9.173 ± 0.022	1.9	368 ± 16	394 ± 5
Anthracene {ANTH}	178	9.264 ± 0.026	2.4	42 ± 7	51 ± 1
Fluoranthene {FLA}	202	12.775 ± 0.024	2.3	578 ± 40	614 ± 12
Pyrene {PYR}	202	12.834 ± 0.022	3.4	469 ± 29	478 ± 3
Benzo[*a*]anthracene {BaA}	228	18.275 ± 0.041	2.5	218 ± 20	209 ± 5
Chrysene/Triphenylene {CHRY+TRIP}	228	18.437 ± 0.040	1.8	415 ± 26	425 ± 10
Benzo[*b*+*j*+k]fluoranthene B[b,j,*k*]FLA}	252	22.454 ± 0.038	3.0	910 ± 64	947 ± 51
Benzo[*a*]pyrene {BaP}	252	23.444 ± 0.047	2.5	261 ± 17	247 ± 17
Indeno[1,2,3-*cd*]pyrene {IcdP}	276	26.461 ± 0.046	3.0	306 ± 20	296 ± 17
Dibenzo[*a*,*h*+*a*,*c*]anthracene D[ah,ac]ANTH}	278	26.569 ± 0.055	3.5	49 ± 4	50 ± 1
Benzo[g,h,i]perylene {BghiP}	276	26.996 ± 0.033	2.9	411 ± 31	394 ± 5

*Reference values, otherwise certified values (from NIST). NR (Not reported in NIST certificate).
[§]Standard deviation of the data for n = 32. DL (Detection limit in pg m^{-3}).

2.4.6 Analysis of water-soluble inorganic species (WSIS)

The analysis of water-soluble cations (Na^+, K^+, NH_4^+, Ca^{2+} and Mg^{2+}) and anions (Cl^-, SO_4^{2-} and NO_3^-) in aerosols were preformed on Ion-Chromatograph (Dionex®). The clear solution of the water-extracts (1/8th of aerosol sample in 40/50 ml Milli-Q water) were transferred to pre-cleaned vials and analyzed for their water-soluble ionic constituents. A mixture of 1.8 mM Na_2CO_3 and 1.7 mM $NaHCO_3$ was used as an eluent for the analysis of anions and an Anion Self Regenerating Suppressor (ASRS) was used to suppress the conductivity.

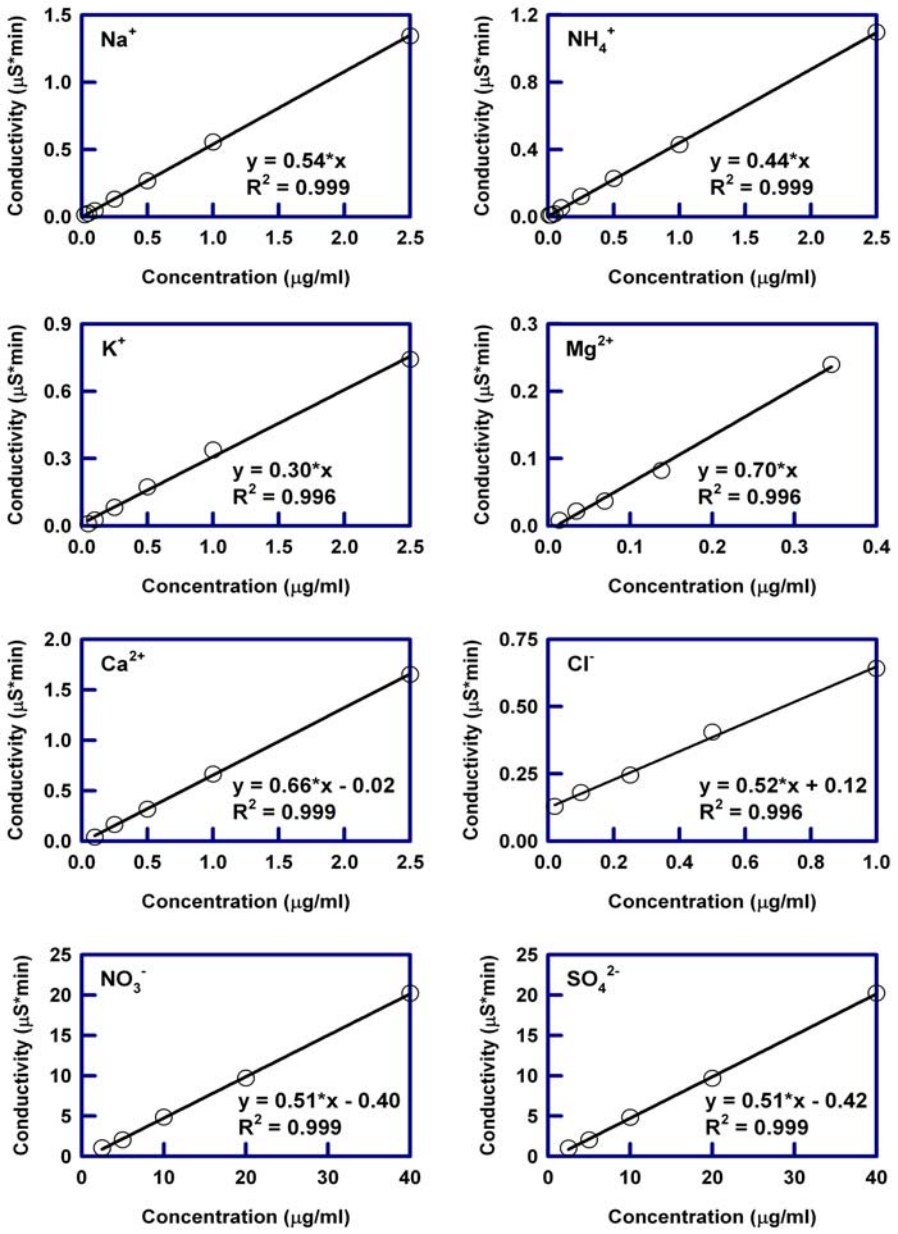

Figure 2.16: : A typical calibration used for the quantification of water-soluble cations and anions in aerosol samples.

For analysis of cations, 20 mM methanesulphonic acid (MSA) was used as an eluent and the conductivity was suppressed with the help of a Cation Self-Regenerating Suppressor (CSRS). The anions and cations were separated using analytical columns, Ionpac-AS14 and Ionpac-CS12, for anions for cations respectively prior to their determination using conductivity detector. A typical

calibration used for the quantification of all the cations and anions (mentioned above) is shown in Figure 2.16.

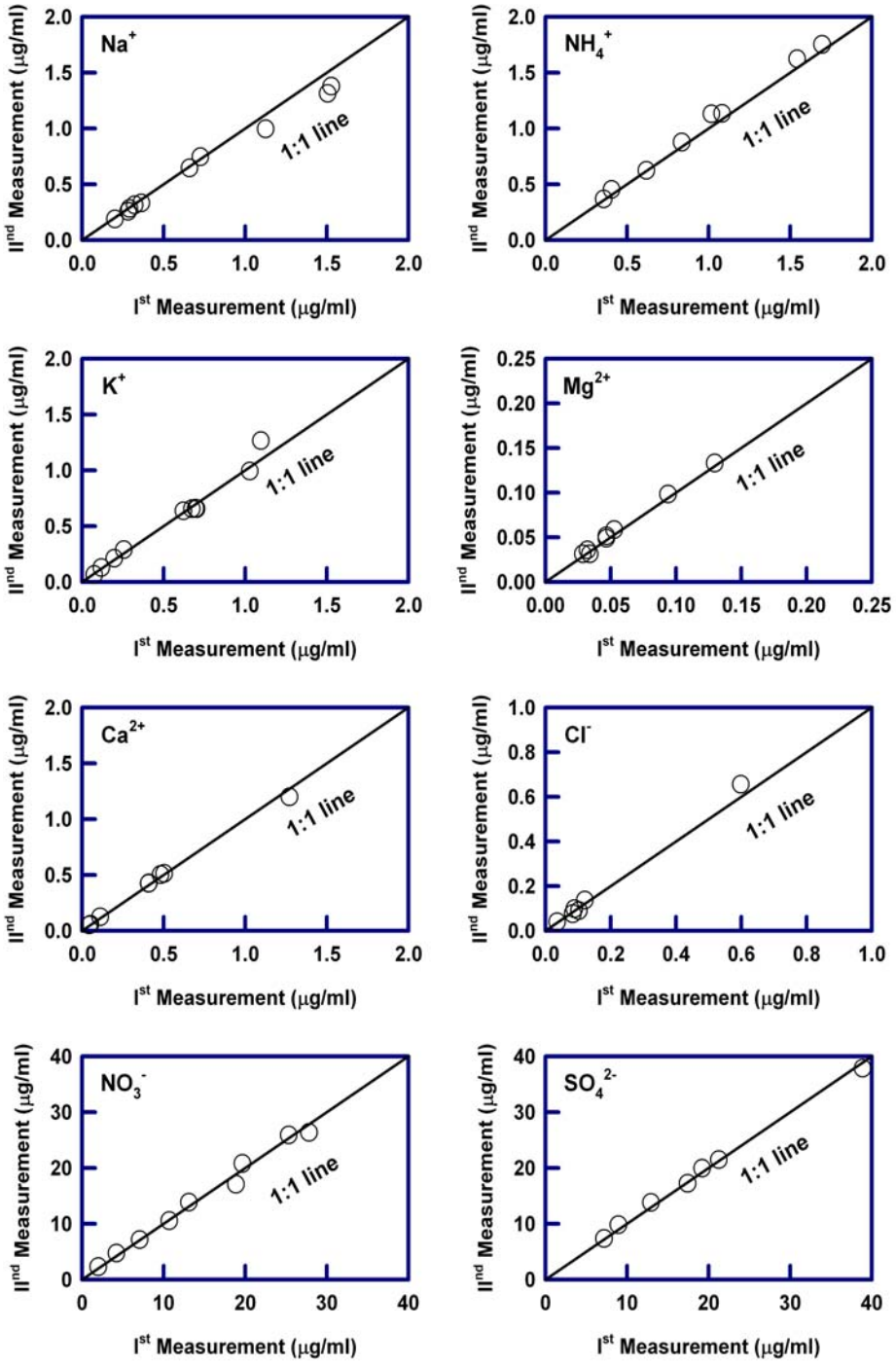

Figure 2.17: Scatter plot of replicate measurements (in ppm; μg mL^{-1}) of cations and anions in aerosols on Ion-Chromatograph.

Simultaneously processed blank filters were also analyzed to obtain blank concentration of cations and anions, and were subtracted from their concentrations in aerosol samples.

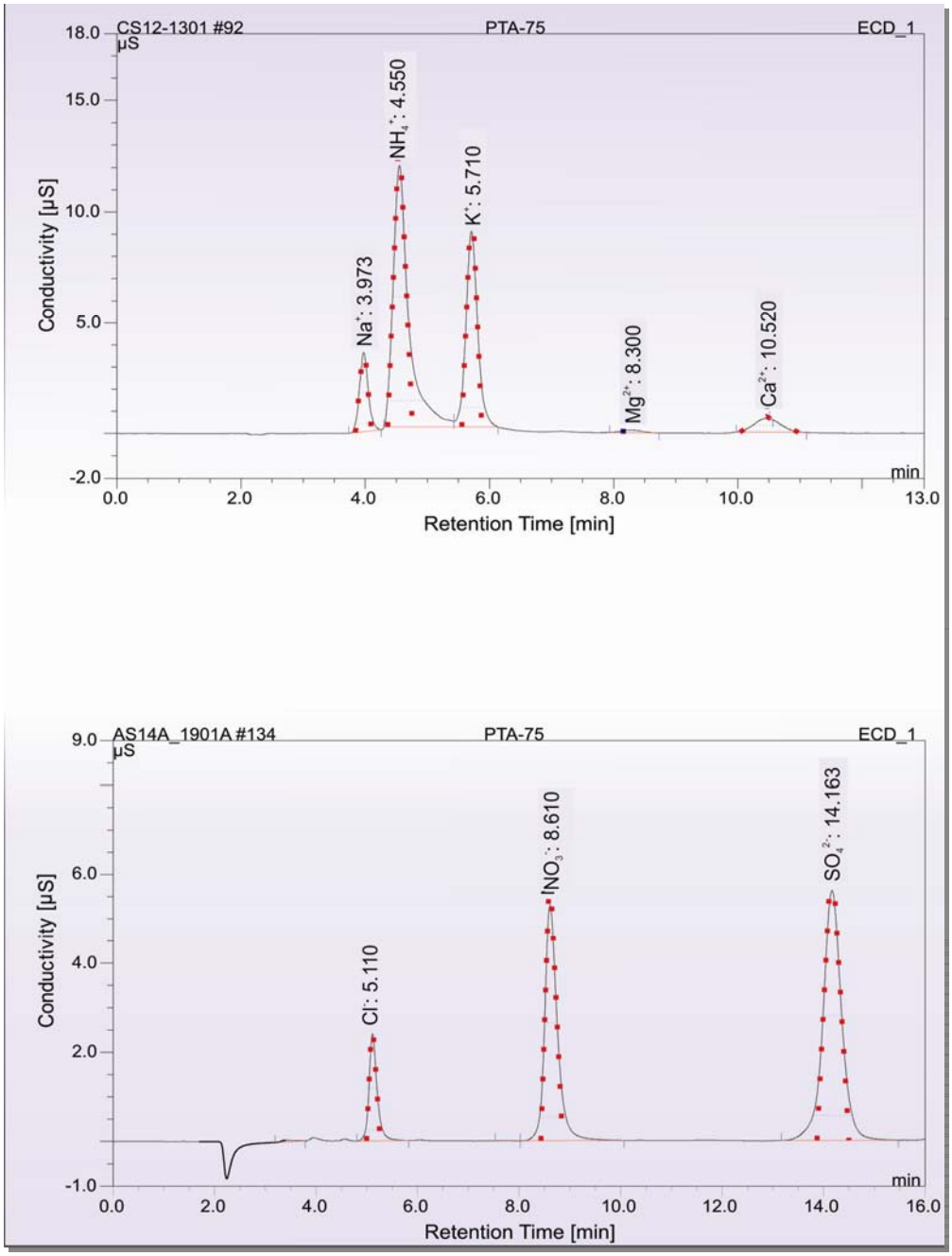

Figure 2.18: Typical chromatographs of cations and anions on Ion-Chromatograph in aerosol sample (PTA-75).

The replicate analyses for Na^+, K^+, Ca^{2+}, Mg^{2+}, Cl^-, SO_4^{2-} and NO_3^- provided uncertainty on the measurements to be within ± 3% while it was ~ ± 6% for NH_4^+ analysis (Figure 2.17). A typical chromatograph showing the separation of cations and anions in aerosol samples on Ion-Chromatograph is represented in Figure 2.18. The details of the analytical procedure for water-soluble ionic constituents are described in earlier publications [*Rastogi and Sarin*, 2005; 2006; *Rengarajan et al.*, 2007].

2.5. Summary

Relevant analytical details adopted in this study for the measurement of WC, OC, WSOC, PAHs and water-soluble ionic species (WSIS) in aerosols is provided in this chapter. An analytical method developed for the quantitative determination of PAHs from standard reference material (NIST-1649b), show analytical accuracy of 100 ± 15%. The adopted protocol for the quantification of PAHs include ASE extraction with DCM at 100 ˚C for 3 static cycles (of 5 min each) at a constant pressure of 1500 psi, followed by the matrix purification on a pre-cleaned silica cartridge and subsequent analysis on GC-MS, operated at 300 ˚C as the optimum ion-source temperature. Analysis of field-based aerosol samples show the average extraction efficiency (equation 2.2) for 4- to 6- ring PAHs is ~100%. The somewhat lower recovery (Av: ~85%) for 2- to 3- ring PAHs in the field-based samples is attributable to their lower concentrations in the aerosols. This protocol for PAHs analysis, is ideal to eliminate the matrix effect from tarry matter, soot and mineral dust associated with high atmospheric aerosols loading.

CHAPTER 3

BIOMASS BURNING EMISSIONS IN NORTHERN INDIA: CHEMICAL CHARACTERIZATION AND ATMOSPHERIC IMPACT

3.1. Introduction

The chemical characteristics of atmospheric aerosols emitted from fossil-fuel and wood-fuel combustion sources have been relatively well studied, for example [*Bond et al.*, 2004; *Fine et al.*, 2002; *Fraser et al.*, 2002a; *Harrison et al.*, 1996; *Rogge et al.*, 1998; *Schauer et al.*, 2002; *Simoneit*, 2002; *Venkataraman et al.*, 2005]. However, data on the chemical composition of aerosols from agricultural-waste burning emissions are rather sparse [*Andreae and Merlet*, 2001; *Hays et al.*, 2005; *Jenkins et al.*, 1996]. Recently, attempts have been made to study the particle size distribution in the emissions from rice-straw and wheat-straw burning [*Hays et al.*, 2005; *Li et al.*, 2007; *Zhang et al.*, 2011]. These laboratory-based experiments have found a unimodal mode with peak, exception being the bimodal size distribution of particles observed for rice-straw burning emissions, one in accumulation-mode and another in coarse-mode [*Keshtkar and Ashbaugh*, 2007]. More recently, the fresh emissions of particles from rice-straw and wheat-straw burning has been found to exhibit a unimodal distribution at 0.10 μm and 0.15 μm respectively [*Zhang et al.*, 2011].

The significance of large-scale biomass burning emissions on the atmospheric chemistry, climate and bio-geochemical cycles has been widely emphasized [*Crutzen and Andreae*, 1990; *Das et al.*, 2008; *Dey and Tripathi*, 2007; *Gustafsson et al.*, 2009; *Menon et al.*, 2002; *Ram and Sarin*, 2010; *Ramanathan et al.*, 2007]. Several top-down studies have suggested for the South Asian region that 50–90% of the BC is derived from the fossil-fuel combustion [*Mayol-Bracero et al.*, 2002a; *Novakov et al.*, 2000; *Ramanathan et al.*, 2007; *Stone et al.*, 2007]. In contrast, recent emission inventories on bottom-up approaches, suggest that biomass burning is a dominant source in South Asia and accounts for nearly 70% of the BC [*Gustafsson et al.*, 2009; *Venkataraman et al.*, 2005]. However, these inferences are derived mainly from OC/EC ratios, and can have influence to some degree by fractionation during chemical processing of carbonaceous aerosols and can thus, mislead in characterization of the sources [*Cabada et al.*, 2004; *Castro et al.*, 1999; *Gustafsson et al.*, 2009; *Ram and Sarin*, 2010; *Schauer et al.*, 1996].

These diverging views on the sources of carbonaceous aerosols demand a comprehensive data set for EC, OC, water-soluble organic carbon (WSOC) and water-soluble inorganic species (WSIS) from biomass burning emissions, as well as for diagnostic tracers such as polycyclic aromatic hydrocarbons (PAHs) [*Li et al.*, 2009; *Tham et al.*, 2008; *Yunker et al.*, 2002].

This chapter presents a first comprehensive study on carbonaceous (EC, OC, WSOC and PAHs) and water-soluble inorganic species (WSIS) in PM2.5 (particles with aerodynamic diameter ≤ 2.5 μm) collected during two distinct agricultural-waste burning practices followed in Punjab, Haryana and western part of Uttar Pradesh in the Indo-Gangetic Plain (IGP). The primary objective is to assess the relative impact of emissions from post-harvest burning of paddy-residue during October–November and wheat-residue during April–May. Such important data set on concentrations of PAHs and their isomer ratios from field burning of agricultural-residues is hitherto lacking in the literature for a dominant source of carbonaceous aerosols in the IGP.

The post-harvest burning of paddy-residue in Punjab region (during October–November) is estimated to be around 100 million tons of rice-straw. The emission strength from wheat-residue burning is about a factor of 2–3 lower during April–May. The time period of December–March is characterized by emissions from bio-fuel (Babool, Cowdung cake, Eucalyptus, Jujube and Shisham) and fossil-fuel combustion sources.

3.2. Field-campaign and meteorology

3.2.1 Sampling site description

The large-scale biomass burning emissions occurring in the states of Punjab, Haryana and western part of Uttar Pradesh (2˚ x 2˚ = 4, 84, 00 sq km; Figure 3.1), extend from north-northwestern part of the Indo-Gangetic Plain (IGP), is a common practice on annual and seasonal basis. It encompasses, post-harvest burning of paddy-residue during October–November and wheat-residue in April–May. The transient emission from bio- and fossil-fuel combustion is dominant during December–March in this basin (IGP).

Moreover, the sampling site at Patiala in Punjab (30.2 ˚N, 76.3 ˚E, 250 m amsl), representing a semi-urban environment, is strategically located ~1 km downwind of the agricultural-fields [*Rajput et al.*, 2011b]. During rest of the year, from July–September (south-west monsoon), the ambient atmosphere remains relatively clean due to frequent precipitation events. As far as atmospheric condition (on a regional scale) is concerned, the period from October–November (post-monsoon) is influenced by haze, and during December–March (wintertime) the heavy fog-formation and shallower planetary boundary layer is a conspicuous feature in this basin. Furthermore, during April–May (pre-monsoon), the high convective mixing of the atmosphere is an important phenomenon in governing the lower concentration of pollutants near the earths' surface. Importantly, during December–March (wintertime), relatively low ambient temperature, shallower boundary layer and poor thermal convection results into efficient trapping of aerosols in the lower atmosphere, and thus, lead to enhance their concentrations. Furthermore, the transport of mineral dust to the northern India from western part of India and northwest Desert regions is a seasonal process occurring during April–June [*Jethva et al.*, 2005].

MODIS (Moderate Resolution Imaging Spectroradiometer) based aerosol optical depth (AOD) over the IGP has been reported to exhibit large spatial and temporal variability during the summer (April–June), varying from 0.6–1.2 at 550 nm wavelength [*Jethva et al.*, 2005]. In addition, the associated fine-mode aerosol fraction (FMAF ratio of the fine-mode AOD to the total-mode AOD) was found to be low (< 0.4). This indicated that the coarse-mode particles are dominant during the summer. The spatial distribution of absorbing aerosol index (AAI) derived from TOMS (Total Ozone Mapping Spectroradiometer), Ångstöm exponent (α) and aerosol volume size distribution measured at Kanpur also indicated the presence of absorbing coarse-mode aerosols in summer. In contrast, the entire IGP was dominated by the fine-mode atmospheric particles during the winter (November–January) with AOD varying from 0.4–0.6. However, their spatial and temporal variability, were quite low as compared to that during summer. Thus, assessing the optical properties of aerosols, the largest aerosol optical depth in India during both the seasons has been found over the IGP [*Jethva*

et al., 2005]. The seasonal influence, due to transport of mineral dust from western part of India and northwest Desert regions during the summer and, from anthropogenic emission sources during winter are the plausible factors resulting into the occurrence of coarse- and fine-mode aerosols during these seasons over the IGP [*Jethva et al.*, 2005].

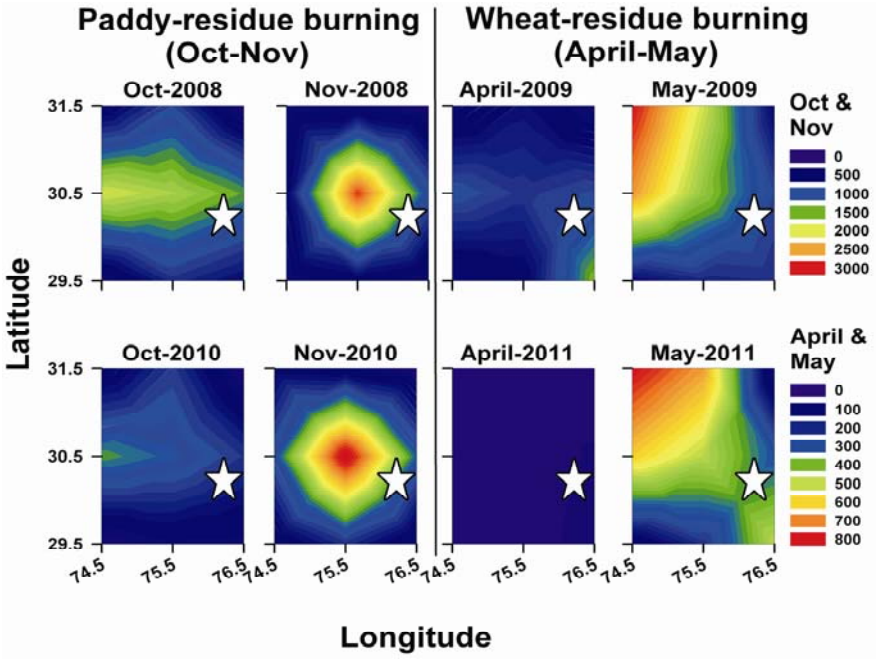

Figure 3.1: MODIS image of fire-counts during paddy- and wheat-residue burning in the IGP. Sampling location at Patiala (shown by star) is strategically downwind of the emission plumes.

3.2.2 Aerosol sampling

Two field campaigns were conducted; during the drier months from October '08–May '09 and during October '10–May '11. A total of 141 PM2.5 (particle with aerodynamic diameter ≤ 2.5 μm) samples were collected that encompass samples from paddy-residue burning (October–November), wheat-residue burning (April–May) and bio- & fossil-fuel combustion (December–March). Aerosol sampling was performed using a high-volume air-sampler (flow rate: ~1.2 m^3 min^{-1}) onto pre-baked (350 ˚C for ~6 h) tissuquartz filters (PALLFLEX^{TM}, 2500QAT-UP, 20 cm x 25 cm) ~15 m above ground level. Due to high aerosol loading, observed in the first campaign during paddy-residue

burning emissions from October–November ’08, the subsequent sampling period was reduced from 24 h to ~12 h. The details on integrated period for aerosol sampling on a seasonal basis are given in Table 3.1.

Table 3.1: Integration period of aerosol sampling for different emission scenario

Emission Source	PM2.5 sampling (October ’08 –May ’09)		PM2.5 sampling (October ’10 –May ’11)	
	Period	Integrated time	Period	Integrated time
Paddy-residue	Oct–Nov '08	~24 h/(Day–Night)	Oct–Nov '10	8–10 h/Daytime
Bio- and fossil-fuel	Dec '08–March '09	~12 h/Daytime	Dec '10–March '11	8–10 h/Daytime
Wheat-residue	April–May '09	8–10 h/Daytime	April–May '11	8–10 h/Daytime

3.2.3 Meteorology

The meteorological winds, surface temperature, relative humidity and precipitation were monitored at the site during the course of aerosol sampling. The ambient temperature and relative humidity (RH) records (monthly averaged; provided by Indian meteorological Department, Punjabi University Campus, Patiala) for the sampling period from October ’08–May ’09 and October ’10–May ’11 exhibit similar inter-annual pattern (Figure 3.2).

The temperature record shows minima during December–March (wintertime) and maxima during April–May (pre-monsoon; summertime), in contrast to RH seasonal pattern. Accordingly, the average ambient temperature varied from 24.5–29.7 °C during October–November (referred to as post-monsoon), 14.4–28.8 °C during December–March (referred to as wintertime) and 33.5–37.7 °C during April–May (referred to as pre-monsoon). The corresponding relative humidity (RH) varied from 51–65%, 49–71% and 34–41%, respectively. The prevailing winds were north-north westerly and weak (intensity: 0.3 km h^{-1}) during October–November, became westerly and moderate (1.1 km h^{-1}) during December–March and frequently south-westerly with relatively high intensity (2.2

km h^{-1}) during April–May (Figure 3.3). Northern India receives rainfall mainly (80–95%) during south-west monsoon (June–September; Figure 3.4).

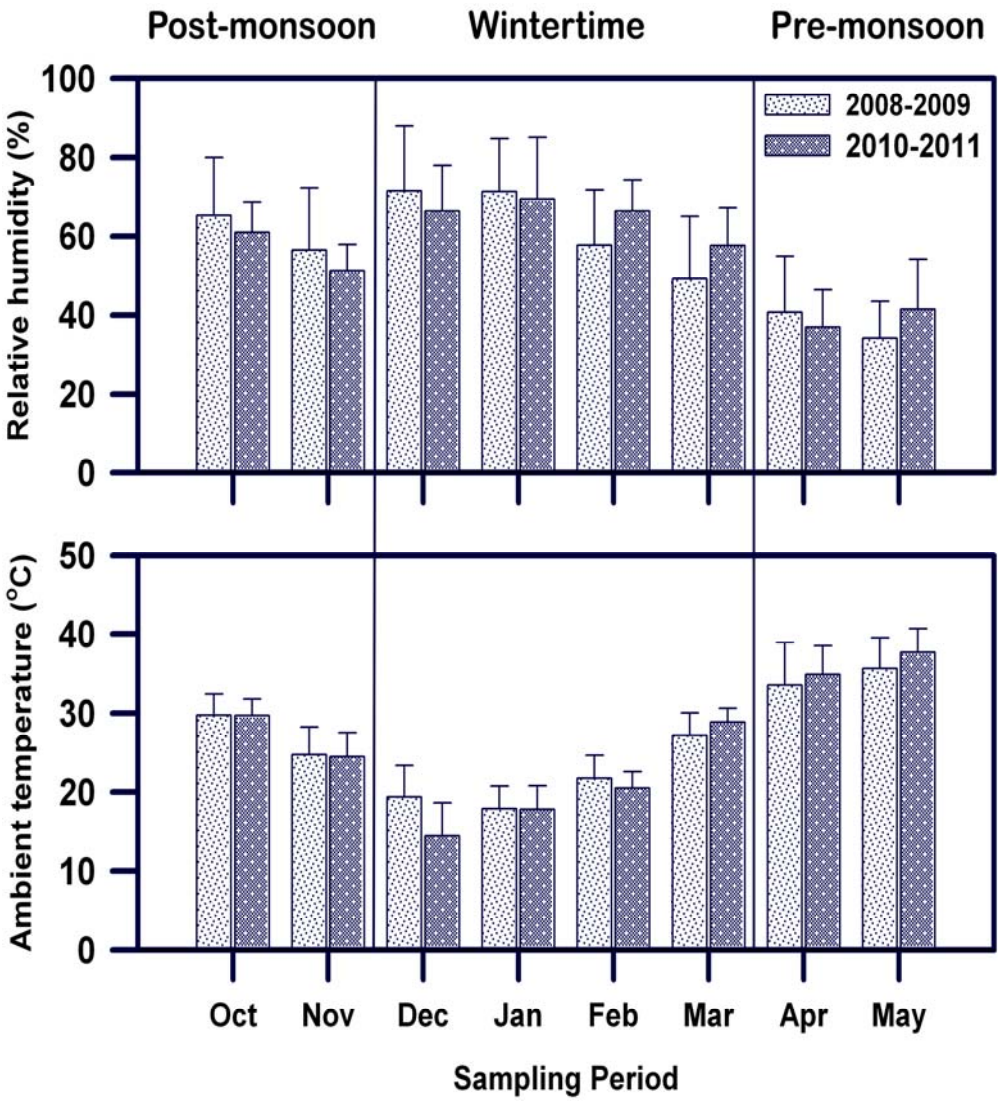

Figure 3.2: The monthly average meteorological record on temperature and relative humidity during the aerosol sampling over Patiala.

As aerosol sampling was conducted during 2008–2011, it is relevant to discuss the rainfall scenario over the region for the entire period. The precipitation records for the year 2008 (annual: 1073 mm), 2009 (550 mm), 2010 (875 mm) and 2011 (802 mm), suggests that 2009 was a drought year (Figure 3.4).

Furthermore, looking at the annual rainfall pattern, it is obvious that from 2008–2011, the amount of precipitation has decreased by almost 30% (not a small number).

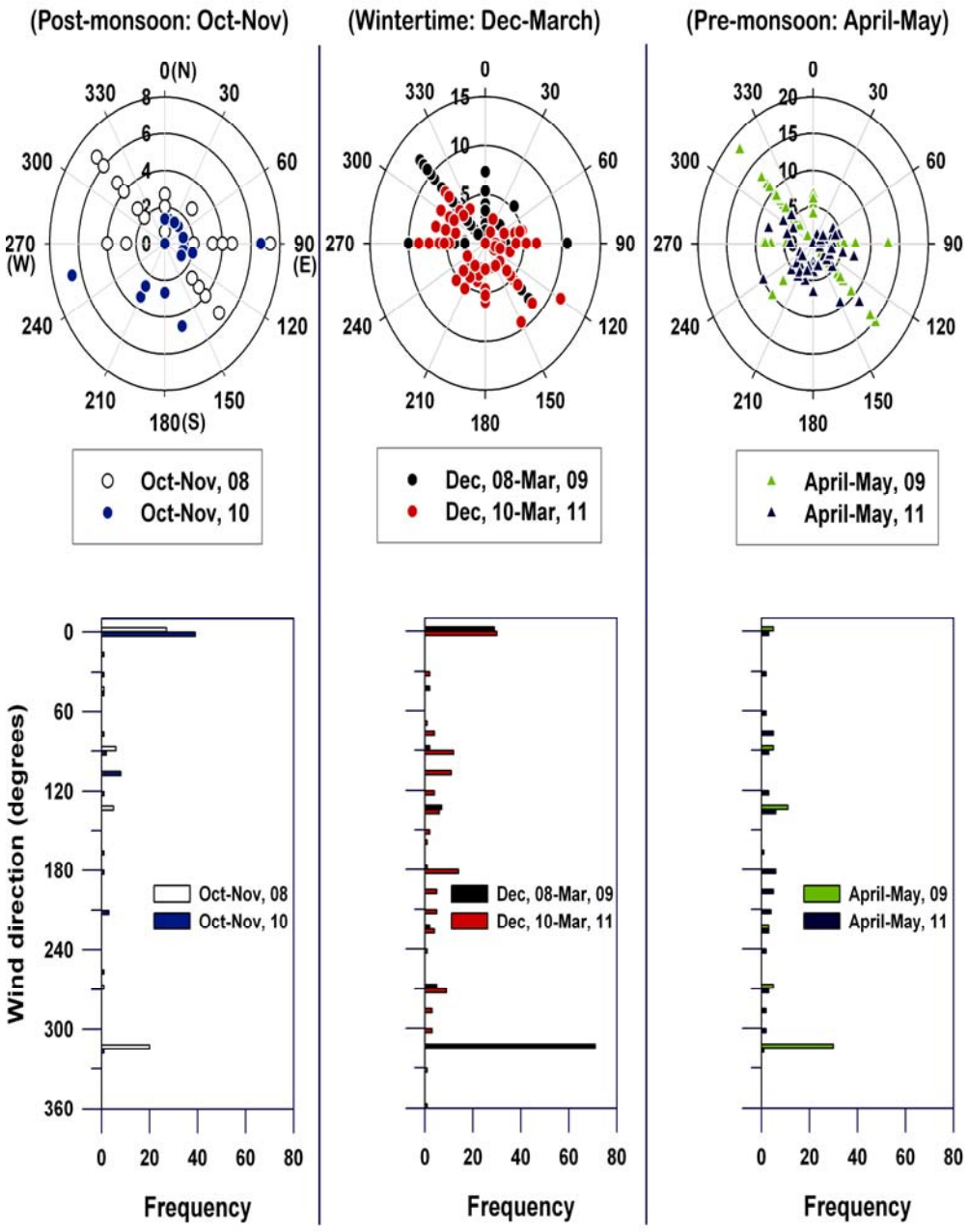

Figure 3.3: Seasonal wind-rose plots for the sampling period from October '08–May '09 and October '10–May '11. N: North; E: East; S: South and W: West.

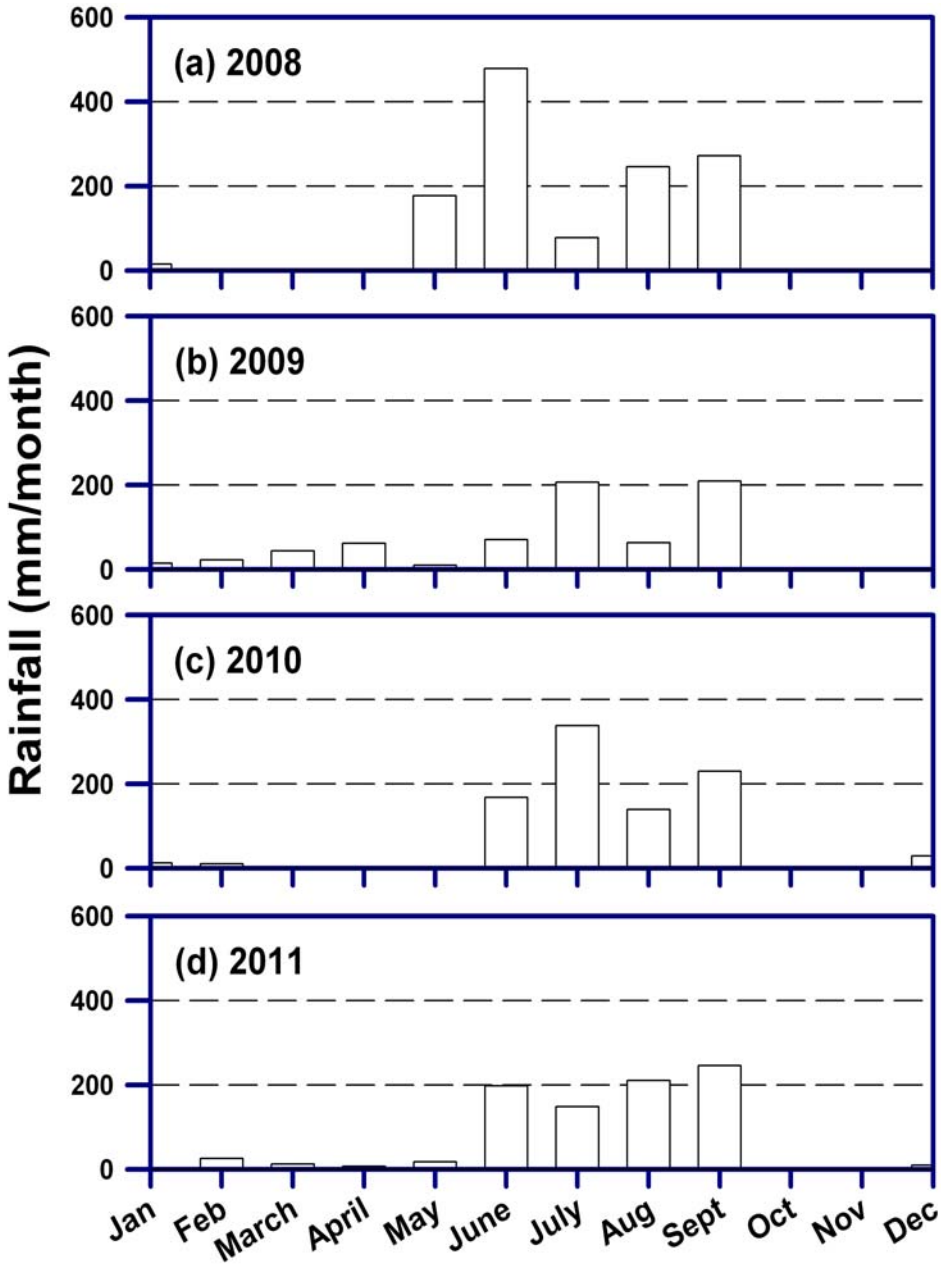

Figure 3.4: Rainfall records over Patiala for the years from 2008–2011 suggest efficient cleaning of the ambient atmosphere during south-west monsoon.

In this chapter, integrated scenario from both the field-campaigns is presented based on the determination of EC, OC, WSOC, WSIS and PAHs in PM2.5 samples (n = 141).

3.3. Results and Discussion

Several studies have documented the composition of fine-particulate matter for bio- and fossil-fuel combustion [*Bond et al.*, 2004; *Fine et al.*, 2002; *Fraser et al.*, 2002b; *Harrison et al.*, 1996; *Rogge et al.*, 1998; *Schauer et al.*, 2002; *Simoneit*, 2002; *Venkataraman et al.*, 2005]. Furthermore, study on agricultural-waste burning emissions is limited, and mostly reported from chamber-based experiments [*Andreae and Merlet*, 2001; *Dhammapala et al.*, 2007; *Hays et al.*, 2005; *Jenkins et al.*, 1996; *Li et al.*, 2007]. However, the field evidence of these emissions in the ambient atmosphere is lacking in the literature. Present study was conducted to constrain on the chemical composition of fine particulate matter emitted from two distinct post-harvest agricultural-wastes burning of paddy- and wheat-residues under ambient atmospheric conditions.

As stated earlier, that north-northwestern part of the Indo-Gangetic Plain (IGP) experience emissions on a large scale from post-harvest paddy- and wheat-residue burning during October–November and April–May respectively. However, the emission from bio- and fossil-fuel combustion is a common practice on annual-basis in the entire IGP, with dominant contributions during December–March. As a consequence, the high aerosol loading in the lower atmosphere is a conspicuous feature in the IGP [*Rajput et al.*, 2011b; *Ram et al.*, 2010b; 2012; *Rengarajan et al.*, 2007; *Tripathi et al.*, 2005]. The present study is strategically conducted from an upwind location in the IGP (at Patiala) to characterize the chemical composition of two distinct agricultural-waste burning emissions from paddy- and wheat-residue. In addition, the chemical composition of carbonaceous aerosols from bio- and fossil-fuel combustion (December–March) is also represented. The absolute concentrations of EC, OC, WSOC, WSIS and PAHs in PM2.5 have been studied along with their relative abundances. Furthermore, fingerprinting of aerosol has been performed using the proxies such as OC/EC, WSOC/OC, nss-K^+/OC, nss-K^+/EC, nss-SO_4^{2-}/OC, ΣPAHs/EC and isomer ratios of PAHs. The initial sections in this chapter will deal only with the aspects related to the carbonaceous species (EC, OC, WSOC and PAHs). The discussion on characteristics of WSIS is made subsequently.

3.3.1 Inter-annual variability

3.3.1.1 Emissions from paddy-residue burning: October–November

As far as day/night variability in aerosol composition is concerned, the discussion is applicable only for the paddy-residue burning emissions, as the sampling was integrated for ~24 h in October–November '08 (day-night) and ~12 h (daytime) in October–November '10. Rest of the samples (in other periods) was collected only during daytime (Table 3.1).

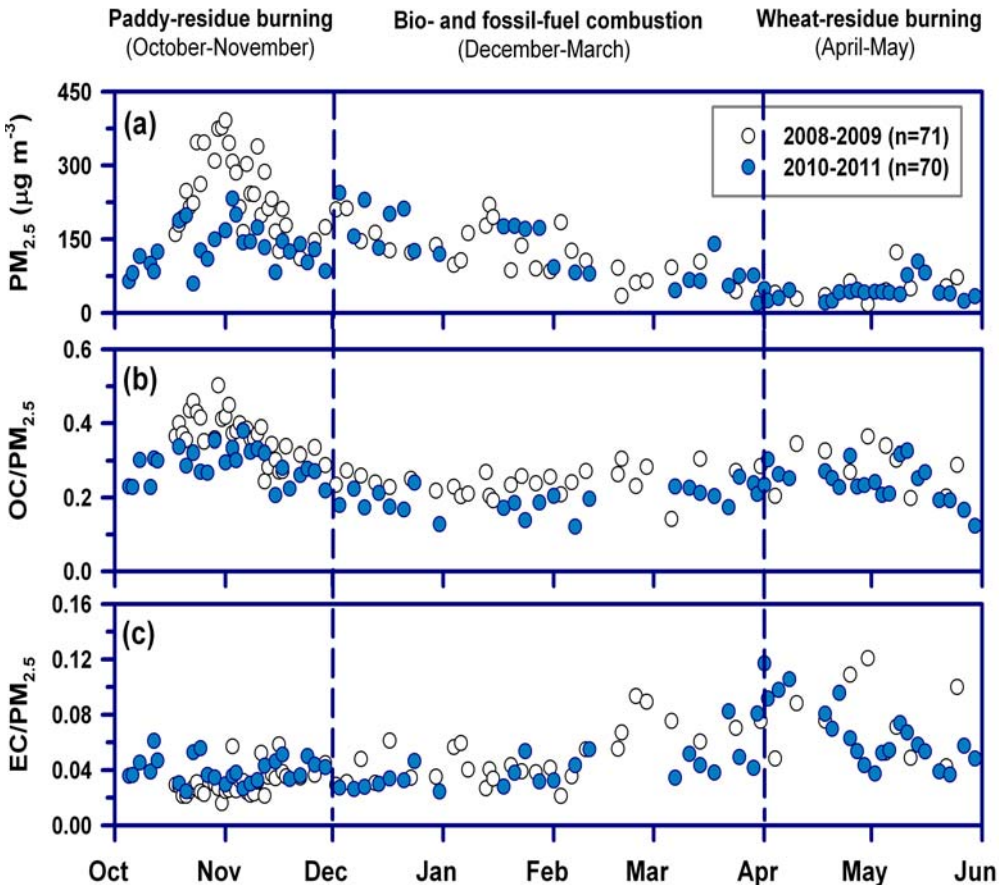

Figure 3.5: Inter-annual variability in: (a) PM2.5; (b) mass fraction of OC and (c) mass fraction of EC. The vertical dotted lines demarcate different emission practices.

PM2.5 concentration varied from 111–391 μg m^{-3} (Av: 246 ± 78) during October–November '08, whereas 60–232 μg m^{-3} (131 ± 44) during October–November '10 (Figure 3.5a). So, about a factor of 2 lower emissions of PM2.5 is

observed during the second-phase of sampling (for October–November ’10) as compared to that during the previous campaign in October–November ’08 [*Rajput et al.*, 2011b]. The mass fraction of OC ranged from 24–50% (Av: 37 ± 6%) and 21–38% (29 ± 5%) in October–November ’08 and ’10, respectively (Figure 3.5b).

However, the mass fraction of EC showed insignificant inter-annual variability from 2–6% (Av: 3 ± 1%) and 2–6% (Av: 4 ± 1%) in the respective periods (Figure 3.5c). Thus, relatively high aerosol loading during October–November ’08 as compared to that during October–November ’10 was observed from paddy-residue burning emission. The OC/EC ratio ranged from 5–26 (Av: 13 ± 5) and 4–14 (8 ±3) during paddy-residue burning in 2008 and 2010 respectively (Figure 3.6a).

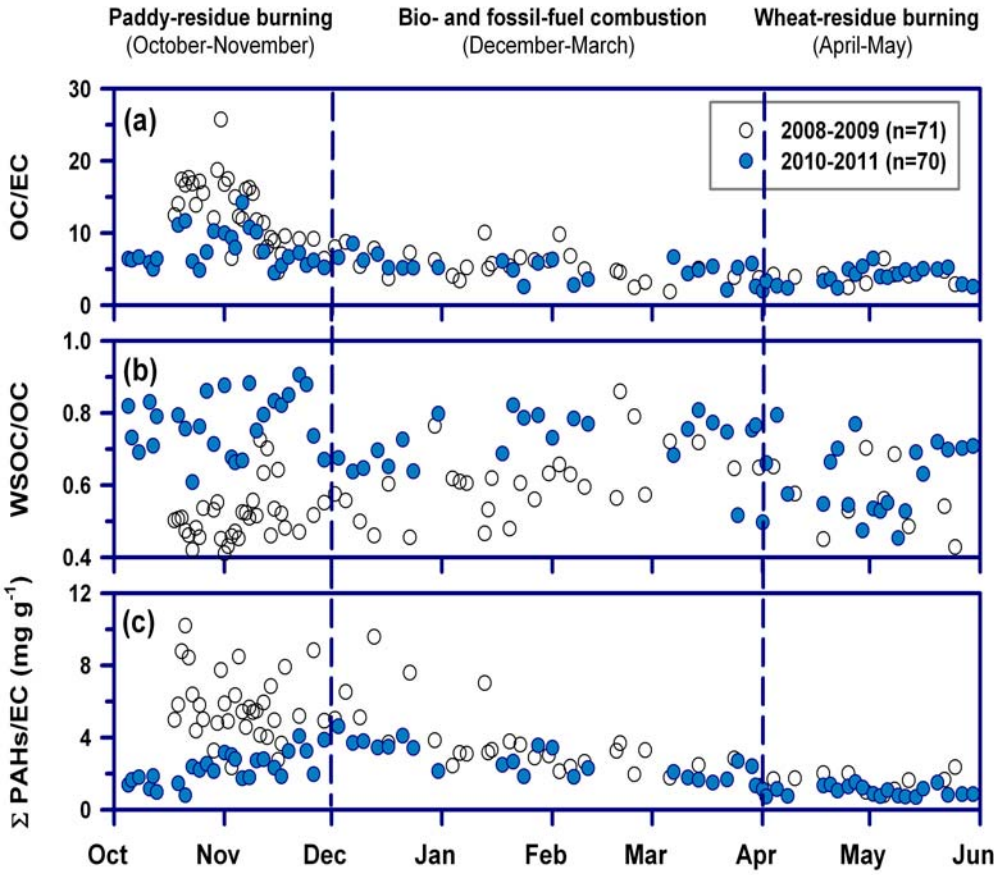

Figure 3.6: Inter-annual variability in the characteristic ratios of: (a) OC/EC (b) WSOC/OC and (c) ΣPAHs/EC. The vertical dotted lines demarcate different emission practices.

Interestingly, relatively low WSOC/OC ratio is associated with paddy-residue burning in October–November '08, varying from 0.41–0.73 (Av: 0.51 ± 0.07), as compared to 0.61–0.91 (0.77 ± 0.08) in 2010 (Figure 3.6b). The amount of the paddy-residue burnt in different years (October–November; in 2008 and 2010), the atmospheric chemistry/dynamics (boundary layer height) during day/night (Table 3.1) and/or the moisture content of biomass could be the probable factors for these variability.

The cause for inter-annual variability in the abundances of particulate matter due to moisture content is ruled out based on similar moisture content (range: 40–50%) in paddy-residues, for the periods October–November '08 and '10 (information on moisture content is provided by the "Punjab Agricultural University").

Furthermore, the amount of paddy-residue burnt in different years (October–November; post-monsoon season) can also influence the concentration ($\mu g/m^3$) of PM2.5 and the associated chemical constituents but could not affect the mass fractions of OC, EC and other constituents in PM2.5. Therefore the dominant factor for inter-annual variability in atmospheric abundances of particulate matter is attributed to the day/night variability and/or differences in the amount of paddy-residues burnt in the two years. Furthermore, the ΣPAHs concentration varied from 20–59 ng m^{-3} (Av: 39 ± 11) and 3–25 ng m^{-3} (12 ± 6) during October–November, in 2008 and 2010 respectively. So, about a factor of 3 lower emissions occurred during paddy-residue burning in 2010 as compared to that in 2008. This is also reflected in the variation of ΣPAHs/EC ratio (Figure 3.6c). The ΣPAHs/EC ratio ranged from 0.8–10.2 mg g^{-1} (5.7 ± 1.8) and 0.8–4.1 mg g^{-1} (2.3 ± 0.9).

However, the ΣPAHs/OC ratio looks similar, varying from 0.26–0.96 mg g^{-1} (Av: 0.48 ± 0.17) and 0.07–0.74 mg g^{-1} (0.33 ± 0.16) in the year 2008 and 2010. Thus, the EC being a conservative constituent, can be used for normalization to assess for the chemical reactivity of organic compounds (such as for the PAHs). In contrast, normalization of a chemical constituent with OC serve to represent its concentration profile from the emission source (Table 3.2).

3.3.1.2 Emissions from bio- and fossil-fuel combustion: December–March

Ambient concentration and composition of PM2.5 do not exhibit significant variability when compared for December '08–March '09 and December '10–March '11 (wintertime). And therefore, the data set is averaged for both the wintertime period (December–March) and represented for their emissions from bio- and fossil-fuel combustion in the further discussion. The concentration of PM2.5 exhibit insignificant inter-annual variability (range: 19–244 μg m^{-3}; Av: 124 ± 58) during December '08–March '09 and December '10–March '11 (Figure 3.5a). The mass fraction of OC and EC in PM2.5 and OC/EC ratio also exhibit insignificant inter-annual variability; OC/PM2.5: ~22 ± 4%, EC/PM2.5: ~5 ± 2% and OC/EC: 5.4 ± 1.9 (Figure 3.5b, 3.5c and 3.6a). Moreover, the WSOC/OC ratio, varying from 0.45–0.86 in both the periods during December '08–March '09 and December '10–March '11, constitute on average 0.66 ± 0.10 (Figure 3.6b). Furthermore, the ΣPAHs concentration varied between 2.1–47.9 ng m^{-3} (Av: 16.9 ± 10.4). The ΣPAHs/EC (range: 1.32–9.58; Av: 3.26 ± 1.61 mg g^{-1}) and ΣPAHs/OC (range: 0.22–1.22; Av: 30.62 ± 0.21 mg g^{-1}) ratios also look similar during the two campaigns in 2008 and 2010 (Figure 3.6c, Table 3.2).

3.3.1.3 Emissions from wheat-residue burning: April–May

PM2.5 concentration varied from 18–123 μg m^{-3} (Av: 53 ± 29) during April–May, 2009, whereas 22–105 μg m^{-3} (48 ± 20) during April–May, 2011 (Figure 3.5a). The concentration of PM2.5 looks similar during the two periods of wheat-residue burning emissions in April–May, 2009 and 2011. The wheat-residue (with moisture content: < 5%) is burnt in open agricultural-fields under prevailing dry weather conditions during April–May (regional summertime: 22–41 ˚C). The mass fractions of OC and EC in PM2.5 and OC/EC ratios also exhibit insignificant inter-annual variability (Figure 3.5b, 3.5c, 3.6a); OC/PM2.5 (range: 19–36%; Av: 26 ± 5%), EC/PM2.5 (range: 4–12%; Av: 6.9 ± 2.5%) and OC/EC ratio (range: 2.0–6.5; Av: 4.2 ± 1.2). Moreover, the WSOC/OC ratio, varied from 0.43–0.79 (0.59 ± 0.10) during the period April–May, in 2009 and 2011 (Figure 3.6b). The ΣPAHs concentration varied between 1.2–17.0 ng m^{-3} (Av: 4.1 ± 3.5).

The ΣPAHs/EC (range: 0.69–2.35 mg g^{-1}; Av: 1.21 ± 0.44 mg g^{-1}) and ΣPAHs/OC (range: 0.12–0.82 mg g^{-1}; Av: 0.32 ± 0.18 mg g^{-1}) ratios for wheat-residue burning emissions also look similar during April–May for the two studied years in 2009 and 2011 (Figure 3.6c).

3.3.1.4 Summary of the field-based concentrations of EC, OC, WSOC and ΣPAHs in PM2.5 during three different emission scenarios:

Table 3.2 provides a wealth of information on the mass concentration of PM2.5 and associated carbonaceous species (EC, OC, WSOC and PAHs), for two distinct agricultural-waste burning emissions of paddy- and wheat-residue. In addition, these mass fractions are also documented for the particulate emission from bio-fuels (Babool, Cowdung cake, Eucalyptus, Jujube and Shisham), and fossil-fuel combustion (Table 3.2). In general, PM2.5 mass concentration is relatively high (a factor of 4) during paddy-residue burning emissions (195 ± 87 μg m^{-3}) as compared to that from wheat-residue (50 ± 23 μg m^{-3}).

In between the two distinct periods of large-scale post-harvest biomass burning emissions from paddy- and wheat-residues, the bio- and fossil-fuel combustion is a dominant source of carbonaceous aerosols during December–March in the Indo-Gangetic Plain (IGP). The PM2.5 concentration (124 ± 58 μg m^{-3}) observed during the emissions from bio- and fossil-fuel combustion is relatively low as compared to that from paddy-residue burning emissions (195 ± 87 μg m^{-3}).

Relatively high mass contribution of OC (33 ± 7%) and, low from EC (3.5 ± 1.1%) in PM2.5, for paddy-residue burning emissions as compared to that from wheat-residue burning (OC/PM2.5: 26 ± 5 %; EC/PM2.5: 6.9 ± 2.5%) and bio- and fossil-fuel combustion (OC/PM2.5: 22 ± 4%; EC/PM2.5: 4.6 ± 1.8%) is revealed from this study (Table 3.2). The overall variability in WSOC/OC ratio exhibits similar characteristics for paddy-residue (0.63 ± 0.15); bio- and fossil-fuel (0.66 ± 0.10) and wheat-residue (0.59 ± 0.10), attributable to their dominant emissions from biomass burning (though of different types). Furthermore, ΣPAHs concentration was also relatively high (27.1 ± 16.7 ng m^{-3}) from paddy-residue burning followed by bio- and fossil-fuel combustion (16.9 ± 10.4 ng m^{-3}) and

Table 3.2: Aerosols concentration (Av ± sd; with range in parenthesis) and characteristic ratios for different emission scenarios

Aerosol	Paddy-residue (Oct–Nov; n=59)	Bio- & fossil- fuel (Dec–March; n=51)	Wheat-residue (April–May; n=31)
PM2.5 (μg m^{-3})	195 ± 87 (60–391)	124 ± 58 (19–244)	50 ± 23 (18–123)
OC/PM2.5 (%)	33 ± 7 (21–50)	22 ± 4 (12–31)	26 ± 6 (12–36)
EC/PM2.5 (%)	3.5 ± 1.1 (2–6)	4.6 ± 1.8 (2–9)	6.9 ± 2.5 (4–12)
OC/EC	10.6 ± 4.6 (4–26)	5.4 ± 1.9 (2–10)	4.0 ± 1.2 (2.0–6.5)
EC/TC	0.10 ± 0.04 (0.04–0.18)	0.17 ± 0.06 (0.09–0.35)	0.20 ± 0.05 (0.13–0.33)
WSOC/OC	0.63 ± 0.15 (0.41–0.91)	0.66 ± 0.10 (0.45–0.86)	0.59 ± 0.10 (0.43–0.79)
ΣPAHs (ng m^{-3})	27.1 ± 16.7 (3.2–59.1)	16.9 ± 10.4 (2.1–47.9)	4.1 ± 3.5 (1.2–17.0)
ΣPAHs/EC (mg g^{-1})	4.20 ± 2.28 (0.8–10.2)	3.26 ± 1.61 (1.32–9.58)	1.21 ± 0.44 (0.69–2.35)
PAHs (mg g^{-1} of OC)			
NAPH	0.006 ± 0.004	0.011 ± 0.015	0.006 ± 0.006
ACY	0.001 ± 0.001	0.002 ± 0.003	0.002 ± 0.003
2-BrNAPH	0.000 ± 0.001	0.001 ± 0.001	0.001 ± 0.004
ACE	0.001 ± 0.001	0.001 ± 0.001	0.001 ± 0.002
FLU	0.001 ± 0.001	0.002 ± 0.001	0.001 ± 0.001
PHEN	0.006 ± 0.004	0.015 ± 0.006	0.017 ± 0.014
ANTH	0.001 ± 0.001	0.003 ± 0.001	0.002 ± 0.002
FLA	0.013 ± 0.010	0.030 ± 0.011	0.018 ± 0.012
PYR	0.016 ± 0.010	0.032 ± 0.011	0.018 ± 0.013
BaA	0.013 ± 0.007	0.016 ± 0.009	0.006 ± 0.006
CHRY+TRIPH	0.036 ± 0.018	0.043 ± 0.025	0.019 ± 0.013
B[b,j,k]FLA	0.125 ± 0.067	0.180 ± 0.087	0.079 ± 0.049
BaP	0.042 ± 0.024	0.065 ± 0.028	0.026 ± 0.018
IcdP	0.069 ± 0.030	0.107 ± 0.036	0.062 ± 0.037
D[ah,ac]ANTH	0.009 ± 0.005	0.011 ± 0.007	0.004 ± 0.004
BghiP	0.071 ± 0.032	0.106 ± 0.034	0.073 ± 0.032
ΣPAHs	0.411 ± 0.182	0.624 ± 0.214	0.325 ± 0.175
PAHs isomer ratios			
ANTH/PHEN	0.25 ± 0.14	0.17 ± 0.07	0.13 ± 0.05
FLA/PYR	0.85 ± 0.08	0.93 ± 0.09	0.98 ± 0.13
BaA/(CHRY+TRIPH)	0.34 ± 0.08	0.39 ± 0.08	0.33 ± 0.15
BaP/B[b,j,k]FLA	0.35 ± 0.10	0.39 ± 0.11	0.35 ± 0.10
IcdP/BghiP	0.98 ± 0.12	1.02 ± 0.20	0.84 ± 0.17
ANTH/(ANTH+PHEN)	0.19 ± 0.08	0.15 ± 0.05	0.11 ± 0.04
FLA/(FLA+PYR)	0.46 ± 0.02	0.48 ± 0.02	0.50 ± 0.03
IcdP/(IcdP+BghiP)	0.49 ± 0.03	0.50 ± 0.05	0.45 ± 0.05

wheat-residue burning emissions (4.1 ± 3.5 ng m^{-3}).

This suggests, that the moist combustion of paddy-residue (moisture content: 40–50%) with relatively poor combustion-efficiency is the primary cause for the high emissions of OC and ΣPAHs, along with lower fraction of EC.

3.3.2 Estimation of primary- and secondary-organic carbon

Particulate organic carbon contains a variety of compounds with a wide range in their volatility. This leads to their occurrence in both the gaseous and particulate phases, enhancing the complications in demarcating between the primary and secondary OC (POC and SOC). Strictly speaking, SOC starts its atmospheric life in gas phase as a VOC, undergoes one or more chemical transformations in the gas phase to a less volatile compound, and finally transfers to the particulate phase by condensation or nucleation. Therefore the term SOC implies both a gas-phase chemical transformation and a change of phase.

Organic compounds that are vapors at the high-temperature conditions of the exhaust of a combustion source and subsequently condense to the particulate phase as the emissions cool are considered as primary because they have not undergone chemical reaction in the gas phase. By the same analogy, organic compounds in an emitted particle are considered primary even if the compounds eventually undergo chemical change in the particulate phas e because these compounds have not undergone a change in phase [*Seinfeld and Pandis*, 2006].

Evaluation of the primary and secondary components of aerosol OC have been difficult. Lack of a direct chemical analysis method for the identification of either of these OC components has led to several indirect methods. The simplest approach to estimating the contributions of primary and secondary sources to measured particulate OC is the EC tracer method.

The gas-phase conversion of volatile organic compound (VOC) has been considered as the major pathway for the formation of secondary organic aerosol (SOA) [*Chan et al.*, 2009; *Miyazaki et al.*, 2007; *Pio et al.*, 2007; *Rajput et al.*, 2011b; *Weber et al.*, 2007; *Zhang and Ying*, 2012].

Table 3.3: Number of data points grouped by lowest OC/EC ratio for different emissions to determine the primary OC in aerosols

% of max OC/EC ratio	Number of data		
	Paddy-residue (October–November)	Bio- and fossil-fuel (December–March)	Wheat-residue (April–may)
5.0	0	0	0
10.0	0	0	0
20.0	4	1	0
30.0	18	5	0
40.0	11	7	5
50.0	9	7	3

In addition, a significant fraction of SOA can also be derived from particulate OC produced from biomass burning vis-à-vis fossil-fuel combustion during chemical processing of aerosols. The EC-tracer method has been used for estimating the primary contribution of organic carbon from its emission source [*Cabada et al.*, 2004; *Cao et al.*, 2007]. Briefly, the method involves the determination of OC/EC primary ratio (source value), utilizing the EC-OC data in samples grouped with low OC/EC ratio (low photo-chemical activity; Table 3.3). The EC-OC data set in aerosols, grouped by samples with lowest 40% of the OC/EC ratio (for a quite significant number of data points, exception being for the wheat-residue burning period), is used to determine the contribution of primary organic carbon (POC). The estimation of primary- and secondary-organic carbon (POC and SOC) can be expressed mathematically as:

$$POC = EC * \left(\frac{OC}{EC} \right)_{\mathrm{Pr}imary} \tag{3.1}$$

$$SOC = OC - POC \tag{3.2}$$

The $(OC/EC)_{Primary}$ can be obtained from the slope of the OC-EC plot (Figure 3.7a, b, c). Here, OC represents the total organic carbon determined on EC-OC analyzer. The underlying and most reliable assumption in using these equations is that the EC has only primary origin. Accordingly, the highest primary OC/EC ratio was observed during paddy-residue burning (6.98; R^2 = 0.78), followed by 2.69 (R^2 = 0.68) from bio- and fossil-fuel combustion and wheat-

residue burning emissions (2.27; R^2 = 0.94, p<0.0001). Subsequently, the contribution of POC and SOC in aerosols is calculated using the above equations (3.1, 3.2).

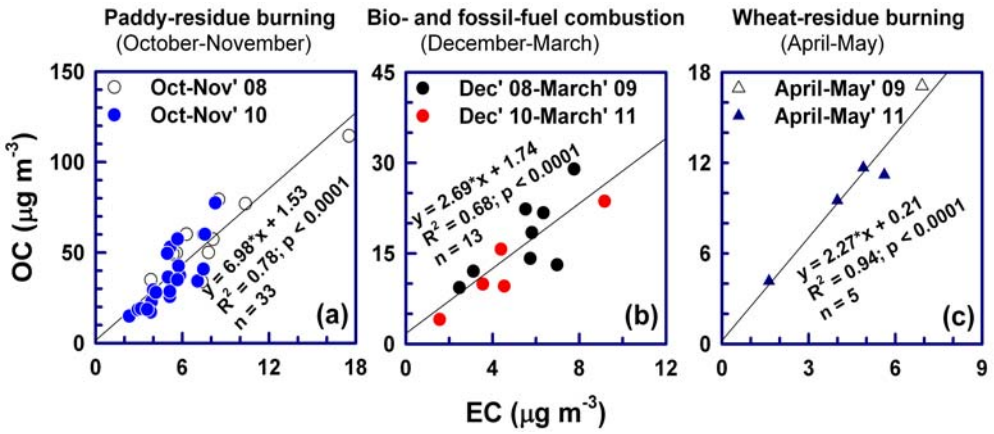

Figure 3.7: The OC and EC concentrations in aerosols with lowest 40% of OC/EC ratio are plotted to obtain primary organic carbon (POC).

The percentage contribution of primary carbonaceous species (POC+EC; primary organic carbon and elemental carbon) to total carbon in aerosols (TC = POC+SOC+EC; secondary organic carbon is referred to as SOC) is about 80% from paddy-residue burning, 63% from bio- and fossil-fuel combustion and 70% from wheat-residue burning emissions (Figure 3.8). In contrary, the SOC component has varying contributions from 20–37%, with highest (36.6%) during bio- and fossil-fuel combustion (December–March). Present study reveals that > 60% of the particulate carbon is derived from primary emission sources (Figure 3.8). Using this approach (of EC tracer method), the SOC in Western Pennsylvania during summer (July 2001) has been estimated to be around 35% of the OC [*Cabada et al.*, 2004]. Assessing the carbonaceous aerosol characteristics from 14-Chinese cities [*Cao et al.*, 2007], that covers northern- and southern-China, has revealed that ~25% of TC (total carbon: OC+EC) is SOC during winter (January), in contrast to enhanced contribution of SOC to TC (~35–40%) during the summer (June–July). The contribution of EC to TC over the northern- and southern-China has been reported to be ~20%, both during winter and summer [*Cao et al.*, 2007].

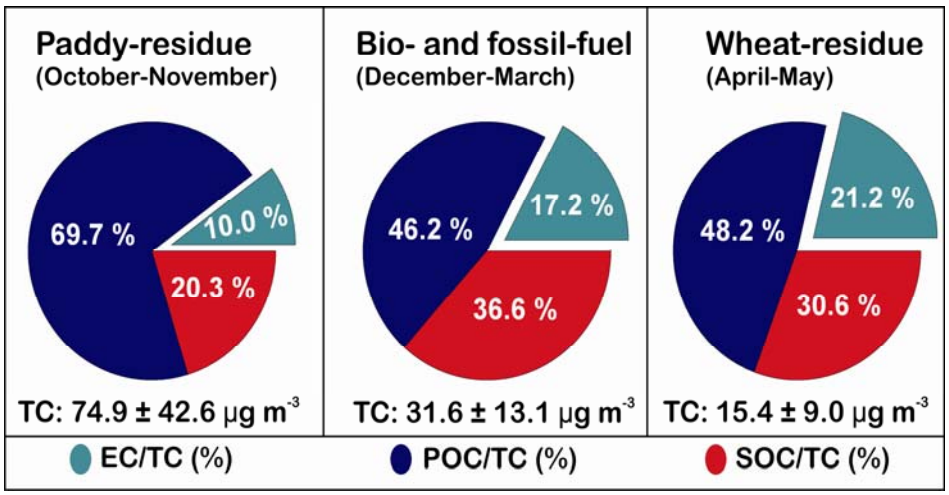

Figure 3.8: Percentage contribution of EC (elemental carbon), POC (primary organic carbon) and SOC (secondary organic carbon) to TC (carbonaceous aerosol) during different emission scenarios.

An study assessing the carbonaceous aerosols from urban and rural areas in Europe, suggests that 50–65% of OC is SOC during summer and 17% during winter in urban Europe, in contrast to 78% of SOC to OC contribution during summer in rural Europe [*Castro et al.*, 1999]. An study assesing the carbonaceous aerosols during wintertime (December–March) from different locations in the IGP (Hisar, Kanpur and Allahabad) has reported that ~30% of the OC is SOC [*Ram and Sarin*, 2010]. Another study from Manora Peak in Central Himalaya, has reported the contribution of SOC to OC of about 30% during winter (December–March), 48% in summer (April–June), 37% in monsoon (July–September) and 20% in post-monsoon (October–November) [*Ram et al.*, 2010a].

3.3.3 Water-soluble OC and the SOA

[*Saxena and Hildemann*, 1996] defined water-soluble organic compounds as those having the solubilities > 1 g/100 g water. They also provided a comprehensive list of water-soluble organic compounds that might be present in atmospheric aerosol, based on their solubility and reported occurrence, if available. Several compounds, including monocarboxylic acids and alcohols up to C4, diols and triols up to C7, or multifunctional acids such as lactic acid are completely miscible with water. The distinction between water-soluble and

insoluble species is based on the solubility of the parent compounds; it should be noted that neutralization by alkaline ions can easily render a water-insoluble compound water-soluble. Furthermore, it has also been reported by them that methanol dissolves a much wider range of organic species than water. The most frequently identified water-soluble species in atmospheric aerosols are low molecular weight dicarboxylic acids, with minor amounts of ketoacids and dicarbonyls, yet they account for only 5–20% of WSOC in urban aerosol. Therefore, there is a large gap in the characterization of the major fraction of WSOC.

Ambient concentration of WSOC (Figure 3.6b; 3.8a, b, c) varied from 11.6–103.6 μg m^{-3} (Av: 38.9 ± 17.8) during paddy-residue burning (October–November), from 3.0–32.2 μm^{-3} (Av: 16.9 ± 6.9) during bio- and fossil-fuel combustion (December–March) and from 3.2–25.6 μg m^{-3} (Av:7.7 ± 4.6) during wheat-residue burning emissions (April–May). However, significant number of data points falling above the 1:1 line indicates biomass burning emission to be a significant primary source for the WSOC (Figure 3.9a, b, c).

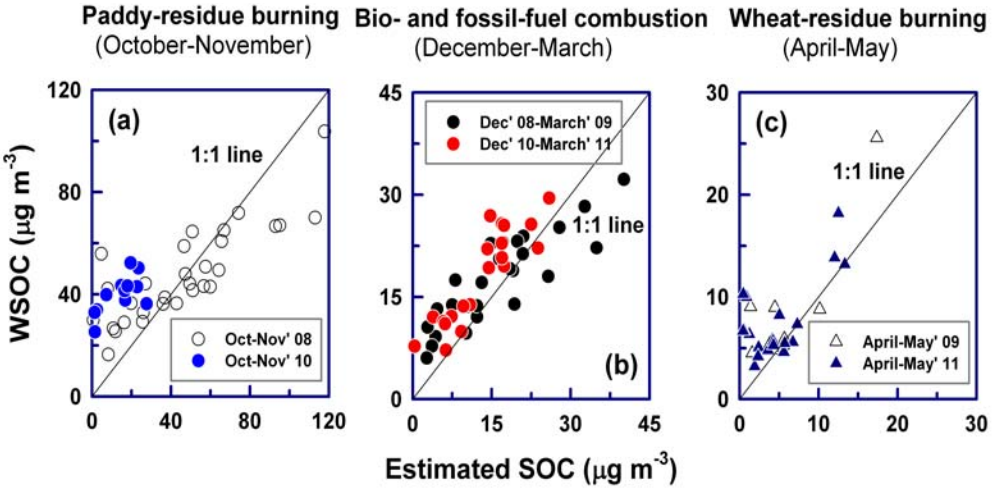

Figure 3.9: Scatter plot of secondary OC (SOC) and WSOC in aerosols during: (a) paddy-residue burning; (b) bio- and fossil-fuel combustion and (c) wheat-residue burning.

The percentage contribution of water soluble-OC (referred to as WSOC/OC; Figure 3.10) is nearly 60% and the remaining fraction of ~40% is

water-insoluble organic carbon (referred to as WIOC/OC). The information on the concentration of WSOC and its relative contribution in OC is reported for the first in this study, from post-harvest agricultural-waste burning emissions (Figure 3.10). In other words, even being the dominant contributor of the OC, such information in the literature on WSOC from biomass burning emissions is absolutely lacking. However, the WSOC data from fossil-fuel combustion sources is available in the literature, for example [*Kondo et al.*, 2007].

Radiocarbon analysis on WSOC extract, from metropolitan Atlanta (Southeastern US) during summer, suggest that 70–80% of the WSOC to be secondary, formed from biogenic emissions of VOC [*Weber et al.*, 2007]. Earlier studies in wintertime (December–March) from different locations in the IGP (Hisar, Kanpur, Allahabad) have estimated about 40% of OC to be SOC [*Ram and Sarin*, 2010; *Ram et al.*, 2010b; *Rengarajan et al.*, 2007].

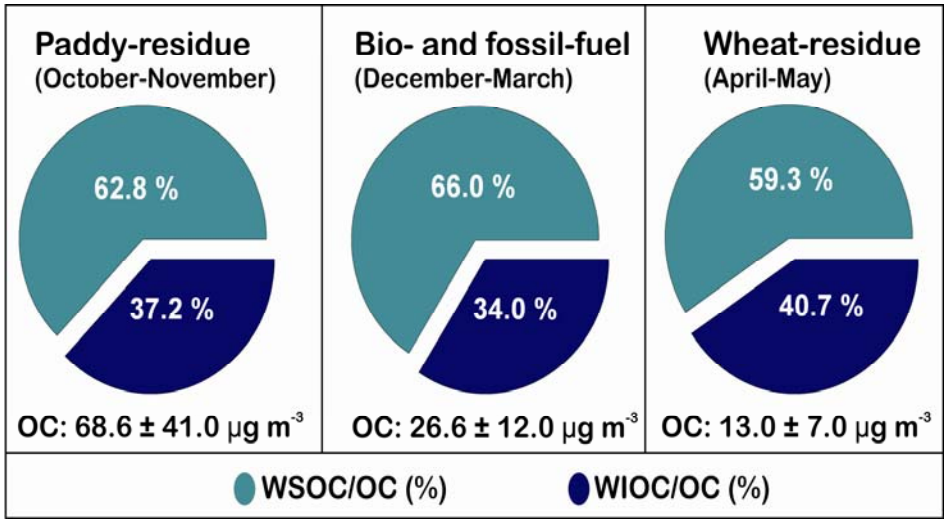

Figure 3.10: Mass closures of organic carbon (OC = WSOC+WIOC), where WSOC and WIOC are referred for water soluble- and water insoluble-organic carbon.

3.3.4 Correlation analysis of particulate ΣPAHs with EC and OC

The ΣPAHs and EC are produced only from the emission sources (primary origin). In addition, OC can be produced within the atmosphere, and thus, can have secondary contribution too. The correlation analysis of ΣPAHs with the EC

and OC content in aerosols is performed in order to infer its association with the EC and/or with organic carbon (Figure 3.11a–f).

The experimental data suggests that, in the aerosol samples with relatively low OC/EC and high EC/PM2.5 ratio (from wheat-residue burning), ΣPAHs correlate significantly with EC (R^2 = 0.64; Figure 3.11c). In rest of the two cases (paddy-residue burning and bio- and fossil-fuel combustion), when OC/EC and OC/PM2.5 ratios are high, a significant correlation (R^2 = 0.57 for paddy- and; 0.66 for bio- and fossil-fuel) exists between the ΣPAHs and OC concentrations (Figure 3.11d, e).

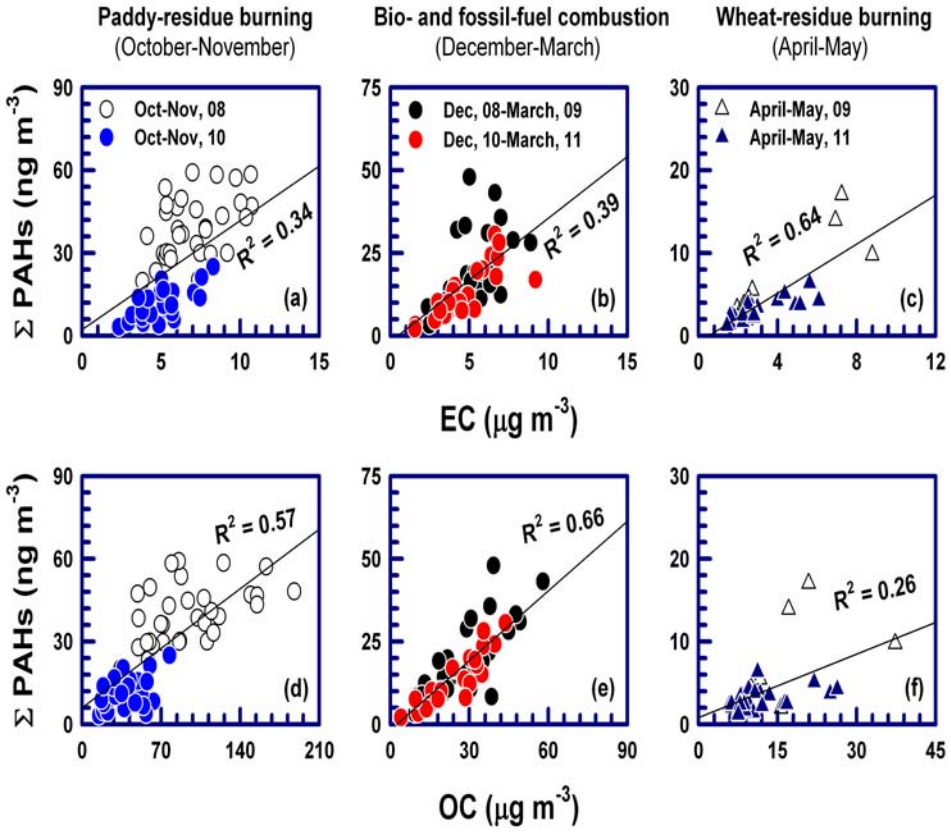

Figure 3.11: Scatter plot of: (a, b, c) EC versus ΣPAHs and (d, e, f) OC versus ΣPAHs for different emissions.

In view of emissions from different types of biomass burning vis-à-vis fossil-fuel combustion, the covariance and/or association of PAHs with the organic matter or elemental carbon appears to depend on the relative abundance of

OC/EC, EC/PM2.5 and OC/PM2.5.The percentage composition of individual PAHs to the ΣPAHs for paddy- and wheat-residues and bio- and fossil-fuel combustion is given in Figure 3.12. Accordingly, the PAHs (contributing > 70% of the ΣPAHs; involving 5-ring PAHs: BaP and B[b,j,k]FLA, and 6-ring PAHs: IcdP and BghiP) follow similar pattern in their percentage contribution: B[b,j,k]FLA (5-ring) > BghiP (6-ring) > IcdP (6-ring) > BaP (5-ring) for paddy-residue burning (October–November), bio- and fossil-fuel combustion (December–March) and wheat-residue burning (April–May) emissions.

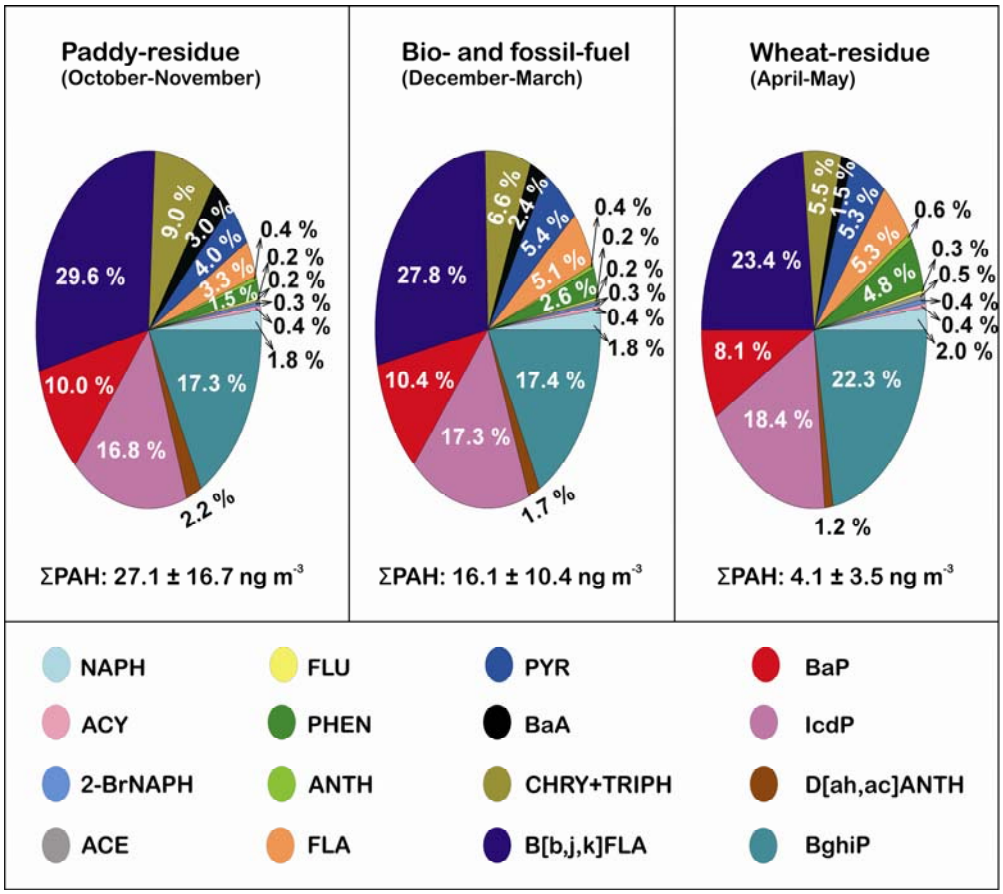

Figure 3.12: Percentage contribution of 16-PAHs for paddy- and wheat-residue burning and bio- and fossil-fuel combustion emissions.

3.3.5 Variability of particulate PAHs

The ambient concentration of 2- and 3-ring PAHs are low (Av: ≤ 0.3 and 0.5 ng m^{-3} respectively) and exhibit least variability for different emission

scenarios during the study period (October–May; Figure 3.13). However, a distinct pattern for 4-, 5- and 6-ring PAHs with the varying sources (biomass vis-à-vis fossil-fuel) is significantly pronounced; with highest concentration from paddy-residue burning (October–November), moderate from bio- and fossil-fuel combustion (December–March) and lowest from wheat-residue burning (April–May).

Accordingly, the 4-ring PAHs concentration for paddy-residue (Av: 5.3 ng m^{-3}), bio- and fossil-fuel combustion (3.2 ng m^{-3}) and, wheat-residue burning (0.7 ng m^{-3}) is evident from Figure 3.13. The concentrations of 5- and 6-ring PAHs are also relatively high (Av: 11.7 and 9.2 ng m^{-3}) during paddy-residue burning followed by lower concentrations associated with bio- and fossil-fuel combustion (7.1 and 5.6 ng m^{-3}) and wheat-residue burning emissions (1.4 and 1.6 ng m^{-3}).

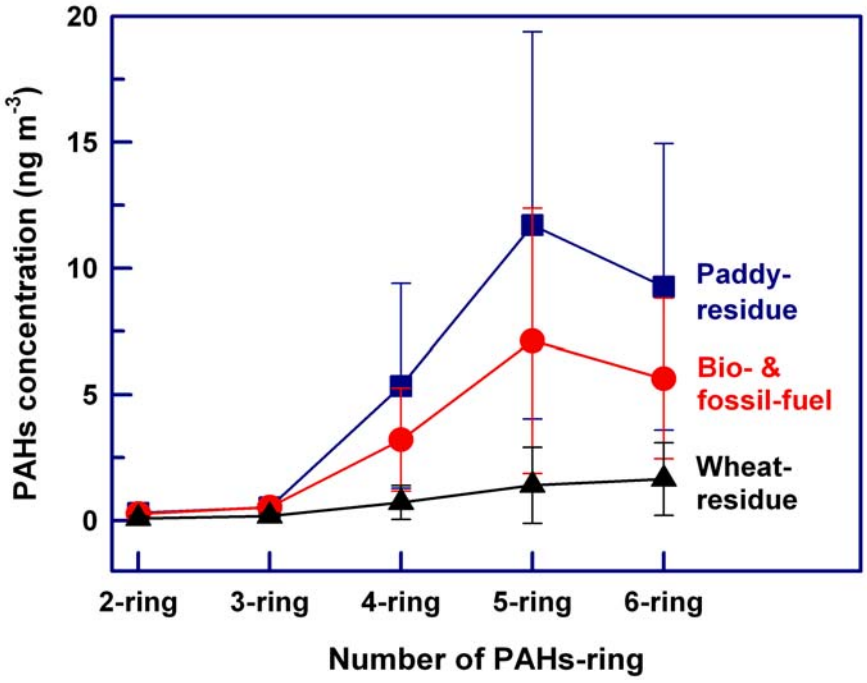

Figure 3.13: Variation of PM2.5-bound PAHs with varying number of aromatic rings for different emission sources.

The mass fraction analysis for low- (sum of 2- to 3-ring PAHs) and high-molecular weight PAHs (sum of 4- to 6-ring PAHs) in total PAHs (ΣPAHs) reveal the dominant contribution from heavier-PAHs (~95%) from all the three different

emissions (paddy-residue, bio- and fossil-fuel and, wheat-residue). One of the striking features of the data suggests that the high-molecular weight compounds are emitted relatively more from moist/poor combustion of biomass.

3.3.6 PAHs isomer ratios and source-characterization

Chemical characterization of emission sources though essential, but a challenging task in the atmospheric sciences, due to alteration in certain proxies during their chemical processing.

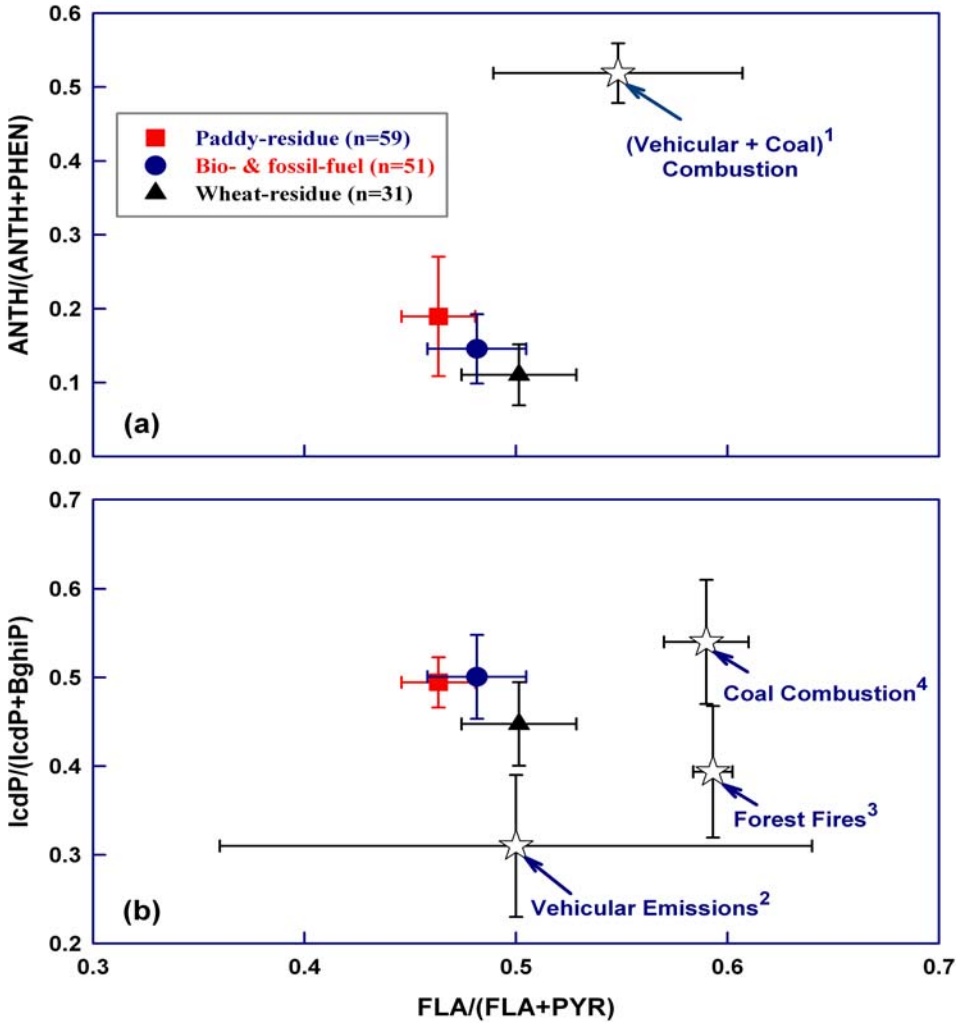

Figure 3.14: Cross plots of diagnostic ratios of PAH isomers: (a) FLA/(FLA+PYR) vs. ANTH/(ANTH+PHEN) and, (b) FLA/(FLA+PYR) vs. IcdP/(IcdP+BghiP). Other data source: [1, 2, 3, 4] [Khalili et al., 1995; Khillare et al., 2005a; Khillare et al., 2005b; Kirton et al., 1991; Li et al., 2010; Masclet et al., 1995; Rajput and Lakhani, 2008; Sharma et al., 2008].

In this regard, PAHs isomer ratios (listed in Table 3.2) have been conventionally used as a robust tracer to apportion their sources [*Yunker et al.*, 2002]. The suitability of various PAHs isomer ratios in assessing their sources has been evaluated in that study from the Fraser river basin. Using PAH ratios and total concentration data it was inferred that contamination sources shift from biomass (e.g. wood and grass) burning to vehicular emissions between remote and urban locations. In contaminated areas ratios show distinct signature for fossil-fuel combustion vis-à-vis biomass burning emission sources. It has been suggested to utilize multiple PAHs ratios for a robust interpretation [*Yunker et al.*, 2002].

Employing the PAHs isomer ratios, ANTH/(ANTH+PHEN) & IcdP/(IcdP+BghiP) against FLA/(FLA+PYR) in the cross plots (Figure 3.14), reveal that the characteristics of post-harvest biomass burning of paddy- and wheat-residues are distinctly different from fossil-fuel combustion sources. The PAHs isomer ratios from field-burning of paddy- and wheat-residues (under ambient atmospheric conditions), documented in this study provide a novel information on their source characterization (Table 3.2; Figure 3.14).

3.3.7 Ambient measurements versus chamber simulation:

3.3.7.1 Paddy-residue burning:

The field-burning of post-harvest paddy-residue is usually performed at very high moisture content (~40–50%) in northern India as compared to that in controlled chamber experiments of biomass (with moisture content: 7–10%) [*Hays et al.*, 2005; *Jenkins et al.*, 1996; *Sheesley et al.*, 2003]. Field-based (ambient; this study) mass fractions of OC and EC in PM2.5 from paddy-residue burning emissions are 33 ± 7% and 3.5 ± 1.1% respectively. Relatively high mass fraction of OC (63 ± 7%) and low fraction of EC (1.2 ± 0.1%) have been reported from chamber-based combustion experiments for paddy-residue [*Hays et al.*, 2005; *Sheesley et al.*, 2003].

The physical and chemical characteristics of particulate matter (PM2.5) emissions from chamber-based simulated agricultural fires (AFs) of residues of

two major grain crops, rice (*Oryza sativa*) and wheat (*Triticum aestivum L.*) has been reported recently [*Hays et al.*, 2005]. In the AF plumes, they observed predominantly accumulation mode (100–1000 nm) aerosols. The mean PM2.5 mass emission factors from wheat- and rice- residues are 4.7 ± 0.04 and 13.0 ± 0.3 g/kg of dry biomass, respectively.

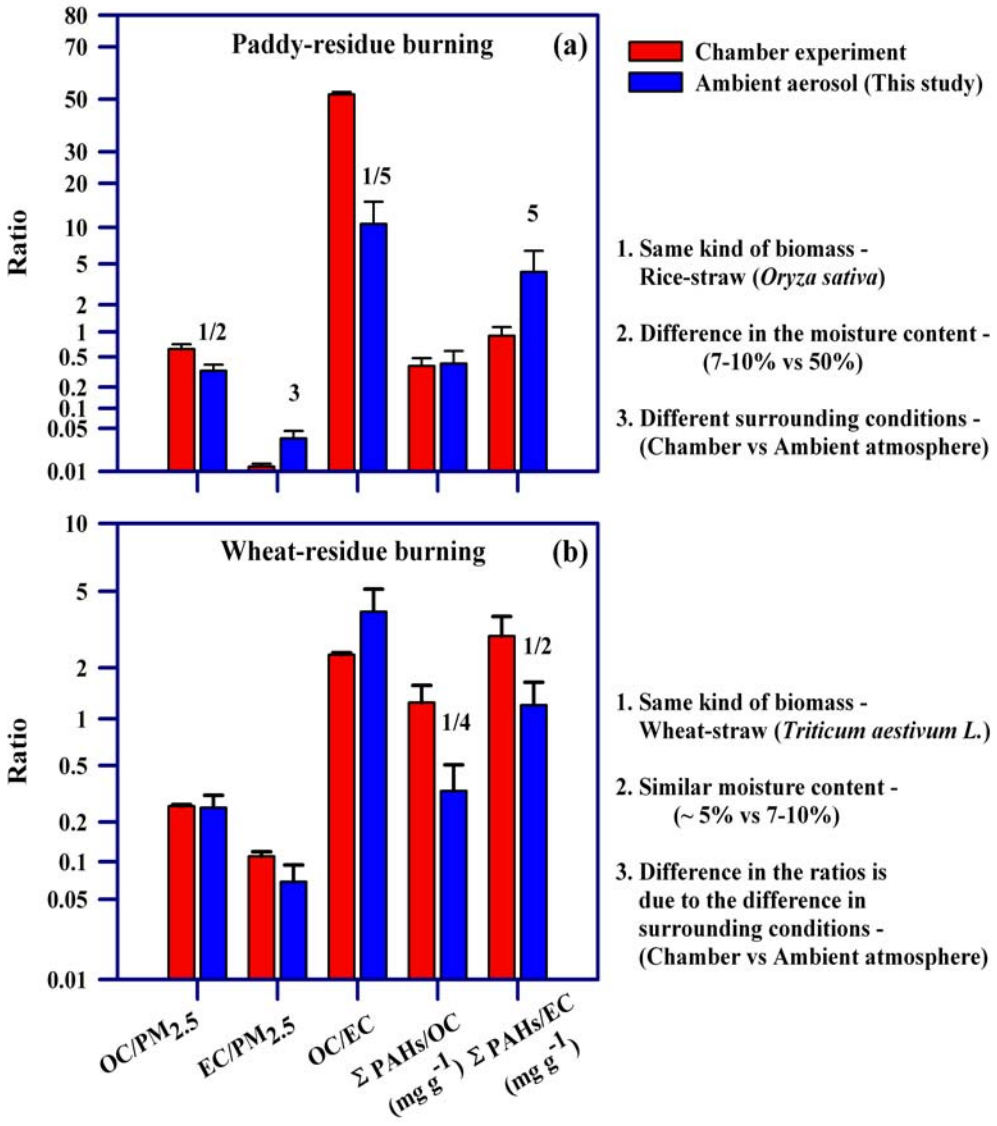

Figure 3.15: Comparison in relative abundances of carbonaceous species in ambient aerosol (this study) and that from chamber-experiment [Dhammapala et al., 2007; Hays et al., 2005; Li et al., 2007; Sheesley et al., 2003] for: (a) paddy- and (b) wheat-residue burning emissions.

The combustion-derived PM emissions from wheat-residue have been reported to be enriched in K (31% weight/weight, w/w) and Cl (36% w/w), whereas the PM emissions from rice-residue are largely carbonaceous (84% w/w). Compound specific analysis of PM2.5 solvent extracts identifies organic matter accounting up to 18% of the PM mass emissions. Hierarchical clustering of source test observations using molecular markers has indicated from their study that agricultural-fuels are distinct from other types of biomass. Furthermore, it was recognized that agricultural-waste burning emissions could significantly contribute to emission inventories at regional, national, and global scale.

The differences in OC/PM2.5 and EC/PM2.5 ratios, associated with field-based paddy-residue burning (this study with moisture content: ~50%) are about a factor of 2–3 (Figure 3.15a), as compared to that from controlled combustion in chamber experiments (moisture content: 7–10%). The OC/EC ratio (10.6 ± 4.6) associated with open burning of paddy-residue (this study) is lower by a factor of 5 when compared to that reported from chamber-experiment (52 ± 1). Thus, a significant difference in the OC/EC ratio reported from ambient and chamber experiment is revealed from this study. However, the ΣPAHs/OC ratio reported from this study (ambient) and that from chamber-experiment looks similar (~0.4 mg g^{-1}). In contrast, the ΣPAHs/EC ratio is about a factor of 5 higher for field-burning of paddy-residue (this study) as compared to that from chamber experiment (Figure 3.15a).

3.3.7.2 Wheat-residue burning:

During wheat-residue burning (under dry weather conditions; April–May), the moisture content of biomass is almost similar (~5%) to that simulated in chamber experiments (7–10%) [*Dhammapala et al.*, 2007; *Hays et al.*, 2005; *Jenkins et al.*, 1996; *Li et al.*, 2007]. The mass fractions of OC and EC in PM2.5 for wheat-residue burning are quite similar from ambient study (OC/PM2.5: 26 ± 5%; EC/PM2.5: 6.9 ± 2.5%) and that from chamber experiments (OC/PM2.5: 26 ± 1%; EC/PM2.5: 11 ± 1%), attributable to similarity in moisture content (~5% versus 7–10% respectively).

Furthermore, the OC/EC ratio (4.2 ± 1.2) from this study (ambient) is also near similar to that reported from chamber studies (2.4 ± 0.1). In contrast, the ΣPAHs/OC and ΣPAHs/EC ratios from ambient study (0.32 ± 0.18 mg g^{-1} and 1.21 ± 0.44 mg g^{-1}) are relatively low by a factor of 4 and 2 respectively as compared to that reported from chamber-experiment (Figure 3.15b).

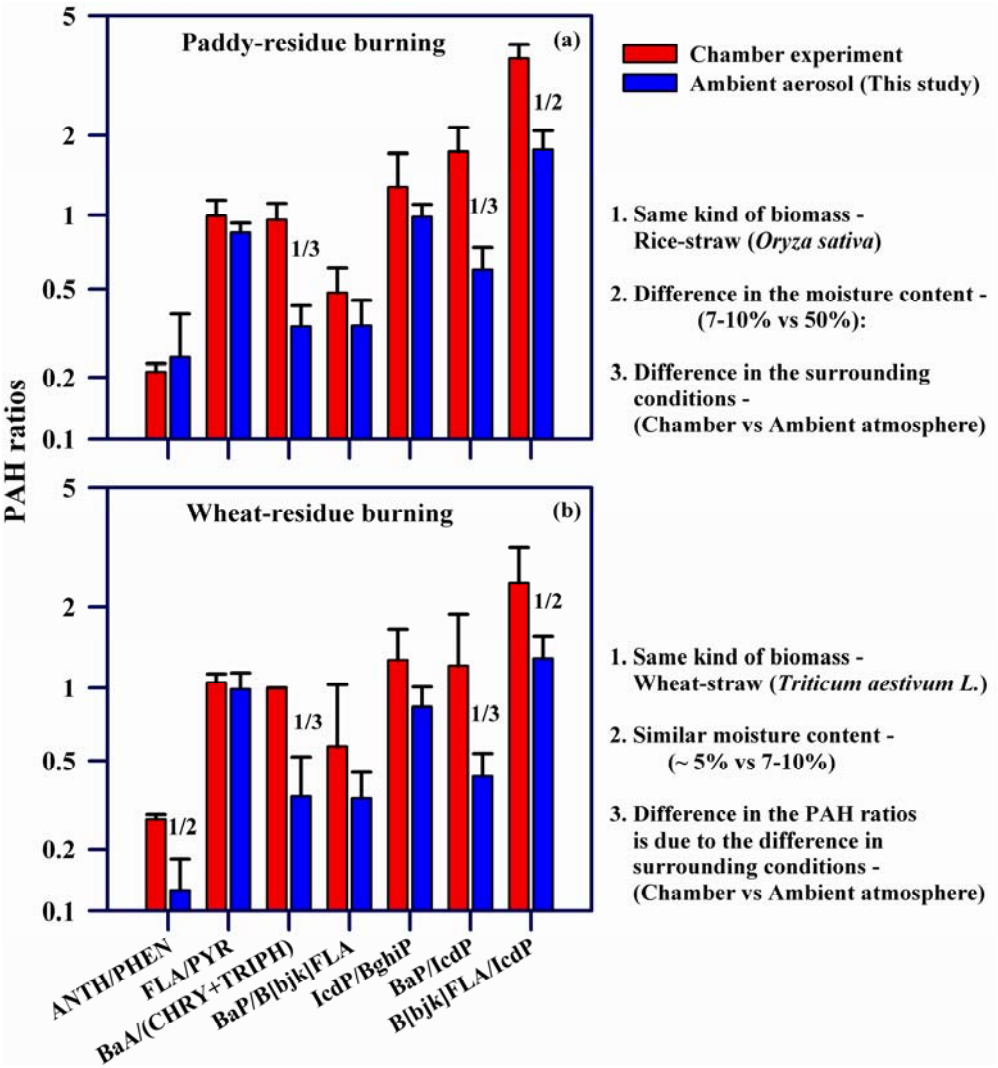

Figure 3.16: PAHs ratios in ambient aerosol (this study) and chamber-experiment [Dhammapala et al., 2007; Hays et al., 2005; Jenkins et al., 1996; Li et al., 2007; Sheesley et al., 2003] for: (a) paddy- and (b) wheat-residue burning emissions.

So far, it has been discussed that the differences in moisture content of paddy-residue and the type of biomass, paddy- vs. wheat-residue can have

pronounced effect on the OC/PM2.5, EC/PM2.5 and OC/EC ratios. The lower mass fractions of PAHs (ΣPAHs/OC and ΣPAHs/EC) observed in this study (ambient) as against the chamber experiments could be attributed to the chemically reactive nature of PAHs [*Chan et al.*, 2009; *Esteve et al.*, 2006; *Kaiser et al.*, 2011; *Lee et al.*, 2012; *Perraudin et al.*, 2007; *Rajput et al.*, 2011b; *Zhang and Ying*, 2012]. It is important to mention here that heterogeneous chemical reactivity of PAHs lowering their mass fractions (Figure 3.15b) is conspicuous for wheat-residue burning in this study (ambient aerosols), when compared to that from chamber-based experiments.

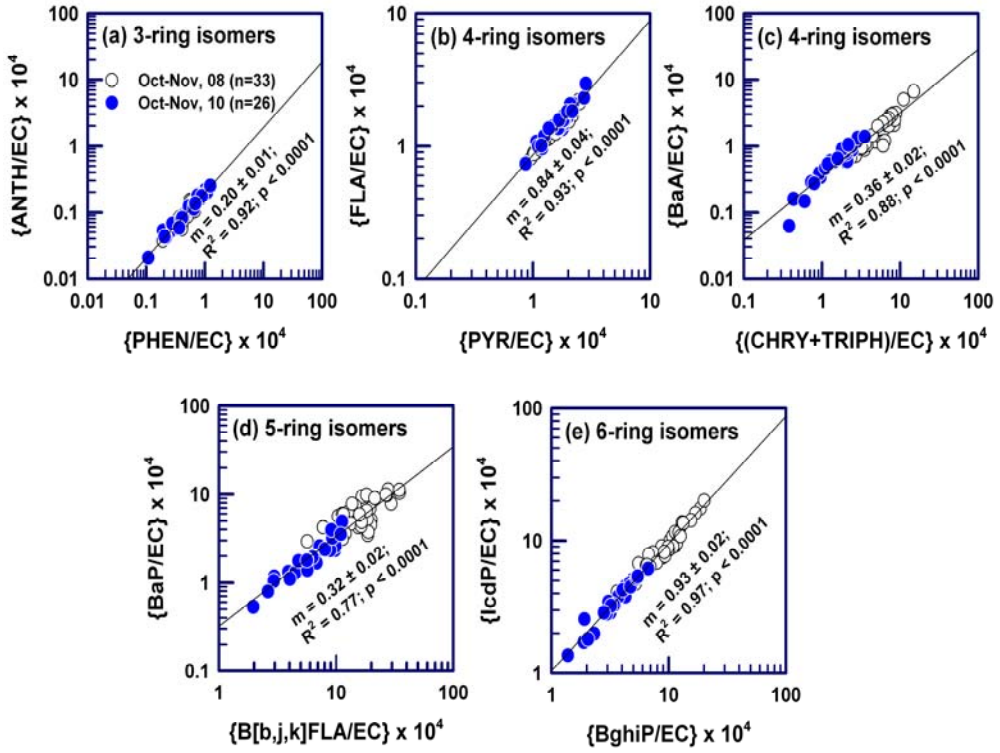

Figure 3.17: Scatter plot showing the relative reactivity of: (a) 3-; (b, c) 4-; (d) 5- and (e) 6-ring PAH isomers under ambient atmospheric conditions, for paddy-residue burning. Slope of the line represents relative rate constant.

However, the reactivity of PAHs affecting the ΣPAHs/OC and ΣPAHs/EC ratios is not obvious for field-burning of paddy-residue as compared to that from controlled combustion in chamber experiment, plausibly due to remarkable difference in the moisture content of biomass (ambient: ~50% vs. chamber: 7–

10%). The differences in the PAHs ratio between ambient (this study) and chamber-based experiment is represented in Figure 3.16a (paddy-residue) and Figure 3.16b (wheat-residue). The value over the ambient PAH ratios (from this study; blue bar, Figure 3.16) represents their ratio between chamber/ambient. For example, a value of 1/3 over BaA/(CHRY+TRIPH) represents that the ratio is 1/3rd in ambient aerosol as compared to that reported from chamber simulation (red bar).

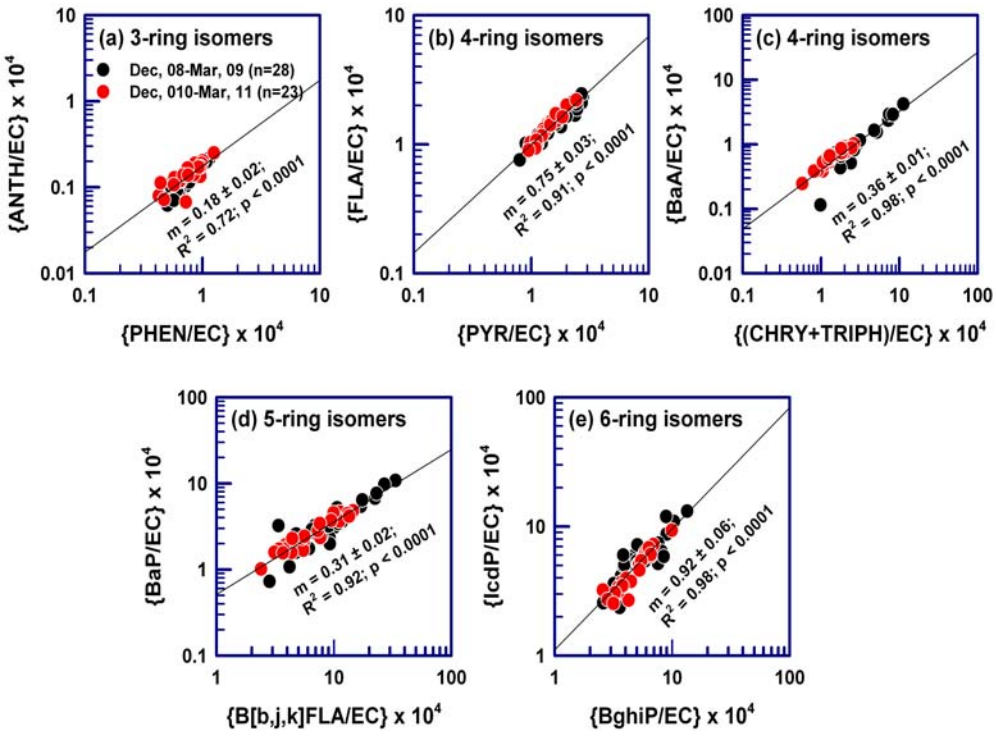

Figure 3.18: Scatter plot showing the relative reactivity of: (a) 3-; (b, c) 4-; (d) 5- and (e) 6-ring PAH isomers under ambient atmospheric conditions, for bio- and fossil-fuel combustion emission.

The relative rate constant of PAH isomers (5-pairs), from three distinct emission scenarios (under ambient atmospheric conditions), are shown in the Figures 3.17, 3.18 and 3.19. The summary is represented in Table 3.4.

The laboratory-based chemical rate constant for different PAHs with atmospheric oxidants (O_3, NO_X and OH radical), adsorbed on to silica (model for mineral dust) and graphite particles (model for soot), has been examined and

represented in a recent literature [Perraudin et al., 2007]. In general, PAHs when adsorbed onto silica has been found to exhibit relatively high reactivity as compared to when adsorbed onto the graphite particles. The heterogeneous reactivity for one of the most reactive PAHs, Benzo[a]pyrene (5-ring compound), has been inferred to be even ~100 times more as compared to that for the anthracene (ANTH), when adsorbed onto silica particles [Perraudin et al., 2007].

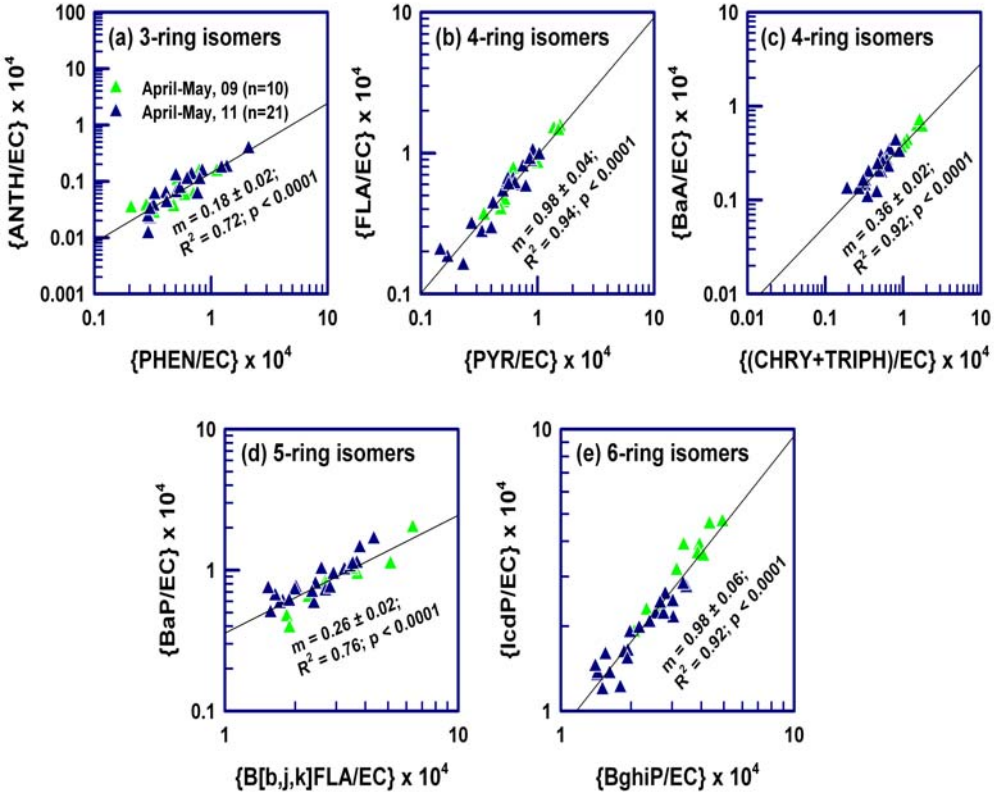

Figure 3.19: Scatter plot showing the relative reactivity of: (a) 3-; (b, c) 4-; (d) 5- and (e) 6-ring PAH isomers under ambient atmospheric conditions, for wheat-residue burning emissions.

High abundance of carbonaceous aerosols during the study period (October–May) and transport of mineral dust during wheat-residue burning period (April–May) from western India and north-west Desert regions to the northern India provided the opportunity to assess the chemical reactivity of PAHs and the relative rate constant of their isomers under ambient atmospheric conditions. For the same reason, the chemical reactivity of PAHs from wheat-residue burning (April–May) is expected to be relatively more (due to influence of mineral dust on

Table 3.4: Relative rate constants (Av ± 1σ) of PAH isomers for their heterogeneous reactivity in ambient aerosols

Relative rate constant (*K*)	Ambient Atmosphere[a]			Chamber study[b]						Relative reactivity[c]
	Paddy-residue	Bio- and fossil-fuel	Wheat-residue	(Onto Graphite)			(Onto silica)			
				OH	NO_2	O_3	OH	NO_2	O_3	
K_{PHEN}/K_{ANTH}	0.20 ± 0.01	0.18 ± 0.02	0.18 ± 0.02	1.1	0.51	0.24 ± 0.13	-	0.002 ± 0.001	0.16 ± 0.04	ANTH > PHEN
K_{PYR}/K_{FLA}	0.84 ± 0.04	0.75 ± 0.03	0.98 ± 0.04	1.00	1.76	1.32	-	0.61	3.93	FLA = PYR
$K_{(CHRY+TRIPH)}/K_{BaA}$	0.36 ± 0.02	0.36 ± 0.01	0.36 ± 0.02	-	-	-	-	-	-	BaA > (CHRY+TRIPH)
$K_{B[b,j,k]FLA}/K_{BaP}$	0.32 ± 0.02	0.31 ± 0.02	0.26 ± 0.02	-	-	-	-	-	-	BaP > B[*b,j,k*]FLA
K_{BghiP}/K_{IcdP}	0.93 ± 0.02	0.92 ± 0.06	0.98 ± 0.06	-	-	1.00 ± 0.49	-	1.32 ± 0.56	0.54 ± 0.14	IcdP ~ BghiP

[a]Present study.

[b] Laboratory-based relative rate constant for PAH isomers, adsorbed onto graphite and onto silica particles is also listed [*Perraudin et al.*, 2007].

[c]Inferred from this study; in ambient aerosols.

chemical reactivity of PAHs) as compared to that during rest of the study period. Heterogeneous reactions of PAHs have potential to alter surface characteristics of aerosol (more hygroscopic) through formation of nitro- and oxygenated-PAHs as secondary organic aerosols [Evagelpoulos et al., 2010; Kaiser et al., 2011; Perraudin et al., 2007]. Furthermore, such reactions are attributable for the low mass fraction of PAHs in ambient aerosols, when compared to that reported from chamber studies.

3.3.8 Inter-annual variability in WSIS for paddy-residue burning emissions

Chemical composition of water-soluble inorganic species (WSIS) in PM2.5 has been studied for two periods from October–November 2008 and October–November 2010 (Figure 3.20). During the October–November 2008, the ΣWSIS concentration varied from 31–92.2 (Av: 56.4 ± 17.2) μg m^{-3}. The ΣWSIS/PM2.5 ratio varied from 0.16–0.36 (Av: 0.24 ± 0.05). The mass fraction in ΣWSIS of: Na^+ varieds from 0.00–0.01 (0.01 ± 0.00); NH_4^+ varied from 0.13–0.26 (0.21 ± 0.04); K^+ varied from 0.04–0.16 (0.10 ± 0.04); Mg^{2+} varied from 0.000–0.002 (0.001 ± 0.001); Ca^{2+} varied from 0.000–0.012 (0.005 ± 0.004); Cl^- varied from 0.00–0.11 (0.02 ± 0.03); NO_3^- varied from 0.22–0.41 (0.31 ± 0.05) and SO_4^{2-} varied from 0.22–0.47 (0.35 ± 0.07).

During the October–November 2010, the ΣWSIS concentration varied from 8.7–67.4 (Av: 28.1 ± 11.4) μg m^{-3}. The ΣWSIS/PM2.5 ratio varied from 0.11–0.34 (Av: 0.22 ± 0.06). The mass fraction in ΣWSIS of: Na^+ varied from 0.01–0.02 (0.01 ± 0.00); NH_4^+ varied from 0.12–0.23 (0.18 ± 0.02); K^+ varied from 0.07–0.24 (0.13 ± 0.05); Mg^{2+} varied from 0.000–0.003 (0.001 ± 0.001); Ca^{2+} varied from 0.000–0.019 (0.007 ± 0.005); Cl^- varied from 0.00–0.08 (0.01 ± 0.02); NO_3^- varied from 0.02–0.29 (0.11 ± 0.08) and SO_4^{2-} varied from 0.41–0.69 (0.56 ± 0.08).

The temporal variability of water-soluble ions for paddy-residue burning emissions during October–November for 2008 and 2010 is shown in Figure 3.20. The mass fraction of primary ions (Na^+, K^+, Mg^{2+}, Ca^{2+} and Cl^-) in water soluble inorganic species (WSIS) exhibit insignificant variability. In contrast, the

secondary water-soluble species (NO_3^- and SO_4^{2-}) mass fractions exhibit significant inter-annual variability (Figure 3.20). However, a secondary water-soluble inorganic species (NH_4^+) mass fraction also does not varied significantly during the two paddy-residue burning emissions.

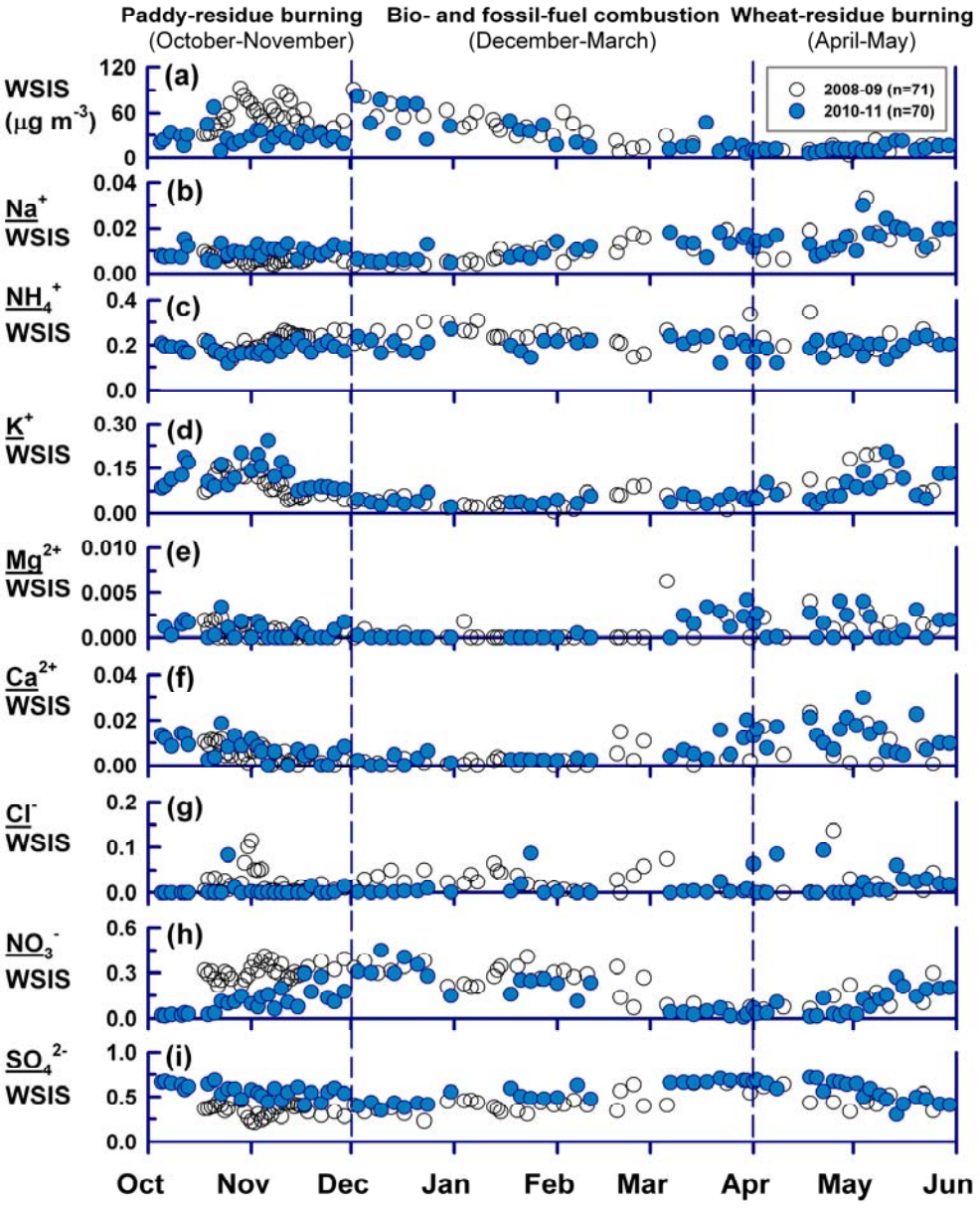

Figure 3.20: Variability in atmospheric abundances of: (a) water-soluble inorganic species (WSIS); and mass fraction of (b) Na^+; (c) NH_4^+; (d) K^+; (e) Mg^{2+}; (f) Ca^{2+}; (g) Cl^-; (h) NO_3^- and (i) SO_4^{2-} for different emission scenario.

It is relevant to reiterate here that during paddy-residue burning (October–November 2008), aerosol sampling was integrated for ~24 h (day-night). Rest of the samples for paddy- (October–November 2010) and wheat-residue burning (April–May 2009 and 2011) was collected for ~12 h (daytime). And therefore, the daytime photo-chemistry and nighttime reactions in context to the inter-annual variability is applicable only for aerosols from paddy-residue burning emissions during October–November in 2008 and 2010.

3.3.9 Inter-annual variability in WSIS for bio- and fossil-fuel combustion emission

Chemical composition of water-soluble inorganic species (WSIS) in PM2.5 have been studied for two periods from December '08–March '09 and December '10–March '11 (Figure 3.20). During the December '08–March '09, the ΣWSIS concentration varied from 8–91 (Av: 41 ± 22) μg m^{-3}. The ΣWSIS/PM2.5 ratio varied from 0.19–0.46 (Av: 0.33 ± 0.09). The mass fraction in ΣWSIS of: Na^+ varied from 0.00–0.05 (0.01 ± 0.01); NH_4^+ varied from 0.15–0.34 (0.24 ± 0.04); K^+ varied from 0.00–0.09 (0.04 ± 0.02); Mg^{2+} varied from 0.000–0.006 (0.000 ± 0.001); Ca^{2+} varied from 0.000–0.052 (0.004 ± 0.010); Cl^- varied from 0.00–0.07 (0.03 ± 0.02); NO_3^- varied from 0.06–0.41 (0.25 ± 0.10) and SO_4^{2-} varied from 0.23–0.65 (0.42 ± 0.11).

During the December '10–March '11, the ΣWSIS concentration varied from 6–82 (Av: 35 ± 23) μg m^{-3}. The ΣWSIS/PM2.5 ratio varied from 0.15–0.36 (Av: 0.26 ± 0.06). The mass fraction in ΣWSIS of: Na^+ varied from 0.00–0.02 (0.01 ± 0.00); NH_4^+ varied from 0.12–0.27 (0.20 ± 0.03); K^+ varied from 0.02–0.07 (0.04 ± 0.01); Mg^{2+} varied from 0.000–0.004 (0.001 ± 0.001); Ca^{2+} varied from 0.000–0.020 (0.005 ± 0.005); Cl^- varied from 0.00–0.09 (0.01 ± 0.02); NO_3^- varied from 0.01–0.45 (0.19 ± 0.14) and SO_4^{2-} varied from 0.35–0.71 (0.54 ± 0.12).

The temporal variability of water-soluble inorganic ions for bio- and fossil-fuel combustion emissions, occurring on annual and seasonal basis in the IGP, during December–March is shown in Figure 3.20. The mass fraction of primary (Na^+, K^+, Mg^{2+}, Ca^{2+} and Cl^-) and secondary water-soluble ionic species

(NH_4^+, NO_3^- and SO_4^{2-}) exhibit insignificant inter-annual variability (Figure 3.20 a–i).

3.3.10 Inter-annual variability in WSIS for wheat-residue burning emissions

Chemical composition of water-soluble inorganic species (WSIS) in PM2.5 has been studied for two periods from April–May 2009 and April–May 2011 (Figure 3.20). During the April–May 2009, the ΣWSIS concentration varied from 3.6–23.4 (Av: 12.5 ± 5.7) μg m^{-3}. The ΣWSIS/PM2.5 ratio varied from 0.16–0.31 (Av: 0.24 ± 0.05). The mass fraction in ΣWSIS of: Na^+ varied from 0.01–0.03 (0.01 ± 0.01); NH_4^+ varied from 0.17–0.35 (0.22 ± 0.05); K^+ varied from 0.07–0.20 (0.12 ± 0.05); Mg^{2+} varied from 0.000–0.004 (0.002 ± 0.001); Ca^{2+} varied from 0.000–0.023 (0.009 ± 0.008); Cl^- varied from 0.00–0.14 (0.02 ± 0.04); NO_3^- varied from 0.06–0.30 (0.13 ± 0.08) and SO_4^{2-} varied from 0.33–0.64 (0.47 ± 0.10). During the April–May 2011, the ΣWSIS concentration varied from 5.6–22.4 (Av: 12.1 ± 4.5) μg m^{-3}. The ΣWSIS/PM2.5 ratio varied from 0.21–0.34 (Av: 0.26 ± 0.04).

The mass fraction in ΣWSIS of: Na^+ varied from 0.01–0.03 (0.02 ± 0.01); NH_4^+ varied from 0.12–0.24 (0.19 ± 0.04); K^+ varied from 0.03–0.20 (0.09 ± 0.05); Mg^{2+} varied from 0.000–0.004 (0.001 ± 0.001); Ca^{2+} varied from 0.005–0.030 (0.014 ± 0.007); Cl^- varied from 0.00–0.09 (0.02 ± 0.03); NO_3^- varied from 0.01–0.27 (0.11 ± 0.08) and SO_4^{2-} varied from 0.30–0.72 (0.56 ± 0.12).

3.3.11 Summary on water-soluble inorganic species in aerosols

Water-soluble inorganic species (WSIS: Na^+, NH_4^+, K^+, Mg^{2+}, Ca^{2+}, Cl^-, NO_3^- and SO_4^{2-}) in PM2.5 have been assessed for paddy-residue burning, bio- and fossil-fuel combustion and wheat-residue burning emissions and compared with the data reported from chamber experiment and that reported for bulk seawater and mineral dust composition in the subsequent section. The chemical composition of WSIS in PM2.5 for different emission scenarios in the Indo-Gangetic Plain (IGP) is given in Table 3.5.

One of the most interesting features revealed from this study is that relatively low NO_3^- and high SO_4^{2-} mass fractions were observed during the day as compared to that during night (inferred from day-night sampling during October–November 2008; open circles; Figure 3.20h, i). This suggests that NO_3^- is less stable during daytime. In contrast, the formation of SO_4^{2-} aerosols is relatively more favored during daytime as compared to that during the night. The sum of cations (Na^+, NH_4^+, K^+, Mg^{2+} and Ca^{2+}) and anions (Cl^-, NO_3^- and SO_4^{2-}) referred to as ΣWSIS varied from 8.7–92.2 (Av: 43.9 ± 20.5) μg m^{-3} for paddy- and 3.6–23.4 (Av: 12.2 ± 4.8) μg m^{-3} for wheat-residue burning emissions (Table 3.5).

The ΣWSIS concentration varied from 5.9–90.7 (Av: 38.1 ± 22.5) μg m^{-3} for bio- and fossil-fuel combustion emission. On average the ΣWSIS contribute 22.8 ± 5.3%, 29.6 ± 8.3% and 25.3 ± 4.2% to the PM2.5 mass for paddy-residue burning, bio- and fossil-fuel combustion and wheat-residue burning emissions, respectively. The mass fraction (%) of anions and cations to the ΣWSIS for paddy-residue burning (n = 59), bio- and fossil-fuel combustion (n = 51) and wheat-residue (n = 31) burning emissions during October–November, December–March and April–May, respectively, is also listed in Table 3.5.

Table 3.5: Chemical composition of water-soluble inorganic species (WSIS) for different emission sources

Ambient Aerosol	Paddy-residue (n=59)	Bio- & fossil-fuel (n=51)	Wheat-residue (n=31)
PM2.5 (μg m^{-3})	195 ± 87	124 ± 58	50 ± 23
WSIS (μg m^{-3})	43.9 ± 20.5	38.1 ± 22.5	12.2 ± 4.8
Mass fraction of WSIS (%)			
Na^+	0.8 ± 0.3	1.0 ± 0.7	1.6 ± 0.6
NH_4^+	19.7 ± 3.4	22.4 ± 4.2	19.9 ± 4.5
K^+	11.1 ± 4.4	4.1 ± 1.9	10 ± 4.9
Mg^{2+}	0.1 ± 0.1	0.1 ± 0.1	0.1 ± 0.1
Ca^{2+}	0.6 ± 0.4	0.4 ± 0.8	1.2 ± 0.7
Cl^-	1.4 ± 2.5	1.9 ± 2.2	2.3 ± 3.3
NO_3^-	21.8 ± 11.9	22.4 ± 12.3	11.5 ± 7.8
SO_4^{2-}	44.6 ± 12.8	47.8 ± 12.5	53.4 ± 12.1

3.3.12 Secondary inorganic species from paddy- and wheat-residue burning emissions

NH_4^+, NO_3^- and SO_4^{2-}, the secondary components of inorganic aerosols, are the dominant contributors to the ΣWSIS, constituting overall 86.1% and 84.8% in aerosols for paddy- and wheat-residue burning emissions (Table 3.5). The average concentrations of NH_4^+, NO_3^- and SO_4^{2-} in aerosols from paddy-residue burning emissions are 8.8 ± 4.7 μg m^{-3}, 10.9 ± 8.4 μg m^{-3} and 18.2 ± 7.9 μg m^{-3}. However, relatively low concentrations of NH_4^+ (2.4 ± 1.0 μg m^{-3}), NO_3^- (1.6 ± 1.6 μg m^{-3}) and SO_4^{2-} (6.2 ± 1.8 μg m^{-3}), by at least a factor of three, has been recorded from wheat-residue burning emission in this study. During the paddy-residue burning emissions (October–November), the mass fractions of SO_4^{2-} and NO_3^- exhibit significant inter-annual variability (in 2008 versus 2010), in contrast to the nearly consistent contributions from other water-soluble ions (Na^+, NH_4^+, K^+, Mg^{2+}, Ca^{2+} and Cl^-; Figure 3.20). The most interesting feature revealed from the inter-annual variability is that relatively low NO_3^- and high SO_4^{2-} mass fractions were observed during the day as compared to that during night (inferred from day-night sampling in 2008; open circles). However, the mass fraction of individual water-soluble ions to the ΣWSIS from the wheat-residue burning emissions (April–May) remained fairly consistent (Figure 3.20). The dominant contribution from SO_4^{2-}, a secondary aerosol, to the ΣWSIS (~50%) is a conspicuous feature for the paddy- and wheat-residue burning emissions.

3.3.13 nss-K^+, nss-SO_4^{2-}, OC and EC

The non-sea-salt (nss) fraction of K^+ and SO_4^{2-} in ambient aerosols has been calculated using the following equations [*Keene et al.*, 1986].

$$nss - K^+ = K^+(\mu g m^{-3}) - 0.037 * Na^+(\mu g m^{-3}) \quad (3.3)$$

$$nss - SO_4^{2-} = SO_4^{2-}(\mu g m^{-3}) - 0.252 * Na^+(\mu g m^{-3}) \quad (3.4)$$

The constants 0.037 and 0.252 represent seawater composition for K^+/Na^+ and SO_4^{2-}/Na^+ ratios (equations 3.3, 3.4).

The nss-K^+/K^+ and nss-SO_4^{2-}/SO_4^{2-} ratios are always greater than or equal to 0.99. This suggests that the contribution from sea-salts to the PM2.5 aerosol composition is negligibly small. How-so-ever small contribution from sea-salts, the atmospheric concentrations for two important constituents (K^+ and SO_4^{2-}) among the measured water-soluble ions has been corrected for their contribution from sea-salts to assess the characteristic ratios nss-K^+/OC, nss-K^+/EC and nss-SO_4^{2-}/OC for different emission scenarios (Figure 3.21a, b, c).

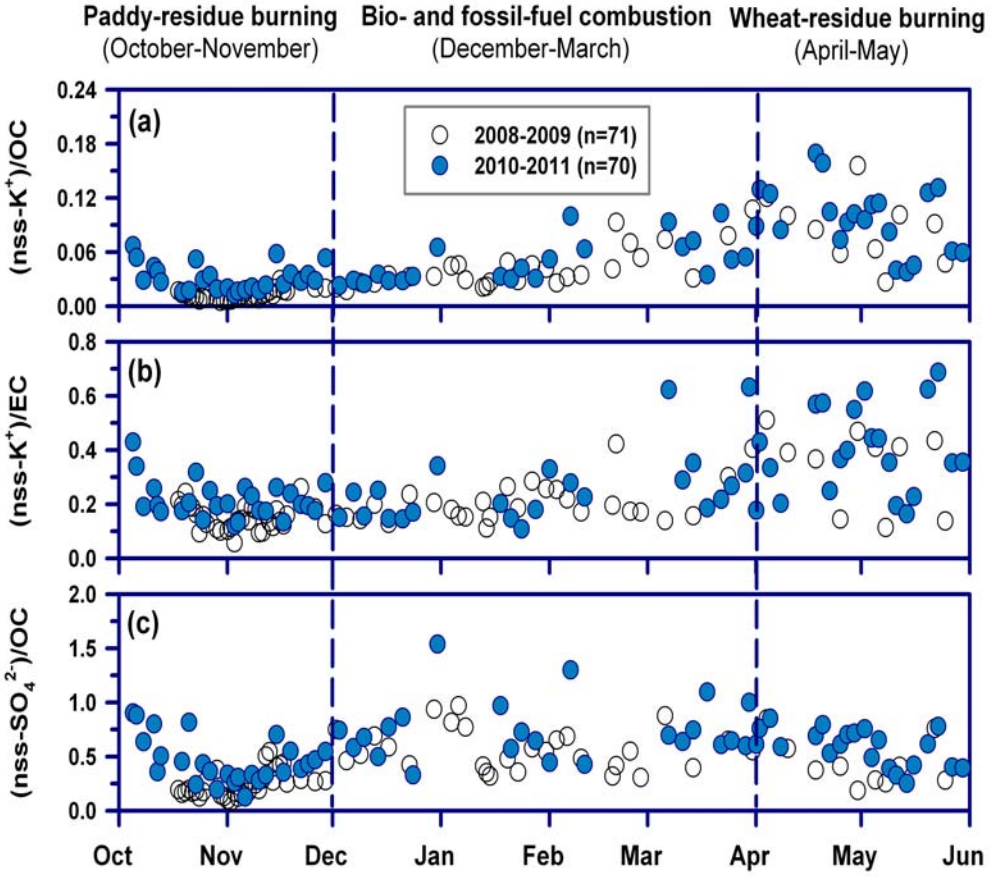

Figure 3.21: Temporal variability in: (a) nss-K^+/OC; (b) nssK^+/EC and (c) nss-SO_4^{2-}/OC concentration ratios. Vertical dashed lines demarcate the three distinct emission scenarios.

The nss-K^+/OC ratio during paddy-residue burning emissions, varied from 0.005–0.029 (Av ± sd: 0.013 ± 0.006) in October–November 2008, and 0.013–0.067 (0.031 ± 0.015) in October–November 2010. During the period, marked by emissions from bio- and fossil-fuel combustion sources, the nss-K^+/OC ratio

varied from 0.017–0.107 (0.042 ± 0.023) in December '08–March '09, and 0.023–0.244 (0.058 ± 0.047) in December '10–March '11.

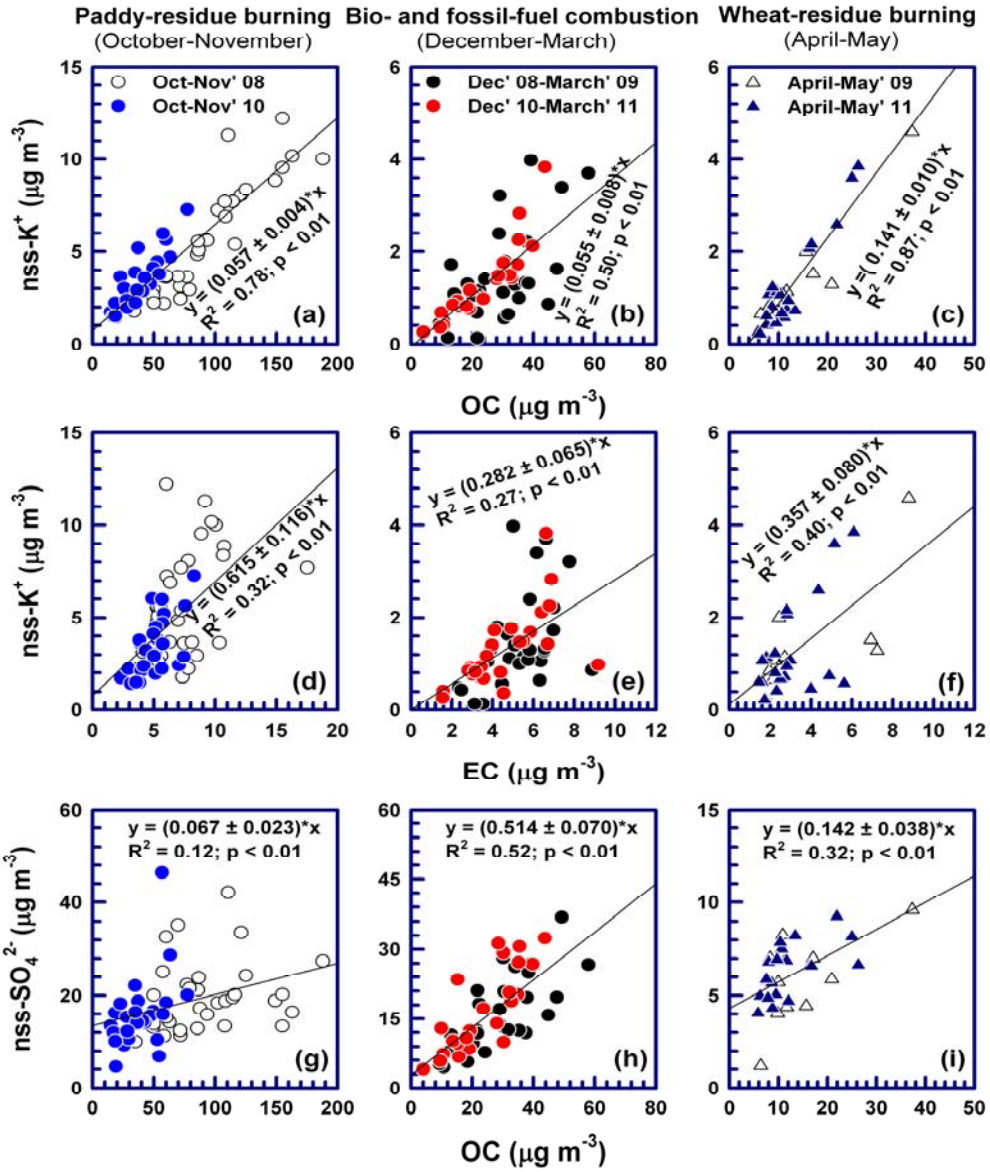

Figure 3.22: Scatter plot among (a, b, c) nss-K^+ and OC; (d, e, f) nss-K^+ and EC; and (g, h, i) nss-SO_4^{2-} and OC for three distinct emission scenarios.

During the wheat-residue burning emission, the nss-K^+/OC ratio varied from 0.027–0.156 (0.085 ± 0.038) in April–May 2009, and 0.038–0.169 (0.097 ± 0.036) in April–May 2011. The nss-K^+/EC ratio during paddy-residue burning

emissions, varied from 0.057–0.261 (Av ± sd: 0.150 ± 0.045) in October–November 2008, and 0.120–0.429 (0.217 ± 0.070) in October–November 2010. During the period, marked by emissions from bio- and fossil-fuel combustion sources, the nss-K^+/EC ratio varied from 0.111–0.422 (0.206 ± 0.076) in December '08–March '09, and 0.108–0.632 (0.259 ± 0.136) in December '10–March '11. During the wheat-residue burning emission, the nss-K^+/EC ratio varied from 0.113–0.510 (0.338 ± 0.148) in April–May 2009, and 0.164–0.687 (0.396 ± 0.169) in April–May 2011. The nss-SO_4^{2-}/OC ratio during paddy-residue burning emissions, varied from 0.086–0.544 (Av ± sd: 0.243 ± 0.116) in October–November 2008, and 0.126–0.904 (0.461 ± 0.213) in October–November 2010.

During the period, marked by emissions from bio- and fossil-fuel combustion sources, the nss- SO_4^{2-}/OC ratio varied from 0.306–0.970 (0.566 ± 0.191) in December '08–March '09, and 0.329–1.539 (0.744 ± 0.0282) in December '10–March '11. During the wheat-residue burning emission, the nss-SO_4^{2-}/OC ratio varied from 0.185–0.847 (0.438 ± 0.221) in April–May 2009, and 0.253–0.852 (0.588 ± 0.171) in April–May 2011. The correlation analysis (Figure 3.22) is performed among the nss-K^+, nss-SO_4^{2-}, OC and EC to determine the characteristic ratios of nss-K^+/OC, nss-K^+/EC and nss-SO_4^{2-}/OC for different emission scenarios, results are integrated in Table 3.6. The nss-K^+/OC, nss-K^+/EC and nss-SO_4^{2-}/OC ratio for different sources and location are listed in Table 3.6. The data from Nepal (at Kathmandu) and New Zealand (Christchurch and Auckland) is represented in Table 3.6 to show these characteric ratios for fossil-fuel combustion sources. The characteristic ratios for several types of natural biomass- (forest and grassland) fires are also listed in Table 3.6.

The present study documents these characteristic ratios for post-harvest agricultural-waste (paddy- and wheat-residues) burning and provides the evidence for dominance of bimass burning emissions in the Indo-Gangetic Plain (from Patiala; Upwind IGP). The characteristic ratios, nss-K^+/OC, nss-K^+/EC and nss-SO_4^{2-}/OC in the IGP are distinctly different with that from fossil-fuel dominated regions. The quantitative impact of biomass burning and fossil-fuel combustion sources to the carbonaceous aerosols in the IGP is presented in chapter 4, using the diagnostic PAHs isomer ratios in aerosol.

Table 3.6: Characteristic ratios of nss-K^+/OC, nss-K^+/EC and SO_4^{2-}/OC for distinct sources

Aerosol Source/Study Region	nss-K^+/OC	nss-K^+/EC	nss-SO_4^{2-}/OC
Paddy-residue burning[a]	0.057 ± 0.004	0.615 ± 0.116	0.067 ± 0.023
Wheat-residue burning[a]	0.141 ± 0.010	0.357 ± 0.080	0.142 ± 0.038
Savanna and Grassland[b]	0.10	0.73	0.10[e]
Tropical forest[b]	0.06	0.44	0.11[e]
Extratropical forests[b]	0.03	0.44	0.11[e]
Upwind IGP[a]	0.055 ± 0.008	0.282 ± 0.065	0.357 ± 0.080
Kathmandu[c]	0.02	0.07	0.16
Christchurch[d]	0.02	0.05	0.05
Auckland[d]	0.02	0.03	0.15

[a]This study: [*Rajput et al.*, 2011b]; [b]Forest- and grassland-fires: [*Andreae and Merlet*, 2001]; [c]fossil-fuel dominated region in Nepal: [*Shakya et al.*, 2010]; [d]fossil-fuel dominated region in New Zealand: [*Wang et al.*, 2005]; [e]All SO_2 is assumed to be converted into SO_4^{2-}.

3.3.14 Field burning versus chamber combustion of paddy-residue

3.3.14.1 Field-based

Assessing the aerosol composition from field burning emissions of paddy-residues in the IGP (studied over Patiala) revealed the average mass fraction in ΣWSIS of: Na^+ is 0.01 ± 0.00; NH_4^+ is 0.20 ± 0.03; K^+ is 0.11 ± 0.04; Mg^{2+} is 0.001 ± 0.001; Ca^{2+} is 0.006 ± 0.004; Cl^- is 0.01 ± 0.03; NO_3^- is 0.22 ± 0.12 and SO_4^{2-} is 0.45 ± 0.13 (Figure 3.23).

3.3.14.2 Chamber experiment

The concentrations of Na^+, NH_4^+, Mg^{2+}, Ca^{2+} and NO_3^- have been reported to be non detectable in chamber experiment [*Hays et al.*, 2005]. The average mass fraction in ΣWSIS of: K^+ is 0.21 ± 0.01; Cl^- is 0.61 ± 0.01 and SO_4^{2-} is 0.17 ± 0.01 (Figure 3.23).

3.3.15 Field burning versus chamber combustion of wheat-residue

3.3.15.1 Field-based

Aerosol composition from wheat-residue burning emissions in fields (in the IGP; studied over Patila) revealed the mass fraction in ΣWSIS of: Na^+ is 0.02

± 0.01; NH_4^+ is 0.20 ± 0.05; K^+ is 0.10 ± 0.05; Mg^{2+} is 0.001 ± 0.001; Ca^{2+} 0.012 ± 0.007; Cl^- is 0.02 ± 0.03; NO_3^- is 0.11 ± 0.08 and SO_4^{2-} is 0.53 ± 0.12 (Figure 3.23).

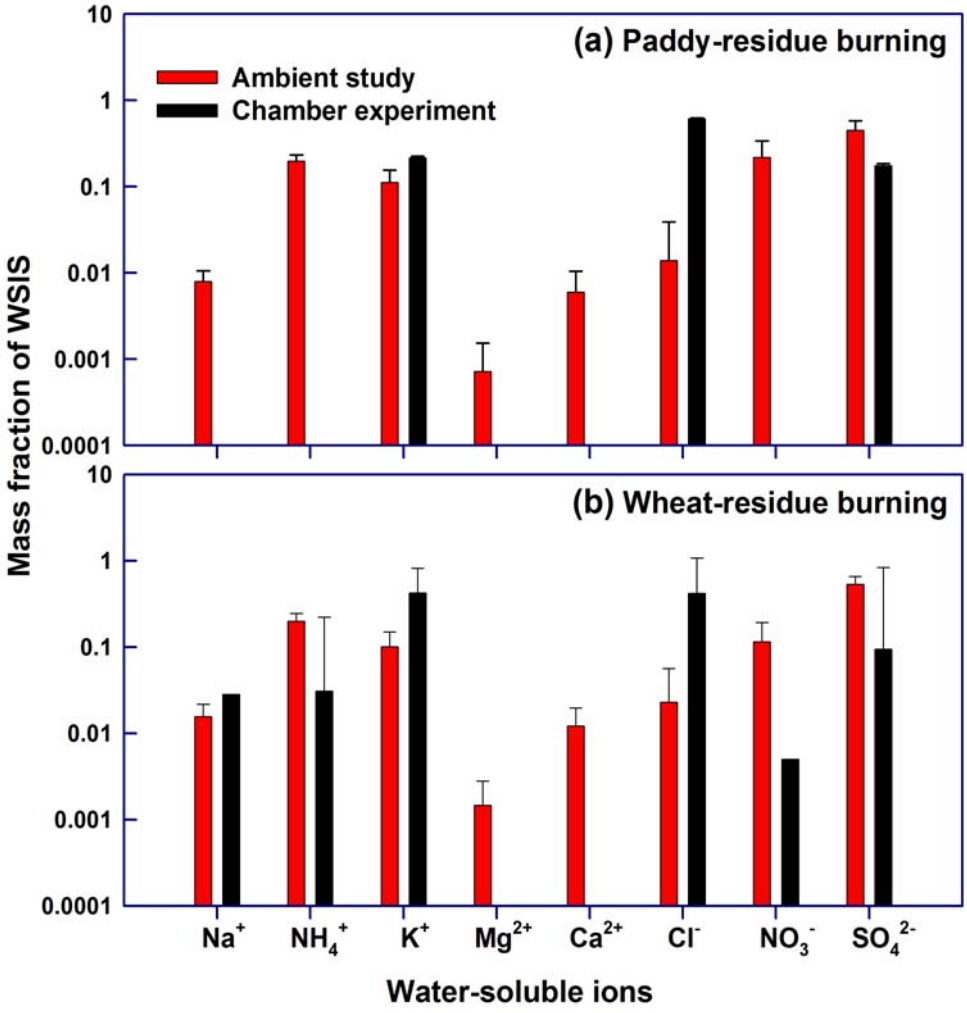

Figure 3.23: Abundances of WSIS measured in ambient aerosols (this study) and that reported from the chamber experiment [Hays et al., 2005] for: (a) paddy-residue and (b) wheat-residue burning emissions.

3.3.15.2 Chamber experiment

The concentrations of Mg^{2+} and Ca^{2+} have been reported to be non detectable in chamber experiment [*Hays et al.*, 2005]. The mass fraction in ΣWSIS of: Na^+ is 0.03 ± 0.00; NH_4^+ is 0.03 ± 0.19; K^+ is 0.42 ± 0.39; Cl^- is 0.42 ± 0.66; NO_3^- is 0.05 ± 0.00 and SO_4^{2-} is 0.09 ± 0.74 (Figure 3.23).

Summing up, the differences in the mass fraction of inorganic constituents in ΣWSIS studied under ambient atmospheric conditions and chamber experiment exists for the secondary inorganic species (NH_4^+, NO_3^- and SO_4^{2-}), exception being the Cl^- (Figure 3.23). Particularly, the contribution of these secondary inorganic species to ΣWSIS from field burning of paddy- and wheat-residues is significantly higher as compared to that simulated from the chamber experiment. However, the contribution of all the primary inorganic species (Na^+, K^+, Mg^{2+}, Ca^{2+}) to the ΣWSIS for paddy- and wheat-residue burning emissions look similar under ambient atmosphere and chamber simulation, exception being the Cl^-. The contribution of Cl^- to the ΣWSIS is significantly lower under ambient atmospheric conditions as compared to that in chamber simulation, for both the paddy- and wheat-residue burning. This evidence is further supported by an order of magnitude lower Cl^-/K^+ equivalent ratio in ambient aerosols (this study) of 0.14 ± 0.22 for paddy- and 0.32 ± 0.54 for wheat-residue burning emissions as compared to that reported from chamber experiment (paddy-: 1.08 and wheat-: 3.13).

The plausible explanation for lower mass fraction of Cl^- associated with the field burning of paddy- and wheat-residues could be due to its reaction with atmospheric oxidants and/or the Cl^- depletion from ambient aerosols in the form of HCl gas, due to the attack of inorganic acids (HNO_3/H_2SO_4) [*Sarin et al.*, 2011].

3.3.15.3 Equivalent ratios of cations and anions for paddy- and wheat-residues burning emissions

The equivalent ratios for several cations and anions for paddy- and wheat-residue burning emissions in ambient aerosols are given in Table 3.7. In addition, the literature based equivalent ratios for mineral dust and bulk seawater is also listed in Table 3.7 [*Formenti et al.*, 2003; *Keene et al.*, 1986]. As far as the scenario on the relative abundances of secondary inorganic species is concerned, the paddy- and wheat-residues burning emission with the equivalent ratios of NH_4^+/NO_3^- (Av: 6.60 for paddy- and 12.35 for wheat-residue) and NO_3^+/SO_4^{2-} (paddy-residue: 0.47 and wheat-residue: 0.20) suggest enhanced formation of nitrate during paddy-residue burning as compared to that from wheat-residue.

However, the equivalent ratio of NH_4^+/SO_4^{2-} for paddy- (1.30 ± 0.51) and wheat-residues burning (1.06 ± 0.38) suggests sulphate to be the limiting reactant.

Table 3.7: Equivalent ratios among water-soluble inorganic ions in aerosol from paddy- and wheat-residue burning emissions

Equivalent Ratio	Paddy-residue[a] (n=59)	Wheat-residue[a] (n=31)	Mineral Dust[b]	Bulk seawater[c]
Ca^{2+}/Na^+	0.89 ± 0.59	1.01 ± 0.68	4.4 ± 0.1	0.044 ± 0.000
Mg^{2+}/Na^+	0.19 ± 0.19	0.19 ± 0.18	1.9 ± 0.2	0.231 ± 0.007
K^+/Na^+	8.81 ± 4.01	3.91 ± 1.48	2.58 ± 0.08	0.022 ± 0.000
Cl^-/Na^+	1.59 ± 3.49	1.13 ± 2.01	0.69 ± 0.02	1.164 ± 0.005
SO_4^{2-}/Na^+	28.62 ± 9.62	20.12 ± 11.51	4.0 ± 0.3	0.121 ± 0.000
Ca^{2+}/Mg^{2+}	3.87 ± 2.99	3.38 ± 1.40	2.316 ± 0.119	0.190 ± 0.006
K^+/Mg^{2+}	29.17 ± 33.56	29.89 ± 46.93	1.358 ± 0.092	0.094 ± 0.004
K^+/SO_4^{2-}	0.33 ± 0.17	0.26 ± 0.18	0.645 ± 0.031	0.179 ± 0.003
Cl^-/Mg^{2+}	4.30 ± 6.98	21.58 ± 69.40	0.363 ± 0.046	5.039 ± 0.149
SO_4^{2-}/Mg^{2+}	135.21 ± 36.04	73.43 ± 31.45	2.105 ± 0.139	0.521 ± 0.016
NH_4^+/NO_3^-	6.60 ± 9.03	12.35 ± 13.40		
NH_4^+/SO_4^{2-}	1.30 ± 0.51	1.06 ± 0.38		
NO_3^-/SO_4^{2-}	0.47 ± 0.35	0.20 ± 0.18	0.400 ± 0.039	

[a] Ambient aerosol in this study; [b] [*Formenti et al.*, 2003]; [c] [*Keene et al.*, 1986].

The cross plot for the equivalent ratio of $K^+/(K^+ + SO_4^{2-})$ and $Na^+/(Na^+ + SO_4^{2-})$ for paddy- (0.5174 ± 0.1851; 0.0343 ± 0.0187) and wheat-residues (0.5626 ± 0.1835; 0.0613 ± 0.0425) exhibit distinctly different signatures than the mineral dust (0.4425 ± 0.0000; 0.3429 ± 0.0000) and bulk seawater (0.1531 ± 0.0002; 0.8921 ± 0.0000) composition (Figure 3.24) [Formenti et al., 2003; Keene et al., 1986].

Thus, the present study provides the scenario on the utility of water-soluble inorganic ions to distinguish their composition among the biomass burning emissions, mineral dust and the seawater.

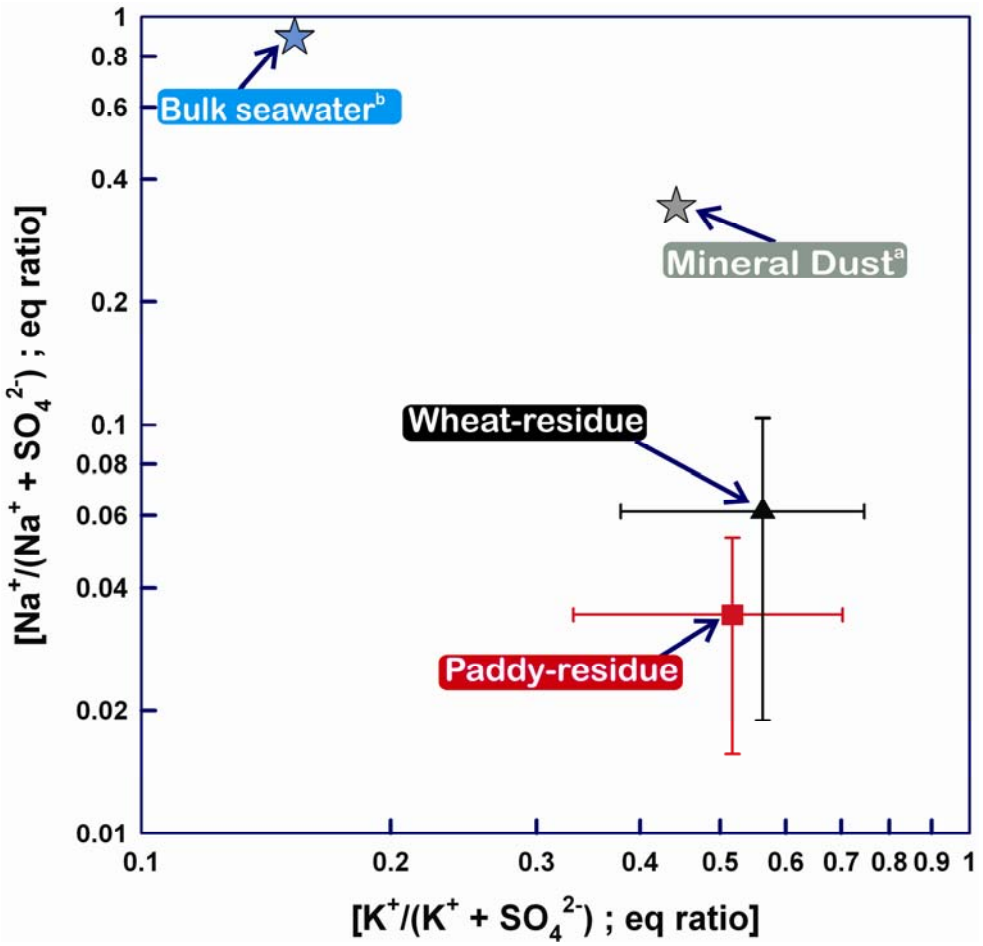

Figure 3.24: Cross plot exhibits distinctly different ratio for paddy- and wheat-residues burning emission (in ambient aerosols; this study) with that from mineral dust: [a][Formenti et al., 2003]; and seawater composition: [b][Keene et al., 1986].

3.4. Inferences

3.4.1 Emission factors and emissions of aerosol from agricultural-waste burning

Though a number of studies exist on aerosol emission estimates for agricultural-waste burning in the literature. [*Streets et al.*, 2003a; *Streets et al.*, 2003b; *Turn et al.*, 1997; *Venkataraman et al.*, 2006]. But these estimates were inferred from laboratory-based studies, where combustion efficiency of biomass is relative high as compared to that in open field burning. As discussed in earlier sections that there are major differences in the composition of aerosols from field-burning and that from combustion experiment in chamber. And therefore, it is

logical to build the emission estimates for different constituents, based on the data set from ambient (from this study) and existing chamber-studies. Emission of particulate matter from paddy- and wheat-residue burning in the Indo-Gangetic Plain (IGP) is estimated using the following equation

$$Emission\ (Gg) = EF\ (g/kg) * FL\ (kg/Km^2) * AB\ (km^2) * 10^{-9} \qquad (3.5)$$

Here, 'EF' is abbreviated for emission factor; 'FL' is for fuel load over the agricultural-fields and 'AB' for the area burned (Table 3.8).

Table 3.8: Estimation of emission factor and emission of aerosols for the agricultural-waste burning of paddy- and wheat-residues

Open biomass **Paddy-residue** (October–November)	**Emission Factor**[a] (g/kg)	**Fuel load**[b] (Kg/sq. km)	**Area burned**[c] (sq. km)	**Emission**[d] (Gg/y)
PM2.5	6.5	11.8 x 10^5	48,400	742
OC	4.5			514
EC	0.5			57
ΣPAHs	1.8[e]			206[f]
Wheat-Residue (April–May)				
PM2.5	4.71	5.94 x 10^5	48,400	271
OC	1.23			71
EC	0.52			30
ΣPAHs	0.4[e]			23[f]

[a]Based on emissions observed in this study for large number of data sets (field-based) and chamber-based experiment [*Hays et al.*, 2005].
[b]Adopted from [*Badarinath et al.*, 2006].
[c]Inferred from high-resolution (1km x 1km) satellite data from MODIS (Aqua/Terra).
[d]Emission factor x Fuel load x Area burned.
[e]Emission factor in mg/kg.
[f]Emission in Mg/y.

As obvious from equation 3.5 that the three parameters (in r.h.s) are required in order to estimate the emission of pollutants from open biomass burning. A factor of 10^{-9} is multiplied to convert the gram-emissions into Giga-grams (Gg). The discussion on estimation of emission factors and emissions of

aerosol for agricultural-waste burning emissions of paddy- and wheat-residues are discussed as follows.

3.4.2 Emission factors (EF)

EF of the particulate matter from agricultural-waste (paddy- and wheat-residues) burning emissions are critically assessed here, based on comparison of their mass fraction from this study (field-based) and those reported from chamber-based simulation experiments. For wheat-residue burning emissions in this study, the mass fractions of OC and EC in PM2.5 are found similar (Figure 3.15b) to that reported from chamber experiment [*Hays et al.*, 2005]. Therefore, the EF of PM2.5, EC and OC is retained similar for field-burning of wheat-residue (Table 3.8) as reported from a chamber experiment [*Hays et al.*, 2005]. However, based on the observation and evaluation for a large discrepancy in OC and EC mass fractions for paddy-residue burning (Figure 3.15a), between field- (this study) and chamber experiment, attributable to difference in moisture content of biomass and its combustion efficiency (refer to earlier sections), the EF of PM2.5, EC, OC for paddy-residue field burning emissions is provided in Table 3.8. Furthermore, the EF of PAHs is estimated (Table 3.8) based on the mass fraction of PAH (ΣPAHs/OC) in this study from a large number of data set for paddy- (n = 59) and wheat-residue burning (n = 31) as follows

$$EF_{PAHs}(mg/kg) = \frac{\sum PAHs(mg)}{OC(g)} * EF_{OC}(g/kg) \qquad (3.6)$$

EF_{OC} is emission factor of OC (Table 3.8).

3.4.3 Fuel load (FL)

The value of fuel-load (Table 3.8) for paddy- and wheat-residues on agricultural-fields is adopted from a recent literature documenting the agricultural-scenario for the states of Punjab in northern India [*Badarinath et al.*, 2006].

3.4.4 Area burned (AB)

Based on analysis of high-resolution (lat-long grid: 1˚ x 1˚) satellite data for open fire-counts from Moderate Resolution Imaging Spectroradiometer MODIS (on-board Aqua/Terra; level 2) during 2008–2011, the fire active (agricultural-waste burning) area is estimated to be to be 48,400 km^2 in the IGP (including states of Punjab, Haryana and western part of Uttar Pradesh; Figure 3.1) [*Justice et al.*, 2002]. The fire-count data (Figure 3.1) has been corrected for Cloud and Overpass. The "Cloud and Overpass corrected fire-pixel count" presents number of pixels corrected for multiple satellite overpasses, missing observations and variable cloud cover [*Justice et al.*, 2002]. Moreover, the area is fire active for a total of four months in a year: occurrence of paddy-residue burning during October–November and wheat–residue burning during April–May. Thus, it is logical, to assess the chemical composition of particulate matter from paddy- and wheat-residue burning emissions from IGP only for two months each, and represented here as the annual emissions (Table 3.8).

3.5. Global scenario on biomass burning emissions

For a global scenario, information on chemical characteristics of aerosols emitted from different types of biomass burning emissions on an annual and seasonal basis is described as below:

(i) Agricultural-waste burning emissions in India (South Asia)
(ii) Agricultural-waste burning emissions in southern China and Korea (East Asia)
(iii) Agricultural-waste burning emissions in Thailand (Southeast Asia)
(iv) Emissions from savanna fires in Africa
(v) Emissions from cerrado/tropical forest fires in the Amazon basin in South America
(vi) Boreal forest fires in US/Canada (North America)

Relevant details on the atmospheric impact due to large-scale biomass burning emissions from two distinguished post-harvest agricultural-waste of

paddy- (October–November) and wheat-residues (April–May), occurring in the Northern India on a seasonal and annual basis have been assessed in this study and represented (earlier sections) in this chapter.

3.5.1 Agricultural-waste burning emissions in southern China and Korea (East Asia)

The characteristic feature associated with the rice-straw burning emissions in Gwangju (South Korea) has been reported through the ground-based PM2.5 sampling [*Ryu et al.*, 2004]. The OC/EC ratio of 8.3 ± 3.8, K^+/EC ratio of 0.19 ± 0.07, K^+/OC ratio of 0.02 ± 0.01, SO_4^{2-}/EC ratio of 1.69 ± 0.65, SO_4^{2-}/OC ratio of 0.21 ± 0.09 and Cl^-/EC ratio of 0.54 ± 0.21, has been observed in PM2.5 samples from the post-harvest rice-straw burning emissions in that study [*Ryu et al.*, 2004]. Another study from southern China (Shandong province), assessing the aerosol characteristics from the wheat-residue burning emissions has reported the OC/EC ratio of 5.0 ± 3.4, K^+/EC ratio of 1.30 ± 0.50, K^+/OC ratio of 0.26 ± 0.10, SO_4^{2-}/EC ratio of 0.20 ± 0.19, SO_4^{2-}/OC ratio of 0.04 ± 0.04 and Cl^-/EC ratio of 1.80 ± 2.13 in PM2.5 samples (ground-based) [*Li et al.*, 2007].

3.5.2 Agricultural-waste burning emissions in Thailand (Southeast Asia)

An study from Thailand in Southeast Asia, has reported OC/EC ratio of 5.8 ± 3.2, K^+/EC ratio of 0.87 ± 0.28, K^+/OC ratio of 0.15 ± 0.04, SO_4^{2-}/EC ratio of 0.17 ± 0.15, SO_4^{2-}/OC ratio of 0.03 ± 0.02 and Cl^-/EC ratio of 1.20 ± 0.80 in PM2.5 samples (ground-based) collected during rice-straw burning emissions [*Kim Oanh et al.*, 2011]. Furthermore, that study has also reported the PAHs isomer ratios: ANTH/PHEN ratio of 0.67 ± 1.59; ANTH/(ANTH+PHEN) of 0.40 ± 0.60; FLA/PYR of 1.72 ± 3.25; FLA/(FLA+PYR) of 0.63 ± 1.15; BaA/CHRY of 0.71 ± 1.37; BaA/(BaA+CHRY) of 0.41 ± 0.74; BaP/B[b,j]FLA of 0.89 ± 1.02 and BaP/(BaP+B[b,j]FLA) of 0.47 ± 0.52.

3.5.3 Emissions from savanna-fires in Africa

As a part of the Southern Africa Fire-Atmosphere Research Initiative (SAFARI-92), assessing the atmospheric aerosol composition and impact of

biomass burning, a study (ground-based) conducted in Kruger National Park (KNP) in eastern South Africa has reported some of the characteristic ratios associated with savanna-fires under two different combustion conditions (flaming and smoldering) [*Maenhaut et al.*, 1996]. The K^+/BC ratio of 0.20, SO_4^{2-}/BC ratio of 0.021 and Cl^-/BC ratio of 0.31 were observed under flaming condition. In contrast, the particulate emission during smoldering exhibit characteristic K^+/BC ratio of 0.17, SO_4^{2-}/BC ratio of 0.033 and Cl^-/BC ratio of 0.22.

As a part of the Experiment for Regional Sources and Sinks of Oxidants (EXPRESSO) conducted over the central Africa in November 1996, several chemical constituents were assessed in airborne aerosol samples, collected using aircraft above the savanna-forest during fire events [*Ruellan et al.*, 1999]. The BC/TC ratio of 0.20 ± 0.08, WSOC/OC ratio of 0.27 ± 0.05, SO_4^{2-}/BC ratio of 0.16, SO_4^{2-}/K^+ ratio of 0.03, ANTH/PHEN ratio of 0.03, ANTH/(ANTH+PHEN) ratio of 0.03 ± 0.05, FLA/PYR ratio of 4.0, FLA/(FLA+PYR) ratio of 0.80 ± 0.53, BaP/B[b,j]FLA ratio of 0.19 and BaP/(BaP+B[b,j]FLA) ratio of 0.16 ± 0.15 have been reported for the savanna-fires.

3.5.4 Emissions from cerrado/tropical forest fires in the Amazon basin in South America

The ground-based measurement of particulate matter in emissions from cerrado biomass (brush and scrub forest; savanna like) burning (August–September 1992) has revealed the K^+/BC ratio of 0.24 ± 0.21, SO_4^{2-}/BC ratio of 0.06 ± 0.04 and Cl^-/BC ratio of 0.17 ± 0.16 under flaming condition [*Yamasoe et al.*, 2000]. Furthermore, similar ratio of K^+/BC (0.2 ± 0.35), SO_4^{2-}/BC (0.05 ± 0.08) and Cl^-/BC (0.15 ± 0.27) under smoldering condition of cerrado fires has also been documented by that study.

Another study, through airborne measurements of the particles emitted from cerrado fires in Brazil, during the Smoke, Clouds and Radiation-Brazil (SCAR-B) study in August–September 1995, has provided the OC/BC ratio of 8.1 ± 5.1, K^+/BC ratio of 0.60 ± 0.43, K^+/OC ratio of 0.07 ± 0.04, SO_4^{2-}/BC ratio of 0.13 ± 0.10 and SO_4^{2-}/OC ratio of 0.02 ± 0.01 [*Ferek et al.*, 1998].

The chemical characterization of particulate matter emissions from tropical rain-forest fires (in the Amazon basin), through the ground-based measurement, has reported the K^+/BC ratio of 0.11 ± 0.12, SO_4^{2-}/BC ratio of 0.12 ± 0.13 and Cl^-/BC ratio of 0.04 ± 0.04 under flaming condition [*Yamasoe et al.*, 2000]. Furthermore, similar ratio of K^+/BC (0.1 ± 0.09), SO_4^{2-}/BC (0.1 ± 0.1) and Cl^-/BC (0.05 ± 0.06) were also observed under smoldering condition in that study.

Airborne measurements (SCAR-B) of the emitted particles from rain forests in Brazil, has characterized the emissions with OC/BC ratio of 6.7 ± 4.2, K^+/BC ratio of 0.61 ± 0.60, K^+/OC ratio of 0.09 ± 0.09, SO_4^{2-}/BC ratio of 0.38 ± 0.40 and SO_4^{2-}/OC ratio of 0.06 ± 0.06 under flaming condition [*Ferek et al.*, 1998]. And near similar ratio of OC/BC (12.6 ± 5.2), K^+/BC (0.47 ± 0.42), K^+/OC (0.04 ± 0.03), SO_4^{2-}/BC (0.40 ± 0.23) and SO_4^{2-}/OC (0.03 ± 0.01) under smoldering condition has also been reported in that study [*Ferek et al.*, 1998].

3.5.5 Boreal forest fires in US/Canada (North America)

A study has documented the chemical characteristics of chaparral fires, occurring in California, through the laboratory-based measurements called as FLAME (Fire Laboratory at Missoula Experiments) [*McMeeking et al.*, 2009]. Accordingly, the particulate matter emitted from chaparral fires are characterized with the OC/EC ratio of 13.2 ± 22.8, EC/TC ratio of 0.07 ± 0.13, K^+/EC ratio of 1.0 ± 1.0, K^+/OC ratio of 0.08 ± 0.12, SO_4^{2-}/EC ratio of 0.40 ± 0.38 and SO_4^{2-}/OC ratio of 0.03 ± 0.05, SO_4^{2-}/K^+ ratio of 0.40 ± 0.31 and Cl^-/EC ratio of 0.40 ± 0.38.

Airborne measurement of emissions from the boreal forest fires in Northern Ontario (in Canada) has revealed the OC/EC ratio of 10–18 under flaming and 21–95 (bulk aerosol sampling) under smoldering condition [*Mazurek et al.*, 1990]. Furthermore, through ground-based measurements the particulate matter with very high OC/EC ratio, of 49 ± 22 under flaming, and 113 ± 10 under smoldering condition for the crown fires (boreal forest) has been characterized [*Conny and Slater*, 2002].

3.6. Summary and Implications

This chapter provides the data set on ambient concentrations of PM2.5, EC, OC, WSOC, WSIS and PAHs (and their isomer ratios) for two distinct post-harvest agricultural-waste (paddy- and wheat-residues) burning emissions. In addition to this, particulate emission from bio- and fossil-fuel combustion (vehicular emission) in the Indo-Gangetic Plain (IGP) is also presented quantitatively. The important conclusions drawn from this study are:

1. The OC/EC (Av: ≥ 4), EC/TC (≥ 0.10), WSOC/OC (Av: ~60%) and ΣPAHs/EC (≥ 1.2 mg g^{-1}) are characteristic for biomass burning emissions. The 5- and 6-ring PAHs concentration exhibit distinct variability depending on their emission source.
2. The average contribution of secondary organic carbon is ~20–37% of the total particulate carbon. The cross plot of PAHs isomer ratios exhibit distinctly different characteristics between post-harvest agricultural-waste burning and fossil-fuel combustion sources.
3. A near similarity in the relative rate constant of PAH isomers, from different emission scenarios, suggests that the isomer ratios preserve the signature and serve as robust tracer of its source.
4. Based on the assessment of particulate emissions from field- and recent chamber-based experiment for agricultural-waste burning, the emission factor and estimates are presented.
5. The contribution of ΣWSIS to the PM2.5 mass is about 23% from paddy- and 25% for wheat-residue burning emissions. The sum of water-soluble ions concentration, of secondary origin (NH_4^+, NO_3^- and SO_4^{2-}) accounts for about 85% to the ΣWSIS for paddy- and wheat-residue burning emissions, with dominant contribution from SO_4^{2-} (~50% of ΣWSIS).
6. Lower ammonium-to-nitrate and higher nitrate-to-sulphate equivalent ratio for paddy- as compared to that from wheat-residue burning emissions suggest enhanced formation of nitrate during the paddy-residue burning emissions (October–November).

7. NH_4^+/SO_4^{2-} equivalent ratio (> 1), suggests sulphate to be the limiting reactant in aerosols.
8. The nss-K^+/OC, nss-K^+/EC and nss-SO_4^{2-}/OC ratios are distinctly different for the paddy- and wheat-residue burning with that from the fossil-fuel combustion sources.
9. The cross plot employing the equivalent ratio of $K^+/(K^+ + SO_4^{2-})$ and $Na^+/(Na^+ + SO_4^{2-})$ provide information on distinctly different signature of paddy- and wheat-residue burning emissions than the mineral dust and bulk seawater composition.

Present study on the chemical characterization of two distinct post-harvest biomass burning emissions highlight the two seasonally active potential sources of organic aerosols in the IGP. Further assessment on the formation of secondary organic aerosols is essential to understand the daytime and nighttime atmospheric chemistry in the IGP on annual-seasonal basis. High abundance of OC, with significant contribution of WSOC (~60% of OC), in conjunction with chemical reactivity of PAHs and formation of SOA have implications to: (1) Cloud-chemistry, (2) Atmospheric and aerosol chemistry affecting the budget of atmospheric oxidants and (3) Aerosol radiation budget – scattering due to hygroscopic aerosol and chemical composition (enriched in WSOC and OC).

CHAPTER 4

ATMOSPHERIC LONG-RANGE TRANSPORT OF CARBONACEOUS AEROSOLS TO NE-HIMALAYA

4.1. Introduction

Carbonaceous aerosols, consisting of primary species (elemental carbon: EC and organic carbon: OC) and secondary organic compounds, contribute significantly to the particulate matter in the lower atmosphere [*Chan et al.*, 2009; *Hallquist et al.*, 2009; *Jimenez*, 2009; *Rudich et al.*, 2007; *Seinfeld and Pankow*, 2003]. Several studies have assessed the chemical composition of carbonaceous aerosols from the source region. However, the complexity in assessing aerosol characteristics after their long-range transport arises mainly due to atmospheric mixing and chemical processing.

The lack of adequate information on aerosol mixing and chemical aging of chemical constituents during their transport is a major cause of uncertainty in assessing the aerosol chemical composition and radiative forcing in the lower atmosphere [*Haywood and Boucher*, 2000; *Novakov and Penner*, 1993; *Sokolik et al.*, 2001]. Furthermore, interaction of several carbonaceous species with trace constituents in the troposphere, not only change the aerosol composition but in turn also influence the abundance of trace gases [*Andreae and Crutzen*, 1997; *Hallquist et al.*, 2009].

Importantly, the water-soluble organic carbon (WSOC) has secondary formation pathway in the atmosphere via photochemical reactions of volatile organic compound (VOC) and/or aging (oxidation) of organic aerosols, besides their primary production from biomass burning emission [*Decesari et al.*, 2002; *Mayol-Bracero et al.*, 2002b; *Saxena and Hildemann*, 1996; *Turpin et al.*, 2000; *Weber et al.*, 2007]. And therefore, this characteristic feature (of secondary formation) of WSOC can be used to provide information on the chemical oxidation of organic compounds during their long-range atmospheric transport by assessing the mass fraction of WSOC to OC in conjunction with OC/EC ratio.

The significance of these water-soluble organic compounds in influencing the number density of cloud condensation nuclei (CCN) by changing the surface characteristics of aerosols from hydrophobic to hydrophilic and also alter the radiation balance of the atmosphere is well known [*Kaiser et al.*, 2011; *Shapiro et al.*, 2009].

The heterogeneous reactivity of PAHs with the atmospheric oxidants (O_3, NO_X and OH radical) has been realized to alter the aerosol surface characteristics (more hydrophilic) and thus expected to enhance the aerosol potential to act as cloud condensation nuclei [*Kaiser et al.*, 2011]. In addition to this, the PAHs isomer ratios have been used for finger-printing of their sources [*Yunker et al.*, 2002].

This chapter provides first data set on the atmospheric concentrations of PM2.5, EC, OC, WSOC and PAHs from a sampling site located at the foot-hills of NE-Himalaya (NE-H).

Under favorable meteorological conditions, during winter months (January–March), sampling site is most ideal to study the chemical composition of carbonaceous aerosols after their long-range atmospheric transport from source regions in the Indo-Gangetic Plain (IGP) and south-east Asia. For rest of the year (April–December), the atmosphere over NE-Himalaya is relatively clean due to widespread rains associated with the SW- and NE-monsoon. In this context, downwind atmospheric transport of fine-mode aerosols from the Northern India can have profound impact on the regional environment [*Rajput et al.*, 2011b; *Ramanathan et al.*, 2001; *Ramanathan et al.*, 2007]. The primary focus of this study is to assess the dominant source and influence of chemical processing on the chemical composition of carbonaceous aerosols after their transport over the foot-hills of NE-H.

4.2. Methodology

4.2.1 Field-campaign

The sampling site at Barapani (25.7 °N; 91.9 °E; 1064 m asl) is located ~20 km upwind of the Shillong town in NE-Himalaya. The annual-average rainfall in this region is ~1100 cm, spread over June–September (SW-monsoon) and October–December (NE-monsoon). In addition, pre-monsoon rain activity begins by early April. This facilitates the removal of ambient aerosols by wet-scavenging important during April–December over NE-Himalaya. During the winter months (January–March), long-range transport of pollutants from the Indo-

Gangetic Plain (IGP) and south-east Asia is a conspicuous feature of the region (Figure 4.1).

With this background information and the importance of study site, PM2.5 samples (n = 51) were collected (whole week, mostly between the first and fourth week of the months) in two campaigns.

First campaign was conducted in March 2009 (n = 12) and second campaign during January and March 2010 (n = 19 and 20, respectively). A high-volume sampler (flow rate: 1.2 m^3 min^{-1}; Thermo Scientific) was deployed at ~10 m above the ground level inside the premises of Space Applications Centre. On average, about 1200 m^3 of ambient air was filtered for each sample (sampling duration: ~18 h) through pre-combusted (at 450 °C for ~6 h) tissuquartz filters (PALLFLEX™, 2500QAT-UP, 20 cm x 25 cm).

After the sample collection, filters were wrapped in Al-foils, sealed in zip-lock plastic bags, and retrieved to the laboratory for analysis as per the protocol described in earlier publications [*Rajput et al.*, 2011a; *Rajput et al.*, 2011b; *Ram et al.*, 2010a; *Ram et al.*, 2012; *Rengarajan et al.*, 2007].

The meteorological parameters; wind direction and speed, relative humidity, surface temperature and precipitation were monitored simultaneously. The daily temperature varied from 6–28 ˚C with relative humidity from 10–99%. The north-westerly winds were dominant; with average wind-speed of 3.3 m s^{-1} during March 2009 and 5 m s^{-1} in March 2010. During the entire sampling period, wet precipitation event (< 15 mm) occurred on 16th March, 2010.

The published data on carbonaceous species from other sites: Patiala (30.2 ˚N, 76.3 ˚E, 250 m asl); Hisar (29.2 ˚N; 75.7 ˚E; 219 m); Kanpur (26.5 ˚N, 80.3 ˚E, 142 m); Allahabad (25.4 ˚N, 81.9 ˚E, 123 m) from the IGP [*Rajput et al.*, 2011b; *Ram and Sarin*, 2010; *Rengarajan et al.*, 2007]; Manora Peak (29.4 ˚N, 79.5 ˚E, 1950 m) from the Central Himalaya [*Ram et al.*, 2010a] and Nepal Climate Observatory Pyramid (NCO-P; 27.95 ˚N, 86.82 ˚E, 5079 m) from the Higher Himalaya [*Decesari et al.*, 2010], have also been used in comparison, as a reference to the aerosol source region in the IGP and to discuss a comparative scenario for the high-altitude locations in the Himalaya.

4.2.2 Air-mass back trajectories:

Seven-day (for the average residence time of atmospheric aerosols) air-mass back trajectories are computed at 12: 00 h (local time) using NOAA-Air Resource Laboratory HYSPLIT-Model (GADS data set) [*Draxler and Rolph*, 2003] at arrival heights of 100 m, 500 m and 1000 m (above ground level; AGL).

As the air-mass back trajectories for a particular day at these heights point to the same origin, for the sake of brevity the wind-regimes over NE-Himalaya (NE-H) is represented in figure 4.1 for an intermediate height of 500 m AGL for all the sampling days (n = 51) during January–March. Furthermore, the air-masses arriving at the sampling site (Figure 4.1) are classified into two groups, those passing over the IGP (referred to as TYPE-I) and those passing over the south-China (referred to as TYPE-II). The air-masses show dominant influence from the IGP (TYPE-I: 80%), with discernible contribution from south-east Asia (south-China; TYPE-II: 20%). Thus, the air-masses during January–March, transport aerosols from the Indo-Gangetic Plain (IGP) and south-east Asia making the aerosol burden relatively high in NE-H, as compared to the rest of the year (April–December) when the site remains relatively clean due to frequent wet precipitation.

4.3. Results and Discussion

4.3.1 Mass concentrations of PM2.5, EC, OC, WSOC and ΣPAHs

4.3.1.1 TYPE-I Air-masses (Passing over the IGP)

The mass concentration of PM2.5 in NE-H (associated with TYPE-I air-masses) varied from 39–211 μg m^{-3} (Av: 91 ± 37 μg m^{-3}). The concentrations of OC, EC, WSOC and ΣPAHs also exhibit large variability (Figure 4.2): 10.1–80.5 μg m^{-3} (Av ± sd: 33.1 ± 16.8); 2.6–11.0 μg m^{-3} (Av: 5.0 ± 1.8); 7.0–51.6 μg m^{-3} (Av: 21.9 ± 9.1) and 4.1–27.7 ng m^{-3} (Av: 13.5 ± 5.4) respectively. The contribution of OC and EC to PM2.5 ranged from 9–48% (Av: 35 ± 8%) and 2–14% (Av: 6 ± 3%), respectively. The OC/TC and EC/TC mass fractions over NE-H (associated with TYPE-I air-masses) account for 85 ± 6% and 15 ± 6% respectively (Figure 4.3;

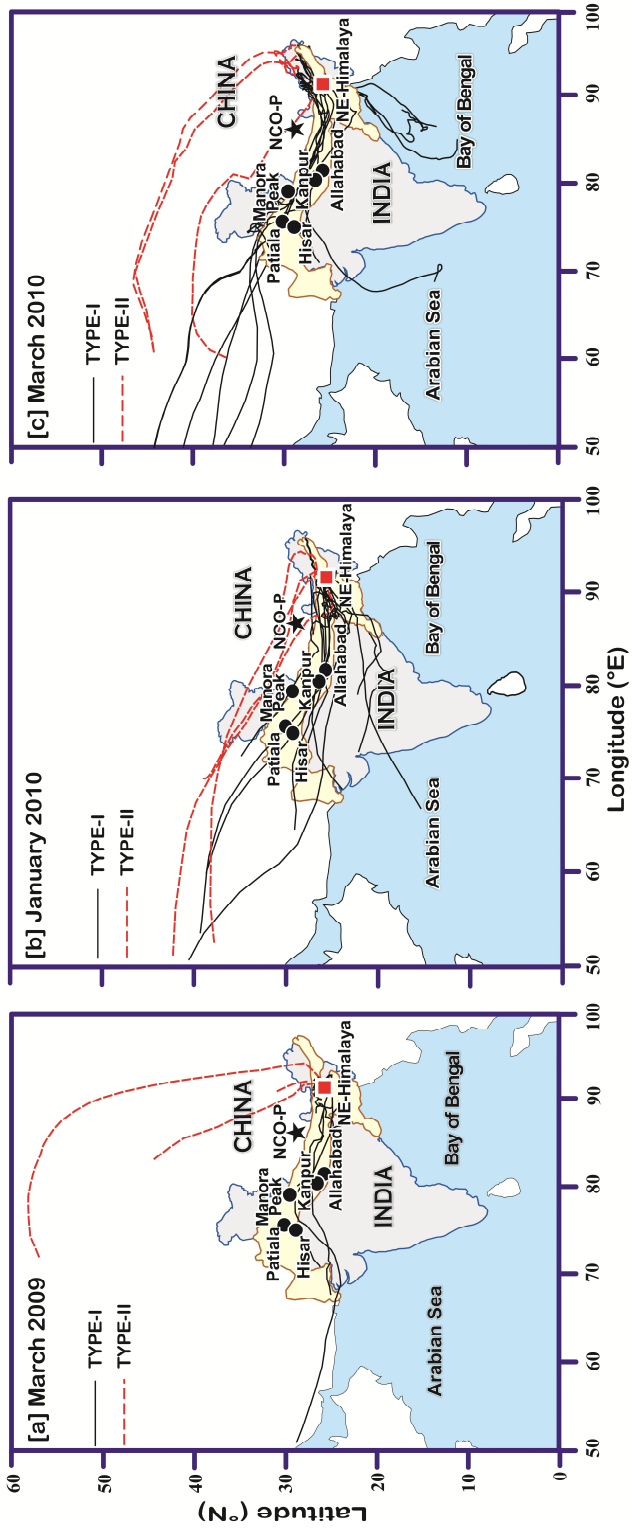

Figure 4.1: Air-mass back trajectories (at 500 m AGL) arriving at Barapani (NE-Himalaya), indicate dominant impact from the IGP (TYPE-I).

total carbon in aerosols, corrected for inorganic carbonates: TC = OC+EC: 38.1 ± 17.7 μg m^{-3}).

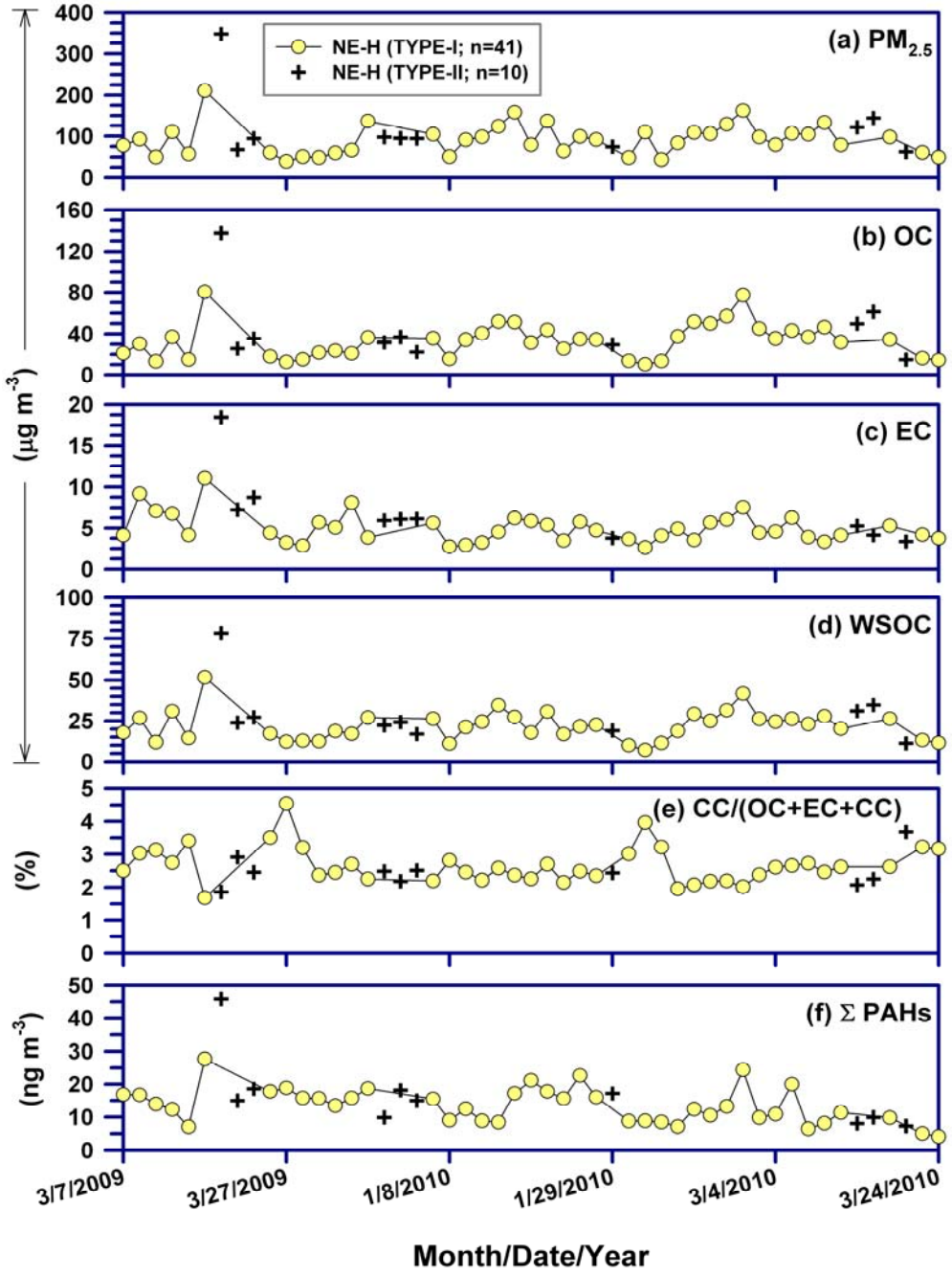

Figure 4.2: Temporal variability of (a) PM2.5 and the associated carbonaceous species: (b) OC; (c) EC; (d) WSOC; (e) carbonate carbon (CC) and (f) ΣPAHs, over NE-H.

In view of the dominant air-mass transport, pointing from the IGP, it is relevant to compare the data from NE-H with those reported from its source region (IGP).

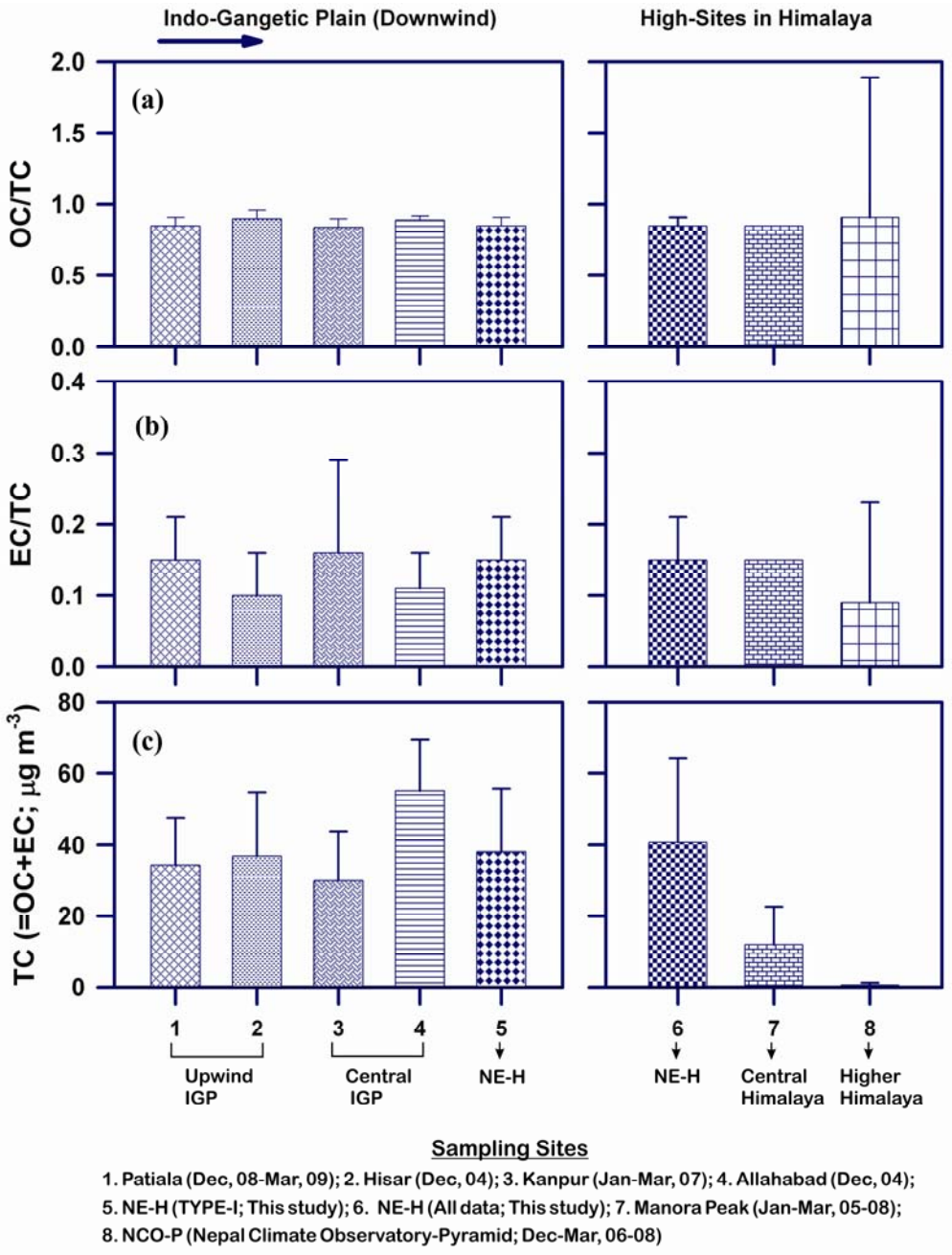

Figure 4.3: Spatial variability in: (a) OC/TC ratio; (b) EC/TC ratio and (b) TC (total carbon: OC+EC) concentration.

Comparing the data from two upwind locations in the IGP, at Patiala and Hisar, revealed similar mass fractions of OC/TC and EC/TC have been reported: 85 ± 6% and 15 ± 6% at Patiala (TC: 34.3 ± 13.3 μg m^{-3}), and 90 ± 6% and 10 ± 6% respectively at Hisar (TC: 36.8 ± 18.0 μg m^{-3}) [*Rajput et al.*, 2011b; *Rengarajan et al.*, 2007]. Furthermore, similar contribution from Central IGP at Kanpur (OC/TC: 84 ± 6% and EC/TC: 16 ± 13%; TC: 29.8 ± 14.1 μg m^{-3}) and Allahabad (OC/TC: 89 ± 3% and EC/TC: 11 ± 5%; TC: 55.2 ± 14.2 μg m^{-3}) have also been reported earlier [*Ram and Sarin*, 2010]. Thus, similarity in OC to TC and EC to TC ratio over a large stretch of IGP and over NE-H suggest carbonaceous aerosol composition to be similar (for winter months: December–March), attributable to the atmospheric impact from similar sources over these locations.

4.3.1.2 TYPE-II Air-masses (Passing over the south-China)

The mass concentration of PM2.5 in NE-H (for TYPE-II air-masses) varied from 62–348 μg m^{-3} (Av: 120 ± 84 μg m^{-3}). The concentrations of associated OC, EC, WSOC and ΣPAHs exhibit large variability too (Figure 4.2): 14.8–137.7 μg m^{-3} (Av: 44.5 ± 35.4); 3.4–18.5 μg m^{-3} (Av: 6.9 ± 4.4); 11.2–78.3 μg m^{-3} (Av: 28.9 ± 18.6) and 7.3–45.9 ng m^{-3} (Av: 16.5 ± 11.1) respectively. The contribution of OC and EC to PM2.5 ranged from 24–43% (Av: 35 ± 6%) and 3–11% (Av: 6 ± 2%), respectively. The OC/TC and EC/TC mass fractions in NE-H (associated with TYPE-II air-masses), account for 85 ± 5% and 15 ± 5% respectively (TC: 51.4 ± 39.2 μg m^{-3}). The overall OC/TC and EC/TC mass fractions in NE-H (n = 51; Figure 4.3), account for 85 ± 6% and 15 ± 6% respectively (TC: 40.7 ± 23.6 μg m^{-3}).

Interestingly, similar contribution from Central Himalaya (Manora Peak; OC/TC: 85% and EC/TC: 15%; TC: 12.1 ± 10.5 μg m^{-3}) have also been reported earlier [*Ram et al.*, 2010a]. Moreover, though the atmospheric concentration of total carbon (TC: OC+EC = 0.67 ± 0.6 μg m^{-3}) is an order of magnitude less over the Nepal Climate Observatory-Pyramid (NCO-P), located in southern-slope of Higher Himalaya [*Decesari et al.*, 2010], as compared to that observed from the

IGP, NE-Himalaya (NE-H; this study) and over the Central Himalaya (Manora Peak), the OC/TC (91%) and EC/TC (9%) mass fractions from the southern-slope of Higher Himalaya look similar to that observed from these locations. The similarity in OC to TC and EC to TC mass fractions over southern-slope of Higher Himalaya, Central Himalaya and NE-Himalaya (NE-H; this study) reveals the impact of long-range transport of carbonaceous aerosols of similar nature over these high-altitude locations in the Himalaya (for winter months: December–March).

The profile of individual PAHs concentration (mg g^{-1} OC) from NE-H, associated with TYPE-I and TYPE-II air-masses, is given in Table 4.1. Furthermore, the earlier reported PAHs profile (mg g^{-1} OC) from Patiala [*Rajput et al.*, 2011b] is also given in Table 4.1 (referred as Upwind IGP).

Table 4.1: Average mass fractions of PM2.5-bound PAHs (mg g^{-1} OC)

PAHs	NE-Himalaya		Upwind IGP[a]
	Air-mass (TYPE-I)	Air-mass (TYPE-II)	
NAPH	0.007 ± 0.005	0.011 ± 0.013	0.015 ± 0.019
ACY	0.003 ± 0.002	0.003 ± 0.003	0.002 ± 0.002
2-BrNAPH	0.003 ± 0.003	0.001 ± 0.001	0.000 ± 0.000
ACE	0.001 ± 0.001	0.001 ± 0.002	0.001 ± 0.001
FLU	0.002 ± 0.001	0.003 ± 0.003	0.002 ± 0.001
PHEN	0.012 ± 0.008	0.016 ± 0.012	0.014 ± 0.006
ANTH	0.003 ± 0.002	0.004 ± 0.004	0.002 ± 0.001
FLA	0.028 ± 0.022	0.045 ± 0.038	0.029 ± 0.011
PYR	0.031 ± 0.024	0.048 ± 0.039	0.033 ± 0.011
BaA	0.020 ± 0.010	0.025 ± 0.015	0.019 ± 0.011
CHRY+TRIPH	0.039 ± 0.017	0.050 ± 0.033	0.054 ± 0.028
B[b,j,k]FLA	0.128 ± 0.052	0.155 ± 0.092	0.201 ± 0.097
BaP	0.055 ± 0.028	0.063 ± 0.035	0.074 ± 0.033
IcdP	0.058 ± 0.032	0.077 ± 0.055	0.115 ± 0.041
D[ah,ac]ANTH	0.008 ± 0.004	0.008 ± 0.005	0.012 ± 0.008
BghiP	0.053 ± 0.027	0.069 ± 0.048	0.110 ± 0.039
ΣPAHs	0.450 ± 0.222	0.580 ± 0.375	0.683 ± 0.243

[a] Data source for Upwind Indo-Gangetic Plain (at Patiala; n=28) is adopted from [*Rajput et al.*, 2011b]. TYPE-I: refers to air-masses passing over the Indo-Gangetic Plain and arriving at NE-Himalaya (NE-H) and those passing over the south-China are referred as TYPE-II (Reference is made to Figure 4.1 for further description).

One of the noticeable features of the data relates to the lower mass fraction of PAHs (mg g^{-1} of OC) over NE-H as compared to that in the Upwind IGP (Table 4.1).

4.3.2 Atmospheric aging/mixing of aerosols during long-range transport

Atmospheric aging and mixing of aerosols (of different origin and age) are the two important atmospheric processes that decide the fate of chemical composition of aerosols, after its emission. So the aerosol composition keeps changing from its source value, due to these two principal governing factors, during the course of transport. Interestingly, aerosol mixing has a pre-defined lower and upper bound values for any chemical proxy.

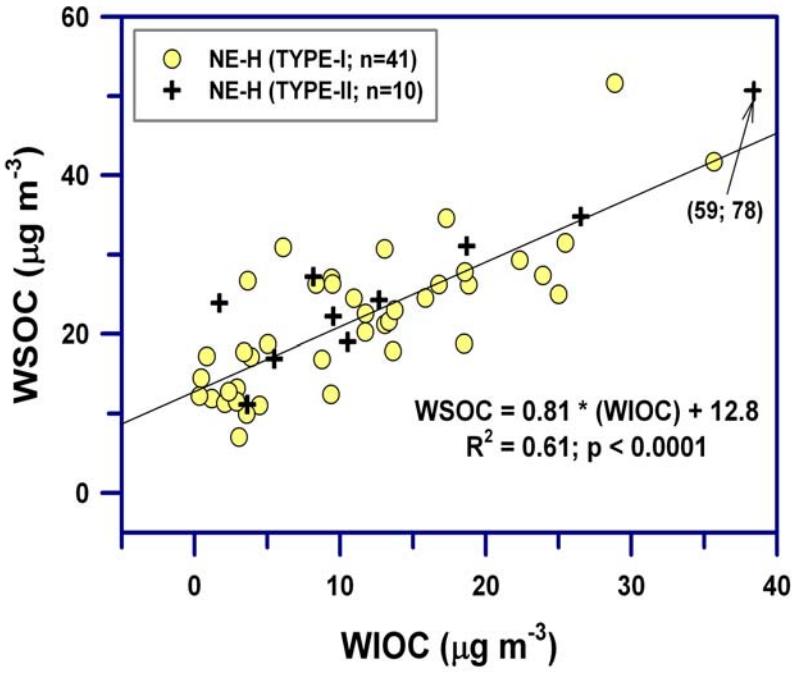

Figure 4.4: Scatter plot showing a significant correlation (TYPE-I air-masses) between water soluble- and water insoluble-organic carbon (WSOC and WIOC) in aerosols.

And therefore the abundance of any chemical proxy, after mixing, can be predicted to fall at a particular point in between the two bounded values of its source, provided the relative contribution from sources in aerosols is known.

In contrast, the influence of atmospheric aging on any chemical constituent is expected to decrease its abundance. The extent of decrease depends on the age of air-mass (decreases with aging). Three ways are utilized to assess the prominent affect between mixing and atmospheric aging of carbonaceous aerosols during their long-range transport over NE-H: (i) Correlation analysis of WSOC with water-insoluble organic carbon (WIOC); (ii) WSOC/OC ratio in conjunction with the OC/EC ratio, and ΣPAHs/EC ratio: comparison between source-region and the study site (NE-H); (iii) Relative abundance of PAHs (normalized to EC): comparison between source value and that observed over NE-H. Statistical analysis of WSOC concentrations with water-insoluble organic carbon (WIOC) has been used to infer about the atmospheric processing of carbonaceous aerosols.

The linear regression between WSOC with WIOC in samples associated with TYPE-I air masses (Figure 4.4, 4.1) is performed, for statistically significant number of data sets (n = 41). As shown in Figure 4.4, WSOC concentrations are positively correlated with WIOC (R^2 = 0.61; $p<0.0001$). This observation indicates towards the potential pathway of secondary organic aerosol (SOA) formation through atmospheric aging of water-insoluble organic aerosols over NE-H. The spatial variability in WSOC/OC ratio in conjunction with OC/EC ratio is shown in figure 4.5. Accordingly, the OC/EC ratio in NE-H, associated with TYPE-I and TYPE-II air-masses, is found to be 4.6 ± 1.3 (R^2 = 0.24, $p<0.01$) and 6.9 ± 1.5 (R^2 = 0.72, $p<0.01$), respectively. The OC/EC ratios (Figure 4.5a) for the upwind locations in the IGP at Patiala and Hisar are 3.8 ± 1.3 (R^2=0.23, $p<0.01$; for data set from December 2008–March 2009) and 6.7 (R^2 = 0.72; December 2004) respectively [Rajput et al., 2011b; Ram and Sarin, 2010]. Furthermore, an earlier study from Central IGP site at Kanpur (26.5 ˚N, 80.3 ˚E, 142 m) and Allahabad (25.4 ˚N, 81.9 ˚E, 123 m) has reported similar OC/EC ratios of 6.2 ± 3.7 for January–March, 2007 and 6.7 (R^2 = 0.72) for December, 2004 respectively [*Ram and Sarin*, 2010]. Interestingly, similar OC/EC ratio of 6.0 (R^2 = 0.80) has also been reported from Central Himalaya.

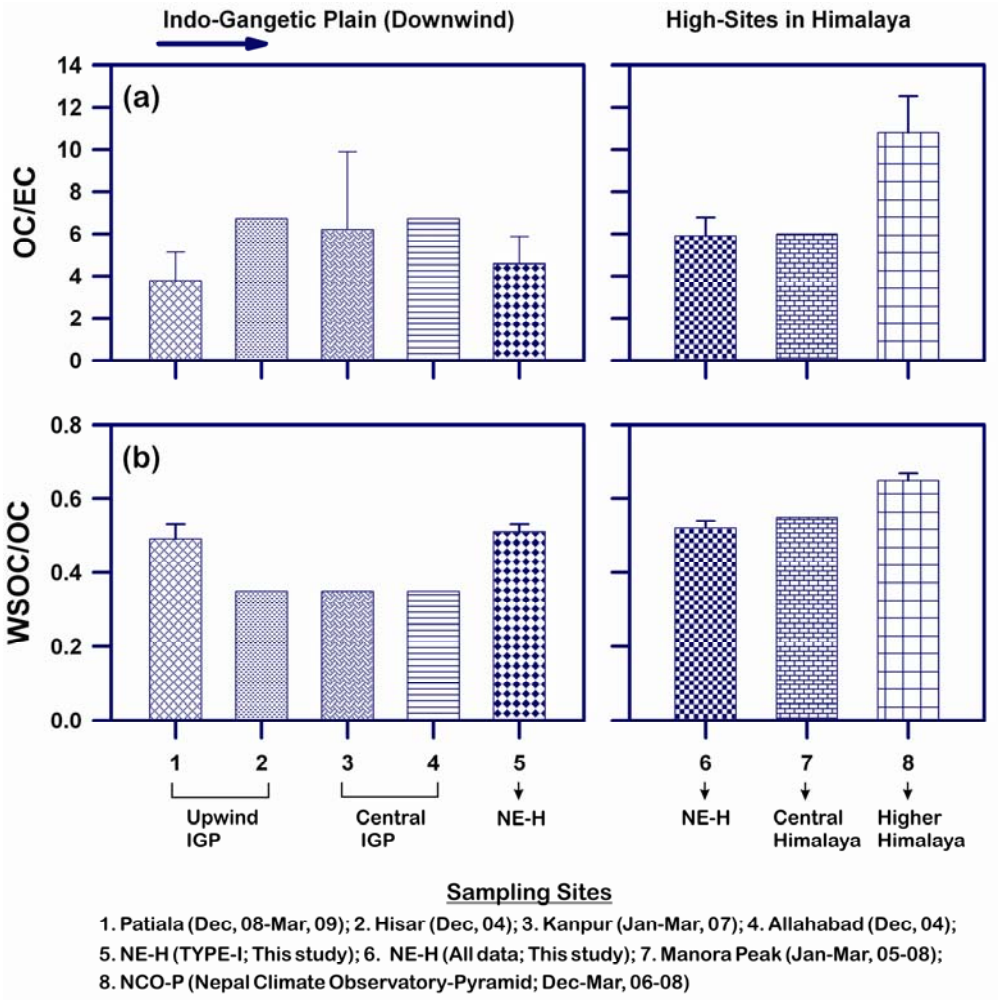

Figure 4.5: Spatial variability in: (a) OC/EC and (b) WSOC/OC ratios to assess the atmospheric aging of aerosols.

From Higher Himalaya (Nepal Climate Observatory-Pyramid; Figure 4.5a), a study has documented OC/EC average ratio of 10.8 ± 1.7 [*Decesari et al.*, 2010]. It would be relevant to state that the data sets on OC/EC ratio from IGP location, Central Himalaya and NE-H are constrained from linear regression analysis, in contrast to the available average ratio from Higher Himalaya [*Decesari et al.*, 2010]. Thus, relatively high OC/EC average ratio from Higher Himalaya as compared to the other locations (discussed above) could be due to high ratios in a few aerosol samples.

Thus, near constancy in OC/EC ratio over NE-H with that in the IGP and Central Himalaya (Figure 4.5a) facilitates of using WSOC to OC ratio as a proxy

to assess the atmospheric aging of carbonaceous aerosols. The logic behind this argument is that for a constant OC to EC ratio, enhancement in WSOC to OC ratio can only be due to atmospheric aging of particulate organic carbon [*Decesari et al.*, 2002]. The WSOC/OC ratio in NE-H, for TYPE-I and TYPE-II air-masses (this study) are 0.51 ± 0.02 (R^2 = 0.89, p<0.0001; OC: 33.1 ± 16.8 μg m^{-3}) and 0.52 ± 0.02 (R^2 = 0.98, p<0.0001; OC: 44.5 ± 35.4 μg m^{-3}) respectively, ranging from 0.50–0.97. Relatively lower WSOC/OC ratio has been reported in aerosols for Central IGP locations: at Kanpur (0.35; R^2 = 0.86; OC: 25.0 ± 13.8 μg m^{-3}) and Allahabad (0.35; R^2 = 0.82; OC: 49.0 ± 14.1 μg m^{-3}) [*Ram and Sarin*, 2010]. Further Upwind IGP locations, Patiala and Hisar are marked by WSOC/OC ratio of 0.49 ± 0.04 (R^2 = 0.88, p<0.0001; OC: 29.0 ± 12.4 μg m^{-3}) and 0.35 (R^2 = 0.86; OC: 33.0 ± 17.9 μg m^{-3}) respectively (Figure 4.5b) [*Ram and Sarin*, 2010].

Moreover, the WSOC/OC ratio over NE-H (0.52 ± 0.02; R^2 = 0.94, p<0.0001) is similar to that reported from Central Himalaya (0.55, R^2 = 0.82; OC: 10.3 ± 5.2 μg m^{-3}; Manora Peak; Figure 4.5b) [*Ram et al.*, 2010a], and relatively low as compared to average ratio reported from the Higher Himalaya (Nepal Climate Observatory-Pyramid; WSOC/OC: 0.65 ± 0.02; OC: 0.36 ± 0.35 μg m^{-3}) [*Decesari et al.*, 2010]. Summing up, relatively high WSOC/OC ratio (Av: 0.51) in NE-H, as compared to that in the IGP, with near constancy in OC/EC ratio ~6, further indicates the potential role of heterogeneous atmospheric oxidation (aging) of particulate OC in enhancing the water-soluble organic carbon content in aerosols. Moreover, enhanced contribution of WSOC to OC reported from NE-Himalaya (this study), Central Himalaya and Higher Himalaya, as compared to that from the source region, highlights the significant role of atmospheric processing of carbonaceous aerosols in altering their chemical composition and thereby its atmospheric impact on a regional scale.

4.3.3 Atmospheric concentration of ΣPAHs and ΣPAHs/EC ratio

The PM2.5-bound ΣPAHs concentration (ng m^{-3}) exhibits significant temporal variability in NE-H. The ΣPAHs concentrations varied from 4.1–27.7 ng m^{-3} (Av ± 1σ: 13.5 ± 5.4) and 7.3–45.9 ng m^{-3} (Av: 16.5 ± 11.1) in the TYPE-I

and TYPE-II air-masses respectively. The ΣPAHs/EC ratio (mg g^{-1}) varied from 1.10–5.88 (1.72 ± 0.39; $R^2 = 0.33$, $p<0.0001$; Figure 4.6) for TYPE-I air-masses.

Furthermore, the ΣPAHs/EC average ratio for TYPE-II air-masses varied from 1.54–4.55 (2.44 ± 0.85) mg g^{-1}. During the wintertime, the ΣPAHs concentration varying from 3.3–47.9 (19.9 ± 11.2) ng m^{-3} and ΣPAHs/EC ratio from 1.32–9.58 (3.54 ± 1.19; $R^2 = 0.25$, $p<0.0001$; Figure 4.6) mg g^{-1} in PM2.5 has been reported recently for an Upwind IGP site at Patiala [*Rajput et al.*, 2011b].

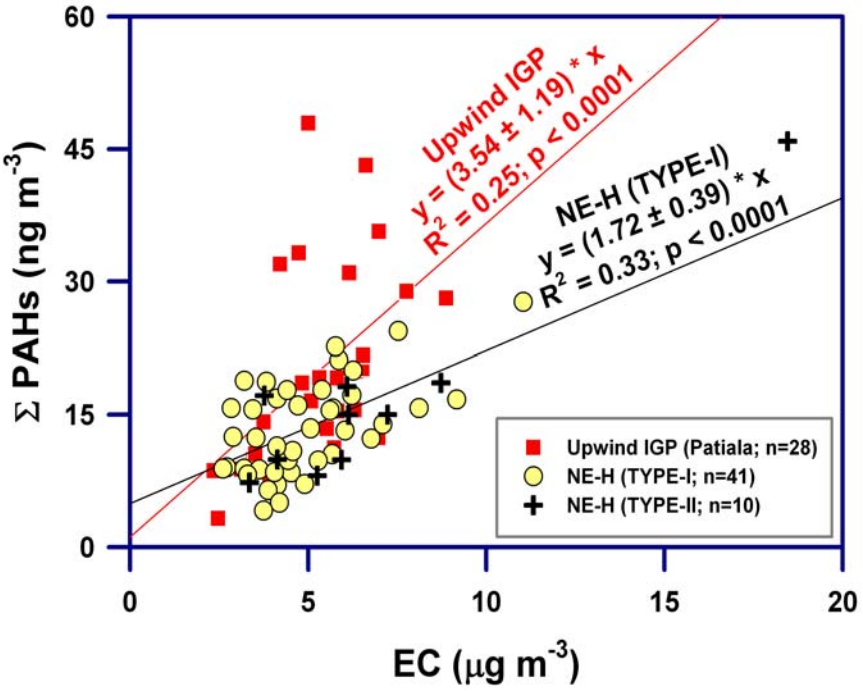

Figure 4.6: Scatter plot shows a significant decrease in ΣPAHs/EC ratio (mg g^{-1}): from 3.54 mg g^{-1} at Upwind IGP (Patiala) to 1.72 mg g^{-1} at NE-H.

Thus, a significant decrease in ΣPAHs concentration and ΣPAHs/EC ratio in NE-Himalaya as compared to that in the Upwind IGP (Patiala) is revealed from this study. At this stage, it would only be relevant to state that the probable cause for this decrease can be attributed either due to mixing of aerosols (of different origin/age) and/or atmospheric aging during their transport from the IGP to NE-H. Further discussion, elucidating the potential role between the mixing and/or

atmospheric aging in lowering the atmospheric abundances of PAHs during their transport over NE-H has been made, using the PAH isomers to EC ratio.

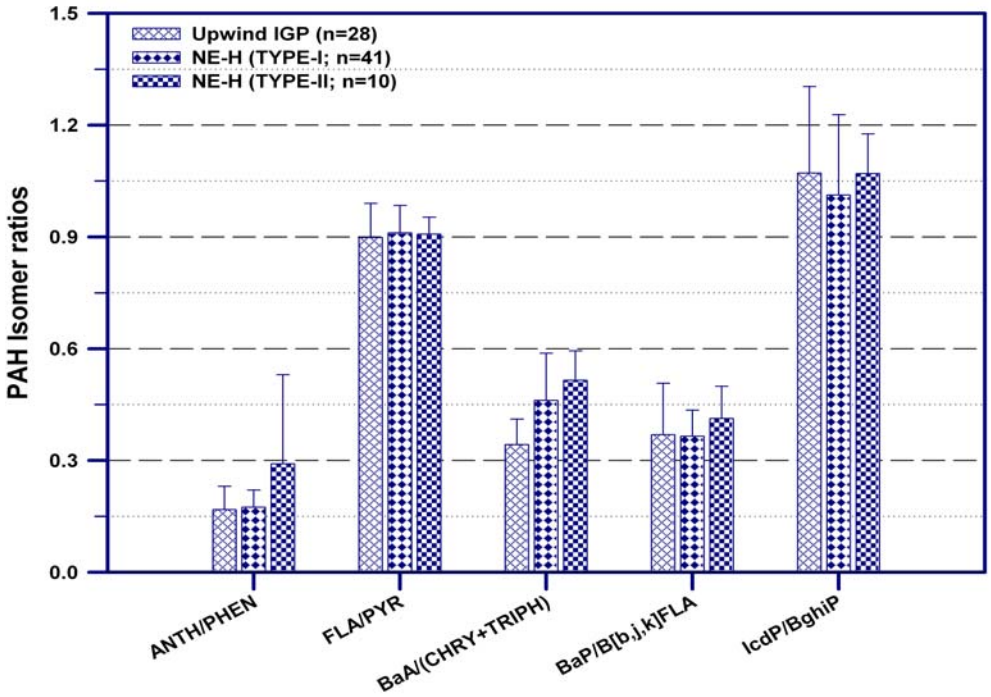

Figure 4.7: Comparison of PAH isomer ratios from NE-H and Upwind IGP. The data for Upwind IGP (Patiala) is adopted from [Rajput et al., 2011b].

However, it would be relevant to first assess for the dominant source of carbonaceous aerosols over NE-H (from source-region in the IGP), using PAHs isomer ratios and then compare the relative abundances of PAH isomers to EC ratios over NE-H with that reported for its dominant source. This approach would facilitate in concluding the potential factor between the two, mixing and atmospheric aging, affecting the composition of carbonaceous aerosols during their long-range transport.

Before the discussion is further made to distinguish the potential role of mixing or atmospheric aging of carbonaceous aerosols using the PAHs, it is relevant to assess the stability of its isomer ratios during the transport (dominant from IGP region) and also the percentage contribution from different sources. In the subsequent sections, percentage contribution from different sources of

carbonaceous aerosols and then the dominant influence between mixing and effect of atmospheric aging has been discussed, using the PAHs isomer pairs.

4.3.4 PAHs isomer ratios

The isomer ratios of PAHs with 3-, 4-, 5- and 6-ring, (ANTH/PHEN; FLA/PYR; BaA/{CHRY+TRIPH}; BaP/B[b,j,k]FLA and IcdP/BghiP) from NE-H have been compared (Figure 4.7) with the available literature-based data that from an Upwind site (Patiala) in the IGP [*Rajput et al.*, 2011b]. It is relevant to state that the data on PAHs for other locations in the IGP is not available in the literature. The ANTH/PHEN ratio reported at Patiala is 0.16 ± 0.06, and that observed in this study over NE-H are 0.29 ± 0.24 (TYPE-I) and 0.26 ± 0.08 (TYPE-II) respectively.

The FLA/PYR ratio at Patiala is 0.90 ± 0.10, and 0.91 ± 0.05 (TYPE-I) and 0.90 ± 0.05 (TYPE-II) in NE-H. The BaA/{CHRY+TRIPH} ratio at Patiala is 0.34 ± 0.06, and 0.52 ± 0.08 (TYPE-I) and 0.51 ± 0.06 (TYPE-II) in NE-H. The BaP/B[b,j,k]FLA ratio at Patiala is 0.36 ± 0.14, and 0.41 ± 0.09 (TYPE-I) and 0.43 ± 0.10 (TYPE-II) in NE-H. The IcdP/BghiP ratio at Patiala is 1.07 ± 0.23, and 1.07 ± 0.11 (TYPE-I) and 1.10 ± 0.14 (TYPE-II) in NE-H. Thus, in general, PAHs isomer ratios looks similar (within ± 1σ) in NE-H with that reported for the Upwind IGP (Patiala; Figure 4.7).

4.3.5 Finger-printing of source regions for carbonaceous aerosols

The simple approach for the qualitative source-apportionment of carbonaceous aerosols using the PAHs isomer ratios has been provided by an earlier study [*Yunker et al.*, 2002]. The similar approach using cross plot of the PAHs isomer ratios, FLA/(FLA+PYR) versus: (Figure 4.8a) ANTH/(ANTH+PHEN); (Figure 4.8b) BaA/(BaA+CHRY+TRIPH); (Figure 4.8c) BaP/(BaP+B[b,j,k]FLA) and (Figure 4.8d) IcdP/(IcdP+BghiP), has been adopted for the present study over the NE-H. The literature based PAH isomer ratios for Upwind IGP (from Patiala), paddy-residue burning, vehicular (gasoline and diesel) emissions, coal combustion and bio-fuels (Cowdung cake and eucalyptus) burning is also shown in figure 4.8 (with reference to the data). As the PAH

isomer ratios from NE-H overlaps with that from Upwind IGP and also with that for biomass (paddy-residue and bio-fuel) burning emissions, the dominant impact of biomass burning emissions in the IGP and its downwind transport to the NE-H is revealed here.

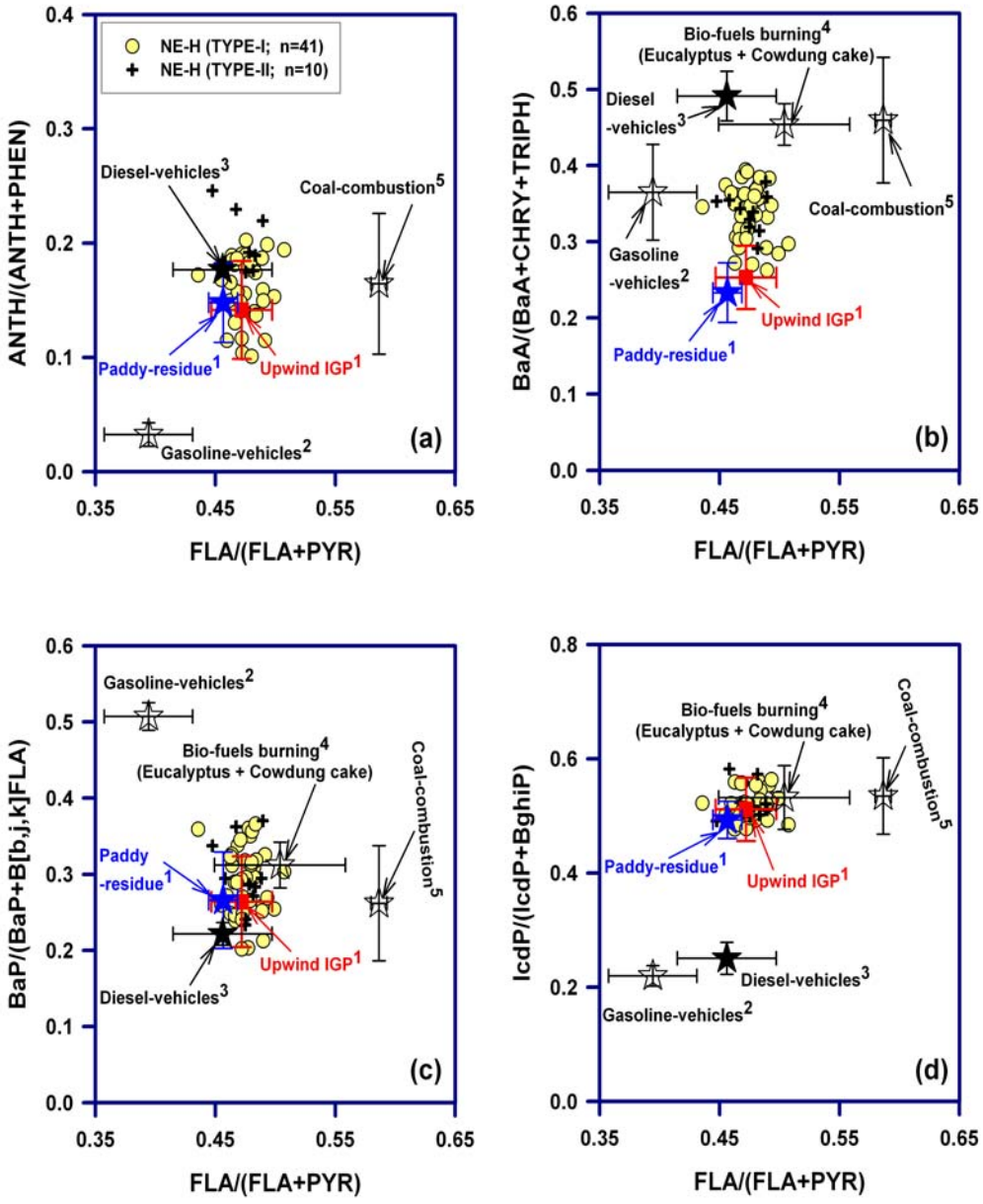

Figure 4.8: Cross plot of FLA/(FLA+PYR) versus: (a) ANTH/(ANTH+PHEN); (b) BaA/(BaA+CHRY+TRIPH); (c) BaP/(BaP+B[b,j,k]FLA) and; (d) IcdP/(IcdP+BghiP). Other data source: [1][Rajput et al., 2011b]; [2][Khillare et al., 2005a]; [3][Khillare et al., 2005b]; [4][Schauer et al., 2001; Sheesley et al., 2003]; [5][Khalili et al., 1995; Kirton et al., 1991; Li et al., 2010].

Furthermore, the quantitative source-apportionment of carbonaceous aerosols has been performed by solving the matrix, as represented below in equations (4.1–4.5), using Mathematica 8.0. The subscript, *G* represents for gasoline-based vehicular emission, *D* for diesel-based vehicular emission, *C* for coal-combustion, *B* for bio-fuels (Cowdung cake and eucalyptus) burning, *R* for rice-straw (also referred as paddy-residue) burning and subscript 0 for the observations in ambient aerosols over NE-H (present study). The unique and exact solution determined for the above matrix for all individual aerosol samples (n = 51) apportions the contribution from five sources: gasoline-based vehicular emission, diesel-based vehicular emission, coal-combustion, bio-fuel (Cowdung cake and eucalyptus) and rice-straw (also referred as paddy-residue) burning.

$$f_G + f_D + f_C + f_B + f_R = 1 \tag{4.1}$$

$$F_G f_G + F_D f_D + F_C f_C + F_B f_B + F_R f_R = F_0 \tag{4.2}$$

$$BA_G f_G + BA_D f_D + BA_C f_C + BA_B f_B + BA_R f_R = BA_0 \tag{4.3}$$

$$BP_G f_G + BP_D f_D + BP_C f_C + BP_B f_B + BP_R f_R = BP_0 \tag{4.4}$$

$$I_G f_G + I_D f_D + I_C f_C + I_B f_B + I_R f_R = I_0 \tag{4.4}$$

Here, *f* represents the fractional contribution for a particular emission source, *F* represents PAHs isomer ratio FLA/(FLA+PYR), *BA* for BaA/(BaA+CHRY+TRIPH), *BP* for BaP/(BaP+B[b,j,k]FLA) and *I* for IcdP/(IcdP+BghiP).

The present study from NE-H (Figure 4.9), demonstrate that about 80% of the carbonaceous aerosols are derived from biomass (bio-fuels and rice-straw) burning from the source region in the Indo-Gangetic Plain (IGP). Result from this study is similar to that concluded by the bottom-up approach based emission inventories (~70% of the black carbon to be derived from biomass burning emission) for the south-Asian region [*Gustafsson et al.*, 2009; *Venkataraman et*

al., 2005], in contrast to the top-down approach suggesting 50–90% of the black carbon derived from fossil-fuel combustion sources [*Mayol-Bracero et al.*, 2002a; *Novakov et al.*, 2000; *Ramanathan et al.*, 2007; *Stone et al.*, 2007]. Now it would be relevant to decouple the prominent affect between the mixing and atmospheric aging of carbonaceous aerosols, based on PAH isomers to EC ratio.

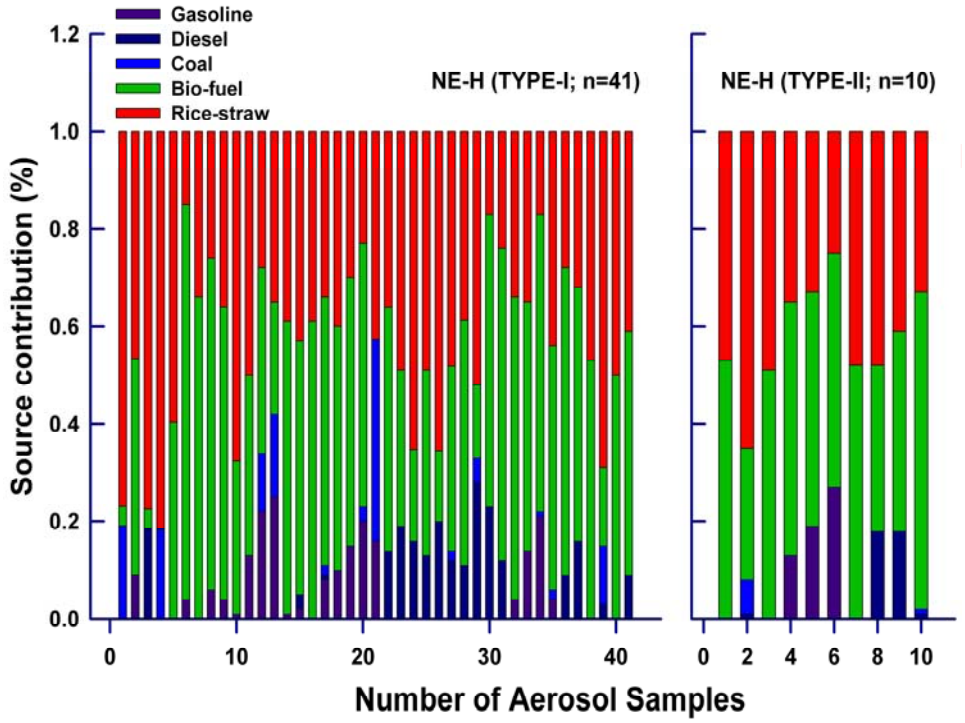

Figure 4.9: Dominant impact of biomass burning emissions accounting for ~80% to the total budget of carbonaceous aerosol over NE-H, from the IGP is depicted.

4.3.6 Atmospheric aging of carbonaceous aerosols: Use of PAH isomers

The above discussion on finger-printing of emissions from source regions has revealed the dominant source (~80%) for carbonaceous aerosols from biomass (agricultural-waste: rice-straw or referred as paddy-residue and bio-fuels: Cowdung cake and eucalyptus) burning. It is obvious from figure 4.10 that the PAH isomers to EC ratio in NE-H are much lower as compared to their abundance ratio from dominant source (biomass burning emission). The aerosol mixing with 80% from biomass burning and 20% from fossil-fuel combustion (as quantified in this study) cannot explain the observed PAH isomers to EC ratio over the NE-H

(Figure 4.10), significantly lower from its dominant source (biomass burning). And therefore, it can be finally concluded that atmospheric aging is the dominant factor over the mixing in changing the aerosol characteristics transported to the NE-H. Summing up, the reactive nature of PAHs provides a tool to assess the atmospheric aging of carbonaceous aerosols (Figure 4.10). On the contrary, the stability of PAHs isomer ratios from its source location (IGP) facilitates for their quantitative estimation from distinct sources (Figure 4.8, 4.9).

4.3.7 Chemical reactivity of PAHs

Recent studies have addressed the issue on secondary organic aerosol (SOA) formation via chemical oxidation of PAHs [Chan et al., 2009; Kaiser et al., 2011]. Several laboratory- and field-based experiments have also observed the potential of PAHs to react with O_3, NOx and OH radical yielding SOA [*Esteve et al.*, 2004; *Perraudin et al.*, 2007; *Rajput et al.*, 2011b]. Relative rate constant for the heterogeneous reactions of PAH isomers in ambient atmosphere is inferred for the wintertime (January–March), using the data from this study (in NE-H), assessing the atmospheric processing of carbonaceous aerosols over NE-H. Ratio-ratio plot of 4-pairs of PAH isomers (abundant in aerosols; normalized to EC, being a conservative constituent) from the NE-H is shown in figure 4.10.

The log-log plot (Figure 4.10) provides the relative rate constant for PAH isomers by the slope of the lines [*Robinson et al.*, 2006a; *Robinson et al.*, 2006b; *Rudich et al.*, 2007]. This approach is elementary to estimate the relative rate constant between two species, since the concentration is inversely related to rate constant [*Robinson et al.*, 2006a]. However, one of the limitations of the relative rate constant is that though it tells about the reactivity of one compound over the other, information on actual rate of reaction cannot be inferred from it. For the sake of comparison with the laboratory-based observations [*Perraudin et al.*, 2007], relative rate constant of isomer pairs, derived from this study (for ambient atmosphere) and laboratory experiments is given in Table 4.2.

A good agreement between relative rate constant from the ambient aerosol data (this study) and that inferred from laboratory experiments is obvious from Table 4.2. Importantly, the mentioned relative rate constants of PAH isomers (for

ambient aerosols) are expected to represent their reactivity when carbonaceous species are dominant in ambient aerosols (based on the chemical composition from this study). From a laboratory-experiment the rate constants for PAHs (coated onto graphite particles) with NO_2/O_3 has been observed to be of the order of 10^{-16}–10^{-17} cm^3 $molecule^{-1}$ s^{-1}, whereas relatively fast rate constants (~10^{-12} cm^3 $molecule^{-1}$ s^{-1}) are observed with OH radical [*Perraudin et al.*, 2007].

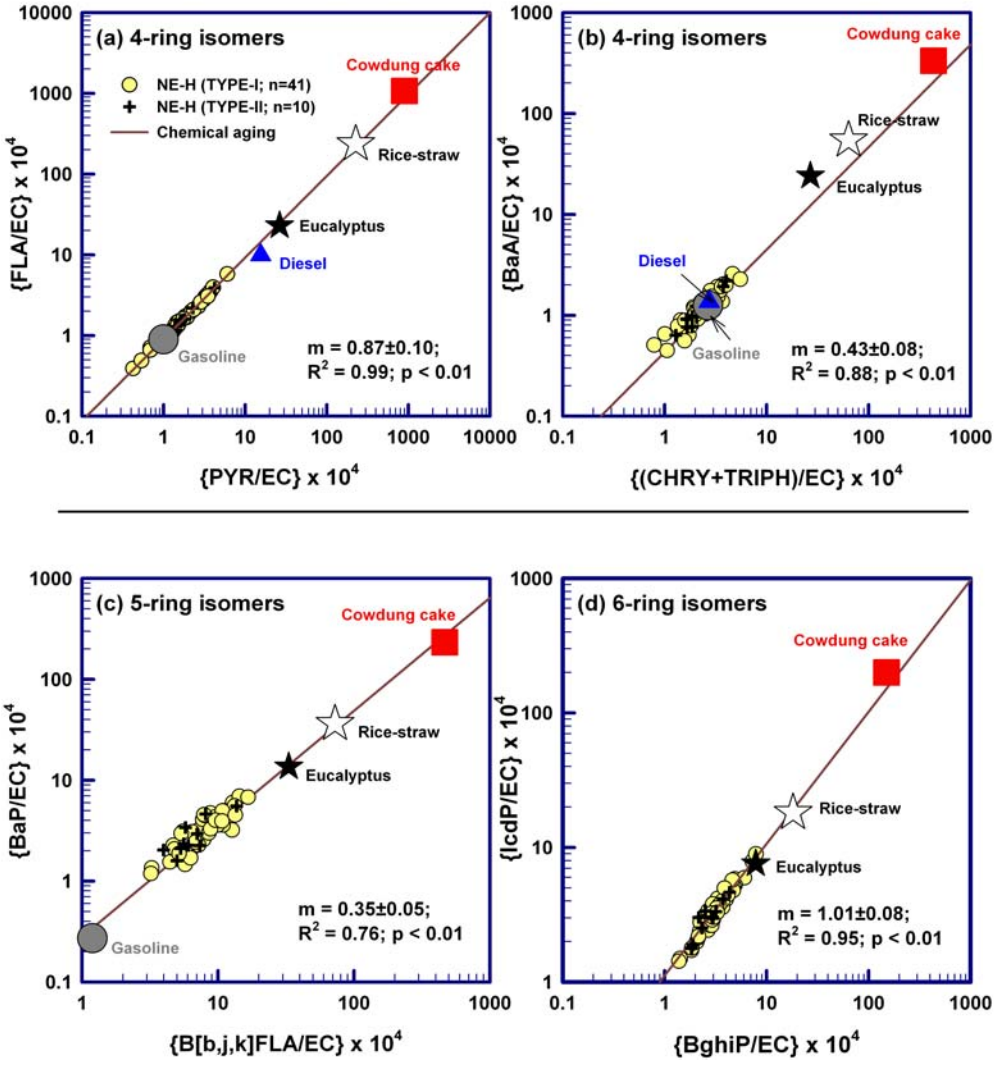

Figure 4.10: Scatter plot of PAH isomers for its potential sources and that from the NE-H to assess atmospheric aging of carbonaceous aerosols. Other relevant data source (average values): $^{Cowdung\ cake}$[Sheesley et al., 2003]; $^{Rice\text{-}straw}$[Sheesley et al., 2003]; ^{Eucalyptus}[Schauer et al., 2001]; ^{Gasoline}[Khillare et al., 2005a]; ^{Diesel}[Khillare et al., 2005b].

It is also obvious from Table 4.2 that BaA and BaP react rapidly than their isomers (CHRY+TRIPH) and B[b,j,k]FLA, in contrast to the other two isomer pairs which exhibit similar reactivity; FLA vs. PYR and IcdP vs. BghiP.

Table 4.2: Relative rate constants (Av ± 1σ) of PAH isomers for heterogeneous-phase reactions in ambient aerosols

Relative Rate constant (k)	*(Ambient Atmosphere)*[a]	*Laboratory study*[b] *(PAHs adsorbed onto Graphite)*		
		OH	**NO_2**	**O_3**
k_{PYR} / k_{FLA}	0.87 ± 0.10	1.00	1.76	1.32
$k_{(CHRY+TRIPH)} / k_{BaA}$	0.43 ± 0.08			
$k_{B[b,j,k]FLA} / k_{BaP}$	0.35 ± 0.05			
k_{BghiP} / k_{IcdP}	1.01 ± 0.08			1.00 ± 0.49

[a][This study].
[b][*Perraudin et al.*, 2007].

4.4. Summary and Implications

The carbonaceous species (OC, EC, WSOC and PAHs) in atmospheric particulate matter (PM2.5) studied from NE-Himalaya (NE-H) suggest their long-range transport and dominant contribution from biomass burning emission sources in the Indo-Gangetic Plain (IGP). The total carbonaceous aerosols (TCA = 1.9*OC+EC) account for 75 ± 15% of PM2.5 [*Turpin and Lim*, 2001], OC/EC ratio centers at 5.9 ± 0.8. Significant linear correlation between WSOC and WIOC, enhancement in WSOC/OC ratio (≈ 0.51) and relatively low ΣPAHs/EC ratio over NE-Himalaya as compared to its source region in the IGP, and lower abundances of PAH isomers (normalized to EC) as compared to that from its source provide evidence for dominant influence of atmospheric aging of organic aerosols during atmospheric transport over NE-H. The percentage contribution of carbonaceous aerosols from different sources, using the PAHs isomer ratios reveals dominant contribution from biomass burning (~80%). The data obtained in this study also provides the relative rate constant of PAH isomers under ambient atmospheric condition. The transport of carbonaceous species (EC, OC and PAHs) and enhancement in WSOC content in aerosols has implications to

increase the number density of cloud condensation nuclei (CCN). This study, assessing the atmospheric processing of carbonaceous aerosols during their long-range transport, emphasizes the importance of ground-based measurements, the information which is not possible through physical and optical properties of aerosols.

CHAPTER 5

SPATIO-TEMPORAL VARIATION OF PAHS FROM DIFFERENT GEOGRAPHICAL LOCATIONS IN INDIA: URBAN, SEMI-URBAN AND HIGH-ALTITUDE SITES

5.1. Introduction

The chemical characteristic of ambient aerosols from a semi-urban location at Patiala (30.2 ˚N, 76.3 ˚E, 250 m amsl) in the IGP and from the foot-hills of NE-Himalaya at Shillong (25.7 °N; 91.9 °E; 1064 m amsl) have been discussed in chapters 3 and 4, respectively. Furthermore, the inferences derived on source-contributions of carbonaceous aerosols and relative rate constant of PAH isomers in ambient aerosols are also reported in those chapters. This chapter provides an overview of the atmospheric abundances of PAHs in aerosols and their isomer ratios from different geographical locations in India: urban (Ahmedabad: 23.03 ˚N; 72.55 ˚E; 49 m amsl) and high-altitude locations (Mt Abu: 24.6 ˚N; 72.7 ˚E; 1680 m amsl) in western India, and two more locations in the IGP at Hisar (semi-urban; 29.2 ˚N; 75.7 ˚E; 219 m amsl) and Kanpur (urban; 26.5 ˚N, 80.3 ˚E, 142 m amsl).

Brief details on the strategic location of the study sites are as follows. Ahmedabad and Mt Abu locations were selected to assess the PAHs characteristics from high-dust region in western India. Moreover, during SW-monsoon (May–June; referred to as summertime), transport of sea salts from the Arabian Sea and presence of other aerosols such as black carbon, organic carbon and sulphate aerosols makes the study at Ahmedabad more interesting. However, the occurrence of aerosol over Mt Abu is largely governed by their long-range transport under prevailing meteorological winds. And therefore, to assess the heterogeneous reactivity of PAHs in chemically aged aerosols, the Mt Abu serves as an ideal location. Furthermore, wintertime study from Hisar and Kanpur sites provide scenario on the spatial distribution of PAHs concentration and their isomer ratios in the IGP.

5.2. Results and Discussion

5.2.1 Meteorological wind-fields over the sampling locations:

Typical wind-fields over the sampling locations at Ahmedabad and Mt Abu for NE-monsoon (November–February; referred to as wintertime) and SW-monsoon (May–August; referred to as summertime) are shown in Figures 5.1 and

5.2, respectively. Transport of sea salts during SW-monsoon and dominance of mineral dust during the drier period from October–May is a conspicuous feature over the Ahmedabad. Moreover, the NE-winds during wintertime influencing the aerosol mixing and composition is also a conspicuous feature (Figure 5.1).

5.2.2 PM2.5, EC, OC and ΣPAHs over Ahmedabad: A Wintertime study

During winters, the prevailing NE-monsoon favors the transport of aerosol from the Northern India over Ahmedabad (Figure 5.1), and thus, influences the regional aerosol composition and chemistry. The mass concentration of PM2.5 at Ahmedabad (during November–December, referred to as wintertime; Figure 5.3a) varied from 32–161 (Av:85 ± 37) μg m^{-3}.

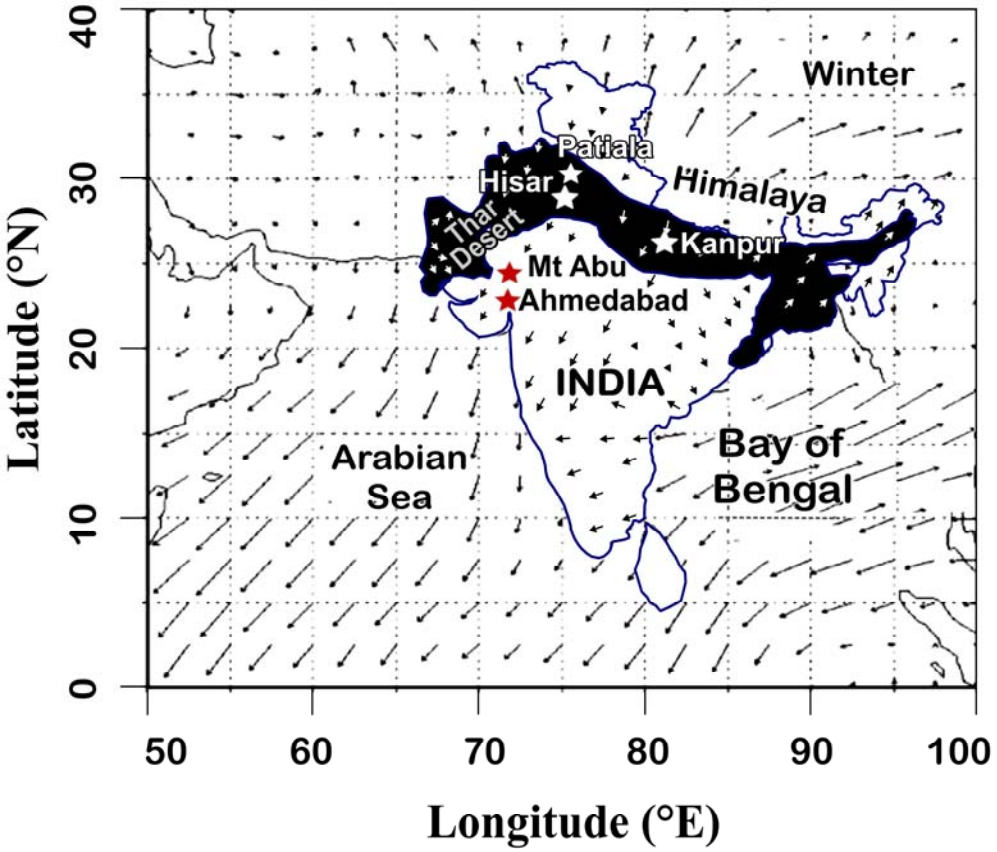

Figure 5.1: Typical wind-fields during wintertime over Ahmedabad and Mt Abu, modified after [Rastogi and Sarin, 2005]. The length of arrow represents the intensity of wind (m s^{-1}).

The concentrations of OC, EC, and ΣPAHs exhibit significant temporal variability: 12–56 (Av: 28 ± 13) μg m^{-3}; 2–8 (Av: 5 ± 2) μg m^{-3}; and 8–92 (Av: 37 ± 27) ng m^{-3}, respectively. The contribution of OC and EC to PM2.5 ranged from 0.18–0.41 (Av: 0.33 ± 0.06) and 0.05–0.08 (Av: 0.06 ± 0.01), respectively (Figure 5.3b). The OC/EC and ΣPAHs/EC ratios varied from 4–8 (6 ± 1) and 4–13 (7 ± 3) mg g^{-1}, respectively (Figure 5.3c). The OC/TC and EC/TC mass fractions over Ahmedabad account for 85% and 15%, respectively (TC: total carbon = OC+EC).

5.2.3 PM2.5, EC, OC and ΣPAHs over Ahmedabad: A Summertime study

During summer, the prevailing SW-monsoon favors the transport of sea-

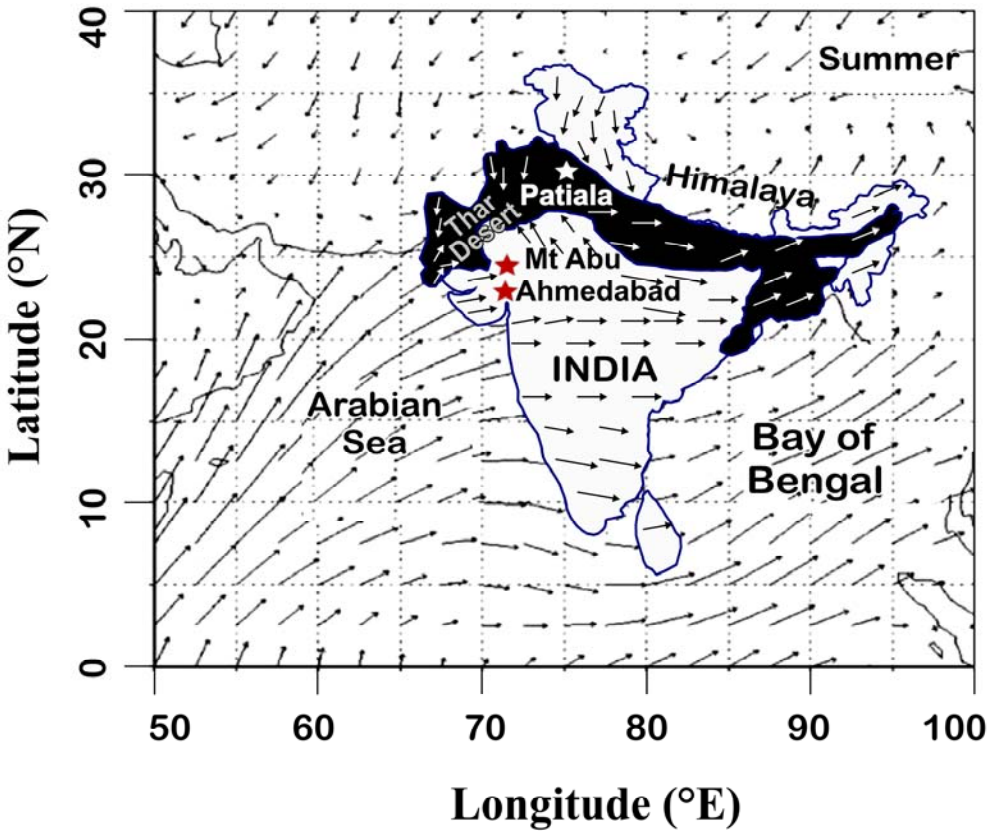

Figure 5.2: Typical wind-fields during summer over Ahmedabad and Mt Abu, modified after [Rastogi and Sarin, 2005].

salts from the Arabian Sea over Ahmedabad (Figure 5.2), and thus, provides a good opportunity to assess the chemical reactivity and mixing of variety of aerosols (Black carbon, organic carbon, sea salts and sulphate) over the region.

Furthermore, due to relatively high wind-speed and high boundary layer height during this period of the year, the ambient atmospheric concentration of particulate matter is lower. The mass concentration of PM2.5 at Ahmedabad (during May–June, referred to as summertime; Figure 5.3a) varied from 15–61 (Av: 25 ± 13) μg m^{-3}.

The concentrations of OC, EC, and ΣPAHs varied from 3–13 (Av: 5 ± 3) μg m^{-3}; 1–2 (Av: 1.1 ± 0.5) μg m^{-3}; and 1–12 (Av: 4 ± 3) ng m^{-3}, respectively. The mass fraction of OC and EC to PM2.5 ranged from 0.11–0.34 (Av: 0.22 ± 0.07) and 0.03–0.08 (Av: 0.05 ± 0.02), respectively (Figure 5.3b). The OC/EC and ΣPAHs/EC ratios varied from 4-7 (5 ± 1) and 2–5 (3 ± 1) mg g^{-1}, respectively (Figure 5.3c). The OC/TC and EC/TC mass fractions over Ahmedabad account for 83% and 17%, respectively.

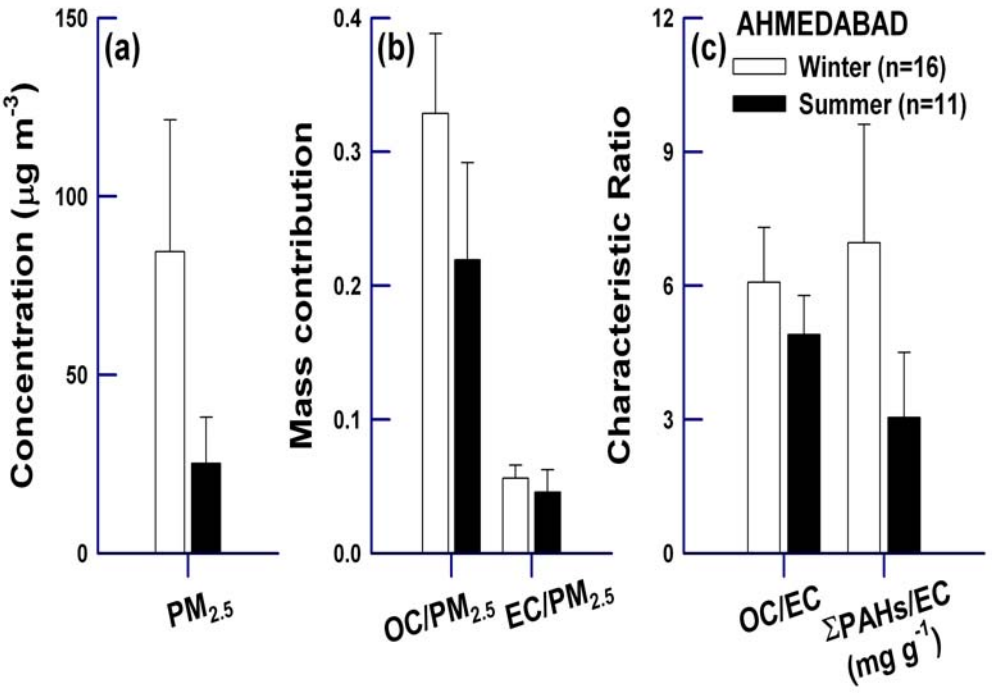

Figure 5.3: (a) Ambient concentration of PM2.5, (b) Contribution of OC and EC to PM2.5 and, (c) Characteristic ratio of OC/EC and ΣPAHs/EC over Ahmedabad during winter and summer.

5.2.4 PAHs isomer ratios from Ahmedabad: Wintertime versus summer

Isomer ratios of PAHs with 3–, 4–, 5– and 6–ring, (ANTH/PHEN; FLA/PYR; BaA/{CHRY+TRIPH}; BaP/B[b,j,k]FLA and IcdP/BghiP) from Ahmedabad have been assessed for the winter and summertime (Figure 5.4). The ANTH/PHEN ratio at Ahmedabad is 0.31 ± 0.05 during wintertime and 0.24 ± 0.18 during the summer. The FLA/PYR ratio is 0.80 ± 0.04 (wintertime) and 0.96 ± 0.24 (summertime) in Ahmedabad.

The BaA/{CHRY+TRIPH} ratio is 0.55 ± 0.09 (wintertime) and 0.57 ± 0.15 (summertime). The BaP/B[b,j,k]FLA ratio is 0.44 ± 0.08 (wintertime) and 0.36 ± 0.15 (summertime). The IcdP/BghiP ratio is 1.03 ± 0.07 (wintertime) and 0.82 ± 0.26 (summertime). Further discussion is essential to summarize on the relative reactivity of PAH isomers.

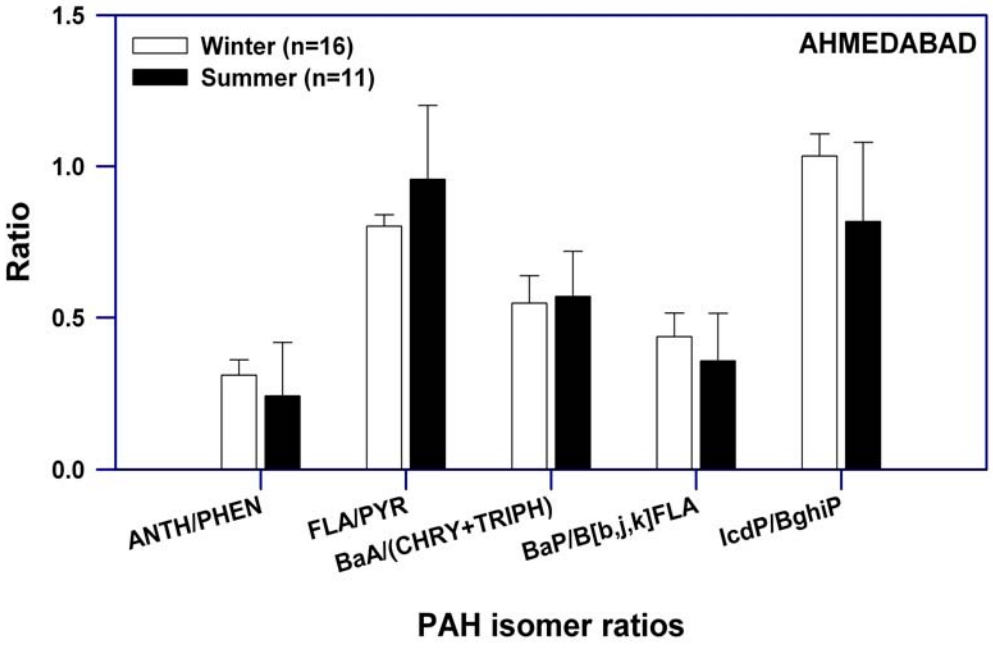

Figure 5.4: PAH isomer ratios (3- to 6-ring) in aerosols for winter and summertime over Ahmedabad.

5.2.5 Aerosol composition over Mt Abu: A wintertime study

Ahmedabad and Mt Abu are located in the semi-arid region of western India, representing typical urban and high-altitude locations, respectively. However, the abundance of particulate matter over Mt Abu is largely governed by

their long-range transport. The mass concentration of PM2.5 during wintertime (February–March '10) at Mt Abu varied from 10–38 (Av: 22 ± 9) μg m^{-3}. The contribution of OC and EC to PM2.5 ranged from 0.02–0.21 (Av: 0.10 ± 0.06) and 0.01–0.06 (Av: 0.03 ± 0.02), respectively. The PM2.5-bound ΣPAHs concentration varied from 0.4–3.3 (Av: 1.5 ± 0.9) ng m^{-3}. The OC/EC and ΣPAHs/EC ratios varied from 1.5–5.1 (3.0 ± 1.0) and 1.2–3.2 (2.2 ± 0.7) mg g^{-1}, respectively. Furthermore, the OC/TC and EC/TC mass fractions account for 74% and 26% over the region, respectively. The mass fraction of PAHs from Ahmedabad (for wintertime and summer) and Mt Abu (winter) is provided in Table 5.1.

Table 5.1: Average mass fractions of PM2.5-bound PAHs (mg g^{-1} OC) from semi-arid locations (Ahmedabad and Mt Abu) in western India

PAHs	Ahmedabad (Nov–Dec '09) (wintertime)	Ahmedabad (May–June '10) (summer)	Mt Abu (Feb–March '10) (wintertime)
NAPH	0.000 ± 0.000	0.004 ± 0.003	0.026 ± 0.026
ACY	0.001 ± 0.001	0.002 ± 0.001	0.000 ± 0.000
2-BrNAPH	0.001 ± 0.002	0.003 ± 0.003	0.051 ± 0.054
ACE	0.000 ± 0.000	0.001 ± 0.002	0.014 ± 0.014
FLU	0.001 ± 0.000	0.001 ± 0.001	0.010 ± 0.008
PHEN	0.012 ± 0.004	0.012 ± 0.004	0.046 ± 0.030
ANTH	0.004 ± 0.001	0.003 ± 0.002	0.007 ± 0.004
FLA	0.048 ± 0.018	0.020 ± 0.008	0.085 ± 0.047
PYR	0.060 ± 0.024	0.022 ± 0.011	0.060 ± 0.032
BaA	0.048 ± 0.019	0.018 ± 0.012	0.040 ± 0.025
CHRY+TRIPH	0.084 ± 0.023	0.029 ± 0.015	0.082 ± 0.049
B[b,j,k]FLA	0.352 ± 0.132	0.155 ± 0.077	0.193 ± 0.104
BaP	0.160 ± 0.076	0.065 ± 0.053	0.071 ± 0.041
IcdP	0.189 ± 0.069	0.134 ± 0.084	0.085 ± 0.036
D[ah,ac]ANTH	0.023 ± 0.010	0.015 ± 0.008	0.018 ± 0.014
BghiP	0.183 ± 0.066	0.159 ± 0.080	0.072 ± 0.032
ΣPAHs	1.167 ± 0.402	0.585 ± 0.278	0.841 ± 0.476

5.2.6 PAHs composition from Hisar and Kanpur during winter in the IGP

During December–March (wintertime), relatively low ambient temperature, shallower atmospheric boundary layer and poor thermal convection leads to efficient trapping of aerosols in the lower troposphere over the entire IGP. Moreover, significantly large amount of carbonaceous aerosols produced along

with the smoke from biomass burning and fossil-fuel combustion emissions during winter, and the fog formation for extended duration (couple of months) is a conspicuous feature in the IGP. Thus, it is essential to assess the atmospheric aerosol composition to infer about the undergoing atmospheric chemistry in the lower troposphere and its radiative impact.

The percentage composition of individual PAHs to the ΣPAHs from the locations Hisar and Kanpur is given in Figure 5.5. The ΣPAHs concentration varied from 2.2–19.1 (Av: 7.7 ± 4.1) ng m^{-3} and ΣPAHs/EC ratio from 1.0–4.7 (2.1 ± 0.9) mg g^{-1} at Hisar. Relatively high concentration of ΣPAHs (range: 3.7–42; Av: 15.4 ± 9.9 ng m^{-3}) with higher ΣPAHs/EC ratio (range: 0.8–7.6; Av: 3.2 ± 1.8 mg g^{-1}) is recorded from a downwind location at Kanpur, attributable to the transport of aerosols from upwind locations in the IGP and/or the change in emission sources as compared to that in the upwind IGP at Hisar. The PAHs involving 5-rings: BaP and B[b,j,k]FLA, and 6-ring PAHs: IcdP and BghiP follow the pattern in their percentage contribution: BghiP (6-ring) > B[b,j,k]FLA (5-ring) > IcdP (6-ring) > BaP (5-ring), contributing ~60% to the ΣPAHs at Hisar and B[b,j,k]FLA (5-ring) > BghiP (6-ring) > IcdP (6-ring) > BaP (5-ring) at Kanpur (overall contribution of ~70% to the ΣPAHs) during winters, when the bio- and fossil-fuel combustion emissions are dominant in the IGP.

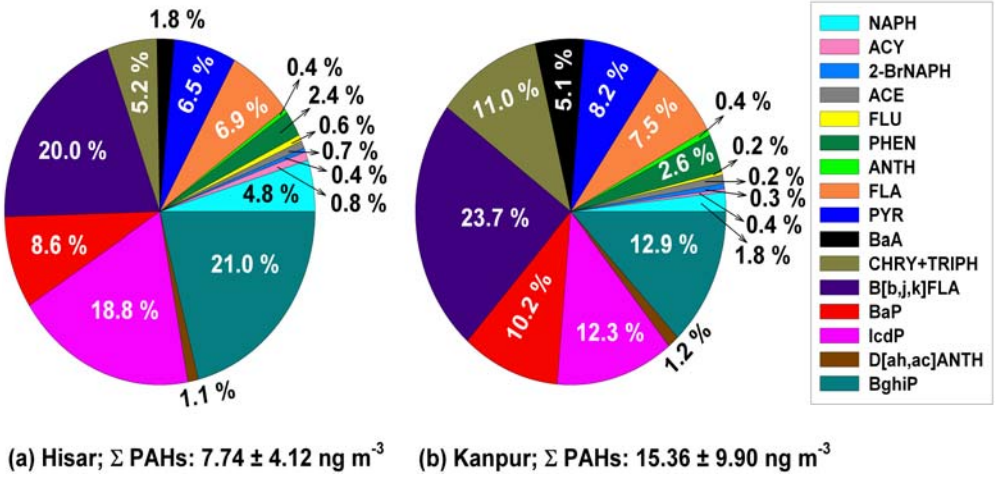

Figure 5.5: Percentage contribution of 16-PAHs from two locations in the IGP (Hisar and Kanpur) during wintertime.

The ambient concentrations of 2- and 3-ring PAHs are low (Av: ≤ 0.3 ng m^{-3}) and exhibit least variability at both the Hisar and Kanpur sites during the wintertime. However, a distinct variability for 4-, 5- and 6-ring PAHs is significantly pronounced. Accordingly, the 4-ring PAHs concentration at Hisar (Av: 0.4 ng m^{-3}) is about three times lower as compared to that from the downwind urban location at Kanpur (1.2 ng m^{-3}).

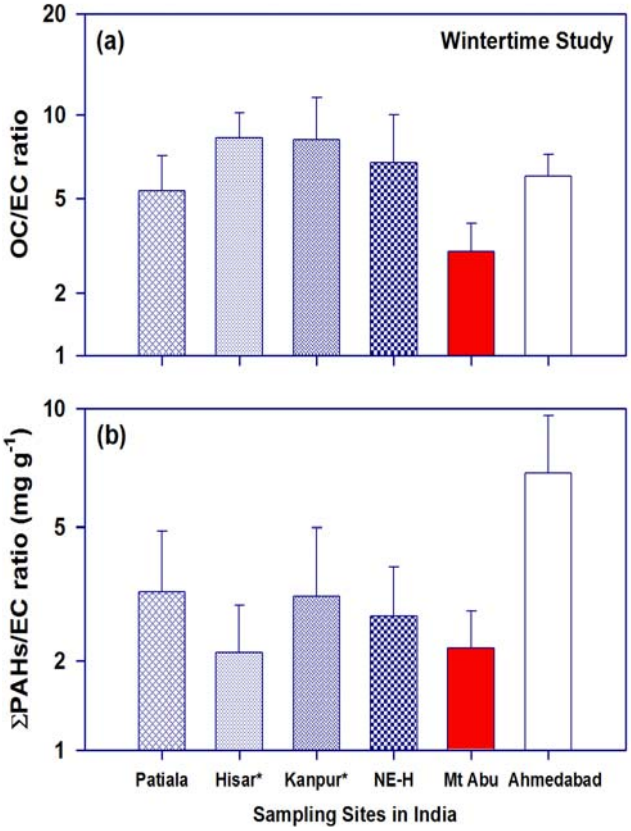

Figure 5.6: Spatial variability in (a) OC/EC and, (b) ΣPAHs/EC ratios for wintertime over India. Star (*) over Hisar and Kanpur, demarcate for PM10 sampling from PM2.5.

Furthermore, the concentrations 5- and 6-ring PAHs are also relatively low at Hisar (0.8 and 1.6 ng m^{-3}) as compared to that at Kanpur (Av: 1.9 and 1.8 ng m^{-3}). However, the mass fraction analysis for low- (sum of 2- to 3-ring PAHs) and high-molecular weight PAHs (sum of 4- to 6-ring PAHs) in ΣPAHs reveal the dominant contribution from heavier-PAHs (~92%) for both these locations in the IGP. This suggests the dominant emission and/or persistence of high-molecular

weight PAHs is aerosols (at these locations) as compared to that for the lighter-PAHs.

5.2.7 Characteristic ratios of OC/EC and ΣPAHs/EC from different geographical locations in India

The OC/EC ratio (Figure 5.6a) close to 7 (on average; during wintertime:

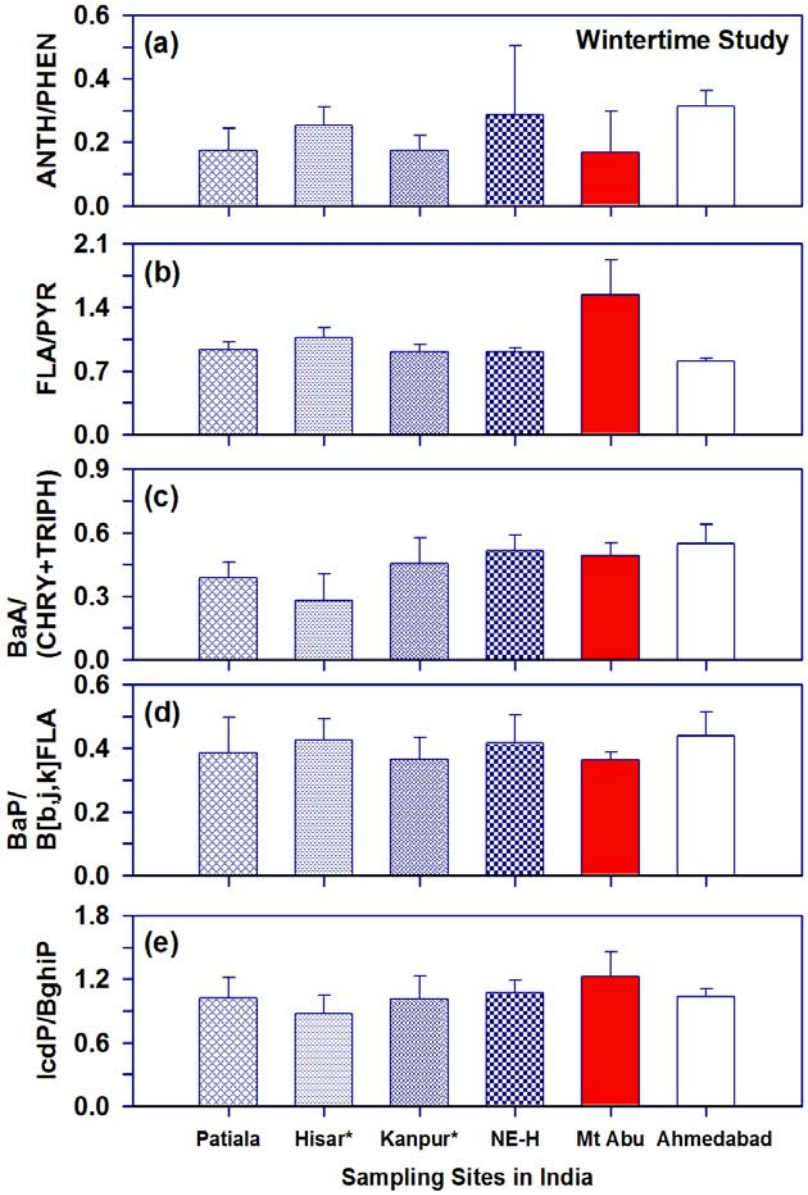

Figure 5.7: Spatial variability in PAHs isomer ratios in aerosols for wintertime in India. Star (*) over Hisar and Kanpur, demarcate for PM10 sampling from PM2.5.

period from December–March) for the sites located in the Indo-Gangetic Plain (IGP; Patiala, Hisar and Kanpur) and over the NE-Himalaya as well as for an urban location at Ahmedabad, suggests the relative proportion of light-scattering carbonaceous aerosol component (OC) is significantly higher as compared to the light-absorbing component (EC), exception being that for a high-altitude location in western India (Mt Abu; OC/EC average ratio: 3.0). The ΣPAHs/EC ratio (mg g^{-1}; Figure 5.6b) close to 3 over the IGP sites (Patiala, Hisar and Kanpur), NE-H and Mt Abu, provide the contribution of PAHs in ambient aerosols to be relatively low over these locations during winters as compared to that over Ahmedabad (ΣPAHs/EC ratio: 7.0 mg g^{-1}; Figure 5.6b). Besides, the relatively low wind-speed (as compared to summertime) and emission from regional sources, the impact of NE-winds, leading to enhancement and accumulation of the carbonaceous species over Ahmedabad is revealed from present study.

5.2.8 PAHs isomer ratios

The PAHs isomer ratios assessed from different geographical locations in the present study (in India), revealed near similarity: ANTH/PHEN ratio ~0.2, FLA/PYR ratio ~0.9 (exception being at Mt Abu: 1.5), BaA/(CHRY+TRIPH) ~0.4, BaP/B[b,j,k]FLA ~0.4 and IcdP/BghiP ~1.0. The significantly high FLA/PYR ratio at Mt Abu suggests the contribution of aerosols from other emission sources too, via long-range atmospheric transport. It is relevant to state here that being a reactive organic compound, the chemical reactivity of PAHs influence on their abundance in ambient atmosphere. In contrast, the similarity in PAHs isomer ratios suggests that they retain their source-signature. Thus, the PAHs isomer ratios serve as a good tracer of their emission sources to the ambient atmosphere.

5.2.9 Chemical reactivity of PAHs

Recent studies have addressed the issue on secondary organic aerosol (SOA) formation via chemical oxidation of PAHs [*Chan et al.*, 2009; *Kaiser et al.*, 2011]. The homogeneous reaction of volatile organic compound (VOC) and heterogeneous reaction of particulate organic aerosols with the atmospheric

oxidants such as O_3, NO_X and OH radical, are important processes occurring in the troposphere [*Zhang et al.*, 2009]. The secondary organic aerosol (SOA) formation, via homogeneous reactions of VOC, can affect aerosol concentration leading to direct effects on human health, visibility, light-scattering and –absorption, as well as indirectly on cloud and haze formation. In contrast, the heterogeneous reactions of particulate organics have potential to alter the chemical composition of aerosols and hence may influence their hygroscopic nature and toxicity.

Using the particle-resolved aerosol model PartMC-MOSAIC for the heterogeneous reactivity of PAHs adsorbed onto soot particles, with the atmospheric oxidants, exhibits that the half-life of PAHs is of the order of seconds during the night, when the PAHs are rapidly oxidised by the gas-surface reaction with NO_X [*Kaiser et al.*, 2011]. In contrast, during daytime, half-life of PAHs is of the order of minutes and determined mostly by the surface layer reaction of PAHs with adsorbed O_3. Such short half-lives of surface-bound PAHs may lead to efficient conversion of hydrophobic soot into more hygroscopic particles, and thus, increasing the aerosol-cloud interaction potential.

However, current atmospheric models do not include secondary organic aerosol (SOA) production from homogeneous reactions of PAHs in the gas-phase [*Chan et al.*, 2009]. Recent studies have shown that primary emissions undergo oxidation in the gas-phase, leading to the formation of SOA. This highlights the possibility that low-volatile gas-phase precursors can act as a potential source for the SOA production. Assessing the SOA formation from gas-phase photo-oxidation of naphthalene and its alkyl derivatives in the chamber, has suggested that the SOA produced under high-NO_X conditions to be semi-volatile, whereas non-volatile organics are produced under low-NO_X conditions. Taking into account for the measured yields of SOA production from the gas-phase reactions of the PAHs, emitted from diesel engines and wood burning, has revealed that within 12 h SOA can be formed 3–5 times more from the PAHs as compared to that from light aromatics. Furthermore, PAHs can account for up to 54% of the total SOA from oxidation of diesel emissions, representing a potentially large source in urban areas.

The chemical oxidation of organic aerosols has potential to alter the physical properties of aerosols, and the process is referred to as atmospheric aging [*Rudich et al.*, 2007]. Atmospheric aerosol contains variety of organic compounds, a large fraction of which has not been identified till date. Laboratory experiments have made significant attempts to assess the chemical reactivity of certain organic compounds. However, most of these experiments are limited to low aerosol loading and relatively under less complex conditions (matrix effects). Nevertheless, addressing the connections between recent laboratory studies and field-measurements in context to the oxidation of organic aerosols, the influence of uptake of oxidants, particle-water interactions, and the evolution of particle density with aging has been assessed. But, recently it has been realized that the chemical composition of aerosols may have a significant role in governing the atmospheric oxidation of organic particles. And therefore, simulating the actual reaction rate of organics in chamber for the ambient atmospheric conditions requires further knowledge and a better understanding on aerosol characteristics through field-based measurements.

Chemical Kinetic experiment in the laboratory-frame, provided heterogeneous reaction rates of 3- to 6-ring PAHs adsorbed onto silica particles with NO_2 radical [*Perraudin et al.*, 2005a]. Measurements were made at 295 K in the absence of light. PAHs were extracted from particles by focused microwave extraction and subsequent determination is formed on GC/MS. Results from that study have shown that heterogeneous rate constants vary from 1.4×10^{-3} to 4×10^{-8} s^{-1}, depending on the structure of the PAH, for NO_2 concentration of 1.5×10^{12} molecules cm^{-3}. Furthermore, benzo[*a*]pyrene was found to be most reactive; with a life-time regarding NO_2 of the order of minutes under polluted air conditions. Finally it was concluded that the heterogeneous reactivity of PAHs seems to be dependent on the nature of the particle.

Investigation has also been made for the heterogeneous reactions of the PAHs in diesel particulate exhaust (NIST SRM 1650a), with NO_2 and OH radical [*Esteve et al.*, 2006]. The relative degradation rate constants were determined by monitoring the decrease in particulate-PAHs concentration with the reaction time, using a fast flow reactor technique. Using internal standards, quantitative

determination of PAHs were performed on GC-MS. Results on relative rate constant of PAHs with NO_2 have shown the effect of their structure on their reactivity. For example, pyrene and benzo[*a*]pyrene were found to be the most reactive with NO_2 whereas all PAHs studied exhibit near similar reactivity with the OH radical. The chemical reactivity of all PAHs appeared to be about four orders of magnitude higher with OH as compared to that with NO_2. These rate constants suggest that the dominant atmospheric loss process of PAHs occurs due to their heterogeneous reactivity with the OH radical as compared to that with NO_2. However, the gas-phase reactivity of PAHs (homogeneous reactivity) would be significantly larger than when associated with carbonaceous particulate substrates.

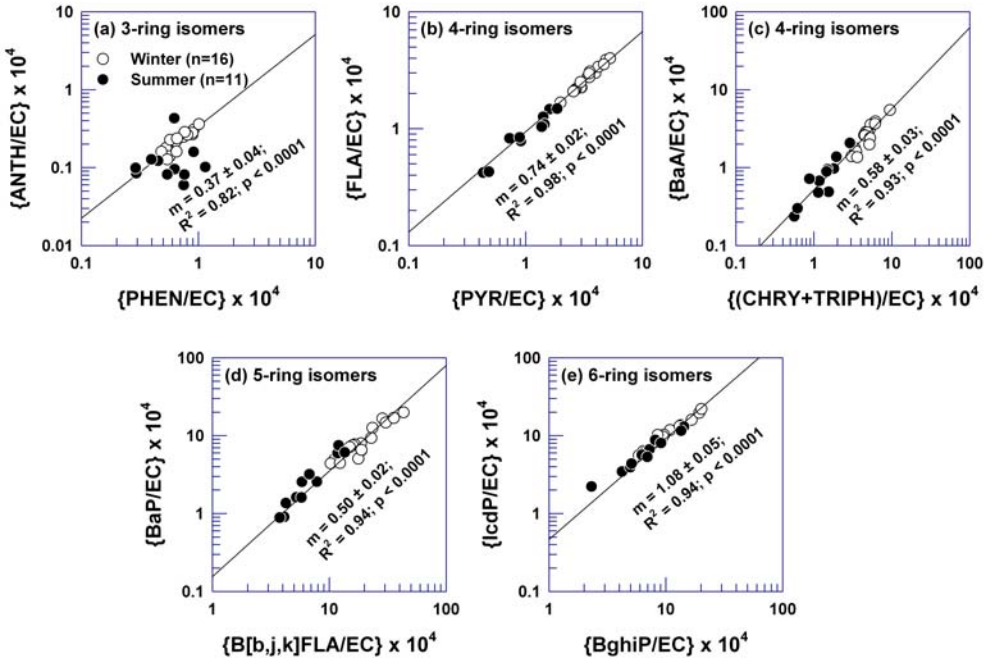

Figure 5.8: Scatter plot of PAH isomers (normalized to EC) in aerosols from Ahmedabad during winter and summertime.

Furthermore, another chamber experiment reports on the heterogeneous chemical reactivity of PAHs adsorbed on different types of particles, with ozone [*Perraudin et al.*, 2007]. As a model of atmospheric carbonaceous aerosols and mineral dust, graphite and silica particles were selected, respectively. The decay

of particulate PAH concentrations with time provided the pseudo-first order rate constants. Second order rate constants were estimated considering the ozone gaseous concentration. At room temperature, rate constants varied: in the case of graphite substrate, between (1.5 ± 0.5) x 10^{-17} and (1.3 ± 0.7) x 10^{-16} cm^3 $molecule^{-1}$ s^{-1} for chrysene and dibenzo[*a,l*]pyrene, respectively, and, in the case of silica substrate, between (1.5 ± 0.3) x 10^{-17} and (1.4 ± 0.3) x10^{-16} cm^3 $molecule^{-1}$ s^{-1} for fluoranthene and benzo[*a*]pyrene, respectively. Heterogeneous reactions of PAHs with ozone exhibit relatively high reactivity as compared to that occurring in the gas-phase, and may be competitive with atmospheric photo-degradation.

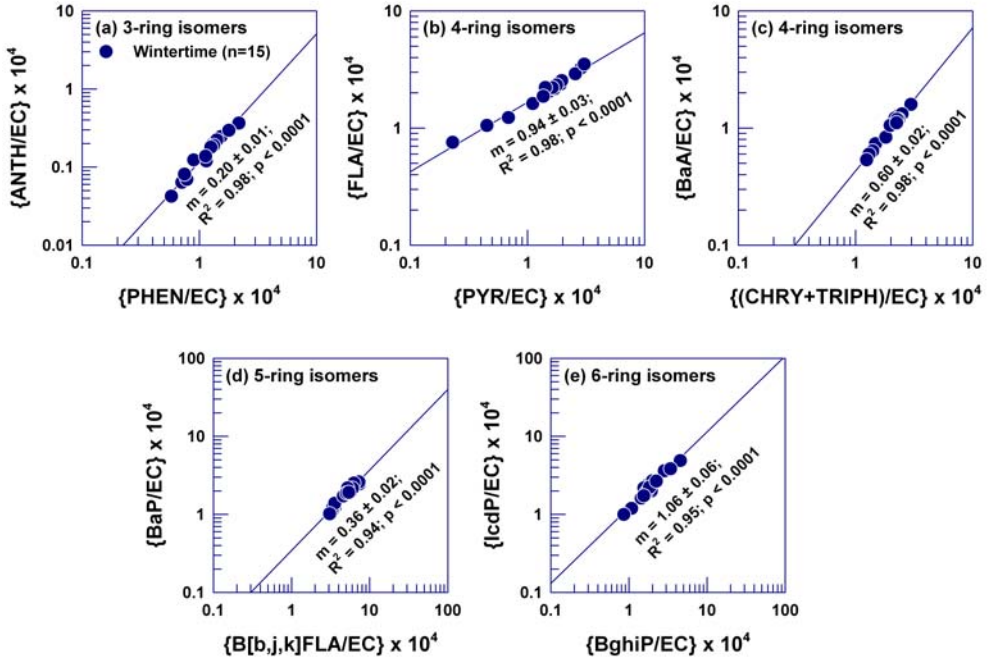

Figure 5.9: Scatter plot of PAH isomers (normalized to EC) in aerosols from Mt Abu during wintertime.

Relative rate constant for the heterogeneous reactions of PAH isomers in ambient atmosphere over Ahmedabad is inferred, using the data from this study. Ratio-ratio plot of 5-pairs of PAH isomers (normalized to EC) for winter and summer is shown in Figure 5.7. The log–log plot (Figure 5.7) provides the relative

rate constant for PAH isomers by the slope of the lines [*Robinson et al.*, 2006a; *Robinson et al.*, 2006b; *Rudich et al.*, 2007].

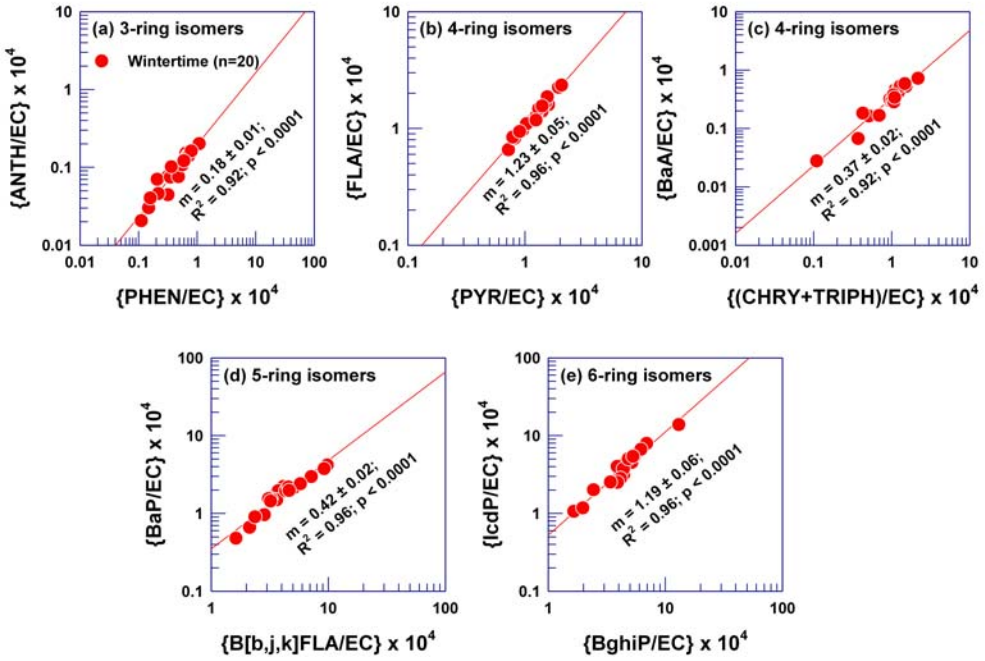

Figure 5.10: Scatter plot of PAH isomers (normalized to EC) in aerosols from Hisar during winter.

Relative rate constant for the heterogeneous reactions of PAH isomers in ambient atmosphere over high-altitude location at Mt Abu is also inferred in this study. Ratio-ratio plot of 5-pairs of PAH isomers (normalized to EC) for wintertime is shown in Figure 5.8. The log–log plot (Figure 5.8) provides the relative rate constant for PAH isomers by the slope of the lines [*Robinson et al.*, 2006a; *Robinson et al.*, 2006b].

This approach is generally used to estimate the relative rate constant between two species, since the concentration is inversely related to rate constant [*Rudich et al.*, 2007]. Accordingly, ANTH, BaA and BaP react rapidly than their isomers PHEN, (CHRY+TRIPH) and B[b,j,k]FLA, respectively. However, the other isomer pairs exhibit similar reactivity; FLA vs. PYR and IcdP vs. BghiP, suggesting their utility as an ideal tracer of their sources. Importantly, the mentioned relative rate constants of PAH isomers (for ambient aerosols) are

expected to represent their reactivity under high abundance of mineral dust mixed with sea salt and black carbon [*Rastogi and Sarin*, 2005].

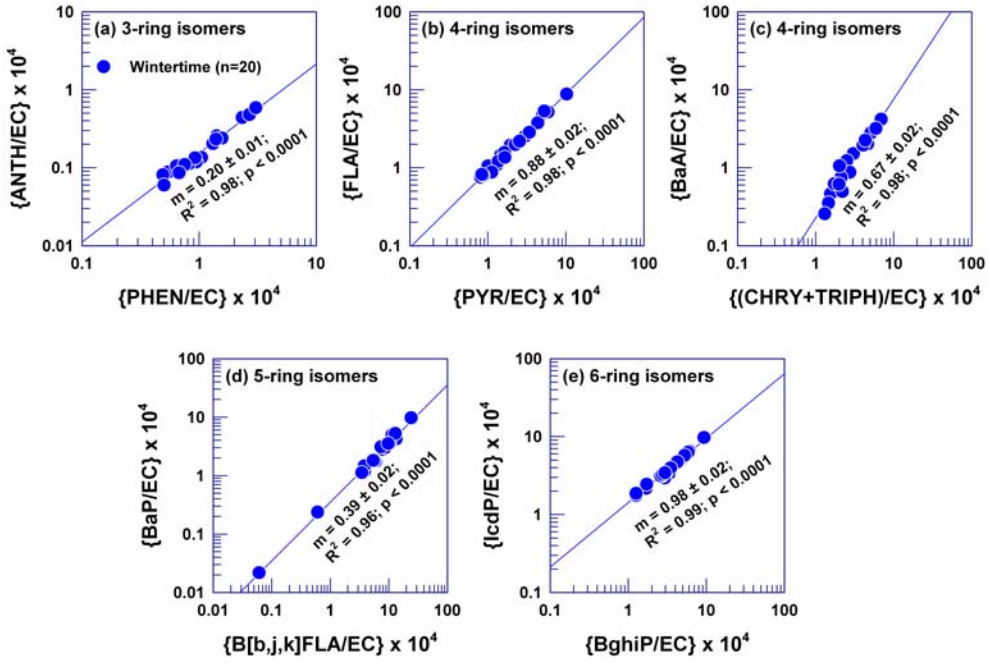

Figure 5.11: Scatter plot of PAH isomers (normalized to EC) in aerosols from Kanpur during winter.

Based on the diagnostic PAHs ratios [*Yunker et al.*, 2002], FLA/(FLA+PYR) and IcdP/(IcdP+BghiP), the cross plot (Figure 5.12) reveals dominant impact of biomass burning emissions over Ahmedabad during winter, whereas the relative contribution of emission from fossil-fuel combustion enhances during the summertime. In contrast, during wintertime the aerosols over the high-altitude location at Mt Abu exhibit their dominant emissions from Cowdung cake (bio-fuels) and coal combustion.

Relative rate constant for the heterogeneous reactions of PAH isomers in ambient atmosphere over the Hisar and Kanpur locations in the IGP is inferred too.

Ratio-ratio plot of 5-pairs of PAH isomers (normalized to EC) for wintertime from Hisar and Kanpur are shown in Figure 5.11 and 5.12. The log–

log plot (Figure 5.11, 5.12) provides the relative rate constant for PAH isomers by the slope of the lines.

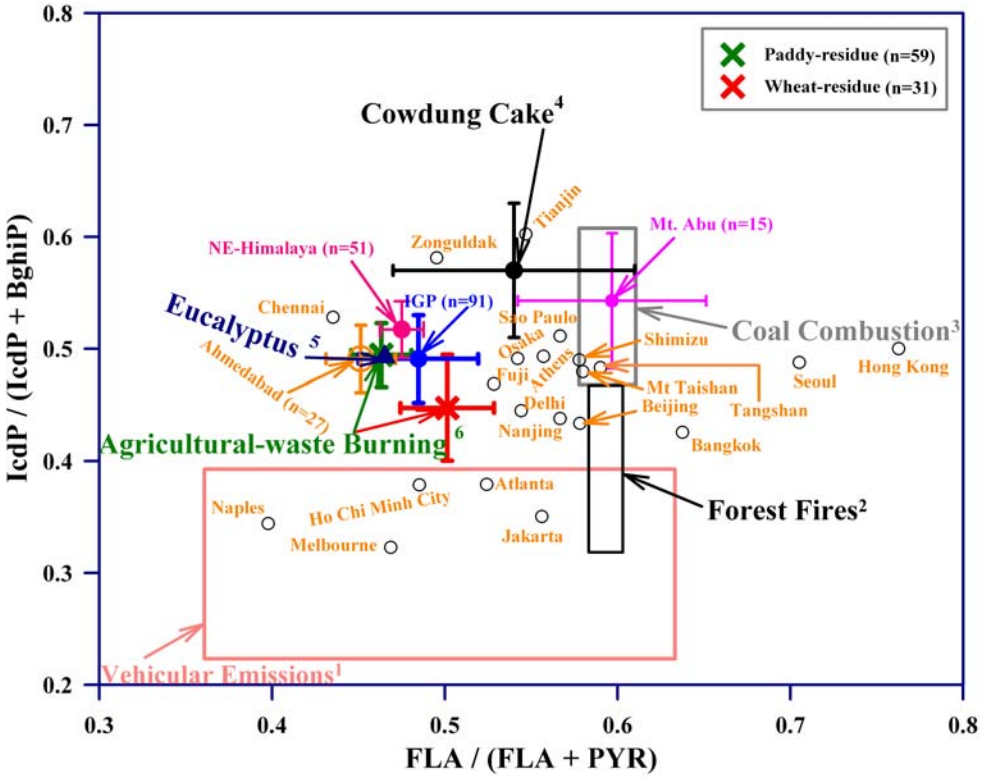

Figure 5.12: Cross-plot of PAH isomer ratios FLA/(FLA+PYR) and IcdP/(IcdP+BghiP) from different geographical location within and outside the India. This plot clearly shows the dominant atmospheric impact of biomass burning emissions over the Indian region. Source data: [1, 2, 3, 4, 5, 6] [Khalili et al., 1995; Khillare et al., 2005a; Khillare et al., 2005b; Kirton et al., 1991; Li et al., 2010; Masclet et al., 1995; Rajput and Lakhani, 2008; Rajput et al., 2011b; Schauer et al., 2001; Sheesley et al., 2003]. Data from other regions are adopted from: [Akyüz and Çabuk, 2008; Bourotte et al., 2005; Caricchia et al., 1999; Fu et al.; Guo et al., 2003; Hien et al., 2007; Li et al., 2010; Li et al., 2009; Mandalakis et al., 2002; Ohura et al., 2003; Okuda et al., 2006; Panther et al., 1999; Sharma et al., 2008; Wang et al., 2006].

Relative rate constant for the heterogeneous reactions of PAH isomers in ambient atmosphere over Ahmedabad, Mt Abu, Hisar and Kanpur is summarized in Table 5.2. Based on the diagnostic PAHs ratios, FLA/(FLA+PYR) and IcdP/(IcdP+BghiP), the cross plot (Figure 5.12) shows the scenario on dominant impact of different sources over various parts of the world. Furthermore, figure

5.12 reveals dominant impact of biomass burning emissions during wintertime over the Indian region.

Table 5.2: Relative rate constants (Av ± 1σ) of PAH isomers for heterogeneous-phase reactions in ambient aerosols from this study

Relative Rate constant (k)	Ahmedabad	Mt Abu	Hisar	Kanpur	Relative reactivity
	Winter/summer	Winter			
k_{PHEN} / k_{ANTH}	0.37±0.04	0.20±0.01	0.18±0.01	0.20±0.01	ANTH > PHEN
k_{PYR} / k_{FLA}	0.74±0.02	0.94±0.03	1.23±0.05	0.88±0.02	FLA ≥ PYR
$k_{(CHRY+TRIPH)} / k_{BaA}$	0.58±0.03	0.60±0.02	0.37±0.02	0.67±0.02	BaA > (CHRY+TRIPH)
$k_{B[b,j,k]FLA} / k_{BaP}$	0.50±0.02	0.36±0.02	0.42±0.02	0.39±0.02	BaP > B[b,j,k]FLA
k_{BghiP} / k_{IcdP}	1.08±0.05	1.06±0.06	1.19±0.06	0.98±0.02	IcdP ≈ BghiP

5.3. Summary and Implications

Atmospheric abundance and chemical reactivity of PAHs under different environmental conditions, presented in this study, provides newer information in the literature. The dominance of biomass burning emissions has been revealed for different geographical locations in India, using the PAHs isomer ratios. Present study summarizes biomass (agricultural-waste and bio-fuels) burning emission to be the dominant source of carbonaceous aerosols over India, as suggested by earlier studies [*Gustafsson et al.*, 2009; *Venkataraman et al.*, 2005]. Assessing the chemical reactivity of particulate PAHs suggests their potential role in atmospheric chemistry. Such reactions can alter the surface characteristics, and therefore, the radiative impact of aerosol [*Kaiser et al.*, 2011].

CHAPTER 6

SYNTHESIS AND SCOPE OF FUTURE RESEARCH

6.1. Synthesis

This chapter summarizes the important findings made in this study and addresses issues for the future research. This thesis highlights the importance of applying the mass spectrometry (GC-MS) technique to the chemical characterization of aerosols. Ambient composition of aerosols is highly variable due to several factors that include variation in their sources (type and strength), chemical reactivity of constituents, mixing and prevailing meteorology. The present study on the chemical characterization of ambient aerosols under different weather and environmental conditions, assess the source-composition of biomass burning vis-à-vis fossil-fuel combustion emission, using several proxies. For examples OC/EC, WSOC/OC, nss-K^+/OC, nss-K^+/EC, nss-SO_4^{2-}/OC, ΣPAHs/EC and PAHs isomer ratios. The chemical characterization for post-harvest paddy- (during October–November) and wheat-residue burning emission (during April–May) provided here, highlights the significant atmospheric impact of biomass burning emissions, occurring on annual and seasonal basis in the Northern India.

Moreover, this study provides the field-based evidence on the heterogeneous chemical reactivity of PAHs and the formation of secondary aerosols. A quantitative information is given on the source characterization of biomass burning emissions, under ambient atmospheric conditions and compared to that reported from the chamber-based combustion experiments. Thus providing, a linkage between the field- and chamber-measurements on source-characterization and the formation of secondary aerosols. The large-scale biomass burning emissions in Northern India, and subsequent transport to the downwind locations, assessed in this study, would bring attention to the variability in aerosol radiative forcing on a regional scale. Furthermore, the long-term measurements of aerosol composition over Northern India and NE-Himalaya, through field-based observation can also be used to validate the satellite data for these regions. In order to assess the atmospheric impact of biomass burning vis-à-vis fossil-fuel combustion on the concentration and composition of ambient aerosol; a long-term sampling was performed during the drier period from an upwind location at Patiala in the Indo-Gangetic Plain (IGP) from October ’08–May ’09 and October

'10–May '11) and a high-altitude site (Barapani in Shillong: January–March '09 and January–March '10) in NE-Himalaya in India. Furthermore, the spatial variability in the atmospheric abundances of carbonaceous species has also been documented through a short-term monitoring from urban (Ahmedabad; November–December '09 and May–June '10) and high-altitude (Mt Abu; February–March '10) locations in western India. In addition, the chemical characteristics of PAHs and their isomer ratios in aerosol has been further examined from two more locations in the IGP: Hisar (for December '04) and Kanpur (for January–March '07 and December '07–February '08).

The PM2.5 mass concentration exhibits a large temporal variability over Patiala and ranged from 60–391 μg m^{-3} during paddy-residue burning (October–November), from 19–244 μg m^{-3} during bio- and fossil-fuel combustion (December–March) and from 18–123 μg m^{-3} during wheat-residue burning emissions (April–May). The mass fractions of OC, EC and ΣWSIS to PM2.5 are: 33%, 3% and 23% for paddy-residue burning, 22%, 5% and 30% for bio- and fossil-fuel combustion and, 26%, 7% and 25% from wheat-residue burning emissions, respectively. On average, the OC/EC ratio of 10.6 (range: 4.5–26) for paddy-residue burning, 5.4 for bio- and fossil-fuel combustion and 4.3 for wheat-residue burning is characteristic to different emission sources. The mass fraction of WSOC to OC was ~60% during these emission scenarios.

The characteristic ratios, nss-K^+/OC, nss-K^+/EC and nss-SO_4^{2-}/OC in the IGP are distinctly different with that from fossil-fuel dominated regions. The ΣPAHs/EC ratio (Av: in mg g^{-1}) was found to be 4.2 for paddy-residue burning, 3.3 for bio- and fossil-fuel combustion and 1.2 for wheat-residue burning emissions. These data sets are constrained based on the long-term sampling (n = 141) during drier periods from October '08–May '09 and October '10–May '11 from an upwind location at Patiala in the Indo-Gangetic Plain (IGP). The cross-plots of PAHs isomer ratios [FLA/(FLA+PYR) versus IcdP/(IcdP+BghiP); and FLA/(FLA+PYR) versus ANTH/(ANTH+PHEN)] show distinct differences for their emission from field-based agricultural-waste burning vis-à-vis fossil-fuel combustion sources.

The long-range atmospheric transport of chemical constituents to the NE-Himalaya (NE-H) is a conspicuous feature during the wintertime (January–March). With this perspective, atmospheric concentrations of PM2.5 (range: 39–348 μg m^{-3}), EC (3–18 μg m^{-3}), OC (10–138 μg m^{-3}), WSOC (7–78 μg m^{-3}) and PAHs (4–46 ng m^{-3}) have been studied during January–March 2009 and 2010 from a site (Barapani: 25.7 ˚N; 91.9 ˚E; 1064 m a.s.l) located at the foot-hills of NE-H. A significant linear correlation (R^2 = 0.61; p<0.0001) between WSOC and water-insoluble organic carbon (WIOC) in aerosols over the NE-H, indicates the influence of atmospheric aging of organic aerosols in enhancing the content of WSOC. Relatively high WSOC/OC ratio (Av: 0.51) in NE-H as compared to that in the source region in the Indo-Gangetic Plain (IGP) in conjunction with near constant OC/EC ratio of ~6.0, also indicates atmospheric aging of organic aerosols.

Relatively low ΣPAHs/EC ratio in NE-H (1.72 mg g^{-1}) as compared to that in the Upwind IGP (3.54 mg g^{-1}) and significantly lower PAH isomers to EC ratio than that reported for their dominant source (biomass burning emission: source-profile), further support the evidence of atmospheric aging of organic aerosols during their long-range transport to the NE-H. Using the PAHs isomer ratios in aerosol, the percentage contribution of the sources of carbonaceous aerosols for the IGP is determined: 80% contribution from biomass burning and the remaining 20% from fossil-fuel combustion sources. Briefly, the potential sources of carbonaceous aerosols over the NE-H is identified using the cross plots of PAH isomer ratios. Accordingly, the mass-closure equations are synthesized for several (4-pairs) PAH isomer ratios for different types of biomass burning and fossil-fuel combustion sources. The solution of the so-formed determined matrix, apportioning the contribution from five distinct sources: paddy-residue, bio-fuel (Cowdung cake and eucalyptus), gasoline-based vehicular emission, diesel-based vehicular emission and coal-combustion, is unique and exact. Estimate on source contribution from this study is similar to the earlier estimates for the south-Asian region, reporting ~70% from biomass burning, using the bottom-up approach.

The mass concentrations of PM2.5 at urban Ahmedabad in the western India, exhibit large seasonal variability: varied from 32–161 μg m^{-3} during

wintertime and 15–61 μg m^{-3} during the summer, respectively. The mass fractions of OC and EC to PM2.5 mass are found to be 33% and 6% during winter, whereas 22% and 5% during the summer, respectively. On average, the OC/EC ratio was 6 during winter and 5 for the summer. Likewise, relatively high ΣPAHs/EC ratio is found in aerosol during wintertime (7 mg g^{-1}) as compared to that during the summer (3 mg g^{-1}). The mass concentrations of PM2.5 and the associated chemical constituents are significantly low at a high-altitude site at Mt Abu in the western India. PM2.5 mass concentration varied from 10–38 μg m^{-3} during the study period from February–March (wintertime). The mass fractions of OC and EC to PM2.5 mass are found to be 10% and 3%, respectively. On average, the OC/EC and ΣPAHs/EC ratio (in mg g^{-1}) was 3.0 and 2.2, respectively over Mt Abu. The cross-plot of PAHs isomer ratios [FLA/(FLA+PYR) versus IcdP/(IcdP+BghiP)] in aerosols from these two locations further re-affirms the dominant impact of biomass burning emission in the western India too.

The mass concentrations of PM10 at semi-urban (Hisar) and urban (Kanpur) locations in the IGP in Northern India, also exhibit large variability during wintertime: varied from 67–295 μg m^{-3} and 53–392 μg m^{-3}, respectively. The mass fractions of OC and EC to PM10 mass were 17% and 2% over Hisar, whereas 19% and 3% over Kanpur, respectively. However, on average, the OC/EC ratio looks similar (8) for these two locations in the IGP during wintertime. The ΣPAHs/EC ratio is found to be 2.1 and 3.2 mg g^{-1} over Hisar and Kanpur. The cross-plot of PAHs isomer ratios [FLA/(FLA+PYR) versus IcdP/(IcdP+BghiP)] in aerosols from these two locations also reveal the dominance of biomass burning emission in the Northern India.

Summing up, based on the assessment of different chemical proxies (OC/EC, ΣPAHs/EC and PAHs isomer ratios), in ambient aerosols from different geographical locations (Northern-, Northeastern- and Western-India), the present study summarizes the biomass burning emission (bio-fuels and agricultural waste) to be the major source of carbonaceous aerosols in Indian region. The WSOC/OC ratio in conjunction with OC/EC ratio has been used to assess the influence of long-range transport on the atmospheric aging of carbonaceous aerosols under the ambient atmospheric conditions.

The strategy on aerosol sampling locations and its collection period has been well explained in context to assess the atmospheric process related to the carbonaceous species in this study. The analytical data also provides the relative rate constants of PAH isomers for heterogeneous phase reactions in the ambient atmosphere. In general, the scatter plots among isomers (normalized to EC) suggest that BaA and BaP are more reactive than their corresponding isomers (CHRY+TRIPH) and B[b,j,k]FLA. In contrast, the reactivity of other two isomer pairs, FLA versus PYR and IcdP versus BghiP, are quite similar.

6.2. Scope of the future research

This study has provided the chemical characteristics of ambient aerosols for two distinct post-harvest agricultural-waste burning emissions of paddy- and wheat-residues, and bio- and fossil-fuel combustion. Furthermore, the chemical characteristics of ambient aerosols from urban, semi-urban and high-altitude sites are also explored from different geographical locations in India. Biomass burning emissions has been inferred as a major source of carbonaceous aerosols in the Indian region, based on several proxies (OC/EC, WSOC/OC, nss-K^+/OC, nss-K^+/EC, nss-SO_4^{2-}/OC, ΣPAHs/EC and PAHs isomer ratios).

The potential role of PAHs in determining the sources of carbonaceous aerosols and atmospheric aging of organic compounds through their measurement in particulate-phase has been studied in detail in this study. Future research need to focus on their heterogeneous-phase chemical reactivity, through simultaneous determination of PAHs and atmospheric oxidants (O_3 and NO_X). This investigation will facilitate in determining their potential role in surface alteration characteristics of aerosols, enhancing the content of water-soluble organic carbon. In contrast, measurement of PAHs in the gaseous-phase over the land (vertical profile) and over the marine boundary layer (from the continent to the open ocean), along with the carbonaceous aerosols and the atmospheric oxidants, would provide the potential role of PAHs in contributing to the secondary organic aerosol production via homogeneous reactivity. The potential loss of O_3 and NO_X through their reactivity with the PAHs can be incorporated in the chemical transport models of these atmospheric oxidants.

Assessing the WSOC/OC ratio in conjunction with the OC/EC ratio in this study has revealed the influence of atmospheric aging of carbonaceous aerosols for enhancement in water-soluble organic carbon fraction, during their long-range transport. The potential reactivity of organic species, and thus, the formation mechanism of secondary species through real-time measurements could be another important subject to atmospheric research, using the mass spectrometry technique. The chemical characterization of the water-soluble organic carbon (WSOC) is an important aspect of atmospheric research to infer on their activation efficiency as cloud condensation nuclei (CCN) and radiative impact.

The application of mass spectrometric techniques would be desirable to quantify various chemical constituents in aerosol and to infer their role in atmospheric chemistry. Furthermore, the evaluation of organic mass as a function of different source and age is another emerging aspect of research, which would be required to constrain the budget of organic aerosol from the south-Asian region.

REFERENCES

Akyüz, M., and H. Çabuk (2008), Particle-associated polycyclic aromatic hydrocarbons in the atmospheric environment of Zonguldak, Turkey, *Sci. Total Environ.*, *405*(1-3), 62-70.

Alexandrou, N., M. Smith, R. Park, K. Lumb, and K. Brice (2001), The Extraction of Polycyclic Aromatic Hydrocarbons from Atmospheric Particulate Matter Samples by Accelerated Solvent Extraction (ASE), *Int. J. Environ. Anal. Chem.*, *81*(4), 257 - 280.

Allen, J. O. (1997), Atmospheric Partitioning of Polycyclic Aromatic Hydrocarbons (PAH) and Oxygenated PAH.

Alvarez-Avilés, O., L. Cuadra-Rodríguez, F. González-Illán, J. Quiñones-González, and O. Rosario (2007), Optimization of a novel method for the organic chemical characterization of atmospheric aerosols based on microwave-assisted extraction combined with stir bar sorptive extraction, *Anal. Chim. Acta*, *597*(2), 273-281.

Andreae, M. O., and P. J. Crutzen (1997), Atmospheric Aerosols: Biogeochemical Sources and Role in Atmospheric Chemistry, *Science*, *276*, 1052-1058.

Andreae, M. O., and P. Merlet (2001), Emission of trace gases and aerosols from biomass burning, *Global Biogeochem. Cycles*, *15*(4), 955-966.

Atkinson, R., and J. Arey (1994), Atmospheric Chemistry of Gas-phase Polycyclic Aromatic Hydrocarbons: Formation of Atmospheric Mutagens, *Environ. Health Perspect.*, *102*(Suppl 4), 117-126.

Badarinath, K. V. S., T. R. K. Chand, and V. K. Prasad (2006), Agricultural crop residue burning in the Indo-Gangetic Plains - A study using IRS-P6 A WiFS satellite data, *Current Science*, *91*(8), 1085-1089.

Baek, S. O., M. E. Goldstone, P. W. W. Kirk, J. N. Lester, and R. Perry (1991), Phase distribution and particle size dependency of polycyclic aromatic hydrocarbons in the urban atmosphere, *Chemosphere*, *22*(5-6), 503-520.

Birch, M. E., and R. A. Cary (1996), Elemental Carbon-Based Method for Monitoring Occupational Exposures to Particulate Diesel Exhaust, *Aerosol Sci. Technol.*, *25*(3), 221 - 241.

Bond, T. C., D. G. Streets, K. F. Yarber, S. M. Nelson, J.-H. Woo, and Z. Klimont (2004), A technology-based global inventory of black and organic carbon emissions from combustion, *J. Geophys. Res.*, *109*(D14), D14203.

Bourotte, C., M.-C. Forti, S. Taniguchi, M. C. Bícego, and P. A. Lotufo (2005), A wintertime study of PAHs in fine and coarse aerosols in São Paulo city, Brazil, *Atmos. Environ.*, *39*(21), 3799-3811.

Cabada, J. C., S. N. Pandis, R. Subramanian, A. L. Robinson, A. Polidori, and B. Turpin (2004), Estimating the Secondary Organic Aerosol Contribution to $PM_{2.5}$ Using the EC Tracer Method Special Issue of Aerosol Science and Technology on Findings from the Fine Particulate Matter Supersites Program, *Aerosol Sci. Technol.*, *38*(12 supp 1), 140-155.

Cachier, H., M. P. Bremond, and P. Buat-MÉNard (1989), Determination of atmospheric soot carbon with a simple thermal method, *Tellus B*, *41B*(3), 379-390.

Cao, J. J., S. C. Lee, J. C. Chow, J. G. Watson, K. F. Ho, R. J. Zhang, Z. D. Jin, Z. X. Shen, G. C. Chen, Y. M. Kang, S. C. Zou, L. Z. Zhang, S. H. Qi, M. H. Dai, Y. Cheng, and K. Hu (2007), Spatial and seasonal distributions of carbonaceous aerosols over China, *J. Geophys. Res.*, *112*(D22), D22S11.

Caricchia, A. M., S. Chiavarini, and M. Pezza (1999), Polycyclic aromatic hydrocarbons in the urban atmospheric particulate matter in the city of Naples (Italy), *Atmos. Environ.*, *33*(23), 3731-3738.

Castro, L. M., C. A. Pio, R. M. Harrison, and D. J. T. Smith (1999), Carbonaceous aerosol in urban and rural European atmospheres: estimation of secondary organic carbon concentrations, *Atmos. Environ.*, *33*(17), 2771-2781.

Chan, A. W. H., K. E. Kautzman, P. S. Chhabra, J. D. Surratt, M. N. Chan, J. D. Crounse, A. Kürten, P. O. Wennberg, R. C. Flagan, and J. H. Seinfeld (2009), Secondary organic aerosol formation from photooxidation of naphthalene and alkylnaphthalenes: implications for oxidation of intermediate volatility organic compounds (IVOCs), *Atmos. Chem. Phys.*, *9*, 3049-3060.

Chee, K. K., M. K. Wong, and H. K. Lee (1997), Microwave-Assisted Solvent Extraction of Air Particulates for the Determination of PAHs, *Environ. Monit. Assess.*, *44*(1), 391-403.

Conny, J. M., and J. F. Slater (2002), Black carbon and organic carbon in aerosol particles from crown fires in the Canadian boreal forest, *J. Geophys. Res.*, *107*(D11), 4116.

Crutzen, P. J., and M. O. Andreae (1990), Biomass Burning in the Tropics: Impact on Atmospheric Chemistry and Biogeochemical Cycles, *Science*, *250*(4988), 1669-1678.

Das, S. K., A. Jayaraman, and A. Misra (2008), Fog-induced variations in aerosol optical and physical properties over the Indo-Gangetic Basin and impact to aerosol radiative forcing, *Ann. Geophys.*, *26*(6), 1345-1354.

Decesari, S., M. C. Facchini, S. Fuzzi, and E. Tagliavini (2000), Characterization of water-soluble organic compounds in atmospheric aerosol: A new approach, *J. Geophys. Res.*, *105*(D1), 1481-1489.

Decesari, S., M. C. Facchini, E. Matta, M. Mircea, S. Fuzzi, A. R. Chughtai, and D. M. Smith (2002), Water soluble organic compounds formed by oxidation of soot, *Atmos. Environ.*, *36*(11), 1827-1832.

Decesari, S., M. C. Facchini, C. Carbone, L. Giulianelli, M. Rinaldi, E. Finessi, S. Fuzzi, A. Marinoni, P. Cristofanelli, R. Duchi, P. Bonasoni, E. Vuillermoz, J. Cozic, J. L. Jaffrezo, and P. Laj (2010), Chemical composition of PM_{10} and PM_1 at the high-altitude Himalayan station Nepal Climate Observatory-Pyramid (NCO-P) (5079 m a.s.l.), *Atmos. Chem. Phys.*, *10*(10), 4583-4596.

Dey, S., and S. N. Tripathi (2007), Estimation of aerosol optical properties and radiative effects in the Ganga basin, northern India, during the wintertime, *J. Geophys. Res.*, *112*(D3), D03203.

Dhammapala, R., C. Claiborn, J. Jimenez, J. Corkill, B. Gullett, C. Simpson, and M. Paulsen (2007), Emission factors of PAHs, methoxyphenols, levoglucosan, elemental carbon and organic carbon from simulated wheat and Kentucky bluegrass stubble burns, *Atmos. Environ.*, *41*(12), 2660-2669.

Draxler, R. R., and G. D. Rolph (2003), HYSPLIT (Hybrid Single-Particle Lagrangian Integrated Trajectory) Model access via NOAA ARL READY Website (http://www.arl.noaa.gov/ready/hysplit4.html), NOAA Air Resources Laboratory, Silver Spring, MD.

Duan, J., X. Bi, J. Tan, G. Sheng, and J. Fu (2005), The differences of the size distribution of polycyclic aromatic hydrocarbons (PAHs) between urban and rural sites of Guangzhou, China, *Atmospheric Research*, *78*(3-4), 190-203.

Ervens, B., B. J. Turpin, and R. J. Weber (2011), Secondary organic aerosol formation in cloud droplets and aqueous particles (aqSOA): a review of laboratory, field and model studies, *Atmos. Chem. Phys.*, *11*, 11069-11102.

Esteve, W., H. Budzinski, and E. Villenave (2004), Relative rate constants for the heterogeneous reactions of OH, NO_2 and NO radicals with polycyclic aromatic hydrocarbons adsorbed on carbonaceous particles. Part 1: PAHs adsorbed on 1-2 μm calibrated graphite particles, *Atmos. Environ.*, *38*(35), 6063-6072.

Esteve, W., H. Budzinski, and E. Villenave (2006), Relative rate constants for the heterogeneous reactions of NO_2 and OH radicals with polycyclic aromatic hydrocarbons adsorbed on carbonaceous particles. Part 2: PAHs adsorbed on diesel particulate exhaust SRM 1650a, *Atmos. Environ.*, *40*(2), 201-211.

Evagelpoulos, V., T. A. Albanis, A. Asvesta, and S. Zoras (2010), Polycyclic Aromatic Hydrocarbons (PAHs) in Fine and Coarse Particles, *Global NEST*, *12*(1), 63-70.

Ferek, R. J., J. S. Reid, P. V. Hobbs, D. R. Blake, and C. Liousse (1998), Emission factors of hydrocarbons, halocarbons, trace gases and particles from biomass burning in Brazil, *J. Geophys. Res.*, *103*(D24), 32107-32118.

Fine, P. M., G. R. Cass, and B. R. T. Simoneit (2002), Chemical Characterization of Fine Particle Emissions from the Fireplace Combustion of Woods Grown in the Southern United States, *Environmental Science & Technology*, *36*(7), 1442-1451.

Formenti, P., W. Elbert, W. Maenhaut, J. Haywood, and M. O. Andreae (2003), Chemical composition of mineral dust aerosol during the Saharan Dust Experiment (SHADE) airborne campaign in the Cape Verde region, September 2000, *J. Geophys. Res.*, *108*(D18), 8576.

Fraser, M. P., K. Lakshmanan, S. G. Fritz, and B. Ubanwa (2002a), Variation in composition of fine particulate emissions from heavy-duty diesel vehicles, *J. Geophys. Res.*, *107*(D21), 8346.

Fraser, M. P., Z. W. Yue, R. J. Tropp, S. D. Kohl, and J. C. Chow (2002b), Molecular composition of organic fine particulate matter in Houston, TX, *Atmos. Environ.*, *36*(38), 5751-5758.

Fu, P. Q., K. Kawamura, C. M. Pavuluri, T. Swaminathan, and J. Chen Molecular characterization of urban organic aerosol in tropical India: contributions of primary emissions and secondary photooxidation, *Atmos. Chem. Phys.*, *10*(6), 2663-2689.

Graber, E. R., and Y. Rudich (2006), Atmospheric HULIS: How humic-like are they? A comprehensive and critical review, *Atmos. Chem. Phys.*, *6*(3), 729-753.

Guo, H., S. C. Lee, K. F. Ho, X. M. Wang, and S. C. Zou (2003), Particle-associated polycyclic aromatic hydrocarbons in urban air of Hong Kong, *Atmos. Environ.*, *37*(38), 5307-5317.

Gustafsson, Ö., M. Kruså, Z. Zencak, R. J. Sheesley, L. Granat, E. Engström, P. S. Praveen, P. S. P. Rao, C. Leck, and H. Rodhe (2009), Brown Clouds over

South Asia: Biomass or Fossil Fuel Combustion?, *Science*, *323*(5913), 495-498.

Hallquist, M., J. C. Wenger, U. Baltensperger, Y. Rudich, D. Simpson, M. Claeys, J. Dommen, N. M. Donahue, C. George, A. H. Goldstein, J. F. Hamilton, H. Herrmann, T. Hoffmann, Y. Iinuma, M. Jang, M. E. Jenkin, J. L. Jimenez, A. Kiendler-Scharr, W. Maenhaut, G. McFiggans, T. F. Mentel, A. Monod, A. S. H. Prévôt, J. H. Seinfeld, J. D. Surratt, R. Szmigielski, and J. Wildt (2009), The formation, properties and impact of secondary organic aerosol: current and emerging issues, *Atmos. Chem. Phys.*, *9*, 5155-5236.

Harrison, R. M., D. J. T. Smith, and L. Luhana (1996), Source Apportionment of Atmospheric Polycyclic Aromatic Hydrocarbons Collected from an Urban Location in Birmingham, U.K, *Environmental Science & Technology*, *30*(3), 825-832.

Hawthorne, S. B., D. J. Miller, M. D. Burford, J. J. Langenfeld, S. Eckert-Tilotta, and P. K. Louie (1993), Factors controlling quantitative supercritical fluid extraction of environmental samples, *J. Chromatogr. A*, *642*(1-2), 301-317.

Hays, M. D., P. M. Fine, C. D. Geron, M. J. Kleeman, and B. K. Gullett (2005), Open burning of agricultural biomass: Physical and chemical properties of particle-phase emissions, *Atmos. Environ.*, *39*(36), 6747-6764.

Haywood, J., and O. Boucher (2000), Estimates of the direct and indirect radiative forcing due to tropospheric aerosols: A review, *Rev. Geophys.*, *38*(4), 513-543.

Hien, T. T., P. P. Nam, S. Yasuhiro, K. Takayuki, T. Norimichi, and B. Hiroshi (2007), Comparison of particle-phase polycyclic aromatic hydrocarbons and their variability causes in the ambient air in Ho Chi Minh City, Vietnam and in Osaka, Japan, during 2005-2006, *Sci. Total Environ.*, *382*(1), 70-81.

Huang, X., R. Qiu, C. K. Chan, and P. Ravi Kant (2011), Evidence of high $PM_{2.5}$ strong acidity in ammonia-rich atmosphere of Guangzhou, China: Transition in pathways of ambient ammonia to form aerosol ammonium at $[NH_4^+]/[SO_4^{2-}] = 1.5$, *Atmospheric Research*, *99*(3-4), 488-495.

Jacobson, M. C., H. C. Hansson, K. J. Noone, and R. J. Charlson (2000), Organic atmospheric aerosols: Review and state of the science, *Rev. Geophys.*, *38*(2), 267-294.

Jacobson, M. Z. (2004), The Short-Term Cooling but Long-Term Global Warming Due to Biomass Burning, *Journal of Climate*, *17*(15), 2909-2926.

Jenkins, B. M., A. Daniel Jones, S. Q. Turn, and R. B. Williams (1996), Particle concentrations, gas-particle partitioning, and species intercorrelations for Polycyclic Aromatic Hydrocarbons (PAH) emitted during biomass burning, *Atmos. Environ.*, *30*(22), 3825-3835.

Jethva, H., S. K. Satheesh, and J. Srinivasan (2005), Seasonal variability of aerosols over the Indo-Gangetic basin, *J. Geophys. Res.*, *110*(D21), D21204.

Jimenez, e. a. (2009), Evolution of Organic Aerosols in the Atmosphere, *Science*, *326*(5959), 1525-1529.

Justice, C. O., L. Giglio, S. Korontzi, J. Owens, J. T. Morisette, D. Roy, J. Descloitres, S. Alleaume, F. Petitcolin, and Y. Kaufman (2002), The MODIS fire products, *Remote Sensing of Environment*, *83*(1-2), 244-262.

Kaiser, J. C., N. Riemer, and D. A. Knopf (2011), Detailed heterogeneous oxidation of soot surfaces in a particle-resolved aerosol model, *Atmos. Chem. Phys.*, *11*, 4505-4520.

Keene, W. C., A. A. P. Pszenny, J. N. Galloway, and M. E. Hawley (1986), Sea-Salt Corrections and Interpretation of Constituent Ratios in Marine Precipitation, *J. Geophys. Res.*, *91*(D6), 6647-6658.

Keshtkar, H., and L. L. Ashbaugh (2007), Size distribution of polycyclic aromatic hydrocarbon particulate emission factors from agricultural burning, *Atmos. Environ.*, *41*(13), 2729-2739.

Khalili, N. R., P. A. Scheff, and T. M. Holsen (1995), PAH source fingerprints for coke ovens, diesel and, gasoline engines, highway tunnels, and wood combustion emissions, *Atmos. Environ.*, *29*(4), 533-542.

Khillare, P., S. Balachandran, and R. Hoque (2005a), Profile of PAH in the Exhaust of Gasoline Driven Vehicles in Delhi, *Environ. Monit. Assess.*, *110*(1), 217-225.

Khillare, P. S., S. Balachandran, and R. R. Hoque (2005b), Profile of PAHs in the Diesel Vehicle Exhaust in Delhi, *Environ. Monit. Assess.*, *105*(1), 411-417.

Kim Oanh, N. T., B. T. Ly, D. Tipayarom, B. R. Manandhar, P. Prapat, C. D. Simpson, and L. J. Sally Liu (2011), Characterization of particulate matter emission from open burning of rice straw, *Atmos. Environ.*, *45*(2), 493-502.

Kirton, P. J., J. Ellis, and P. T. Crisp (1991), The analysis of organic matter in coke oven emissions, *Fuel*, *70*(12), 1383-1389.

Kiss, G., Z. Varga-Puchony, and J. Hlavay (1996), Determination of polycyclic aromatic hydrocarbons in precipitation using solid-phase extraction and column liquid chromatography, *J. Chromatogr. A*, *725*(2), 261-272.

Kiss, G., A. Gelencsér, Z. Krivácsy, and J. Hlavay (1997), Occurrence and determination of organic pollutants in aerosol, precipitation, and sediment samples collected at Lake Balaton, *J. Chromatogr. A*, *774*(1-2), 349-361.

Kondo, Y., Y. Miyazaki, N. Takegawa, T. Miyakawa, R. J. Weber, J. L. Jimenez, Q. Zhang, and D. R. Worsnop (2007), Oxygenated and water-soluble organic aerosols in Tokyo, *J. Geophys. Res.*, *112*(D1), D01203.

Kondo, Y., H. Matsui, N. Moteki, L. Sahu, N. Takegawa, M. Kajino, Y. Zhao, M. J. Cubison, J. L. Jimenez, S. Vay, G. S. Diskin, B. Anderson, A. Wisthaler, T. Mikoviny, H. E. Fuelberg, D. R. Blake, G. Huey, A. J. Weinheimer, D. J. Knapp, and W. H. Brune (2011), Emissions of black carbon, organic, and inorganic aerosols from biomass burning in North America and Asia in 2008, *J. Geophys. Res.*, *116*(D8), D08204.

Lee, J. Y., D. A. Lane, J. B. Heo, S.-M. Yi, and Y. P. Kim (2012), Quantification and seasonal pattern of atmospheric reaction products of gas phase PAHs in $PM_{2.5}$, *Atmos. Environ.*, *55*(0), 17-25.

Li, P.-h., Y. Wang, Y.-h. Li, Z.-f. Wang, H.-y. Zhang, P.-j. Xu, and W.-x. Wang (2010), Characterization of polycyclic aromatic hydrocarbons deposition in $PM_{2.5}$ and cloud/fog water at Mount Taishan (China), *Atmos. Environ.*, *44*(16), 1996-2003.

Li, X., S. Wang, L. Duan, J. Hao, C. Li, Y. Chen, and L. Yang (2007), Particulate and Trace Gas Emissions from Open Burning of Wheat Straw and Corn Stover in China, *Environmental Science & Technology*, *41*(17), 6052-6058.

Li, Z., E. N. Porter, A. Sjödin, L. L. Needham, S. Lee, A. G. Russell, and J. A. Mulholland (2009), Characterization of $PM_{2.5}$-bound polycyclic aromatic hydrocarbons in Atlanta--Seasonal variations at urban, suburban, and rural ambient air monitoring sites, *Atmos. Environ.*, *43*(27), 4187-4193.

Liu, S., S. Tao, W. Liu, Y. Liu, H. Dou, J. Zhao, L. Wang, J. Wang, Z. Tian, and Y. Gao (2007), Atmospheric Polycyclic Aromatic Hydrocarbons in North China: A Winter-Time Study, *Environmental Science & Technology*, *41*(24), 8256-8261.

Maenhaut, W., I. Salma, J. Cafmeyer, H. J. Annegarn, and M. O. Andreae (1996), Regional atmospheric aerosol composition and sources in the eastern Transvaal, South Africa, and impact of biomass burning, *J. Geophys. Res.*, *101*(D19), 23631-23650.

Mandalakis, M., M. Tsapakis, A. Tsoga, and E. G. Stephanou (2002), Gas-particle concentrations and distribution of aliphatic hydrocarbons, PAHs, PCBs and PCDD/Fs in the atmosphere of Athens (Greece), *Atmos. Environ.*, *36*(25), 4023-4035.

Mandalakis, M., Ö. Gustafsson, T. Alsberg, A.-L. Egebäck, C. M. Reddy, L. Xu, J. Klanova, I. Holoubek, and E. G. Stephanou (2005), Contribution of Biomass Burning to Atmospheric Polycyclic Aromatic Hydrocarbons at Three European Background Sites, *Environmental Science & Technology*, *39*(9), 2976-2982.

Masclet, P., H. Cachier, C. Liousse, and H. Wortham (1995), Emissions of Polycyclic aromatic hydrocarbons by savanna fires, *Journal of Atmospheric Chemistry*, *22*(1), 41-54.

Mayol-Bracero, O. L., R. Gabriel, M. O. Andreae, T. W. Kirchstetter, T. Novakov, J. Ogren, P. Sheridan, and D. G. Streets (2002a), Carbonaceous aerosols over the Indian Ocean during the Indian Ocean Experiment (INDOEX): Chemical characterization, optical properties, and probable sources, *J. Geophys. Res.*, *107*(D19), 8030.

Mayol-Bracero, O. L., P. Guyon, B. Graham, G. Roberts, M. O. Andreae, S. Decesari, M. C. Facchini, S. Fuzzi, and P. Artaxo (2002b), Water-soluble organic compounds in biomass burning aerosols over Amazonia 2. Apportionment of the chemical composition and importance of the polyacidic fraction, *J. Geophys. Res.*, *107*(D20), 8091.

Mazurek, M. A., W. R. I. Cofer, and J. S. Levine (1990), *Carbonaceous aerosols from prescribed burning of a boreal forest ecosystem. Revision*, Medium: ED; Size: 22 p. pp.

McMeeking, G. R., S. M. Kreidenweis, S. Baker, C. M. Carrico, J. C. Chow, J. L. Collett, Jr., W. M. Hao, A. S. Holden, T. W. Kirchstetter, W. C. Malm, H. Moosmüller, A. P. Sullivan, and C. E. Wold (2009), Emissions of trace gases and aerosols during the open combustion of biomass in the laboratory, *J. Geophys. Res.*, *114*(D19), D19210.

Menon, S., J. Hansen, L. Nazarenko, and Y. Luo (2002), Climate Effects of Black Carbon Aerosols in China and India, *Science*, *297*(5590), 2250-2253.

Miet, K., K. Le Menach, P. M. Flaud, H. Budzinski, and E. Villenave (2009a), Heterogeneous reactivity of pyrene and 1-nitropyrene with NO_2: Kinetics, product yields and mechanism, *Atmos. Environ.*, *43*(4), 837-843.

Miet, K., K. Le Menach, P. M. Flaud, H. Budzinski, and E. Villenave (2009b), Heterogeneous reactions of ozone with pyrene, 1-hydroxypyrene and 1-nitropyrene adsorbed on particles, *Atmos. Environ.*, *43*(24), 3699-3707.

Miyazaki, Y., Y. Kondo, S. Han, M. Koike, D. Kodama, Y. Komazaki, H. Tanimoto, and H. Matsueda (2007), Chemical characteristics of water-soluble organic carbon in the Asian outflow, *J. Geophys. Res.*, *112*(D22), D22S30.

Novakov, T., and J. E. Penner (1993), Large contribution of organic aerosols to cloud-condensation-nuclei concentrations, *Nature*, *365*(6449), 823-826.

Novakov, T., M. O. Andreae, R. Gabriel, T. W. Kirchstetter, Mayol, O. L. Bracero, and V. Ramanathan (2000), Origin of carbonaceous aerosols over the tropical Indian Ocean: Biomass burning or fossil fuels?, *Geophys. Res. Lett.*, *27*(24), 4061-4064.

Ohura, T., T. Amagai, M. Fusaya, and H. Matsushita (2003), Spatial Distributions and Profiles of Atmospheric Polycyclic Aromatic Hydrocarbons in Two Industrial Cities in Japan, *Environmental Science & Technology*, *38*(1), 49-55.

Okuda, T., D. Naoi, M. Tenmoku, S. Tanaka, K. He, Y. Ma, F. Yang, Y. Lei, Y. Jia, and D. Zhang (2006), Polycyclic aromatic hydrocarbons (PAHs) in the aerosol in Beijing, China, measured by aminopropylsilane chemically-bonded stationary-phase column chromatography and HPLC/fluorescence detection, *Chemosphere*, *65*(3), 427-435.

Panther, B. C., M. A. Hooper, and N. J. Tapper (1999), A comparison of air particulate matter and associated polycyclic aromatic hydrocarbons in some tropical and temperate urban environments, *Atmos. Environ.*, *33*(24-25), 4087-4099.

Pathak, R. K., W. S. Wu, and T. Wang (2009), Summertime $PM_{2.5}$ ionic species in four major cities of China: nitrate formation in an ammonia-deficient atmosphere, *Atmos. Chem. Phys.*, *9*(5), 1711-1722.

Pavuluri, C. M., K. Kawamura, T. Swaminathan, and E. Tachibana (2011), Stable carbon isotopic compositions of total carbon, dicarboxylic acids and glyoxylic acid in the tropical Indian aerosols: Implications for sources and photochemical processing of organic aerosols, *J. Geophys. Res.*, *116*(D18), D18307.

Perraudin, E., H. Budzinski, and E. Villenave (2005a), Kinetic study of the reactions of NO_2 with polycyclic aromatic hydrocarbons adsorbed on silica particles, *Atmos. Environ.*, *39*(35), 6557-6567.

Perraudin, E., H. Budzinski, and E. Villenave (2005b), Analysis of polycyclic aromatic hydrocarbons adsorbed on particles of atmospheric interest using pressurised fluid extraction, *Anal. Bioanal. Chem.*, *383*(1), 122-131.

Perraudin, E., H. Budzinski, and E. Villenave (2007), Kinetic Study of the Reactions of Ozone with Polycyclic Aromatic Hydrocarbons Adsorbed on Atmospheric Model Particles, *Journal of Atmospheric Chemistry*, *56*(1), 57-82.

Pio, C. A., M. Legrand, T. Oliveira, J. Afonso, C. Santos, A. Caseiro, P. Fialho, F. Barata, H. Puxbaum, A. Sanchez-Ochoa, A. Kasper-Giebl, A. Gelencsér, S. Preunkert, and M. Schock (2007), Climatology of aerosol composition (organic versus inorganic) at nonurban sites on a west-east transect across Europe, *J. Geophys. Res.*, *112*(D23), D23S02.

Poster, D., M. Schantz, L. Sander, and S. Wise (2006), Analysis of polycyclic aromatic hydrocarbons (PAHs) in environmental samples: a critical review of gas chromatographic (GC) methods, *Analytical and Bioanalytical Chemistry*, *386*(4), 859-881.

Rajput, N., and A. Lakhani (2008), Measurements of polycyclic aromatic hydrocarbons at an industrial site in India, *Environ. Monit. Assess.*, *150*(1), 273-284.

Rajput, P., M. M. Sarin, and R. Rengarajan (2011a), High-precision GC-MS analysis of atmospheric polycyclic aromatic hydrocarbons (PAHs) and isomer ratios from biomass burning emissions, *Journal of Environmental Protection*, *2*(4), 445-453.

Rajput, P., M. M. Sarin, R. Rengarajan, and D. Singh (2011b), Atmospheric polycyclic aromatic hydrocarbons (PAHs) from post-harvest biomass burning emissions in the Indo-Gangetic Plain: Isomer ratios and temporal trends, *Atmos. Environ.*, *45*(37), 6732-6740.

Ram, K., and M. M. Sarin (2009), Absorption Coefficient and Site-Specific Mass Absorption Efficiency of Elemental Carbon in Aerosols over Urban, Rural, and High-Altitude Sites in India, *Environmental Science & Technology*, *43*(21), 8233-8239.

Ram, K., and M. M. Sarin (2010), Spatio-temporal variability in atmospheric abundances of EC, OC and WSOC over Northern India, *J. Aerosol Sci*, *41*(1), 88-98.

Ram, K., M. M. Sarin, and P. Hegde (2010a), Long-term record of aerosol optical properties and chemical composition from a high-altitude site (Manora Peak) in Central Himalaya, *Atmospheric Chemistry and Physics*, *10*(3), 11791-11803.

Ram, K., M. M. Sarin, and S. N. Tripathi (2010b), A 1 year record of carbonaceous aerosols from an urban site in the Indo-Gangetic Plain: Characterization, sources, and temporal variability, *J. Geophys. Res.*, *115*(D24), D24313.

Ram, K., M. M. Sarin, and S. N. Tripathi (2012), Temporal Trends in Atmospheric $PM_{2.5}$, PM_{10}, Elemental Carbon, Organic Carbon, Water-Soluble Organic Carbon, and Optical Properties: Impact of Biomass Burning Emissions in The Indo-Gangetic Plain, *Environmental Science & Technology*, *46*(2), 686-695.

Ramana, M. V., V. Ramanathan, Y. Feng, S. C. Yoon, S. W. Kim, G. R. Carmichael, and J. J. Schauer (2010), Warming influenced by the ratio of black carbon to sulphate and the black-carbon source, *Nature Geosci*, *3*(8), 542-545.

Ramanathan, V., P. J. Crutzen, J. Lelieveld, A. P. Mitra, D. Althausen, J. Anderson, M. O. Andreae, W. Cantrell, G. R. Cass, C. E. Chung, A. D. Clarke, J. A. Coakley, W. D. Collins, W. C. Conant, F. Dulac, J. Heintzenberg, A. J. Heymsfield, B. Holben, S. Howell, J. Hudson, A. Jayaraman, J. T. Kiehl, T. N. Krishnamurti, D. Lubin, G. McFarquhar, T. Novakov, J. A. Ogren, I. A. Podgorny, K. Prather, K. Priestley, J. M. Prospero, P. K. Quinn, K. Rajeev, P. Rasch, S. Rupert, R. Sadourny, S. K. Satheesh, G. E. Shaw, P. Sheridan, and F. P. J. Valero (2001), Indian Ocean Experiment: An integrated analysis of the climate forcing and effects of the great Indo-Asian haze, *J. Geophys. Res.*, *106*(D22), 28371-28398.

Ramanathan, V., M. V. Ramana, G. Roberts, D. Kim, C. Corrigan, C. Chung, and D. Winker (2007), Warming trends in Asia amplified by brown cloud solar absorption, *Nature*, *448*(7153), 575-578.

Rastogi, N., and M. M. Sarin (2005), Long-term characterization of ionic species in aerosols from urban and high-altitude sites in western India: Role of mineral dust and anthropogenic sources, *Atmos. Environ.*, *39*(30), 5541-5554.

Rastogi, N., and M. M. Sarin (2006), Chemistry of aerosols over a semi-arid region: Evidence for acid neutralization by mineral dust, *Geophys. Res. Lett.*, *33*(23), L23815.

Rastogi, N., and M. M. Sarin (2008), Atmospheric ^{210}Pb and ^{7}Be in ambient aerosols over low- and high-altitude sites in semiarid region: Temporal variability and transport processes, *J. Geophys. Res.*, *113*(D11), D11103.

Rengarajan, R., M. M. Sarin, and A. K. Sudheer (2007), Carbonaceous and inorganic species in atmospheric aerosols during wintertime over urban and high-altitude sites in North India, *J. Geophys. Res.*, *112*(D21), D21307.

Richter, B. E., B. A. Jones, J. L. Ezzell, N. L. Porter, N. Avdalovic, and C. Pohl (1996), Accelerated Solvent Extraction: A Technique for Sample Preparation, *Anal. Chem.*, *68*(6), 1033-1039.

Robinson, A. L., N. M. Donahue, and W. F. Rogge (2006a), Photochemical oxidation and changes in molecular composition of organic aerosol in the regional context, *J. Geophys. Res.*, *111*(D3), D03302.

Robinson, A. L., R. Subramanian, N. M. Donahue, and W. F. Rogge (2006b), Source Apportionment of Molecular Markers and Organic Aerosol1. Polycyclic Aromatic Hydrocarbons and Methodology for Data Visualization, *Environmental Science & Technology*, *40*(24), 7803-7810.

Rogge, W. F., L. M. Hildemann, M. A. Mazurek, and G. R. Cass (1998), Sources of Fine Organic Aerosol. 9. Pine, Oak, and Synthetic Log Combustion in Residential Fireplaces, *Environmental Science & Technology*, *32*(1), 13-22.

Rudich, Y. (2003), Laboratory Perspectives on the Chemical Transformations of Organic Matter in Atmospheric Particles, *Chem. Rev.*, *103*(12), 5097-5124.

Rudich, Y., N. M. Donahue, and T. F. Mentel (2007), Aging of Organic Aerosol: Bridging the Gap Between Laboratory and Field Studies, *Annu. Rev. Phys. Chem.*, *58*(1), 321-352.

Ruellan, S., H. Cachier, A. Gaudichet, P. Masclet, and J.-P. Lacaux (1999), Airborne aerosols over central Africa during the Experiment for Regional Sources and Sinks of Oxidants (EXPRESSO), *J. Geophys. Res.*, *104*(D23), 30673-30690.

Ryu, S. Y., J. E. Kim, H. Zhuanshi, Y. J. Kim, and G. U. Kang (2004), Chemical Composition of Post-Harvest Biomass Burning Aerosols in Gwangju, Korea, *Journal of the Air & Waste Management Association*, *54*(9), 1124-1137.

Sarin, M., A. Kumar, B. Srinivas, A. K. Sudheer, and N. Rastogi (2011), Anthropogenic sulphate aerosols and large Cl-deficit in marine atmospheric boundary layer of tropical Bay of Bengal, *Journal of Atmospheric Chemistry*, *66*(1-2), 1-10.

Saxena, P., and L. M. Hildemann (1996), Water-soluble organics in atmospheric particles: A critical review of the literature and application of thermodynamics to identify candidate compounds, *Journal of Atmospheric Chemistry*, *24*(1), 57-109.

Schantz, M. M., J. J. Nichols, and S. A. Wise (1997), Evaluation of Pressurized Fluid Extraction for the Extraction of Environmental Matrix Reference Materials, *Anal. Chem.*, *69*(20), 4210-4219.

Schauer, J. J., W. F. Rogge, L. M. Hildemann, M. A. Mazurek, G. R. Cass, and B. R. T. Simoneit (1996), Source apportionment of airborne particulate

matter using organic compounds as tracers, *Atmos. Environ.*, *30*(22), 3837-3855.

Schauer, J. J., M. J. Kleeman, G. R. Cass, and B. R. T. Simoneit (2001), Measurement of Emissions from Air Pollution Sources. 3. C1 - C29 Organic Compounds from Fireplace Combustion of Wood, *Environmental Science & Technology*, *35*(9), 1716-1728.

Schauer, J. J., M. J. Kleeman, G. R. Cass, and B. R. T. Simoneit (2002), Measurement of Emissions from Air Pollution Sources. 5. C1 - C32 Organic Compounds from Gasoline-Powered Motor Vehicles, *Environmental Science & Technology*, *36*(6), 1169-1180.

Schauer, J. J., B. T. Mader, J. T. DeMinter, G. Heidemann, M. S. Bae, J. H. Seinfeld, R. C. Flagan, R. A. Cary, D. Smith, B. J. Huebert, T. Bertram, S. Howell, J. T. Kline, P. Quinn, T. Bates, B. Turpin, H. J. Lim, J. Z. Yu, H. Yang, and M. D. Keywood (2003), ACE-Asia Intercomparison of a Thermal-Optical Method for the Determination of Particle-Phase Organic and Elemental Carbon, *Environmental Science & Technology*, *37*(5), 993-1001.

Seinfeld, J. H., and J. F. Pankow (2003), Organic Atmospheric Particulate Material, *Annu. Rev. Phys. Chem.*, *54*(1), 121-140.

Seinfeld, J. H., and S. N. Pandis (2006), Atmospheric Chemistry and Physics - From Air Pollution to Climate Change (2nd Edition), edited, John Wiley & Sons.

Shakya, K. M., L. D. Ziemba, and R. J. Griffin (2010), Characteristics and Sources of Carbonaceous, Ionic, and Isotopic Species of Wintertime Atmospheric Aerosols in Kathmandu Valley, Nepal, *Aerosol and Air Quality Research*, *10*, 219-230.

Shapiro, E. L., J. Szprengiel, N. Sareen, C. N. Jen, M. R. Giordano, and V. F. McNeill (2009), Light-absorbing secondary organic material formed by glyoxal in aqueous aerosol mimics, *Atmos. Chem. Phys.*, *9*(7), 2289-2300.

Sharma, H., V. Jain, and Z. Khan (2008), Atmospheric polycyclic aromatic hydrocarbons (PAHs) in the urban air of Delhi during 2003, *Environ. Monit. Assess.*, *147*(1), 43-55.

Sheesley, R. J., J. J. Schauer, Z. Chowdhury, G. R. Cass, and B. R. T. Simoneit (2003), Characterization of organic aerosols emitted from the combustion of biomass indigenous to South Asia, *J. Geophys. Res.*, *108*(D9), 4285.

Simoneit, B. R. T. (2002), Biomass burning - a review of organic tracers for smoke from incomplete combustion, *Appl. Geochem.*, *17*(3), 129-162.

Sokolik, I. N., D. M. Winker, G. Bergametti, D. A. Gillette, G. Carmichael, Y. J. Kaufman, L. Gomes, L. Schuetz, and J. E. Penner (2001), Introduction to special section: Outstanding problems in quantifying the radiative impacts of mineral dust, *J. Geophys. Res.*, *106*(D16), 18015-18027.

Song, J., L. He, P. a. Peng, J. Zhao, and S. Ma (2012), Chemical and Isotopic Composition of Humic-Like Substances (HULIS) in Ambient Aerosols in Guangzhou, South China, *Aerosol Sci. Technol.*, *46*(5), 533-546.

Srinivas, B., M. M. Sarin, and V. V. S. S. Sarma (2011), Atmospheric dry deposition of inorganic and organic nitrogen to the Bay of Bengal: Impact of continental outflow, *Mar. Chem.*, *127*(1-4), 170-179.

Stone, E. A., G. C. Lough, J. J. Schauer, P. S. Praveen, C. E. Corrigan, and V. Ramanathan (2007), Understanding the origin of black carbon in the atmospheric brown cloud over the Indian Ocean, *J. Geophys. Res.*, *112*(D22), D22S23.

Streets, D. G., T. C. Bond, G. R. Carmichael, S. D. Fernandes, Q. Fu, D. He, Z. Klimont, S. M. Nelson, N. Y. Tsai, M. Q. Wang, J. H. Woo, and K. F. Yarber (2003a), An inventory of gaseous and primary aerosol emissions in Asia in the year 2000, *J. Geophys. Res.*, *108*(D21), 8809.

Streets, D. G., K. F. Yarber, J. H. Woo, and G. R. Carmichael (2003b), Biomass burning in Asia: Annual and seasonal estimates and atmospheric emissions, *Global Biogeochem. Cycles*, *17*(4), 1099.

Tham, Y. W. F., K. Takeda, and H. Sakugawa (2008), Polycyclic aromatic hydrocarbons (PAHs) associated with atmospheric particles in Higashi Hiroshima, Japan: Influence of meteorological conditions and seasonal variations, *Atmospheric Research*, *88*(3-4), 224-233.

Tripathi, S. N., S. Dey, V. Tare, and S. K. Satheesh (2005), Aerosol black carbon radiative forcing at an industrial city in northern India, *Geophys. Res. Lett.*, *32*(8), doi:10.1029/2005GL022515.

Turn, S. Q., B. M. Jenkins, J. C. Chow, L. C. Pritchett, D. Campbell, T. Cahill, and S. A. Whalen (1997), Elemental characterization of particulate matter emitted from biomass burning: Wind tunnel derived source profiles for herbaceous and wood fuels, *J. Geophys. Res.*, *102*(D3), 3683-3699.

Turpin, B. J., P. Saxena, and E. Andrews (2000), Measuring and simulating particulate organics in the atmosphere: problems and prospects, *Atmos. Environ.*, *34*(18), 2983-3013.

Turpin, B. J., and H.-J. Lim (2001), Species Contributions to $PM_{2.5}$ Mass Concentrations: Revisiting Common Assumptions for Estimating Organic Mass, *Aerosol Sci. Technol.*, *35*(1), 602 - 610.

Turrio-Baldassarri, L., C. L. Battistelli, and A. L. Iamiceli (2003), Evaluation of the efficiency of extraction of PAHs from diesel particulate matter with pressurized solvents, *Analytical and Bioanalytical Chemistry*, *375*(4), 589-595.

Venkataraman, C., and S. K. Friedlander (1994), Size Distributions of Polycyclic Aromatic Hydrocarbons and Elemental Carbon. 2. Ambient Measurements and Effects of Atmospheric Processes, *Environmental Science & Technology*, *28*(4), 563-572.

Venkataraman, C., G. Habib, A. Eiguren-Fernandez, A. H. Miguel, and S. K. Friedlander (2005), Residential Biofuels in South Asia: Carbonaceous Aerosol Emissions and Climate Impacts, *Science*, *307*(5714), 1454-1456.

Venkataraman, C., G. Habib, D. Kadamba, M. Shrivastava, J. F. Leon, B. Crouzille, O. Boucher, and D. G. Streets (2006), Emissions from open biomass burning in India: Integrating the inventory approach with high-resolution Moderate Resolution Imaging Spectroradiometer (MODIS) active-fire and land cover data, *Global Biogeochem. Cycles*, *20*(2), GB2013.

Wang, G., L. Huang, Z. Xin, H. Niu, and Z. Dai (2006), Aliphatic and polycyclic aromatic hydrocarbons of atmospheric aerosols in five locations of Nanjing urban area, China, *Atmospheric Research*, *81*(1), 54-66.

Wang, H., K. Kawamura, and D. Shooter (2005), Carbonaceous and ionic components in wintertime atmospheric aerosols from two New Zealand cities: Implications for solid fuel combustion, *Atmos. Environ.*, *39*(32), 5865-5875.

Weber, R. J., A. P. Sullivan, R. E. Peltier, A. Russell, B. Yan, M. Zheng, J. de Gouw, C. Warneke, C. Brock, J. S. Holloway, E. L. Atlas, and E. Edgerton (2007), A study of secondary organic aerosol formation in the anthropogenic-influenced southeastern United States, *J. Geophys. Res.*, *112*(D13), D13302.

Wise, S. A., B. A. Benner, S. N. Chesler, L. R. Hilpert, C. R. Vogt, and W. E. May (1986), Characterization of the polycyclic aromatic hydrocarbons from two standard reference material air particulate samples, *Anal. Chem.*, *58*(14), 3067-3077.

Wise, S. A., L. C. Sander, M. M. Schantz, M. J. Hays, and B. A. Benner (2000), Recertification of Standard Reference Material (SRM) 1649, Urban Dust, for the Determination of Polycyclic Aromatic Hydrocarbons (PAHs), *Polycyclic Aromat. Compd.*, *13*(4), 419 - 456.

Xie, M.-X., F. Xie, Z.-W. Deng, and G.-S. Zhuang (2003), Determination of polynuclear aromatic hydrocarbons in aerosol by solid-phase extraction and gas chromatography-mass spectrum, *Talanta*, *60*(6), 1245-1257.

Yamasoe, M. r. A., P. Artaxo, A. H. Miguel, and A. G. Allen (2000), Chemical composition of aerosol particles from direct emissions of vegetation fires in the Amazon Basin: water-soluble species and trace elements, *Atmos. Environ.*, *34*(10), 1641-1653.

Yunker, M. B., R. W. Macdonald, R. Vingarzan, R. H. Mitchell, D. Goyette, and S. Sylvestre (2002), PAHs in the Fraser River basin: a critical appraisal of PAH ratios as indicators of PAH source and composition, *Org. Geochem.*, *33*(4), 489-515.

Zhang, H., D. Hu, J. Chen, X. Ye, S. X. Wang, J. M. Hao, L. Wang, R. Zhang, and Z. An (2011), Particle Size Distribution and Polycyclic Aromatic Hydrocarbons Emissions from Agricultural Crop Residue Burning, *Environmental Science & Technology*, *45*(13), 5477-5482.

Zhang, H., and Q. Ying (2012), Secondary organic aerosol from polycyclic aromatic hydrocarbons in Southeast Texas, *Atmos. Environ.*, *55*(0), 279-287.

Zhang, Y., B. Yang, J. Meng, S. Gao, X. Dong, and J. Shu (2009), Homogeneous and heterogeneous reactions of phenanthrene with ozone, *Atmos. Environ.*, *44*(5), 697-702.

LIST OF PUBLICATIONS

(i) Papers published in peer reviewed International Journals:

1. **Prashant Rajput,** Manmohan Sarin and Ramabadran Rengarajan **(2011)**, High-Precision GC-MS Analysis of Atmospheric Polycyclic Aromatic Hydrocarbons (PAHs) and Isomer Ratios from Biomass Burning Emissions, ***Journal of Environmental Protection***, 2, 445–453.

2. **Prashant Rajput,** M. M. Sarin, R. Rengarajan and Darshan Singh **(2011)**, Atmospheric polycyclic aromatic hydrocarbons (PAHs) from post-harvest biomass burning emissions in the Indo-Gangetic Plain: Isomer ratios and temporal trends, ***Atmospheric Environment,*** 45, 6732–6740.

(ii) Manuscript Under Review:

3. **Prashant Rajput,** M. M. Sarin and S. S. Kundu **(2012)**, Atmospheric PM2.5, EC, OC, WSOC and PAHs from NE-Himalaya: Sources and long-range transport, ***Journal of Geophysical Research-Atmospheres*** (Rivision submitted).

(iii) Abstract in National/International Conference:

1. **Prashant Rajput**, M. M. Sarin, Darshan Singh and Deepti Sharma **(2012)**, Carbonaceous aerosols from biomass burning emissions in Northern India: Chemical characterization and temporal trends, **22nd V. M. Goldschmidt Conference**, 24–29th June 2012, **Montreal Canada**.

Journal of Environmental Protection, **2011, 2, 445-453**
doi: 10.4236/jep.2011.24051 Published Online June 2011 (http://www.SciRP.org/journal/jep)

High-Precision GC-MS Analysis of Atmospheric Polycyclic Aromatic Hydrocarbons (PAHs) and Isomer Ratios from Biomass Burning Emissions

Prashant Rajput, Manmohan Sarin*, Ramabadran Rengarajan

Geosciences-Division, Physical Research Laboratory, Ahmedabad, India.
Email: sarin@prl.res.in

Received February 19th, 2011; revised March 25th, 2011; accepted April 27th, 2011.

ABSTRACT

This manuscript describes an analytical method for the quantitative determination of 16*-polycyclic aromatic hydrocarbons* (*PAHs*) *using accelerated solvent extraction* (*ASE*), *followed by purification on a silica cartridge, and subsequent measurement by gas chromatograph coupled to a mass spectrometer* (*GC-MS*). *The solvent extraction parameters* (*T* = 100 ˚*C*, *P* = 1500 *psi*, *t* = 30 *min*, *V* = 30 *ml*) *are optimized with dichloromethane* (*DCM*) *in order to avoid fractionation effect, thereby achieving quantitative mass recovery of PAHs. The purification of PAHs on silica cartridge eliminates the matrix effect*, *facilitates their enrichment from extracted solution and quantitative determination in presence of an internal-standard* (*Pyrene-D*10). *The analytical protocol has been successfully used for the quantification of 16-PAHs and their isomer ratios in atmospheric aerosols collected from northern India dominated by agricultural-waste* (*post-harvest paddy and wheat residue*) *burning emissions. Based on the analysis of ambient aerosols*, *collected from different sites, the overall recovery efficiency for* 2- *to* 3*-ring PAHs is* 85% *and near* 100% *recovery for* 4- *to* 6*-ring compounds.*

***Keywords*:** *Agricultural-Waste Burning*, *PAHs*, *Accelerated Solvent Extraction*, *GC-MS*

1. Introduction

Atmospheric aerosols are composed of mineral dust, inorganic constituents (sulphate and nitrate), carbonaceous matter (organic carbon and elemental carbon) and sea-salts [1-5]. Among the various components, physical adsorption characteristics of mineral dust, sea-salt (polar), and graphitic carbon (non-polar) are well understood [6-8]. These characteristics affect the high precision measurements of organic compounds and compromise their application as proxies to trace the aerosol sources and to understand their chemical reactivity with the atmospheric oxidants (O_3, OH and NO_x) [9-12]. It is, thus, essential to establish an analytical protocol for the measurements of organic compounds in atmospheric aerosols with varying mass concentration and matrix.

Analytical schemes for the quantitative determination of PAHs in environmental samples and standard reference materials are available in the literature e.g. [12-18]. However, suitability of many of these is limited to low aerosol loading. More importantly, these analytical methods have not adequately investigated the matrix effect of tarry matter (emitted from agricultural-waste burning) on mass recovery of PAHs. Therefore, development of an analytical protocol is required for the quantitative mass recovery of PAHs, by eliminating the matrix from high atmospheric loading of aerosols. We report here a quantitative method for the determination of PAHs by suitable combination of accelerated solvent extraction (ASE), followed by purification on a silica cartridge and subsequent determination on a gas chromatograph coupled to a mass spectrometer (GC-MS). The suitability of the analytical method has been ascertained from the field-based samples collected from different geographical locations in India.

The analyses of organic compounds by the conventional extraction techniques such as Soxhlet extraction and ultrasonication [14,19,20], though provide their quantitative recovery, require large volume of solvents (>100 mL) and are often labour intensive. In spite of this, the Soxhlet extraction technique has been successfully used for the extraction of PAHs from standard reference materials (SRM-National Institute of Standards and Tech-

nology) [14,18]. However, the current demand for eco-friendly environment requires minimum consumption of solvents and rapid sample preparation, without compromising the accuracy and precision. Among the two conventional techniques (ultrasonication and Soxhlet extraction), the former provides rapid sample preparation with comparatively lower consumption of solvent. An alternative extraction technique involving supercritical fluid extraction (SFE) requires longer extraction time and also suffers from the incomplete recovery of PAHs in environmental samples due to analyte-matrix interactions [21]. In contrast, the microwave-assisted solvent extraction (MASE) and the accelerated solvent extraction (ASE) approach are beneficial in terms of lower consumption of solvent and perform extraction in shorter time [12,15, 22-24]. However, the MASE technique requires centrifugation and filtration; thus, amounting to the loss of analyte. For the quantitative determination of PAHs, gas chromatography (GC), for its high-resolution and sensitivity, is often preferred rather than liquid chromatography (LC). Recently, the wide range of applications of GC-MS technique has been reviewed [25].

2. Experimental Section

2.1. Materials and Method

The aerosol samples (n = 17) analyzed in this study are collected from three different sites in India: Patiala (30.2 N; 76.3 E; 250 m asl); Hisar (29.2 N; 75.7 E; 219 m asl) and Shillong (25.7 N; 91.9 E; 1064 m asl). The first two sites are located in the Indo-Gangetic Plain (IGP) whereas the third site lies in the high rainfall region of Northeastern India. The aerosol samples from Patiala and Hisar represent by and large emissions from large-scale agricultural-waste burning emissions [26-28] in the IGP. However, aerosol composition at Shillong is influenced by the long-range transport of chemical constituents from Southeast Asia. It is relevant to state that the contribution from sea-salts is insignificant at all the three sites for the sampling during Oct-May. The ambient samples were collected onto pre-combusted quartz-fibre filters (PALLFLEX™, 2500QAT-UP, 20 cm × 25 cm) using high-volume samplers at a flow rate of ~1.2 $m^3 \cdot min^{-1}$. Soon after their retrieval, filters were covered with Al-foil, sealed in zip-lock plastic bags and stored at ~ 4˚C until analysis. The aerosol mass is determined gravimetrically on a high precision analytical balance (Sartorius, Model LA130S-F; 0.1 mg) after equilibrating the filters at relative humidity of 40% ± 5% at 24 ± 2˚C for ~ 10 hrs. The concentrations of elemental carbon (EC) and organic carbon (OC) are measured on a EC-OC analyzer (Model 2000, Sunset Laboratory, Forest Grove, USA) using a thermal-optical transmittance (TOT) protocol [2,9].

The HPLC grade solvents (≥95%), dichloromethane (DCM), acetone and hexane (Chromasolv® Plus, Sigma-Aldrich) are used for the extraction and sample preparation. The 16-PAHs mixture (QTM PAH Mix; 47930-U, in Methylene Chloride, Supelco) and Pyrene-D10 (in methanol, 71390 Absolute Standards INC.) are used as the external and internal standards respectively. The analytical accuracy of PAHs is determined using a standard reference material (SRM-1649b), procured from the National Institute of Standards & Technology (NIST, Gaithersburg, USA). In SRM, PAHs are extracted using the accelerated solvent extraction system (ASE 200, Dionex Corporation, Sunnyvale, USA), followed by evaporation in an evaporator (Turbo Vap LV® II, Caliper Life Sciences, Hopkinton, USA). Subsequently, extract was purified on silica-solid phase extraction cartridge (SPE; WAT020810, Waters Sep-Pak®, 3cc/500mg) placed over the vacuum manifold (20 positions, WAT200606). After removal of matrix, **extracts** were analyzed for PAHs on a GC-MS (Agilent: 7890A/5975C). The detailed approach involving optimization of experimental conditions for the determination of 16-PAHs is described in the following sections.

2.2. Optimization of GC-MS Parameters

After several initial tests, a 30 min GC programme **(Table 1)** was adopted for the separation of 16-PAHs **(**listed in **Table 2)**. Subsequently the MS conditions, especially the ion-source (filament) temperature were standardized for optimum intensity of PAHs. The PAHs were analyzed on a GC-MS in electron impact mode (70 eV). A 1-μL solution of 400 ppb (16-PAHs; QTM mixture) spiked with 200 ng of Pyrene-D10 (internal standard) is separated on a GC capillary column (30 m × 0.25 mm × 0.25 μm; Agilent HP-5MS) at a constant flow rate of 1.3 mL/min of helium gas and analyzed at different filament temperatures; 280˚C (n = 4), 300˚C (n = 4) and 320˚C (n = 4). The PAHs are identified by comparing their retention times (RT) with those for 16-PAHs standard and their quantification is achieved by comparing the peak areas with those of the internal standard (Pyrene-D10). The filament temperature at 300˚C appeared to be the threshold for optimum relative response factors (RRF) for 16-PAHs, calculated as

$$RRF = \frac{\{Area_{Analyte} * Conc_{ISTD}\}}{\{Area_{ISTD} * Conc_{Analyte}\}} \quad (1)$$

The ISTD stands for Internal Standard. Likewise, retention time of PAHs at varying filament temperatures (as above), are investigated, and are found to be invariable

Table 1. Experimental parameters for the measurement of PAHs.

ASE		GC-MS		
Parameters	Optimized conditions	GC		
		Inlet temp: 300˚C		
Solvent	DCM (30 mL)	Heating Rate	Temp	Hold Time
System pressure	1500 psi	˚C/min	˚C	Min
			50	1
Oven temperature	100˚C	25	150	-
		25	200	-
Oven heating time	5 min	3	230	-
		8	310	3
Static Cycles	3 (of 5 min each)	MS		
		Interface temp.	280	
Nitrogen purge	60 s	Ion-source temp.	300	
Extraction Time	30 min	Quadrupole temp.	180	

Table 2. Analysis of 16-PAHs in SRM 1649b, Urban Dust (n=19).

16-PAHs	Molecular weight	Retention time	Detection limit	Measured Conc.[§]	Reported Conc.
		(min)	(n = 12; pg·m^{-3})	(ng/100mg SRM)	
Naphthalene {NAPH}*	128	5.448 ± 0.002	1.9	90 ± 18	112 ± 42
Acenaphthylene {ACY}*	152	7.000 ± 0.004	3.7	15 ± 3	18 ± 3
2-Bromonaphthalene {2-BrNAPH}	206	7.154 ± 0.019	2.5	NR	
Acenaphthene {ACE}*	154	7.180 ± 0.003	1.2	10 ± 1	19 ± 4
Fluorene {FLU}*	166	7.760 ± 0.016	1.5	17 ± 2	22 ± 2
Phenanthrene {PHEN}	178	9.173 ± 0.022	2.3	373 ± 18	394 ± 5
Anthracene {ANTH}	178	9.264 ± 0.026	2.6	44 ± 8	51 ± 1
Fluoranthene {FLA}	202	12.775 ± 0.024	2.1	587 ± 45	614 ± 12
Pyrene {PYR}	202	12.834 ± 0.022	1.6	481 ± 31	478 ± 3
Benzo[*a*]anthracene {BaA}	228	18.275 ± 0.041	2.3	224 ± 22	209 ± 5
Chrysene/Triphenylene {CHRY + TRIP}	228	18.437 ± 0.040	1.9	413 ± 28	425 ± 10
Benzo[b + j + k]fluoranthene {B[b,j,*k*]FLA}	252	22.454 ± 0.038	2.4	923 ± 72	947 ± 51
Benzo[a]pyrene {BaP}	252	23.444 ± 0.047	2.0	267 ± 19	247 ± 17
Indeno[1,2,3-cd]pyrene {IcdP}	276	26.461 ± 0.046	1.6	314 ± 20	296 ± 17
Dibenzo[a,h + a,c]anthracene D[ah,ac]ANTH}	278	26.569 ± 0.055	3.6	49 ± 4	50 ± 1
Benzo[g,h,i]perylene {BghiP}	276	26.996 ± 0.033	2.5	421 ± 35	394 ± 5

*Reference values, otherwise certified values (from NIST). NR (Not reported in NIST certificate).[§]Standard deviation of the data for n = 19.

(RT < 0.001% shift). The optimized GC-MS conditions for the determination of PAHs are listed in **Table 1**, and are used for the measurement of 16-PAHs in ambient aerosols. Data acquisition and processing for the GC-MS analysis is performed on a HP-Enhanced Chemstation Data System.

2.3. Optimization of Purification Step on Silica Cartridge

Aerosol samples contain a wide range of matrices involving mineral dust, organic carbon and elemental carbon. These matrices cause mass interferences with the analytes and affect the resolution of measurements, particularly for the measurements of PAHs on GC-MS. In this study, we have used the silica-SPE cartridge for the purification of PAHs [30]. Prior to the application of silica-SPE cartridges for purification of PAHs in aerosol samples, the elution recovery from 16-PAHs standard is investigated. Accordingly, the silica cartridges, installed over the vacuum manifold are conditioned through 10 mL DCM followed by 10 mL hexane under the vacuum (<340 millibar). The cartridges are dried under normal conditions for 5 min. Subsequently, the 16-PAHs liquid mixture of varying amount 100 ng (n = 3), 400 ng (n = 3) and, 800 ng (n = 3), in 3 mL hexane are loaded on silica cartridges. The matrix is allowed to fall under gravity, and is discarded. The cartridges are dried again for 5 min. The affect of cartridge drying on the PAHs mass recovery has been discussed elsewhere [30]. Subsequently, the elution of PAHs from each cartridge is performed under gravity with 3 mL, 20% DCM in hexane (v/v). The eluate is evaporated to ~ 500 µL under gentle nitrogen gas stream, to which 200 ng of Pyrene-D10 is added. The final solution is made to 1 mL in hexane and stored in amber coloured glass vials at −19˚C until analysis on GC-MS.

2.4. Optimization of Extraction Parameters on ASE

The extraction parameters on ASE such as solvent selection, temperature and extraction time on the recovery efficiency of PAHs were investigated at a constant pressure of 1500 psi (103 bars). The extraction at 1500 psi pressure is considered to be optimal for the aerosol samples [12]. The extraction protocol was developed based on the analysis of standard reference material (NIST, SRM-1649b, Urban Dust). The toxic solvents e.g. benzene and its derivatives were not used to assess the extraction efficiency of PAHs. Furthermore, the loss of analyte during sample processing [16], if any, was checked with the low boiling point solvents e.g. DCM (40˚C), which not only extract PAHs quantitatively from aerosols but also can undergo rapid evaporation. Furthermore, the PAHs were also extracted from SRM in two different solvents viz. DCM (n = 6) and DCM: Acetone (n = 6; 1:1 v/v) at 100˚C, 1500 psi and 3 static cycles of 5 min each. These extracts were evaporated to 1 mL in evaporator (<30˚C) and further to near dryness by gentle nitrogen gas purge. The residue was dissolved in 3 mL hexane. Subsequently, the optimized protocol, described in the previous sections is used for the purification and sample preparation for PAHs analysis. The results suggest that, within the uncertainty of measurements on GC-MS, the yields for individual PAHs were equal with DCM or DCM:Acetone (1:1 v/v). However, DCM was used for the PAHs extraction, due to its rapid evaporation (b.p. 40˚C) in comparison to its mixture with acetone (56.3˚C). The analytical accuracy **(Table 2)** of the protocol was determined by the SRM analysis (n = 19) following the protocol listed in **Table 1**. The molecular weight (quantification ion), retention times and the detection limits (inferred from analyses of n = 12 blanks) for 16-PAHs are also given in **Table 2**.

3. Results & Discussion

3.1. Temporal Variations in $PM_{2.5}$ and Carbonaceous Species (OC, EC)

The $PM_{2.5}$ samples, selected for the evaluation of analytical protocol for PAHs analysis, show temporal variability in aerosol mass from 48 to 391 $\mu g \cdot m^{-3}$. The organic and elemental carbon (OC, EC) varied from 15 to 188 $\mu g \cdot m^{-3}$ and 2.2 to 18.5 $\mu g \cdot m^{-3}$ respectively, whereas Σ PAHs varied from 2 to 46 $ng \cdot m^{-3}$. The high OC/EC ratios (range: 4 to 19) indicate the dominant contributions of carbonaceous species from biomass burning emissions (agricultural-waste burning and the wood fuel combustion) [2,3,31].

3.2. Sample Preparation for PAHs Analysis

The elution recovery of 16-PAHs on silica-SPE cartridge is optimized using 16-PAHs standard, prior to the analysis of aerosol samples (**Figure 1**). The 16-PAHs standard of varying concentrations; 100 ng (n = 3), 400 ng (n = 3) and, 800 ng (n = 3) in 3 mL hexane was eluted from the silica-SPE cartridges. A near quantitative recovery for all 16-PAHs (**Figure 1**) was achieved with the adopted protocol (as discussed in section 2.3). The assessment of extraction parameters (**Figure 2**) on ASE suggests that extraction at 100˚C for 30 min (@ 1500 psi) is optimum for the quantification of PAHs in SRM. Moreover, analysis of SRM extracts (n = 12) for different conditions on ASE (tested range: 90˚C - 120˚C; 5 - 15 min static cycle), suggest that though the mass recovery of PAHs

depends on the extraction conditions, their isomers do not fractionate under these conditions on ASE **(Figure 2)**. A one-eighth or one-fourth portion of the quartz filter (based on Total Carbon/ Aerosol Mass) was cut into strips and loaded on the ASE. The PAHs were extracted following a developed protocol **(Table 1)** in 30 mL DCM.

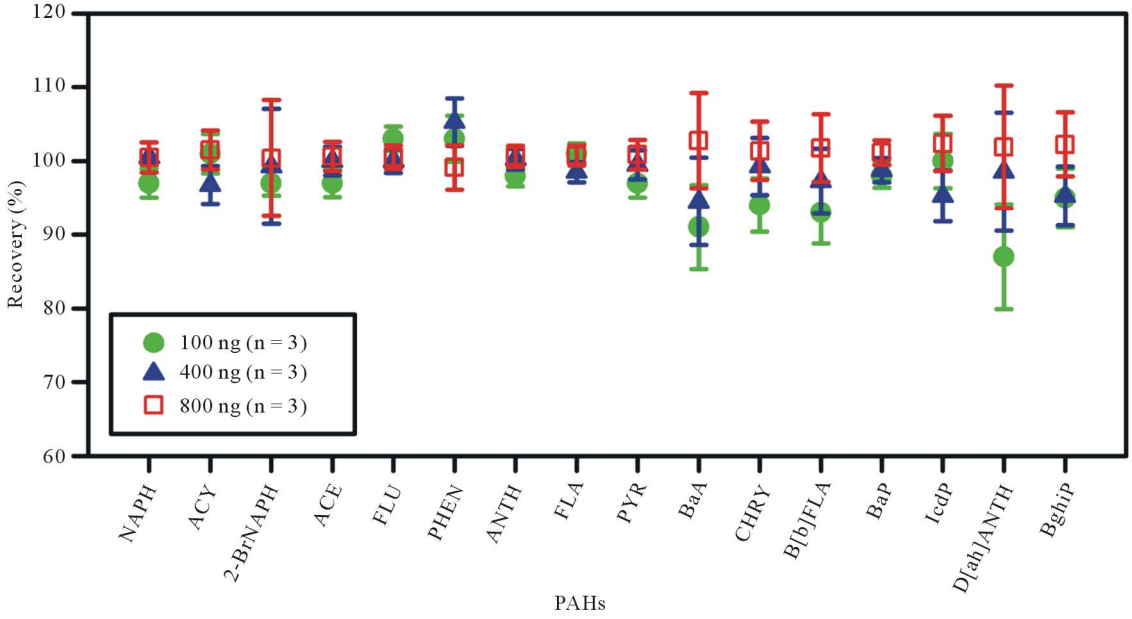

Figure 1. Recovery of 16-PAHs after purification on silica cartridge, as ascertained from a standard (QTM PAH Mix; 47930-U, in Methylene Chloride). The consistent recovery of PAHs (~100%) at varying concentrations of standard solution is noteworthy.

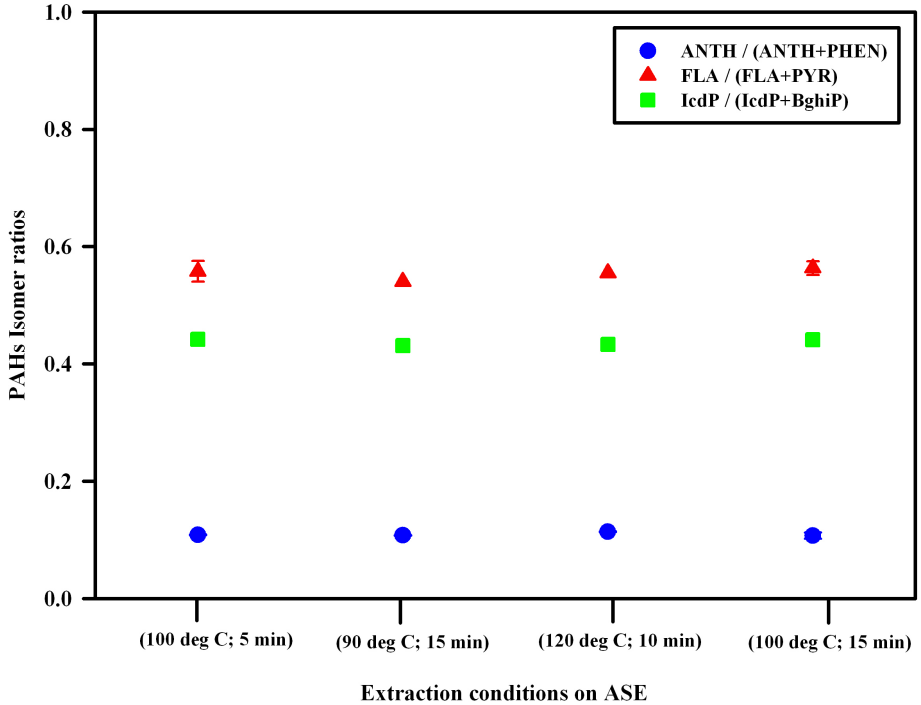

Figure 2. Replicate analysis (n = 12) of three different isomer pairs in SRM ascertain that accelerated solvent extraction (ASE) does not lead to fractionation of PAHs isomers. The extraction of PAHs at 100 ˚C for 15 min has been used as an optimized step for quantitative recovery in aerosol samples.

The extracts were concentrated to 1 mL in the evaporator (<30˚C) and further to near dryness under a gentle stream of nitrogen gas. The residue was dissolved in 3 mL hexane for purification on a silica-SPE cartridge (for details refer to experimental section 2.3). The analytical accuracy for an individual PAH (except 2-BrNAPH, not reported in SRM certificate) was monitored, based on the analysis of SRM with every batch of samples. Quality-control of the data was checked by analyzing the blank filters routinely.

3.3. PAHs Analyses on GC-MS: Evaluation of Protocol for High Aerosol Mass Loading

The operating conditions for PAHs analysis on GC-MS are given in **Table 1**. The DCM based commercial standard of 16-PAHs mixture is diluted in hexane to prepare a 2 ppm stock solution. From this stock **solution**, seven working standards between the concentration ranges from 0 to 1500 ppb are prepared in hexane and analyzed routinely on GC-MS. The one year record in temporal variations (insignificant for n = 35 injections of 16-PAHs standard) of the RRF of 16-PAHs (equation 1) show the stability of GC-MS **(Figure 3)**. Furthermore, several analyses of SRM aliquots (~100 mg; n = 19) over a period of one year, determine the analytical accuracy **(Table 2)**. A total of (n = 17) ambient aerosol samples, collected from different geographical locations in India; from Patiala (n = 8), Hisar (n = 2) and Shillong (n = 7), were

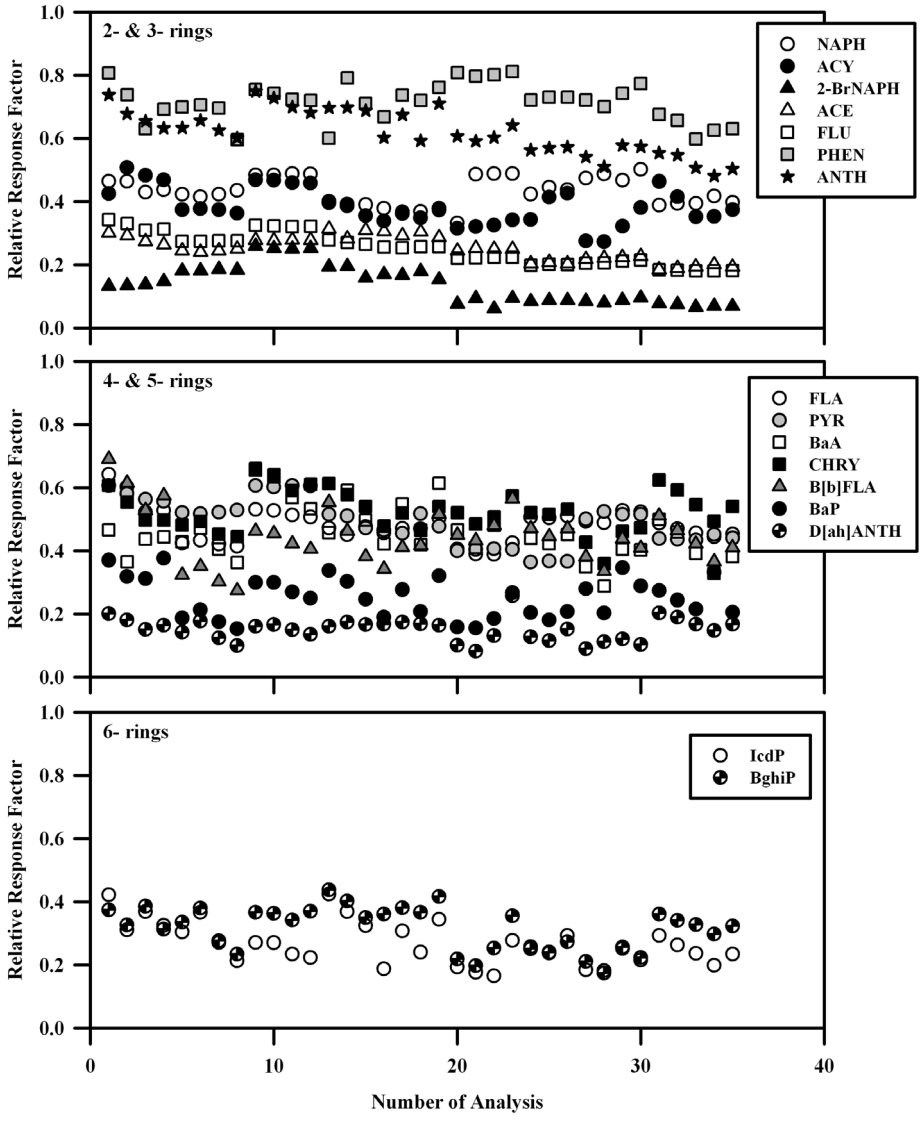

Figure 3. Time dependent analyses (n = 35; over 250 days) of 16-PAHs (QTM PAH Mix; 47930-U, in Methylene Chloride) studied to ascertain the variability in response factors on GC-MS.

analyzed for the mass recovery of PAHs. Repeat extractions and analyses of these samples (n = 17; **Figure 4)** reveal that the extraction efficiency for 2- to 3-ring PAHs is 85 % whereas the recovery is ~100% for 4- to 6-ring compounds. The overall extraction efficiency of PAHs is 97% ± 2%. The extraction efficiency of PAHs in aerosol samples **(Figure 4)** is calculated as

$$100 * \frac{\text{PAHs recovery in first extraction}}{\text{PAHs recovery in}\{\text{first}+\text{second}\}\text{extraction}} \quad (2)$$

Analysis of several sample repeats (n = 17) showed that on an average the external precision of the measurements is ± 4 %. We reemphasis that these samples are representative of tarry matter and soot (along with the mineral dust), and therefore, the analytical protocol investigate the extraction efficiency of PAHs in the presence of varying matrices.

3.4. Investigation of Loss of 2- to 3- ring PAHs During Sample Processing

The 100 ng of 16-PAHs mixture (QTM PAH Mix; 47930-U, in Methylene Chloride, Supelco) was spiked on pre-cleaned quartz fibre filters (1.5 sq cm; n = 6). The extraction of PAHs, followed by matrix purification and sample preparation is done in the similar way to aerosol samples. The analyses on GC-MS ensure recovery close to 100% for the individual PAHs. In contrast to the low recovery for 2- to3-ring PAHs in aerosol samples, the high recovery for all 16-PAHs from spiked filters (~100%), indicate the low concentrations of these PAHs (lighter mass) in aerosol samples lead to their low recovery.

4. Conclusions

An analytical method developed for the quantitative determination of PAHs from standard reference material (NIST-1649b), show analytical accuracy of (100% ± 15%). The adopted protocol for the quantification of PAHs include ASE extraction with DCM at 100˚C for 3 static cycles (of 5 min each) at a constant pressure of 1500 psi, followed by the matrix purification on a pre-cleaned silica cartridge and subsequent analysis on GC-MS, operated at 300˚C as the optimum ion-source temperature. Analysis of field-based aerosol samples show the average extraction efficiency (equation 2) for 4- to 6- ring PAHs is ~100%. The somewhat lower recovery (mean ~85%) for 2- to 3- ring PAHs in the field-based samples is attributable to their lower concentrations in the aerosols. The analytical protocol, for PAHs analysis is ideal to eliminate the matrix effect from tarry matter, soot and mineral dust associated with high atmospheric loading of aerosols.

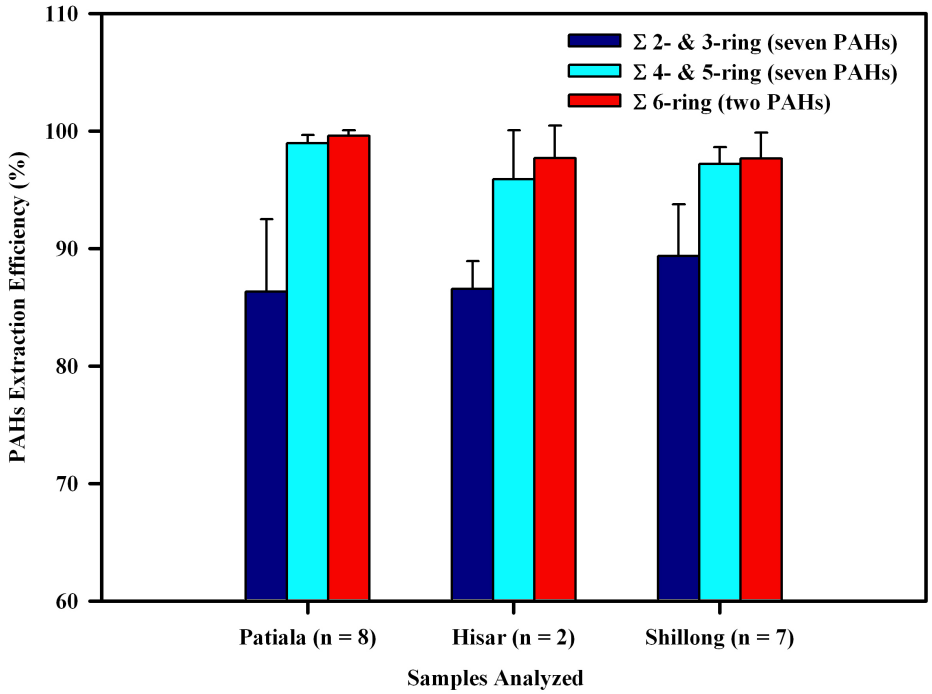

Figure 4. The extraction efficiency of PAHs, as determined in aerosol samples collected from different geographical regions. The 4- to 6- ring PAHs are recovered with ~100 % efficiency, whereas 2- to 3- ring PAHs show somewhat lower recovery (~85%) in the first extraction.

5. Acknowledgements

We acknowledge the partial financial support from the ISRO-Geosphere Biosphere Programme (Bangaluru, India).

REFERENCES

[1] O. L. Mayol-Bracero, P. Guyon, B. Graham, G. Roberts, M. O. Andreae, S. Decesari, M. C. Facchini, S. Fuzzi and P. Artaxo, "Water-Soluble Organic Compounds in Biomass Burning Aerosols over Amazonia 2. Apportionment of the Chemical Composition and Importance of the Polyacidic Fraction," *Journal of Geophysical Research,* Vol. 107, No. D20, 2002. doi:10.1029/2001JD000522

[2] R. Rengarajan, M. M. Sarin and A. K. Sudheer, "Carbonaceous and Inorganic Species in Atmospheric Aerosols during Wintertime over Urban and High-Altitude Sites in North India," *Journal of Geophysical Research,* Vol. 112, No. D21307, 2007.

[3] K. Ram and M. M. Sarin, "Spatio-Temporal Variability in Atmospheric Abundances of EC, OC and WSOC over Northern India," *Journal of Aerosol Science,* Vol. 41, No. 1, 2010, pp. 88-98. doi:10.1016/j.jaerosci.2009.11.004

[4] J. H. Seinfeld and J. F. Pankow, "Organic Atmospheric Particulate Material," *Annual Review of Physical Chemistry,* Vol., 54, 2003, pp. 121-140. doi:10.1146/annurev.physchem.54.011002.103756

[5] J. H. Seinfeld and S. N. Pandis, "Atmospheric Chemistry and Physics—From Air Pollution to Climate Change," 2nd Edition, John Wiley & Sons, New York, 2006.

[6] S. O. Baek, M. E. Goldstone, P. W. W. Kirk, J. N. Lester and R. Perry, "Phase Distribution and Particle Size Dependency of Polycyclic Aromatic Hydrocarbons in the Urban Atmosphere," *Chemosphere,* Vol. 22, No. 5-6, 1991, pp. 503-520. doi:10.1016/0045-6535(91)90062-I

[7] Y. Rudich, N. M. Donahue and T. F. Mentel, "Aging of Organic Aerosol: Bridging the Gap Between Laboratory and Field Studies," *Annual Review of Physical Chemistry,* Vol. 58, 2007, pp. 321-352. doi:10.1146/annurev.physchem.58.032806.104432

[8] M. C. Jacobson, H. C. Hansson, K. J. Noone and R. J. Charlson, "Organic Atmospheric Aerosols: Review and State of the Science," *Reviews of Geophysics,* Vol. 38, No. 2, 2000, pp. 267-294. doi:10.1029/1998RG000045

[9] E. Perraudin, H. Budzinski and E. Villenave, "Analysis of Polycyclic Aromatic Hydrocarbons Adsorbed on Particles of Atmospheric Interest using Pressurised Fluid Extraction," *Analytical Bioanalytical Chemistry,* Vol. 383, No. 1, 2005, pp. 122-131. doi:10.1007/s00216-005-3398-7

[10] K. Miet, K. Le Menach, P. M. Flaud, H. Budzinski and E. Villenave, "Heterogeneous Reactivity of Pyrene and 1-Nitropyrene with NO_2: Kinetics, Product Yields and Mechanism," *Atmospheric Environment,* Vol. 43, No. 4, 2009, pp. 837-843. doi:10.1016/j.atmosenv.2008.10.041

[11] K. Miet, K. Le Menach, P. M. Flaud, H. Budzinski and E. Villenave, "Heterogeneous Reactions of Ozone with Pyrene, 1-Hydroxypyrene and 1-Nitropyrene Adsorbed on Particles," *Atmospheric Environment,* Vol. 43, No. 24, 2009, pp. 3699-3707. doi:10.1016/j.atmosenv.2009.04.032

[12] B. E. Richter, B. A. Jones, J. L. Ezzell, N. L.Porter, N. Avdalovic and C. Pohl, "Accelerated Solvent Extraction: A Technique for Sample Preparation," *Analytical Chemistry,* Vol. 68, No. 6, 1996, pp. 1033-1039. doi:10.1021/ac9508199

[13] G. Kiss, Z. Varga-Puchony and J. Hlavay, "Determination of Polycyclic Aromatic Hydrocarbons in Precipitation using Solid-Phase Extraction and Column Liquid Chromatography," *Journal of Chromatography A,* Vol. 725, No. 2, 1996, pp. 261-272. doi:10.1016/0021-9673(95)00940-X

[14] S. A. Wise, L. C. Sander, M. M. Schantz, M. J. Hays and B. A. Benner, "Recertification of Standard Reference Material (SRM) 1649, Urban Dust, for the Determination of Polycyclic Aromatic Hydrocarbons (PAHs)," *Polycyclic Aromatic Compounds,* Vol. 13, No. 4, 2000, pp. 419-456. doi:10.1080/10406630008233854

[15] M. M. Schantz, J. J. Nichols and S. A. Wise, "Evaluation of Pressurized Fluid Extraction for the Extraction of Environmental Matrix Reference Materials," *Analytical Chemistry,* Vol. 69, No. 20, 1997, pp. 4210-4219. doi:10.1021/ac970299c

[16] N. Alexandrou, M. Smith, R. Park, K. Lumb and K. Brice, "The Extraction of Polycyclic Aromatic Hydrocarbons from Atmospheric Particulate Matter Samples by Accelerated Solvent Extraction (ASE)," *International Journal of Environmental Analytical Chemistry,* Vol. 81, No. 4, 2001, pp. 257 - 280. doi:10.1080/03067310108044248

[17] G. Kiss, A.Gelencsér, Z. Krivácsy and J. Hlavay, "Occurrence and Determination of Organic Pollutants in Aerosol, Precipitation, and Sediment Samples Collected at Lake Balaton," *Journal of Chromatography A,* Vol. 774, Nos. 1-2, 1997, pp. 349-361. doi:10.1016/S0021-9673(97)00265-3

[18] S. A. Wise, B. A. Benner, S. N. Chesler, L. R. Hilpert, C. R. Vogt and W. E. May, "Characterization of the Polycyclic Aromatic Hydrocarbons from Two Standard Reference Material Air Particulate Samples," *Analytical Chemistry,* Vol. 58, No. 14, 1986, pp. 3067-3077. doi:10.1021/ac00127a036

[19] J. Duan, X. Bi, J. Tan, G. Sheng and J. Fu, "The Differences of the Size Distribution of Polycyclic Aromatic Hydrocarbons (PAHs) between Urban and Rural Sites of Guangzhou, China," *Atmospheric Research,* Vol. 78, Nos. 3-4, 2005, pp. 190-203. doi:10.1016/j.atmosres.2005.04.001

[20] M. Mandalakis, Ö. Gustafsson, T. Alsberg, A.-L. Egebäck, C. M. Reddy, L. Xu, J. Klanova, I. Holoubek and E. G. Stephanou, "Contribution of Biomass Burning to Atmospheric Polycyclic Aromatic Hydrocarbons at Three European Background Sites," *Environmental Science & Technology,* Vol. 39, No. 9, 2005, pp. 2976-2982.

doi:10.1021/es048184v

[21] S. B. Hawthorne, D. J. Miller, M. D. Burford, J. J. Langenfeld, S. Eckert-Tilotta and P. K. Louie, "Factors Controlling Quantitative Supercritical Fluid Extraction of Environmental Samples," *Journal of Chromatography A,* Vol. 642, No. 1-2, 1993, pp. 301-317. doi:10.1016/0021-9673(93)80095-P

[22] O. Alvarez-Avilés, L. Cuadra-Rodríguez, F. González-Illán, J. Quiñones-González and O. Rosario, "Optimization of a Novel Method for the Organic Chemical Characterization of Atmospheric Aerosols Based on Microwave-Assisted Extraction Combined with Stir Bar Sorptive Extraction," *Analytica Chimica Acta,* Vol. 597, No. 2, 2007, pp. 273-281. doi:10.1016/j.aca.2007.07.004

[23] K. K. Chee, M. K. Wong and H. K. Lee, "Microwave-Assisted Solvent Extraction of Air Particulates for the Determination of PAHs," *Environmental Monitoring and Assessment,* Vol. 44, Nos. 1-3, 1997, pp. 391-403. doi:10.1023/A:1005708117992

[24] L. Turrio-Baldassarri, C. L. Battistelli and A. L. Iamiceli, "Evaluation of the Efficiency of Extraction of PAHs from Diesel Particulate Matter with Pressurized Solvents," *Analytical Bioanalytical Chemistry,* Vol. 375, No. 4, 2003, pp. 589-595.

[25] D. L. Poster, M. M. Schantz, L. C. Sander and S. A. Wise, "Analysis of Polycyclic Aromatic Hydrocarbons (PAHs) in Environmental Samples: A Critical Review of Gas Chromatographic (GC) Methods," *Analytical Bioanalytical Chemistry,* Vol. 386, No. 4, 2006, pp. 859-881. doi:10.1007/s00216-006-0771-0

[26] M. Punia, V. P. Nautiyal and Y. Kant, "Identifying Biomass Burned Patches of Agricultural Residue using Satellite Remote Sensing Data," *Current Science,* Vol. 94, No. 9, 2008, pp. 1185-1190.

[27] P. K. Gupta, S. Sahai, N. Singh, C. K. Dixit, D. P. Singh, C. Sharma, M. K. Tiwari, R. K. Gupta and S. C. Garg, "Residue Burning in Rice-Wheat Cropping System: Causes and Implications," *Current Science,* Vol. 87, No. 12, 2004, pp. 1713-1717.

[28] K. V. S. Badarinath, T. R. K. Chand and V. K. Prasad, "Agricultural Crop Residue Burning in the Indo-Gangetic Plains - A Study using IRS-P6 A WiFS Satellite Data," *Current Science,* Vol. 91, No. 8, 2006, pp. 1085-1089.

[29] J. J. Schauer, B. T. Mader, J. T. DeMinter, G. Heidemann, M. S. Bae, J. H. Seinfeld, R. C. Flagan, R. A. Cary, D. Smith, B. J. Huebert, T. Bertram, S. Howell, J. T. Kline, P. Quinn, T. Bates, B. Turpin, H. J. Lim, J. Z. Yu, H. Yang and M. D. Keywood, "ACE-Asia Intercomparison of a Thermal-Optical Method for the Determination of Particle-Phase Organic and Elemental Carbon," *Environmental Science & Technology,* Vol. 37, No. 5, 2003, pp. 993-1001. doi:10.1021/es020622f

[30] M. -X. Xie, F. Xie, Z.-W. Deng and G.-S. Zhuang, "Determination of Polynuclear Aromatic Hydrocarbons in Aerosol by Solid-Phase Extraction and Gas Chromatography-Mass Spectrum," *Talanta,* Vol. 60, No. 6, 2003, pp. 1245-1257. doi:10.1016/S0039-9140(03)00224-8

[31] K. Ram, M. M. Sarin and P. Hegde, "Atmospheric Abundances of Primary and Secondary Carbonaceous Species at Two High-Altitude Sites in India: Sources and Temporal Variability," *Atmospheric Environment,* Vol. 42, No. 28, 2008, pp. 6785-6796. doi:10.1016/j.atmosenv.2008.05.031

Atmospheric Environment 45 (2011) 6732–6740

Contents lists available at SciVerse ScienceDirect

Atmospheric Environment

journal homepage: www.elsevier.com/locate/atmosenv

Atmospheric polycyclic aromatic hydrocarbons (PAHs) from post-harvest biomass burning emissions in the Indo-Gangetic Plain: Isomer ratios and temporal trends

Prashant Rajput [a], M.M. Sarin [a,*], R. Rengarajan [a], Darshan Singh [b]

[a] Physical Research Laboratory, Ahmedabad 380 009, India
[b] Punjabi University, Patiala 147 002, India

ARTICLE INFO

Article history:
Received 5 January 2011
Received in revised form
5 August 2011
Accepted 8 August 2011

Keywords:
Agricultural-waste burning
Rice-straw
Wheat-straw
$PM_{2.5}$
PAHs
Indo-Gangetic Plain

ABSTRACT

Atmospheric concentrations of particulate polycyclic aromatic hydrocarbons (PAHs) and their isomer ratios have been studied for two distinct biomass burning emissions (post-harvest burning of paddy-residue in Oct–Nov and wheat-residue burning during April–May) in the Indo-Gangetic Plain (IGP). The mass concentrations of $PM_{2.5}$ (Av: 246 μg m^{-3}), OC (92 μg m^{-3}), EC (7 μg m^{-3}) and ΣPAHs (40 ng m^{-3}) are significantly higher from the paddy-residue burning. In contrast, for wheat-residue burning emissions, concentrations of $PM_{2.5}$ (53 μg m^{-3}), OC (15 μg m^{-3}), EC (4 μg m^{-3}) and ΣPAHs (7 ng m^{-3}) are about 4–5 times lower. The large temporal variability in the concentrations of particulate species and OC/EC ratio (range: 1.9–25.7) is attributed to differences in the two biomass burning emissions and their relative source strength. The mass fraction of EC (Av: 3.1%), associated with the poor combustion efficiency of moist paddy-residue, is significantly lower than that from the wheat-residue burning (EC/$PM_{2.5}$ = 7.6%) during dry weather conditions. Furthermore, OC mass fractions from paddy- and wheat-residue burning emissions are 37% and 28% respectively; whereas ΣPAHs/EC ratios are significantly different, 5.7 and 1.6 mg g^{-1}, from the two emission sources. The particulate concentrations of 5- and 6-ring isomers (normalized to EC) from paddy-residue burning are about 3–5 times higher than those from the wheat-residue burning emissions. The cross plots of PAHs show distinct differences in isomer ratios from agricultural-waste burning emissions vis-à-vis fossil-fuel combustion.

1. Introduction

The chemical characteristics of atmospheric aerosols from fossil-fuel combustion and biomass burning emissions have been reasonably well studied and represented in the literature (Bond et al., 2004; Fine et al., 2002; Fon et al., 2007; Fraser et al., 2002; Harrison et al., 1996; Rengarajan et al., 2007; Rogge et al., 1998; Schauer et al., 2002; Simoneit, 2002; Venkataraman et al., 2005; Wang et al., 2009). However, detailed information on the chemical composition of aerosols particularly from agricultural-waste burning emissions is rather lacking (Andreae and Merlet, 2001; Hays et al., 2005; Jenkins et al., 1996). Recently, attempts have been made to study the particle-size distribution in the controlled combustion experiments conducted for rice- and wheat-straw (Hays et al., 2005; Li et al., 2007; Zhang et al., 2011). These laboratory based experiments have reported a unimodal size peaking at less than 0.5 μm, with the exception of one set of results on bimodal-size distribution of particles from rice-straw combustion (Keshtkar and Ashbaugh, 2007). More recently, study based on freshly emitted particles from rice- and wheat-straw burning has reported a unimodal size distribution at 0.10 μm and 0.15 μm respectively (Zhang et al., 2011).

The significance of large-scale biomass burning emissions on the atmospheric chemistry, climate and bio-geochemical cycles has been widely emphasized (Crutzen and Andreae, 1990; Das et al., 2008; Dey and Tripathi, 2007; Gustafsson et al., 2009; Menon et al., 2002; Ram et al., 2010; Ramanathan et al., 2007). Several studies with top-down approach have been carried out from the South Asian region, suggesting that 50–90% of the black carbon (BC) is derived from the fossil-fuel combustion sources (Mayol-Bracero et al., 2002; Novakov et al., 2000; Ramanathan et al., 2007; Stone et al., 2007). In contrast, bottom-up approach based on emission inventories suggest that biomass burning is a dominant source in the South Asia and accounts for nearly 70% of the BC (Gustafsson et al., 2009; Rengarajan et al., 2007; Venkataraman et al., 2005). However, these inferences are derived mainly from OC/EC ratios, and can be biased to some degree by fractionation of carbonaceous

* Corresponding author. Tel.: +91 79 26314306; fax: +91 79 26301502.
E-mail address: sarin@prl.res.in (M.M. Sarin).

1352-2310/$ – see front matter © 2011 Elsevier Ltd. All rights reserved.
doi:10.1016/j.atmosenv.2011.08.018

aerosols during chemical processing in the atmosphere and can, thus, have misleading conclusions drawn on their source characterization (Cabada et al., 2004; Castro et al., 1999; Gustafsson et al., 2009; Ram and Sarin, 2010; Schauer et al., 1996). These diverging views on the sources of carbonaceous aerosols require a comprehensive data set for EC and OC from biomass burning emissions, as well as for some of the diagnostic tracers such as polycyclic aromatic hydrocarbons (PAHs) (Mandalakis et al., 2005; Li et al., 2009a,b; Sheesley et al., 2009; Tham et al., 2008; Thornhill et al., 2008; Yunker et al., 2002).

This manuscript presents a first comprehensive data set on airborne PAHs (and isomer ratios), OC and EC in $PM_{2.5}$ (particles with aerodynamic diameter $\leq$ 2.5 μm) collected during two distinct agricultural-waste burning practices followed in the Punjab and Haryana regions of the Indo-Gangetic Plain (IGP). Our primary objective is to assess the relative impact of emissions from post-harvest burning of paddy-residue during Oct–Nov and wheat-residue burning emissions during April–May. Detailed information on concentrations of PAHs and their isomer ratios from agricultural-waste burning emissions is lacking in the literature for this dominant source of carbonaceous aerosols in the IGP. The post-harvest burning of paddy-residue in Punjab region (during Oct–Nov) is estimated to be around 100 million tons of rice-straw (Badarinath et al., 2006; Gupta et al., 2004; Punia et al., 2008). The emission strength from wheat-residue burning is about a factor of 2–3 lower during April–May. The time period of December–March is characterized by emissions from bio-fuels (Babool, Cowdung cake, Eucalyptus, Jujube and Shisham) and fossil-fuel combustion sources.

2. Aerosol sampling and methodology

2.1. Site description & meteorology

The sampling site at Patiala (30.2 N, 76.3 E; 250 m amsl) is located upwind of the major industrial pollution sources in the Indo-Gangetic Plain (IGP), Fig. 1. The site is mainly influenced by the downwind transport of carbonaceous aerosols from two distinct and seasonal post-harvest biomass burning emissions in Oct–Nov and April–May. In order to characterize the chemical constituents from agricultural-waste burning emissions, $PM_{2.5}$ samples were collected during drier months (from Oct 2008 to May 2009). The sampling during the wet period (south-west monsoon; July–Sept) is not relevant due to wash-out of the atmosphere by frequent rain events. During summer months (May–June), transport of mineral dust from western India and northwest Desert regions is a conspicuous feature (Jethva et al., 2005). The entire study period from Oct–May is sub-divided into three phases: Oct–Nov, referred to as post-monsoon, is influenced by emissions from post-harvest burning of paddy-residue; Dec–Mar (wintertime) is dominated by bio-fuel (Babool, Cowdung cake, Eucalyptus, Jujube and Shisham) and fossil-fuel combustion, with occasional fog events. The time period of April–May is influenced by emissions from post-harvest burning of wheat-residue. The daily temperature varied from 19 to 33 °C during Oct–Nov, 11–31 °C during Dec–Mar and 22–41 °C during April–May, with corresponding relative humidity of 61 ± 15%, 62 ± 15% and 37 ± 12% respectively. The winds were north-westerly and weak (1 m s^{-1}) during the Oct–Nov, changing to moderate intensity (4 m s^{-1}) during Dec–Mar from north-westerly

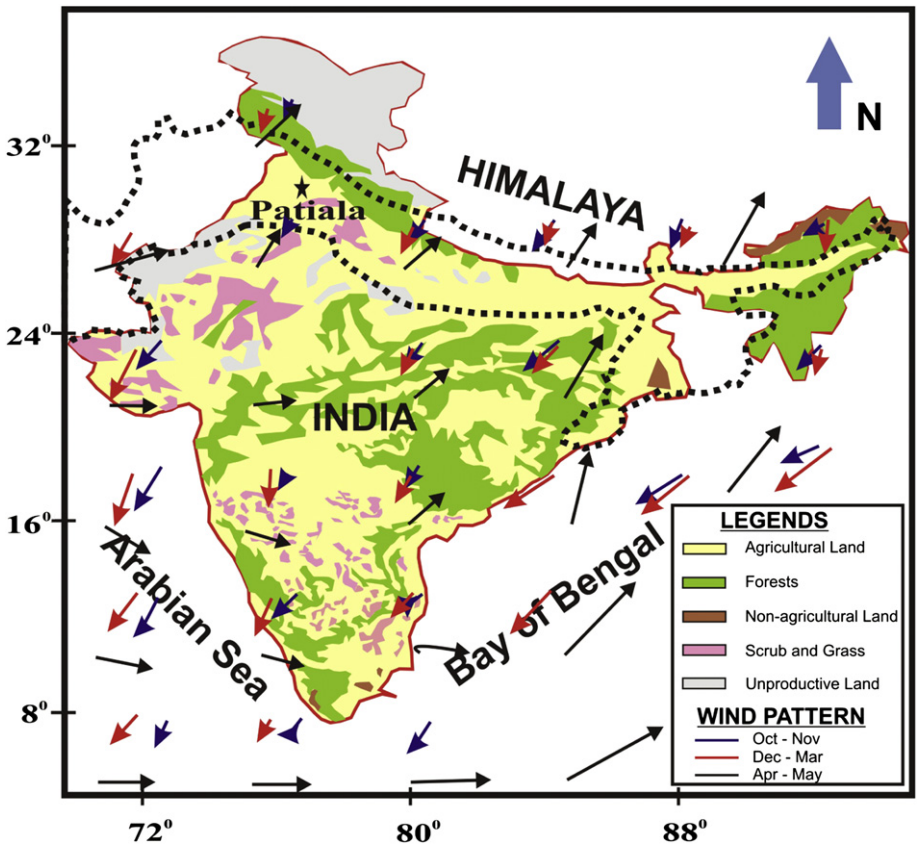

Fig. 1. Aerosol sampling site at Patiala (shown by star) in the Indo-Gangetic Plain (area marked by dotted line). Typical wind-fields (during the sampling period) and major land use patterns in India are also shown (adapted from maps of India.com).

to westerly. The south-westerly winds were relatively strong (8 m s^{-1}) in April–May.

2.2. Aerosol sampling

A high-volume aerosol sampler (Thermo Scientific), with $PM_{2.5}$ size cut-off, was set up on the terrace (~15 m above ground level) of the Physics Department, Punjabi University, Patiala. The aerosol samples were collected onto pre-combusted (@ 350 °C for ~6 h) tissuquartz filters (PALLFLEX™, 2500QAT-UP, 20 cm × 25 cm), by filtering air at a flow rate of ~1.2 m^3 min^{-1} for ~20 h. A total of 71 samples were collected over a period of eight months from Oct 2008 to May 2009. Soon after their retrieval from the sampler, filters were wrapped in Al-foils, sealed in zip-lock bags and stored at ~4 °C until analysis. The $PM_{2.5}$ mass was determined gravimetrically on a high precision analytical balance (0.1 mg; Sartorius, model LA130S-F) after equilibrating the filters at relative humidity of 37 ± 2% and temperature of 24 ± 2 °C for nearly 10 h.

2.3. Analysis of elemental carbon and organic carbon (EC, OC)

The concentrations of elemental carbon (EC) and organic carbon (OC) were measured on EC–OC analyzer (Model 2000, Sunset Laboratory, USA) using a thermal–optical transmittance (TOT) protocol reported earlier from our laboratory (Ram and Sarin, 2009; Rengarajan et al., 2007; Ram et al., 2010). The average blank level of OC was 3.9 ± 0.3 μg cm^{-2} for ($n = 8$, ±1σ), and has been corrected for all measured concentrations in aerosol samples. The average ratio of measured carbon to expected carbon in a standard solution of Potassium Hydrogen Phthalate (KHP; $n = 16$) is 1.05 ± 0.04. Based on replicate analysis of samples ($n = 45$), the precision of measurements for OC and EC are ± 3% (1σ) and ±7% respectively.

2.4. Sample preparation and analysis of PAHs on GC–MS

A total of 16-PAHs are measured in this study. These include Naphthalene {NAPH}, Acenaphthylene {ACY}, 2-Bromonaphthalene {2-BrNAPH}, Acenaphthene {ACE}, Fluorene {FLU}, Phenanthrene {PHEN}, Anthracene {ANTH}, Fluoranthene {FLA}, Pyrene {PYR}, Benzo[*a*]anthracene {BaA}, Chrysene/Triphenylene {CHRY + TRIPH}, Benzo[$b + j + k$]fluoranthene {B[b,j,k]FLA}, Benzo[*a*]pyrene [BaP], Indeno[1,2,3-*cd*] pyrene {IcdP}, Dibenzo[$a,h + a,c$]anthracene {D[ah,ac]ANTH}, and Benzo[*ghi*]perylene {BghiP}. The extremely low levels of PAHs in aerosols require their enrichment solvent extraction and matrix removal prior to their quantitative analysis on a gas chromatograph coupled to a mass spectrometer (GC–MS; HP 7890A/5975C, Agilent). The analytical protocol adopted in this study and relevant details have been described in our earlier publication (Rajput et al., 2011). Briefly, accelerated solvent extraction (ASE) of PAHs is carried out using HPLC grade solvents, dichloromethane (DCM:Chromasolv® Plus, Sigma–Aldrich) and matrix clean-up on a silica-solid phase extraction cartridge (SPE; WAT020810, Waters Sep-Pak®, 3 cc/500 mg). Subsequently PAHs are measured on GC-MS in presence of 200 ng Pyrene-D10 (71390 Absolute Standards INC.) as an internal standard. The analytical accuracy of PAHs, as determined from a standard reference material (NIST, SRM-1649b, Urban dust) on a GC–MS equipped with a capillary column (30 m × 0.25 mm × 0.25 μm), are listed in (Table 1). Helium is used as a carrier gas, and the mass spectrometer is operated in electron-impact mode at 70 eV. The calibration on GC–MS is performed with standards prepared in hexane from a 16-PAHs mixture (QTM PAH Mix; 47930-U, Supelco). The mass recovery of an individual PAH (except that of 2-Bromonaphthalene) in aerosol samples is corrected using the analytical accuracy from SRM. Replicate extractions and analyses of several field-based samples ($n = 12$) ensures that more than 95% mass of the total PAHs (ΣPAHs) is extractable during the first extraction. Replicate analyses of several samples ($n = 9$) also provide external precision (uncertainty in the heterogeneity of sample) of measurements to be ±4%.

Table 1
Detection limits (DL; $n = 10$ blanks) and analytical accuracy of PAHs based on analysis ($n = 13$) of standard reference material (NIST, SRM-1649b, Urban Dust).

PAHs	Molecular weight	DL (pg m^{-3})	Measured conc.[b] (ng/100 mg SRM)	Reported conc. (ng/100 mg SRM)
NAPH[a]	128	1.9	83 ± 12	112 ± 42
ACY[a]	152	3.7	14 ± 3	18 ± 3
2-BrNAPH	206	2.5	NR	NR
ACE[a]	154	1.2	10 ± 1	19 ± 4
FLU[a]	166	1.5	16 ± 2	22 ± 2
PHEN	178	2.3	376 ± 17	394 ± 5
ANTH	178	2.6	47 ± 7	51 ± 1
FLA	202	2.1	605 ± 43	614 ± 12
PYR	202	1.6	492 ± 31	478 ± 3
BaA	228	2.3	231 ± 23	209 ± 5
CHRY + TRIPH	228	1.9	413 ± 16	425 ± 10
B[b,j,k]FLA	252	2.4	950 ± 65	947 ± 51
BaP	252	2.0	274 ± 19	247 ± 17
IcdP	276	1.6	318 ± 21	296 ± 17
D[ah,ac]ANTH	278	3.6	48 ± 5	50 ± 1
BghiP	276	2.5	428 ± 36	394 ± 5

NR (Not Reported in SRM).
[a] Reference values, otherwise certified values (NIST).
[b] Standard deviation of the data for $n = 13$ (This study).

3. Results and discussion

3.1. Temporal variations of $PM_{2.5}$ and carbonaceous species (OC and EC)

In this study, temporal variability of particulate-bound species have been studied for three distinct emission sources: post-harvest burning of paddy-residue during Oct–Nov (post-monsoon); bio-fuel burning and fossil-fuel combustion during Dec–Mar (winter) and post-harvest burning of wheat-residue in April–May (summer). The temporal variability in $PM_{2.5}$ mass concentration and mass fractions of OC and EC ($OC/PM_{2.5}$, $EC/PM_{2.5}$) is presented in Fig. 2. The atmospheric concentration of $PM_{2.5}$ (Fig. 2a) is significantly higher during paddy-residue burning emissions (Oct–Nov), range: 111–391 μg m^{-3} (Av: 246 ± 78); whereas $OC/PM_{2.5}$ and $EC/PM_{2.5}$ mass fractions (Fig. 2b and c) varied from 24 to 50% (Av: 37 ± 6%) and 1.6–5.8% (3.1 ± 1.0%) respectively. During Dec–Mar (emissions from bio-fuel and fossil-fuel combustion), $PM_{2.5}$ concentration decreases by a factor of two, Av: 122 ± 54 μg m^{-3}, with a parallel decrease in the mass fraction of OC (range: 14–31%, Av: 24 ± 4%). However, an increase in the $EC/PM_{2.5}$ fraction (2.1–9.3%), compared to that from paddy-residue burning is noteworthy. Emissions from post-harvest burning of wheat-residue (April–May) exhibit further characteristic decrease in the $PM_{2.5}$ mass concentration (range: 18–123 μg m^{-3}, Av: 53 ± 29 μg m^{-3}). However, average OC mass fraction during April–May (28 ± 6%; range: 20–36%) is comparatively higher than that from fossil-fuel combustion (Dec–Mar). The $EC/PM_{2.5}$ fraction (4.3–12.1%) from wheat-residue burning (Fig. 2c) is significantly high compared to that from paddy-residue burning. The cause for this is attributed to high-moisture content in the paddy-residue (40–50%) as compared to that in the wheat-residue (<5%). The chamber based experiments on wheat- and rice-straw combustion, with moisture content in the range of 7–10%, have been reported in the literature (Table 2). In general, the chamber based rice-straw combustion experiments suggest negative relationship between moisture

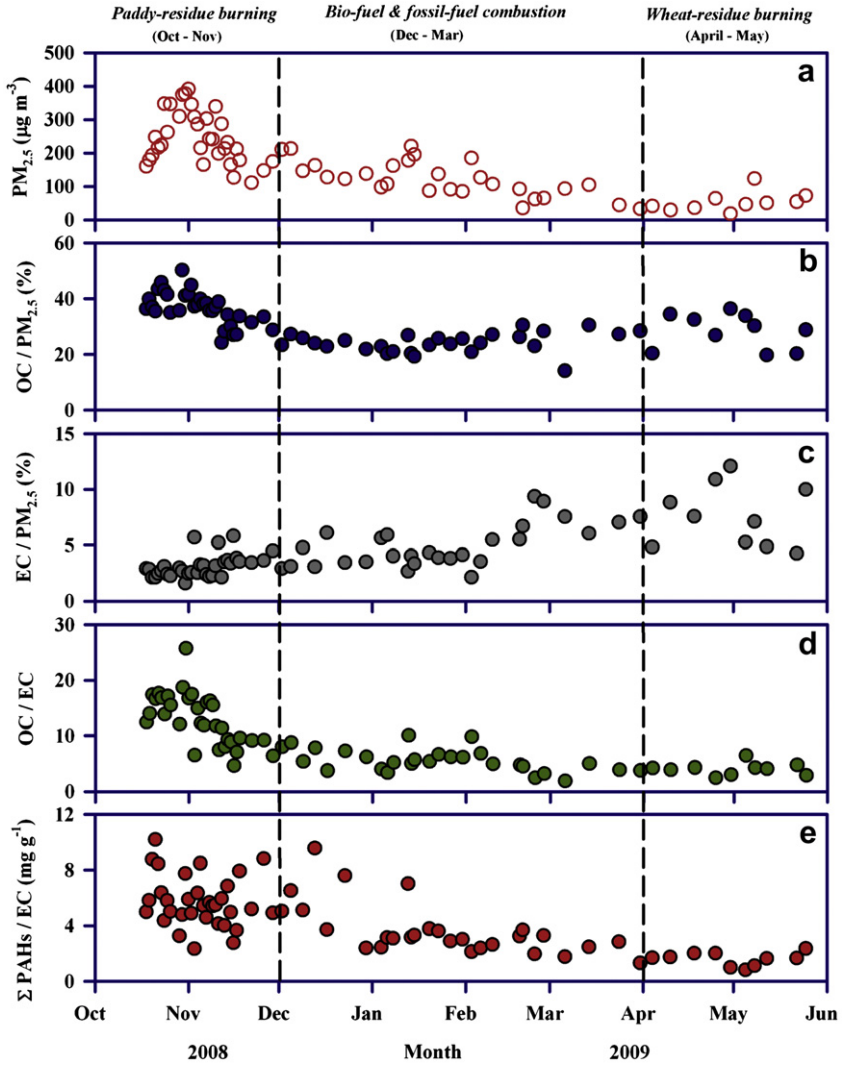

Fig. 2. Temporal variability in $PM_{2.5}$ and atmospheric concentrations of carbonaceous species is shown for sampling during Oct 2008 to May 2009. Vertical dotted lines demarcate different post-harvest biomass burning emissions.

content and mass fraction of total carbon (TC = OC + EC) in $PM_{2.5}$ (Hays et al., 2005; Korenaga et al., 2001). In contrast, the particulate TC and PAHs from wood-fuel (rubber) combustion and wheat-straw burning show a positive correlation with moisture content (Chomanee et al., 2009; Dhammapala et al., 2007; Hays et al., 2005; Li et al., 2007; Sheesley et al., 2003). A comparison of the mass fractions of carbonaceous species (OC, EC and PAHs) analyzed in the ambient atmospheric aerosols and chamber experiments (as summarized in Table 2) must take into account differences in the respective moisture content and combustion efficiency (open field burning vis-à-vis controlled laboratory combustion).

3.2. OC/EC and ΣPAHs/EC ratios

The temporal variation of OC/EC ratios provide useful information on varying nature of combustion sources and their strength; especially for biomass burning vis-à-vis fossil-fuel emissions (Ram et al., 2008; Rengarajan et al., 2007). The atmospheric abundance of $PM_{2.5}$ and the temporal variability in OC/EC ratios (Fig. 2a and d) reflect differences in the intensity and type of emission sources. The concentrations of OC and EC, during paddy-residue burning, varied from 34 to 188 μg m^{-3} and 3.8 to 17.5 μg m^{-3} respectively; with significantly high OC/EC ratios varying from 4.6 to 25.7 μg m^{-3} (Av: 13.0 ± 4.6). Similar to the temporal variability of $PM_{2.5}$, the concentrations of OC (range: 9–58 μg m^{-3}) and EC (range: 2.3–8.9 μg m^{-3}) are significantly lower during Dec–Mar when emissions from bio-fuel and fossil-fuel combustion are relatively significant. A simultaneous decrease in the OC/EC ratios in Dec–Mar (range: 1.9–10.1; Fig. 2d) further suggests relative dominance of EC from the fossil-fuel combustion. It is noteworthy that OC concentrations and OC/EC ratios further decrease during wheat-residue burning (April–May; Fig. 2d). The emissions from post-harvest burning of wheat-residue with relatively low moisture content, is a likely cause for the decrease in OC and increase in EC concentration and, hence, decrease in OC/EC ratios. This is also reflected in the contribution of EC to $PM_{2.5}$ (Av: 8%); comparatively high during wheat-residue burning as compared to those from paddy-residue burning (Av: ~3%). The low contribution of EC is associated with the emission from paddy-residue burning in Oct–Nov.

The total PAHs concentrations (ΣPAHs) also exhibit distinct temporal variability, similar to those recorded in the abundances of OC and EC. The ΣPAHs varied from 19.8 to 59.1 ng m^{-3} (Av: 39.4) during paddy-residue burning, 3.3–47.9 ng m^{-3} (Av: 19.7) during emissions from bio-fuels and fossil-fuel combustion and,

Table 2
Average mass fractions of EC and OC in $PM_{2.5}$ for rice- and wheat-straw burning.

References	Type of measurement	OC/$PM_{2.5}$ (%)	EC/$PM_{2.5}$ (%)	Moisture content (%)
Hays et al., 2005	Chamber simulation			
Rice-straw		69	1.3	8.6
Wheat-straw		26	11	8.8
Dhammapala et al., 2007	Chamber simulation			
Wheat-straw		63	11.7	10–11
Sheesley et al., 2003	Controlled combustion			
Rice-straw		56	1.1	
Li et al., 2007	Ambient aerosol			
Wheat-straw	(T = 25–30 °C; RH = 53–71%)[a]	36	6.5	9.6
This study	Ambient aerosol			
Rice-straw	(T = 19–33 °C; RH = 61 ± 15%)[a]	37 ± 6	3.1 ± 1.0	40–50
Fossil- & bio-fuels	(T = 11–31 °C; RH = 62 ± 15%)[a]	24 ± 4	5.0 ± 1.9	
Wheat-straw	(T = 22–41 °C; RH = 37 ± 12%)[a]	28 ± 6	7.6 ± 2.8	<5

[a] Ambient atmospheric conditions.

2.0–17.0 ng m^{-3} (Av: 6.6) during wheat-residue burning. Furthermore, the concentrations of OC, EC and ΣPAHs from bio-fuels and fossil-fuel combustion (Dec–Mar), show intermediate values with respect to those associated with burning of paddy- and wheat-residue. The average ΣPAHs/EC ratios (in mg g^{-1}; Fig. 2e) are 5.7, 3.7, and 1.6, respectively during the three biomass burning events. A systematic decrease in the ΣPAHs, ΣPAHs/EC and OC/EC ratios from Oct to May (Fig. 2d and e) is attributed to the decrease in the source strength, combustion efficiency and types of biomass burning. A recent investigation on the concentration of OC, EC and PAHs, studied from rubber–wood burning, had reported that the concentrations of these species increases with high-moisture content of the wood, whereas they are inversely related to the duration of burning (Chomanee et al., 2009). A likely cause for the high mass fraction of carbonaceous aerosols and concentrations of ΣPAHs in Oct–Nov is attributed to high-moisture content of the paddy-residue (relative humidity was 61 ± 15% and that in April–May was 37 ± 12%). In addition, a strong convective mixing and high abundance of mineral dust during summer months is a likely process suggested for the lower concentrations of carbonaceous species during wheat-residue burning emissions. However, mass ratios of carbonaceous species are expected to be more source-specific and are not affected by environmental conditions. It is important to reiterate that high ratios of OC/EC and ΣPAHs/EC are associated with paddy-residue burning (Fig. 2d and e).

The mass fractions (mg g^{-1}) of light-PAHs (2- to 3-ring) during paddy-residue burning, bio-fuels and fossil-fuel combustion and, wheat-residue burning emissions are 0.01 ± 0.01, 0.04 ± 0.03 and 0.03 ± 0.01 respectively. The mass fractions of light molecular weight PAHs in $PM_{2.5}$ (Table 3) are relatively low compared to chamber based experiments (e.g. Hays et al., 2005). Relative differences in the moisture content of biomass (40–50% in paddy-residue; and <5% in wheat-residue), high particulate reactivity of PAHs in the presence of O_3, NO_x and OH radicals and their physical scavenging onto atmospheric mineral dust (as against chamber based experiments in the laboratory) are the likely mechanism proposed for the lower mass fractions of light-PAHs (Table 3). The estimated emission of pollutants during wheat-

Table 3
Average mass fractions of $PM_{2.5}$-bound PAHs (mg g^{-1} OC) for biomass burning emissions vis-à-vis fossil-fuel combustion.

PAHs	Paddy-residue (Oct–Nov)	Bio- & fossil-fuel (Dec–Mar)	Wheat-residue (April–May)
NAPH	0.004 ± 0.003	0.015 ± 0.019	0.008 ± 0.006
ACY	0.001 ± 0.000	0.002 ± 0.002	0.001 ± 0.001
2-BrNAPH	0.000 ± 0.000	0.000 ± 0.000	0.000 ± 0.000
ACE	0.001 ± 0.002	0.001 ± 0.001	0.000 ± 0.000
FLU	0.001 ± 0.000	0.002 ± 0.001	0.000 ± 0.000
PHEN	0.004 ± 0.003	0.014 ± 0.006	0.014 ± 0.010
ANTH	0.001 ± 0.001	0.002 ± 0.001	0.004 ± 0.010
FLA	0.011 ± 0.006	0.029 ± 0.011	0.023 ± 0.016
PYR	0.013 ± 0.007	0.033 ± 0.011	0.024 ± 0.016
BaA	0.015 ± 0.007	0.019 ± 0.011	0.006 ± 0.009
CHRY + TRIPH	0.046 ± 0.015	0.054 ± 0.028	0.031 ± 0.015
B[b,j,k]FLA	0.150 ± 0.070	0.201 ± 0.097	0.116 ± 0.067
BaP	0.052 ± 0.024	0.074 ± 0.033	0.029 ± 0.028
IcdP	0.082 ± 0.029	0.115 ± 0.041	0.084 ± 0.054
D[ah,ac]ANTH	0.011 ± 0.005	0.012 ± 0.008	0.005 ± 0.007
BghiP	0.085 ± 0.031	0.110 ± 0.039	0.097 ± 0.035
ΣPAHs	0.476 ± 0.174	0.683 ± 0.243	0.440 ± 0.220

residue burning in the month of May, in the Punjab state (with land cultivated area ≈ 5500 sq. km) are 113 Gg of CO (1 Gg = 10^9 g), 8.6 Gg of NO_x and 1.33 Gg of CH_4 (Badarinath et al., 2006). In contrast, for paddy-residue burning (land cultivated area ≈ 12,700 sq. km; for Oct 2005) a factor of two higher emissions were estimated (Badarinath et al., 2006). This further supports our data that concentrations of carbonaceous species are relatively high during paddy-residue burning emissions (Oct–Nov) as compared to those during wheat-residue burning (April–May).

3.3. Variations in particulate PAHs

The 3-ring PAHs (with average concentrations below 0.1 ng m^{-3}) exhibit the least difference in their variability for different biomass burning emissions during the study period (Oct–May); whereas minor variations for 4-ring PAHs are evident in Fig. 3. However, PAHs with 5- and 6-ring show distinct variation,

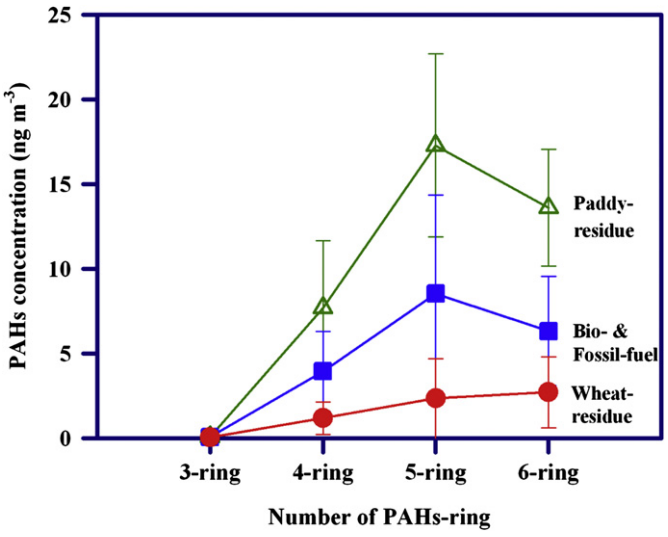

Fig. 3. Variation in $PM_{2.5}$-bound PAHs with varying number of aromatic rings for different emission scenario; 5- and 6-ring PAHs exhibit large variability for different emissions.

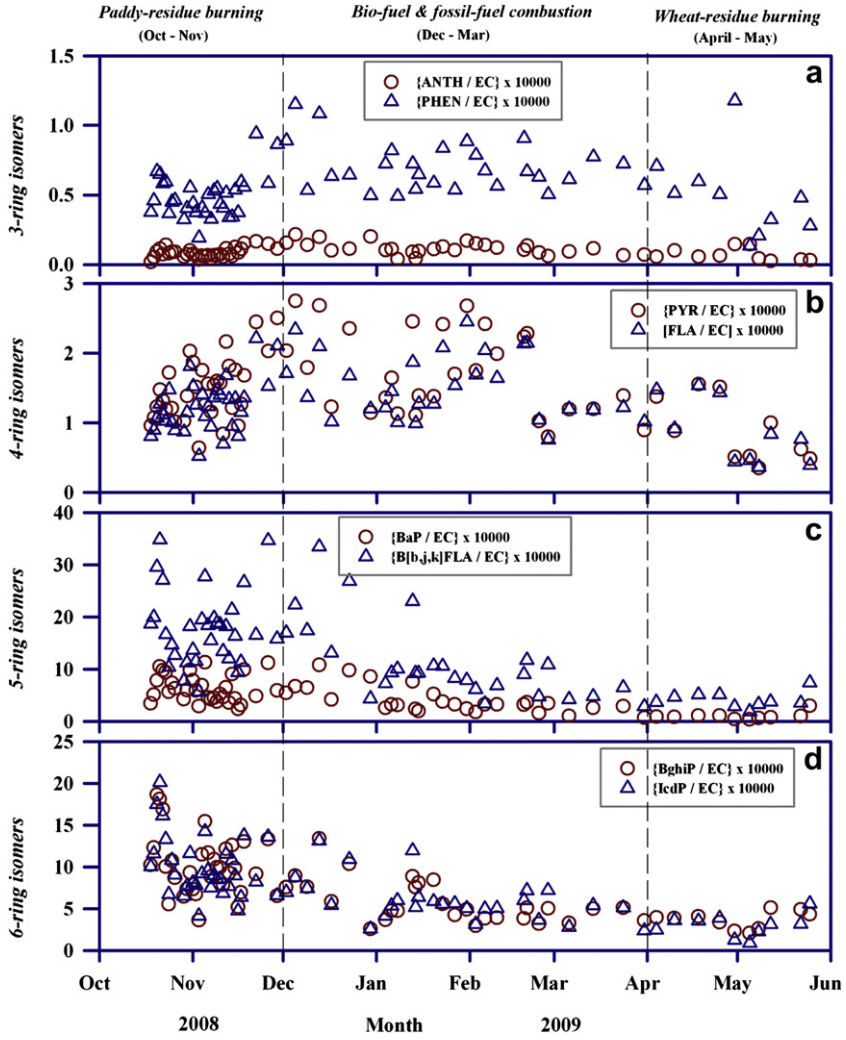

Fig. 4. PAH–EC ratio plots for different isomers. A systematic decrease in the EC normalized concentrations of 5- and 6-ring PAHs reflects the difference in paddy- and wheat-residue burning emissions.

with relatively high average concentrations (17 and 14 ng m^{-3}), during paddy-residue burning followed by lower concentrations associated with bio-fuels and fossil-fuel combustion and, wheat-residue burning emissions. The pronounced difference in the concentrations of 5- and 6-ring PAHs, by a factor of two, for three emission sources is evident in Fig. 3. The relative mass fractions of high-molecular weight PAHs (4- to 6-ring PAHs) and light-PAHs (2- to 3-ring PAHs), normalized to ΣPAHs, reveal that the contribution of heavier-PAHs to ΣPAHs from all three different emissions (paddy-residue, bio-fuels and fossil-fuel and, wheat-

Table 4
Diagnostic PAHs isomer ratios (this study) are compared with the literature data including NIST, SRM-1649b (Range; Mean ± SD, in parenthesis).

Biomass sources	ANTH/(ANTH + PHEN)	FLA/PYR	FLA/(FLA + PYR)	BaP/IcdP	BaP/BghiP	IcdP/BghiP	IcdP/(IcdP + BghiP)
Chamber experiment							
Paddy-residue[a,b]	0.17 ± 0.01	0.97 ± 0.21	0.49 ± 0.05	1.63 ± 0.45	2.20 ± 0.20	1.43 ± 0.51	0.58 ± 0.09
Wood-fuel[c]	0.18 ± 0.03	0.75 ± 0.12	0.43 ± 0.04	–	–	–	–
Wheat-residue[a,b]	0.21 ± 0.01	1.05 ± 0.08	0.51 ± 0.02	1.22 ± 0.66	1.43 ± 0.37	1.28 ± 0.39	0.55 ± 0.08
This study (ambient aerosol)							
Paddy-residue (Oct–Nov)	0.05–0.22 (0.15 ± 0.03)	0.74–0.92 (0.84 ± 0.04)	0.42–0.48 (0.46 ± 0.01)	0.34–0.97 (0.64 ± 0.16)	0.34–1.07 (0.64 ± 0.21)	0.80–1.33 (0.98 ± 0.13)	0.45–0.57 (0.49 ± 0.03)
Fossil- & bio-fuels (Dec–Mar)	0.07–0.29 (0.14 ± 0.04)	0.71–1.13 (0.90 ± 0.09)	0.42–0.53 (0.47 ± 0.03)	0.31–3.33 (0.70 ± 0.54)	0.20–3.32 (0.74 ± 0.54)	0.66–1.57 (1.07 ± 0.23)	0.40–0.61 (0.51 ± 0.06)
Wheat-residue (April–May)	0.01–0.17 (0.10 ± 0.05)	0.81–1.23 (0.97 ± 0.13)	0.45–0.55 (0.49 ± 0.03)	0.23–0.53 (0.34 ± 0.09)	0.15–0.69 (0.27 ± 0.15)	0.43–1.29 (0.80 ± 0.27)	0.30–0.56 (0.43 ± 0.08)
NIST, SRM-1649b[d]	0.11	1.28	0.56	0.83	0.63	0.75	0.43
NIST, SRM-1649b ($n = 13$)[e]	0.11 ± 0.01	1.23 ± 0.05	0.55 ± 0.01	0.86 ± 0.06	0.64 ± 0.06	0.75 ± 0.08	0.43 ± 0.03

[a] Hays et al., 2005.
[b] Jenkins et al., 1996.
[c] Bari et al., 2010.
[d] NIST reported.
[e] This study.

residue) is consistently greater than 95%, implying that they predominantly reside in the particulate form.

3.4. Variability in PAHs isomers

The concentrations of 3- and 4-ring PAHs, normalized to EC (Fig. 4a and b), show relatively high values during Dec–Mar; whereas distinct temporal variability for 5- and 6-ring PAHs (Fig. 4c and d) follows a trend similar to that of $PM_{2.5}$, OC/EC and ΣPAHs/EC. It is, thus, imperative that the signature of the type of biomass burning and its source strength is retained in the temporal variability of ΣPAHs/EC ratio, particularly for the 5- and 6-ring isomers.

The PAHs ratios from the simulated experiments for the agricultural-waste burning and wood-fuel combustion (Bari et al., 2010; Hays et al., 2005; Jenkins et al., 1996) and those observed in this study are summarized in Table 4. The PAHs ratios reported from this study, for paddy- and wheat-residue burning, are in sharp contrast to those reported from chamber based experiments (Hays et al., 2005; Jenkins et al., 1996) (Table 4). For example, if we consider the most reactive PAHs e.g. Bap, the ratios BaP/IcdP and BaP/BghiP (this study) is at least a factor of 2 lower than the ratios reported from the simulated experiments (Table 4). Moreover, these ratios are considerably depleted for the wheat-residue burning emissions (April–May) as compared to those for the paddy-residue (Oct–Nov). The reaction kinetics of PAHs (adsorbed onto silica particles) with NO_2 and O_3 has revealed high reactivity for Benzo[*a*]pyrene ($k_{ANTH,\ NO2} = 0.01 \times k_{BaP,\ NO2}$) as compared to its reactivity when adsorbed onto graphite particles (Perraudin et al., 2007). During wheat-residue burning in April–May, and high abundances of mineral dust, it is likely that some of the highly reactive PAHs (e.g. Benzo[a]pyrene and Anthracene) form nitro- and oxy-derivatives (Esteve et al., 2004; Evagelpoulos et al., 2010; Lal et al., 2008; Perraudin et al., 2005, 2007). This is one of the plausible causes for the low mass fractions of PAHs during April–May.

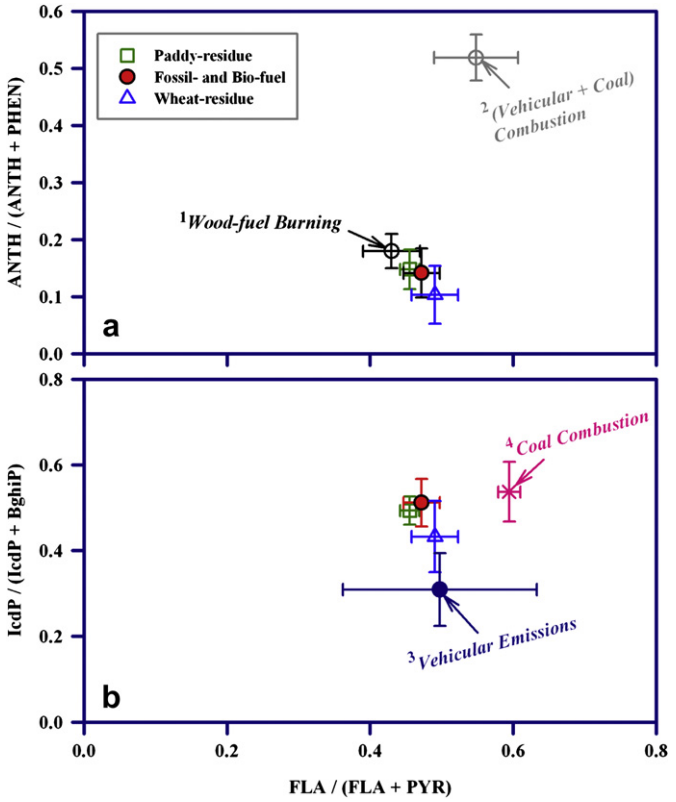

Fig. 5. Cross plots for the isomer ratios (a) FLA/(FLA + PYR) vs. ANTH/(ANTH + PHEN) and, (b) FLA/(FLA + PYR) vs. IcdP/(IcdP + BghiP) based on data from post-harvest agricultural-waste burning emissions (this study). Other data source: [1](Bari et al., 2010); [2](Sharma et al., 2008); [3](Khillare et al., 2005a,b; Rajput and Lakhani, 2008); [4](Khalili et al., 1995; Kirton et al., 1991; Li et al., 2010).

4. Conclusions & implications

The atmospheric mass concentrations of $PM_{2.5}$, OC, EC and PAHs (and isomer ratios), associated with the post-harvest biomass burning emissions, have been studied over the annual seasonal cycle from a sampling site (Patiala) located in the north-west region of the Indo-Gangetic Plain. The important conclusions drawn from our study are:

(1) Among the three different emission sources, the highest concentrations of $PM_{2.5}$, $OC/PM_{2.5}$, $EC/PM_{2.5}$ and ΣPAHs/EC ratios are recorded for post-harvest burning of paddy-residue in Oct–Nov. In contrast, the emissions from post-harvest burning of wheat-residue, during April–May (summer), are characterized by lowest concentrations of $PM_{2.5}$, ΣPAHs/EC and OC/EC ratios. The bio-fuel and fossil-fuel combustion sources dominate during Dec–Mar.
(2) The difference in biomass burning emissions is reflected in the variability of OC/EC ratios and concentrations of 5- and 6-ring PAHs (when normalized to EC).
(3) Summing up, difference in the moisture content of biomass (paddy- and wheat-straw) and their combustion efficiency, occurrence of mineral dust in the ambient atmosphere and chemical reactivity of PAHs with the oxidants like O_3 and NO_x are the major factors for the lower mass fraction of PAHs (mg g^{-1} of OC) associated with field-based measurements in contrast to laboratory experiments. A factor of 2 lower PAHs ratios, involving BaP (this study), compared to the laboratory simulation experiments indicates the enhanced chemical reactivity of BaP via heterogeneous reactions.

A notable feature of the data relates to the high abundance of particulate-bound PAHs associated with high OC/EC ratios; suggesting that high-molecular weight compounds are emitted relatively more during poor (incomplete) combustion of biomass with high-moisture content. Our evaluation of isomer ratios, based on the cross plots (Fig. 5), suggest that ANTH/(ANTH + PHEN) & IcdP/(IcdP + BghiP) against FLA/(FLA + PYR) from post-harvest biomass burning of paddy- and wheat-residue are distinguishable from fossil-fuel combustion sources. The isomer ratios from agricultural-waste burning (this study) provide important information to fill the existing gap in the conventional cross plots (Fig. 5) of ambient data on PAHs (Yunker et al., 2002).

Acknowledgements

This study was funded by the ISRO-Geosphere-Biosphere Programme office (Bangaluru, India). We are thankful to Ms. Deepti Sharma for help in sample collection at Patiala. We express our gratitude to Indian Meteorological Department (Punjabi University, Patiala) for providing the relevant meteorological data. The authors are thankful to the three anonymous reviewers for their critical comments and suggestions.

References

Andreae, M.O., Merlet, P., 2001. Emission of trace gases and aerosols from biomass burning. Global Biogeochemical Cycles 15, 955–966.
Badarinath, K.V.S., Chand, T.R.K., Prasad, V.K., 2006. Agricultural crop residue burning in the Indo-Gangetic Plains – a study using IRS-P6 A WiFS satellite data. Current Science 91, 1085–1089.

Bari, M.A., et al., 2010. Characterisation of particulates and carcinogenic polycyclic aromatic hydrocarbons in wintertime wood-fired heating in residential areas. Atmospheric Environment. doi:10.1016/j.atmosenv.2010.11.053.

Bond, T.C., et al., 2004. A technology-based global inventory of black and organic carbon emissions from combustion. Journal of Geophysical Research – Atmospheres 109, D14203. doi:10.1029/2003JD003697.

Cabada, J.C., et al., 2004. Estimating the secondary organic aerosol contribution to $PM_{2.5}$ using the EC tracer method special issue of aerosol science and technology on findings from the fine particulate matter supersites program. Aerosol Science and Technology 38, 140–155.

Castro, L.M., et al., 1999. Carbonaceous aerosol in urban and rural European atmospheres: estimation of secondary organic carbon concentrations. Atmospheric Environment 33, 2771–2781.

Chomanee, J., et al., 2009. Effect of moisture content and burning period on concentration of smoke particles and particle-bound polycylic aromatic hydrocarbons from rubber-wood combustion. Aerosol and Air Quality Research 9, 404–411.

Crutzen, P.J., Andreae, M.O., 1990. Biomass burning in the tropics: impact on atmospheric chemistry and biogeochemical cycles. Science 250, 1669–1678.

Das, S.K., Jayaraman, A., Misra, A., 2008. Fog-induced variations in aerosol optical and physical properties over the Indo-Gangetic Basin and impact to aerosol radiative forcing. Annales Geophysicae 26, 1345–1354.

Dey, S., Tripathi, S.N., 2007. Estimation of aerosol optical properties and radiative effects in the Ganga basin, northern India, during the wintertime. Journal of Geophysical Research – Atmospheres 112, D03203. doi:10.1029/2006JD007267.

Dhammapala, R., et al., 2007. Emission factors of PAHs, methoxyphenols, levoglucosan, elemental carbon and organic carbon from simulated wheat and Kentucky bluegrass stubble burns. Atmospheric Environment 41, 2660–2669.

Esteve, W., Budzinski, H., Villenave, E., 2004. Relative rate constants for the heterogeneous reactions of OH, NO_2 and NO radicals with polycyclic aromatic hydrocarbons adsorbed on carbonaceous particles. Part 1: PAHs adsorbed on 1–2 μm calibrated graphite particles. Atmospheric Environment 38, 6063–6072.

Evagelpoulos, V., et al., 2010. Polycyclic aromatic hydrocarbons (PAHs) in fine and coarse particles. Global NEST 12, 63–70.

Fine, P.M., Cass, G.R., Simoneit, B.R.T., 2002. Chemical characterization of fine particle emissions from the fireplace combustion of woods grown in the southern United States. Environmental Science and Technology 36, 1442–1451.

Fon, T., Noriatsu, O., Hiroshi, S., 2007. Polycyclic aromatic hydrocarbons (PAHs) in the aerosol of Higashi Hiroshima, Japan: pollution scenario and source identification. Water, Air, & Soil Pollution 182, 235–243.

Fraser, M.P., et al., 2002. Variation in composition of fine particulate emissions from heavy-duty diesel vehicles. Journal of Geophysical Research – Atmospheres 107 (D21), 8346. doi:10.1029/2001JD000558.

Gupta, P.K., et al., 2004. Residue burning in rice-wheat cropping system: causes and implications. Current Science 87, 1713–1717.

Gustafsson, Ö, et al., 2009. Brown clouds over south Asia: biomass or fossil fuel combustion? Science 323, 495–498.

Harrison, R.M., Smith, D.J.T., Luhana, L., 1996. Source apportionment of atmospheric polycyclic aromatic hydrocarbons collected from an urban location in Birmingham, U.K. Environmental Science and Technology 30, 825–832.

Hays, M.D., et al., 2005. Open burning of agricultural biomass: physical and chemical properties of particle-phase emissions. Atmospheric Environment 39, 6747–6764.

Jenkins, B.M., et al., 1996. Particle concentrations, gas-particle partitioning, and species intercorrelations for polycyclic aromatic hydrocarbons (PAH) emitted during biomass burning. Atmospheric Environment 30, 3825–3835.

Jethva, H., Satheesh, S.K., Srinivasan, J., 2005. Seasonal variability of aerosols over the Indo-Gangetic basin. Journal of Geophysical Research – Atmospheres 110, D21204. doi:10.1029/2005JD005938.

Keshtkar, H., Ashbaugh, L.L., 2007. Size distribution of polycyclic aromatic hydrocarbon particulate emission factors from agricultural burning. Atmospheric Environment 41, 2729–2739.

Khalili, N.R., Scheff, P.A., Holsen, T.M., 1995. PAH source fingerprints for coke ovens, diesel and, gasoline engines, highway tunnels, and wood combustion emissions. Atmospheric Environment 29, 533–542.

Khillare, P.S., Balachandran, S., Hoque, R.R., 2005a. Profile of PAHs in the diesel vehicle exhaust in Delhi. Environmental Monitoring and Assessment 105, 411–417.

Khillare, P.S., Balachandran, S., Hoque, R.R., 2005b. Profile of PAHs in the exhaust of gasoline driven vehicles in Delhi. Environmental Monitoring and Assessment 110, 217–225.

Kirton, P.J., Ellis, J., Crisp, P.T., 1991. The analysis of organic matter in coke oven emissions. Fuel 70, 1383–1389.

Korenaga, T., Liu, X., Huang, Z., 2001. The influence of moisture content on polycyclic aromatic hydrocarbons emission during rice straw burning. Chemosphere – Global Change Science 3, 117–122.

Lal, S., et al., 2008. Emission characteristic of ozone related trace gases at a semi-urban site in the Indo-Gangetic plain using inter-correlations. Journal of Atmospheric Chemistry 60, 189–204.

Li, X., et al., 2007. Particulate and trace gas emissions from open burning of wheat straw and corn stover in China. Environmental Science and Technology 41, 6052–6058.

Li, Z., et al., 2009a. Characterization of $PM_{2.5}$-bound polycyclic aromatic hydrocarbons in Atlanta-Seasonal variations at urban, suburban, and rural ambient air monitoring sites. Atmospheric Environment 43, 4187–4193.

Li, Z., et al., 2009b. Characterization of $PM_{2.5}$-bound polycyclic aromatic hydrocarbons in Atlanta. Atmospheric Environment 43, 1043–1050.

Li, P.-h., Wang, Y., Li, Y.-h., Wang, Z.-f., Zhang, H.-y., Xu, P.-j., Wang, W.-x., 2010. Characterization of polycyclic aromatic hydrocarbons deposition in $PM_{2.5}$ and cloud/fog water at Mount Taishan (China). Atmospheric Environment 44, 1996–2003.

Mandalakis, M., et al., 2005. Contribution of biomass burning to atmospheric polycyclic aromatic hydrocarbons at three European background sites. Environmental Science and Technology 39, 2976–2982.

Mayol-Bracero, O.L., et al., 2002. Carbonaceous aerosols over the Indian Ocean during the Indian Ocean Experiment (INDOEX): chemical characterization, optical properties, and probable sources. Journal of Geophysical Research – Atmospheres 107 (D19), 8030. doi:10.1029/2000JD000039.

Menon, S., et al., 2002. Climate effects of black carbon aerosols in China and India. Science 297, 2250–2253.

Novakov, T., et al., 2000. Origin of carbonaceous aerosols over the tropical Indian Ocean: biomass burning or fossil fuels? Geophysical Research Letters 27, 4061–4064.

Perraudin, E., Budzinski, H., Villenave, E., 2005. Kinetic study of the reactions of NO_2 with polycyclic aromatic hydrocarbons adsorbed on silica particles. Atmospheric Environment 39, 6557–6567.

Perraudin, E., Budzinski, H., Villenave, E., 2007. Kinetic study of the reactions of ozone with polycyclic aromatic hydrocarbons adsorbed on atmospheric model particles. Journal of Atmospheric Chemistry 56, 57–82.

Punia, M., Nautiyal, V.P., Kant, Y., 2008. Identifying biomass burned patches of agricultural residue using satellite remote sensing data. Current Science 94, 1185–1190.

Rajput, N., Lakhani, A., 2008. Measurements of polycyclic aromatic hydrocarbons at an industrial site in India. Environmental Monitoring and Assessment 150, 273–284.

Rajput, P., Sarin, M.M., Rengarajan, R., 2011. High-precision GC–MS analysis of atmospheric polycyclic aromatic hydrocarbons (PAHs) and isomer ratios from biomass burning emissions. Journal of Environmental Protection 2, 445–453.

Ram, K., Sarin, M.M., 2009. Absorption coefficient and site-specific mass absorption efficiency of elemental carbon in aerosols over urban, rural, and high-altitude sites in India. Environmental Science and Technology 43, 8233–8239.

Ram, K., Sarin, M.M., 2010. Spatio-temporal variability in atmospheric abundances of EC, OC and WSOC over Northern India. Journal of Aerosol Science 41, 88–98.

Ram, K., Sarin, M.M., Hegde, P., 2008. Atmospheric abundances of primary and secondary carbonaceous species at two high-altitude sites in India: sources and temporal variability. Atmospheric Environment 42, 6785–6796.

Ram, K., Sarin, M.M., Hegde, P., 2010. Long-term record of aerosol optical properties and chemical composition from a high-altitude site (Manora Peak) in Central Himalaya. Atmospheric Chemistry and Physics 10, 11791–11803.

Ramanathan, V., et al., 2007. Warming trends in Asia amplified by brown cloud solar absorption. Nature 448, 575–578.

Rengarajan, R., Sarin, M.M., Sudheer, A.K., 2007. Carbonaceous and inorganic species in atmospheric aerosols during wintertime over urban and high-altitude sites in North India. Journal of Geophysical Research – Atmospheres 112, D21307. doi:10.1029/2006JD008150.

Rogge, W.F., et al., 1998. Sources of fine organic aerosol. 9. Pine, oak, and synthetic log combustion in residential fireplaces. Environmental Science and Technology 32, 13–22.

Schauer, J.J., et al., 2002. Measurement of emissions from air pollution sources. 5. C1–C32 organic compounds from gasoline-powered motor vehicles. Environmental Science and Technology 36, 1169–1180.

Schauer, J.J., et al., 1996. Source apportionment of airborne particulate matter using organic compounds as tracers. Atmospheric Environment 30, 3837–3855.

Sharma, H., Jain, V., Khan, Z., 2008. Atmospheric polycyclic aromatic hydrocarbons (PAHs) in the urban air of Delhi during 2003. Environmental Monitoring and Assessment 147, 43–55.

Sheesley, R.J., et al., 2003. Characterization of organic aerosols emitted from the combustion of biomass indigenous to South Asia. Journal of Geophysical Research – Atmospheres 108 (D9), 4285. doi:10.1029/2002JD002981.

Sheesley, R.J., et al., 2009. Source apportionment of elevated wintertime PAHs by compound-specific radiocarbon analysis. Atmospheric Chemistry and Physics 9, 3347–3356.

Simoneit, B.R.T., 2002. Biomass burning – a review of organic tracers for smoke from incomplete combustion. Applied Geochemistry 17, 129–162.

Stone, E.A., et al., 2007. Understanding the origin of black carbon in the atmospheric brown cloud over the Indian Ocean. Journal of Geophysical Research – Atmospheres 112, D22S23. doi:10.1029/2006JD008118.

Tham, Y.W.F., Takeda, K., Sakugawa, H., 2008. Polycyclic aromatic hydrocarbons (PAHs) associated with atmospheric particles in Higashi Hiroshima, Japan: influence of meteorological conditions and seasonal variations. Atmospheric Research 88, 224–233.

Thornhill, D.A., et al., 2008. Spatial and temporal variability of particulate polycyclic aromatic hydrocarbons in Mexico City. Atmospheric Chemistry and Physics 8, 3093–3105.

Venkataraman, C., et al., 2005. Residential biofuels in south Asia: carbonaceous aerosol emissions and climate impacts. Science 307, 1454–1456.
Wang, X., et al., 2009. Characteristics and sources of atmospheric polycyclic aromatic hydrocarbons (PAHs) in Shanghai, China. Environmental Monitoring and Assessment 165, 295–305.
Yunker, M.B., et al., 2002. PAHs in the Fraser River basin: a critical appraisal of PAH ratios as indicators of PAH source and composition. Organic Geochemistry 33, 489–515.
Zhang, H., et al., 2011. Particle size distribution and polycyclic aromatic hydrocarbons emissions from agricultural crop residue burning. Environmental Science and Technology 45, 5477–5482.